INFORMATION TO USERS

This manuscript has been reproduced from the microfilm master. UMI films the text directly from the original or copy submitted. Thus, some thesis and dissertation copies are in typewriter face, while others may be from any type of computer printer.

The quality of this reproduction is dependent upon the quality of the copy submitted. Broken or indistinct print, colored or poor quality illustrations and photographs, print bleedthrough, substandard margins, and improper alignment can adversely affect reproduction.

In the unlikely event that the author did not send UMI a complete manuscript and there are missing pages, these will be noted. Also, if unauthorized copyright material had to be removed, a note will indicate the deletion.

Oversize materials (e.g., maps, drawings, charts) are reproduced by sectioning the original, beginning at the upper left-hand corner and continuing from left to right in equal sections with small overlaps.

Photographs included in the original manuscript have been reproduced xerographically in this copy. Higher quality 6" x 9" black and white photographic prints are available for any photographs or illustrations appearing in this copy for an additional charge. Contact UMI directly to order.

University of Alberta

PHOTODYNAMIC THERAPY OF UROLOGIC MALIGNANCIES: STRATEGIES
FOR SELECTIVE PHOTOSENSITIZATION

By

Zhengwen XIAO ©

A THESIS

SUBMITTED TO THE FACULTY OF GRADUATE STUDIES AND RESEARCH
IN PARTIAL FULFILLMENT OF THE REQUIREMENTS FOR THE DEGREE OF
DOCTOR OF PHILOSOPHY

In

Experimental Surgery

Department of Surgery

Edmonton, Alberta

Fall, 1999

Your file Votre référence

Our file Notre référence

The author has granted a non-exclusive licence allowing the National Library of Canada to reproduce, loan, distribute or sell copies of this thesis in microform, paper or electronic formats.

The author retains ownership of the copyright in this thesis. Neither the thesis nor substantial extracts from it may be printed or otherwise reproduced without the author's permission.

L'auteur a accordé une licence non exclusive permettant à la Bibliothèque nationale du Canada de reproduire, prêter, distribuer ou vendre des copies de cette thèse sous la forme de microfiche/film, de reproduction sur papier ou sur format électronique.

L'auteur conserve la propriété du droit d'auteur qui protège cette thèse. Ni la thèse ni des extraits substantiels de celle-ci ne doivent être imprimés ou autrement reproduits sans son autorisation.

0-612-46949-2

Canada

UNIVERSITY OF ALBERTA

Library Release Form

Name of Author: Zhengwen XIAO

Title of Thesis: Photodynamic Therapy of Urologic Malignancies: Strategies of Selective Photosensitization

Degree: Doctor of Philosophy

Year this degree granted: 1999

Permission is hereby granted to the University of Alberta Library to reproduce single copies of this thesis and to lend or sell such copies for private, scholarly or scientific research purposes only.

The author reserves all other publication and other rights in association with the copyright in the thesis, and except as hereinbefore provided, neither the thesis nor any substantial portion thereof may be printed or otherwise reproduced in any material form whatever without the author's prior written permission.

(Signed) _____

10423 – 58 Avenue

Edmonton, Alberta

Canada, T6H 1B8

Date: _Aug. 16, 1999_

University of Alberta

Faculty of Graduate Studies and Research

The undersigned certify they have read and recommend to the Faculty of Graduate Studies and Research for acceptance, a thesis entitled *"Photodynamic Therapy of Urologic Malignancies: Strategies For Selective Photosensitization"* submitted by Zhengwen Xiao in partial fulfillment of the requirements for the degree of Doctor of Philosophy in Experimental Surgery.
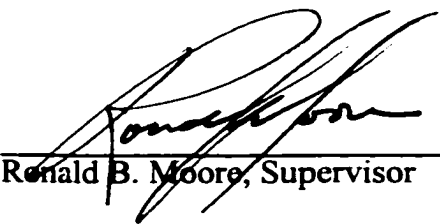
_____
Ronald B. Moore, Supervisor
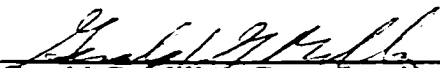
_____
Gerald G. Miller, Co-supervisor
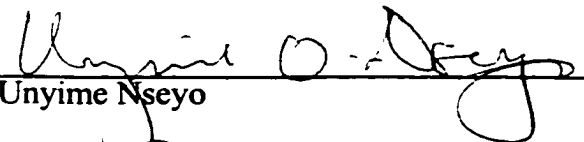
_____
Unyime Nseyo

_____
Theresa M. Allen
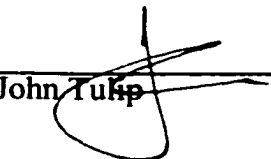
_____
John Tulip

_____
David Rayner

Date _____

DEDICATION

To My Family

And

My Supervisors

ABSTRACT

Photodynamic therapy (PDT) requires three components for cytotoxicity: a photosensitizer, light, and oxygen. To selectively destroy cancer, a photosensitizer needs to be accumulated in tumor and to be locally activated by light to elicit a series of photochemical reactions. Photofrin® is the only approved photosensitizer for clinical use. To avoid prolonged skin phototoxicity and bladder contracture, the feasibility of intravesical (i.b.) administration of Photofrin for whole bladder PDT was investigated in an orthotopic rat bladder tumor model. Second-generation photosensitizers with short elimination half-life or better tumor selectivity were examined for their photoefficiency and toxicity.

To establish an orthotopic rat bladder tumor model, tumor cells from the rat transitional cell carcinoma cell line AY-27, were instilled into rat bladders. Tumor growth was assessed by magnetic resonance imaging. Tumor take was close to 100%, the majority of tumors were superficial by 16 days. Rats bearing bladder tumors were treated with i.b. or i.v. Photofrin or 5-aminolevulinic acid (ALA). The biodistribution times for ALA were 2, 4, or 6 h, and for Photofrin, 4 h. The porphyrin fluorescence intensities, representative of photosensitizer levels within tumor, bladder wall and abdominal muscle were semi-quantitated by confocal microscopy. While both i.v. and i.b. drug administrations reached comparable tumor photosensitization, porphyrin fluorescence was detected only within tumor and urothelium after bladder instillation, sparing the bladder muscle.

Studies of whole bladder PDT of superficial bladder cancers demonstrated that i.b. instillation of Photofrin was as effective as i.v. injection, but with much less toxicity to the bladder and other organs. ALA-mediated PDT exerted similar tumor destruction to Photofrin after i.b. instillation. Interstitial PDT with multiple optical fibers in tumor broadens the application of PDT from superficial to solid tumors. Small, subcutaneous rat prostate and bladder tumors could be completely eliminated after ALA injection and 3000 J irradiation. Intraspheroid distribution, clonogenic assays, and photobleaching studies suggest that hypocrellins are promising second generation photosensitizers.

The orthotopic rat bladder tumor model is an ideal model system for pre-clinical evaluation of new treatments for bladder cancer. Intravesical instillation is an effective and safe route of drug administration for whole bladder PDT.

ACKNOWLEDGMENT

Without the contributions of many people who shared their time and expertise, this thesis project were not accomplished. I would especially like to thank Dr. R. B. Moore, my supervisor, for the opportunity to train in the Departments of Experimental Surgery and Oncology. His steadfast pursuit of excellence in research and its application to clinical medicine had inspired this project. Special thanks to Dr. G. G. Miller, my co-supervisor, for his help in shaping my study and English writing. His constant support made it possible for my thesis to be finished in time.

I would also like to thank Dr. J. Tulip, Mr. Dwayne Dickey, for providing their expertise in lasers, optics and photodosimetry.

I am especially grateful to Dr. T. M. Allen, Mr. C. B. Hansen, who provided their expert opinion in liposomal formulation of photosensitizers.

Dr. Judith Hugh and her staff in the Department of Pathology generously provided their expertise and time. Special thanks are extended to: Jan Spivak-Steele and Richard Linford who did histological sectioning and staining, Laith Dabbagh who did immuno-cytology, for this project.

Special thanks to Dr. David Rayner in the Department of Pathology, University of Alberta Hospitals, who provided his expert opinion in immunocytochemical study of the bladder tumor model.

I thank K. M. Brown, our former technologist, Dr. T. J. McCallum, Dr. R. kilani and Dr. Ian Parney who provided much appreciated assistance with various technical aspects of the project.

Dr. S. B. Halls, Irene I. Piva, RTR.CMR, and Doris Jeske, RTR.CMR in the Department of Oncologic Imaging provided excellent technical support with MRI imaging for the rats. Their expertise and time are highly appreciated.

I would also like to thank Carrie Moris, Cathy Helps, in the Nuclear Medicine Department generously provided their time, expertise and equipment to allow the imaging of the rats.

TABLE OF CONTENTS

LIST OF TABLES

LIST OF FIGURES

Figure 1.3   (B) Staining with anti-cytokeratin 13 shows that only basal and intermediate cells (arrows) of normal urothelium are weakly positive (light brown), while tumor cells (*) are negative. Bar = 100 μm.

Figure 1.4   Fas and FasL expression on AY-27 TCC cells. Cells were incubated first with either anti-Fas (A), anti-FasL (B), or isotype-matched mouse IgG (control), then with goat anti-mouse-Ig-FITC. Samples were read on FL 1 parameter using a flow cytometer. The fluorescence distribution profiles are not significantly different among control (I) and treated samples (II).

Figure 2.1   Mean PpIX fluorescence levels (± SEM) in flank tumor and normal bladder wall 2 h after various doses of ALA i.v. injection. Each value represents the mean of 30 measurements. Single asterisks represent statistically significant ($p < 0.01$) values when compared with the flank tumor at the 1000 mg/kg dose. Double asterisks represent statistical values of $p < 0.05$ with respect to the same tumor reference. (a.u. = arbitrary fluorescence units).

Figure 2.2   Mean PpIX fluorescence levels (± SEM) in flank tumor and normal bladder wall 4 h after various doses of ALA i.v. injection. Each value represents the mean of 30 measurements. * Significantly different ($p < 0.01$) from flank tumor PpIX level in the 1000 mg/kg group. (a.u. = arbitrary fluorescence units).

Figure 2.3   Mean PpIX fluorescence levels (± SEM) in flank tumor and normal bladder wall 6 h after various doses of ALA i.v. injection. Each value represents the mean of 30 measurements. (* $p < 0.01$, ** $p < 0.05$, compared with the flank tumor in 1000 mg/kg dose), (a.u. = arbitrary fluorescence units).

Figure 2.4   Confocal images of , (a) normal bladder wall with background fluorescence (no drug); (b) bladder papilloma sensitized with 25 mM (14 mg/ml) PpIX intravesically for 4 h, showing superficial, focal fluorescence distribution.

Figure 2.5   Confocal images of, (a) flank tumor sensitized with 1000 mg/kg; (b) flank tumor sensitized with 250 mg/kg; (c) normal bladder wall sensitized with 250 mg/kg; and (d) orthotopic bladder papilloma (stage T2) sensitized with 1000 mg/kg of ALA intravenously for 4 h. (Bar = 25 μm).

Figure 2.6   Mean PpIX fluorescence levels (± SEM) in orthotopic bladder tumors and normal bladder wall 4 h after various doses of ALA i.v. injection. Each value represents the mean of 30 measurements. (* $p < 0.01$, ** $p < 0.05$, compared with the papilloma level in 1000 mg/kg dose), (a.u. = arbitrary fluorescence units).

Figure 2.7   Mean PpIX fluorescence levels (± SEM) in orthotopic bladder tumors and normal bladder wall 2 h after various doses of ALA i.b. instillation. Each value represents the mean of 30 measurements. (* $p < 0.01$, compared with papilloma in 600 mM dose), (a.u. = arbitrary fluorescence units).

Figure 2.8   Mean PpIX fluorescence levels (± SEM) in orthotopic bladder tumors and normal bladder wall 4 h after various doses of ALA i.b. instillation. Each value represents the mean of 30 measurements. * Significantly different ($p < 0.01$) from papilloma PpIX level in 600 mM group. The muscularis and submucosa within the 400 mM ALA dose group also had significantly less PpIX fluorescence than the bladder papilloma ($p < 0.01$ and 0.05), respectively), (a.u. = arbitrary fluorescence units).

Figure 2.9   Mean PpIX fluorescence levels (± SEM) in orthotopic bladder tumors and normal bladder wall 6 h after various doses of ALA i.b. instillation. Each value represents the mean of 30 measurements. * Significantly different ($p < 0.01$) from papilloma PpIX level in 600 mM group. (a.u. = arbitrary fluorescence units).

Figure 2.10   Confocal images of, (a) bladder papilloma sensitized with 100 mM ALA; (b & c) bladder papilloma and carcinoma *in situ* sensitized with 600 mM ALA; and (d) bladder papilloma sensitized with 2 mg/ml Photofrin; intravesically for 4 h.

Figure 2.11   Mean porphyrin levels (± SEM) in orthotopic bladder tumors and normal bladder wall 4 h after various doses of PII i.b. instillation or i.v. injection of 5 mg/kg PII. Each value represents the mean of 30 measurements. * Significantly different ($p < 0.01$) from papilloma porphyrin level in 2 mg/ml i.b. group. (a.u. = arbitrary fluorescence units).

Figure 3.1   Schematic biosynthetic pathway of heme. The first intermediate is 5-aminolevulinic acid , which is formed by the condensation of glycine and succinyl CoA. This rate-limiting step can be bypassed by administration of exogenous ALA at high concentrations. Therefore, protoporphyrin IX, which is the potential photosensitizer, is synthesized

and accumulated in cells. Reactions above the dotted line take place in the mitochondria. Others take place in the cytosol.

Figure 3.2   The schematic of in vitro measurement of light distribution.

Figure 3.3   Setup of whole bladder PDT of rats bearing orthotopic bladder tumors. (A) The bladder was catheterized and filled with 0.5 ml of 1% intralipid, and the laser output at the fiber tip was checked before and after each session. (B) The fiber was inserted into the bladder *per urethra* and positioned in the center of the bladder.

Figure 3.4   (A) Histology of untreated rat bladder wall showing mucosa, submucosa, and muscularis. There are some mononuclear cells scattering in the well-vescularized thin submucosal layer. (B) 14 days after bladder tumor was treated with 100 J/cm^2 light only, no evident histologic change in tumor and submucosa (x 125, H&E stain).

Figure 3.5   Untreated bladder wall showing scanty collagen fibrils (blue) in submucosa and serosa, especially surrounding small blood vessels. (x 125, Masson Trichrome stain).

Figure 3.6   Bladder section showing total denudation of the urothelium (arrows), extensive intramural hemorrhage and tissue necrosis except the serosa of the bladder, 3 days after PDT with Photofrin 5 mg/kg, i.v. and light dose of 100 I/cm^2 (x 125, H&E stain).

Figure 3.7   Bladder section showing total denudation of the urothelium (arrows), blood vessel dilatation with congestion in the edematous submucosa and muscular layers, which were also infiltrated with inflammatory cells, 5 days after PDT with Photofrin 5 mg/kg, i.v. and light dose of 50 J/cm^2 (x 125, H&E stain).

Figure 3.8   Dynamic scintigrams of a rat during continuous filling cysto-metrography show the bladder (b) and kidneys (k) after 0.8 mL of ^{99m}Tc-saline is infused into the bladder pre-implantation of tumor cells (A); and (B) a shrunken bladder (b) with left side vesico-ureteric reflux and hydroureteronephrosis in the same rat 30 days after whole bladder PDT with Photofrin injection and 50J/cm² irradiation. Insets are magnifications of images A-15 and B-15. 'c' denotes the cannula in the urethra; 'u' denotes the ureter.

Figure 3.9   Bladder section showing slight increase in collagen fibrils in the bladder wall with small blood vessel proliferation in the submucosa 67

days after PDT with Photofrin 5 mg/kg, i.v. and light dose of 50 J/cm^2 (x 125, Masson Trichrome stain).

Figure 3.10 Bladder section showing moderate increase in collagen fibrils in the bladder wall with small blood vessel proliferation in the submucosa 67 days after PDT with Photofrin 5 mg/kg, i.v. and light dose of 100 J/cm^2 (x 125, Masson Trichrome stain).

Figure 3.11 Histology of bladder wall showing patchy urothelium sloughing (right upper corner with areas of undamaged CIS (right lower corner), 12 days after PDT with Photofrin 2 mg/ml, i.b. and light dose of 50 J/cm^2. There are many mononuclear cells infiltrating the bladder wall (x 125, Masson Trichrome stain).

Figure 3.12 Histology of bladder wall 67 days after PDT with ALA 300 mM, i.b. and a light dose of 75 J/cm^2 showing apparently normal bladder architecture without abnormal collagen fibril deposition (x 125, Masson Trichrome stain).

Figure 3.13 Kaplan-Meier probability of survival for Fischer rats implanted with AY-27 TCC cells and treated with whole bladder PDT at 14 days post-implantation.

Figure 3.14 Bladder pressure as a function of filled bladder volume in rats prior to, 30 days and 60 days after whole bladder PDT. The bladders were constantly filled with ^{99m}Tc-saline at infusion rate of 0.1 ml/mim. The bladder pressure was measured simultaneously.

Figure 4.1 Experimental setup of interstitial laser therapy of subcutaneous rat AY-27 and R3327-H frank tumors. The argon-pumped dye laser (λ= 630 nm) was split and coupled to optic fibers which were inserted into the tumor through a template.

Figure 4.2 Relative mean PpIX fluorescence intensity in s.c. rat R3327-H prostate tumor after i.v. injection of ALA. Each value represents the mean of 30 measurements.

Figure 4.3 Effect of total light dose in PDT of the AY-27 tumors growing s.c. in flanks of Fischer rats. Points, % pre-treatment tumor volume from 3 rats in each group.

Figure 5.12 Intraspheroid drug distribution and intensity profile in the central section of a spheroid incubated with PpIX 10 μM for 4 h.

Figure 5.13 Intraspheroid drug distribution and intensity profile in the central section of a spheroid incubated with Stealth liposomal HBEA-R1/R2 10 μM for 2 h.

Figure 5.14 Intraspheroid drug distribution and intensity profile in the central section of a spheroid incubated with Stealth liposomal HBBA-R2 10 μM for 2 h.

Figure 5.15 Intraspheroid drug distribution and intensity profile in the central section of a spheroid incubated with classic liposomal HBBA-R2 10 μM for 4 h.

Figure 5.16 Intraspheroid drug distribution and intensity profile in the central section of a spheroid incubated with Stealth liposomal HBBA-R2 10 μM for 4 h.

Figure 5.17 Intraspheroid drug distribution and intensity profile in the central section of a spheroid incubated with specific SIL-HBBA-R2 10 μM for 2 h.

Figure 5.18 Intraspheroid drug distribution and intensity profile in the central section of a spheroid incubated with non-specific SIL-HBBA-R2 10 μM for 2 h.

Figure 5.19 Intraspheroid drug distribution and intensity profile in the central section of a spheroid incubated with ALA 1 mM for 4 h.

Figure 5.20 Intraspheroid drug distribution and intensity profile in the central section of a spheroid incubated only with serum-free medium (no drug) for 4 h.

Figure 6.1 Phototoxicity of different drugs to AY-27 monolayer cells by clonogenic assay. The argon-pumped dye laser was tuned to 630 nm and 150 mW of output power except for illumination of AlPC (690 nm and 150 – 200 mW). The surviving fraction is the % control. 1 μM HBER-R1 = 0.6 μg/ml, 1 μM HBBA-R2 = 0.63 μg/ml.

Figure 6.2 Effect of wavelength on PpIX photobleaching. PpIX was first dissolved in DMSO, then diluted with PBS to a final concentration of 100 ng/ml, and illuminated with light of different wavelength.

ABBREVIATIONS

a.u.	arbitrary units
ALA	5-aminolevulinic acid
AlPC	Aluminum phthalocyanine chloride
ANOVA	analysis of variance
AY-27	a rat bladder tumor cell line
BCG	Bacillus Calmette-Guérin
C*IS*	carcinoma *in situ*
CL	classic liposome
CLSM	confocal laser scanning microscopy
DAB	diaminobenzidine
DMSO	dimethyl sulfoxide
DPPC	dipalmitoyphosphatidylcholine
DPPG	dipalmitoyphosphatidylglycerol
DSPC	distearolphosphatidylcholine
DSPE	distearolphosphatidylethanolamine
EDTA	ethylenediaminetetraacetic acid
EMT6/Ed	experimental mammary tumor cell line
FANFT	*N*-[4-(5-nitro-2-furyl)-2-thiazolyl]formamide
FasL	Fas-ligand
gp	glycoprotein
H&E	hematoxylin-eosin
HB	Hypocrellin B
HBBA	n-butylaminated HB
HBEA	ethanolaminated HB
HBSS	Hank's Balanced Salts Solution
HMPAO	hexamethylpropyleneamine oxime
HpD	hematoporphyrin derivative
i.b.	intravesical
i.p.	intraperitoneal
i.v.	intravenous
IF	immunofluorescence
ILS	increased life span compared with control
J	Joules
KeV	kiloelectron volts
laser	light amplified by stimulated emission radiation
LDL	low density lipoprotein
LTS	long-term survivor
M.T.	Masson Trichrome
mAb	monoclonal antibody
MBq	megabecquerel
MBT-2	a murine bladder tumor cell line

MGH-U3	a human bladder TCC cell line
mL	milliliter
mM	millimolar
μM	micromolar
MNU	N-methyl-N-nitrosourea
M_r	molecular weight
MRI	magnetic resonance imaging
MST	mean survival time
mW	milliwatts
N/C	nuclear-to-cytoplasmic
nm	nanometer
nSIL	Stealth® immunoliposome with non-specific mAb
$^1O_2$	singlet oxygen
PBS	phosphate-buffered saline
PDT	photodynamic therapy
PEG2000	polyethylene glycol, (Mr 2000)
PII or PF	Photofrin
PpIX	protoporphyrin-IX
R3327-H	a well-differentiated rat prostate cancer cell line
ROI	region of interest
s.c.	subcutaneous
SEM	scanning electron microscopy
SIL	Stealth® immunoliposome
SL	sterically stabilized liposome or Stealth® liposome
sSIL	Stealth® immunoliposome with specific mAb
STIR	Short-T1 Inversion Recovery Sequence in MRI
T1	clinical stage 1
Ta	clinical stage A
^{99m}Tc	^{99}Technetium
TCC	transitional cell carcinoma
TFS	tumor-free survivor
TUR	transurethral resection
v/v	volume/volume

INTRODUCTION

Photodynamic therapy (PDT) is a novel approach in the treatment for cancer which has great potential as a primary therapeutic modality for superficial lesions as well as for prophylaxis of bladder cancer.[1,2,3] The principle of PDT involves exposing a photosensitizing drug (a photosensitizer) to specific wavelengths of light in the presence of oxygen. Cytotoxicity is attributed to the generation of active chemical species such as singlet oxygen ($^1O_2$) and/or free radicals resulting from an energy transfer reaction between the photoactivated triplet photosensitizer and tissue oxygen.[4] The therapeutic efficacy of PDT using a systemically administrated hematoporphyrin derivative (HpD) or the active fraction of HpD (Photofrin®) has been demonstrated in numerous animal models[4] and in clinical trials.[1,2,3] The drawbacks of systemically administrated Photofrin are: 1) Photofrin-PDT is accompanied with a generalized skin photosensitivity that can last for 4 to 8 weeks; 2) The 630 nm light which is used to activate Photofrin has limited tissue penetration; 3) Since the drug is a mixture of porphyrins, it has a complicate pharmacokinetics; and 4) for whole bladder PDT, the main drawback has been contracted bladders.[5,6] To avoid these problems, second generation photosensitizers with short elimination half-lives or better tumor selectivity have been investigated,[7,8] and local photosensitizer administration via topical or intravesical routes has been advocated.[9,10]

While the basic concept of PDT dates from 1903, when von Tappeiner and Jesionek[11] applied eosin to the lesions of skin cancer patients and exposed them to sunlight, the modern era of PDT treatment of cancer did not occur until 1972, when Dougherty et al.[12,13] at Roswell Park Cancer Institute started the first major studies of PDT in animal tumors using Lipson's hematoporphyrin derivative, a mixture of porphyrins.[14] Dougherty and associates showed that some of the components of HpD were not photoactive, and separated the active components which were eventually termed Photofrin (Porfimer Sodium).[15] In 1976, Kelly and Snell[16] treated one patient with bladder cancer transurethrally using HpD and white light. However, this was not followed up with additional patients in the following several years, probably due to

1

lack of sophisticated laser and laser delivery systems at that time. Therefore PDT was largely applied to skin lesions since other light sources could also be used for skin cancer PDT. With the development of suitable lasers and optical light delivery systems, the interests of PDT treatment for bladder cancer, as well as diseases in other hollow organs re-surged during the 1980's. More than 10,000 cancer patients, including bladder cancer, were treated with Photofrin-based PDT from 1981 to 1989.[17]

Photofrin is a mixture of porphyrins with the chemical structure of di-, tri-, or tetra-hematoporphyrin ethers or esters. Photofrin uptake may be mediated in part *via* an active transport mechanism, as several studies have shown that the distribution of the different circulating porphyrin structures determines their localization in the tissue.[18,19] Porphyrin esters circulate bound to lipoproteins; unbound aggregated components (*e.g.* micelle-like structures from porphyrin oligomers) are easily available for uptake in macrophages and endothelial or neoplastic cells; hematoporphyrin and other monomeric components form low affinity bonds with albumin and globulins. In malignant tissues, those sensitizers bound with albumin and globulins are mainly released to the extracellular matrix, and the lipoprotein-bound oligomers and porphyrin esters are endocytosed by a lower-density lipoprotein (LDL) receptor-mediated process in the neoplastic cells, released in the cytoplasm and bound to apolar endocellular matrices.[20,21,22] Peak tissue Photofrin levels are reached in rodents between 4 and 10 hours after intravenous (i.v.) injection. However, PDT usually is started 24 – 48 hours following administration, since the photosensitizer might be retained in tumor tissue for a longer period of time than in the surrounding normal tissue. Therefore phototoxicity to normal tissue might be minimized. Although the serum half-life is about 25 hours in humans, the photosensitizer will be present in the skin at a photosensitizing level for at least 6 weeks.

Porphyrins (HpD, Photofrin) have an intense absorption in the blue region of the spectrum around 400 nm (Soret band) and four additional absorption bands (with decreasing intensity) between 500 nm and 650 nm. As the penetration of light in

2

tissue increases with higher wavelengths, the weakest absorption band of 630 nm is normally used for illumination of Photofrin sensitized tissue.[23] The maximum depth of necrosis in tumor tissue is typically no more than 5 mm when the 630 nm band is used.[24] For this reason, Photofrin-based PDT is best for small or superficial tumors, e.g. tumors of skin, bladder, bronchus, or esophagus, although larger tumors, e.g. prostate carcinoma may be treated by inserting multiple optical fibers into the tumor.[24,25]

The main target of Photofrin-based PDT toxicity is still uncertain due to the efficient interaction of toxic substrates with many cellular sites. *In vitro* photobiology studies have documented that these sites include many biomolecules and subcellular organelles such as microsomes, mitochondria, and to a lesser extent the nucleus.[24,26] There is evidence that the cellular membranes are important targets for damage.[27,28,29] Unsaturated fatty acids can be photooxidized, and lipid peroxidation as well as membrane protein crosslinking have been found following PDT. This damage can lead to increased membrane permeability and inhibited transport of amino acids, nucleosides and sugars.[30] As mitochondria are major sites for porphyrin localization, these organelles are thought to be important targets for PDT.[31,32] Porphyrin photosensitization can also induce DNA single-strand breaks, alkali-labile lesions or sister chromatin exchange.[33,34] However, nuclear damage or repair are probably not of primary importance in photodynamic destruction, since PDT has been shown to induce similar levels of cytotoxicity in normal human fibroblasts and in DNA repair-deficient fibroblasts.[35]

Although *in vitro* studies have shown direct tumor cell killing, it has been suggested that the microvasculature is a primary target of Photofrin-PDT *in vivo*.[24,31,36] Tumor cells showed much higher viability when removed from tumor immediately after PDT than those removed 24 hours after PDT.[24,31] Fingar and Henderson[37] have studied the important effects of vascular injury using the rat cremaster muscle as a model. They showed that the earliest event following PDT is damage to the endothelial cell, which contracts, allowing exposure of the endothelial basement

3

membrane with consequent thrombosis. Serum levels of thromboxane and leukotriene B_4 increase following PDT. Other vasoactive eicosanoids are released, causing vessel constriction and changes in macromolecular permeability. Finally, platelet aggregation and vascular constriction lead to vascular stasis, and eventual vessel degeneration and hemorrhage with resultant tissue starvation and oxygen deprivation.

Photofrin is not an ideal photosensitizer because of weak absorption in the therapeutically useful wavelength, poor chemical characterization, and poor tumor selectivity with prolonged skin phototoxicity. And when applied clinically these properties have contributed to bladder volume reduction resulting from muscular fibrosis following whole bladder PDT.[5,6] These limitations might be partly overcome by second generation photosensitizers such as phthalocyanines,[38] chlorins,[39] bacteriochlorins,[40] benzoporphyrin derivatives,[41] hypocrellins,[8] and protoporphyrin IX endogenously produced from exogenous 5-aminolevulinic acid (ALA).[10] Furthermore, tumor selectivity may be enhanced by topical administration of photosensitizers and the systemic side effects avoided.[9,10]

Kennedy et al. introduced a novel approach which appears to combine short sensitizer half-life, the absence of prolonged skin photosensitivity and topical applicability.[42] Selective destruction of skin cancers was achieved utilizing the topically applied prodrug 5-aminolevulinic acid.[42,43] ALA is the first intermediate of the heme synthesis pathway,[44] the second last step of which is the production of protoporphyrin IX (PpIX), a potent photosensitizer. Under normal conditions the synthesis of heme is controlled by a feedback mechanism in which the presence of free heme inhibits the synthesis of ALA from glycine and succinyl CoA in mitochondria. However, an excess of exogenous ALA overcomes this negative feedback control mechanism and results in transient intracellular accumulation of PpIX. Some malignant cells may produce more porphyrins than their slower growing normal counterparts, leading to an increased accumulation of PpIX in tumor cells. The concept of using ALA as a prodrug for photosensitization was based on a

4

disorder called human porphyria. The skin of patients with porphyria is highly sensitive to sunlight due to abnormally high levels of ALA-induced porphyrins in the circulation.[45] Subsequent studies in rodents showed that after systemic ALA administration, selective accumulation of porphyrins (predominantly PpIX, with small amounts of coproporphyrin) was found in surface-lining tissues such as epidermis, mucosae of bladder and gastrointestinal tract, endometrium *etc.*, but not in underlying muscle layers.[43,46,47,48] Relatively selective porphyrin accumulation in tumor has also been reported.[49] With ALA administered intravesically to rat bladder, PpIX is preferentially accumulated in mucosa, and to a much lesser extent in submucosa and muscularis.[47,50] ALA-induced PpIX is rapidly eliminated from the body when ALA is given systemically, therefore, the risk of skin photosensitivity is limited to 24 hours.[43,51] Preliminary clinical results of whole bladder PDT after intravesical ALA instillation did not show any sign of bladder contracture.[10]

However, much of the experimental work on the distribution of ALA-induced PpIX and PDT was conducted in animals free of tumor or in tumors transplanted subcutaneously in rodents and compared with the adjacent skin and muscle.[46,47,48,50,52] What is important clinically for whole bladder PDT is the differential retention of PpIX and phototoxicity between the orthotopic bladder tumor and adjacent tissue, especially bladder muscle. Furthermore, the efficacy of ALA-based PDT for superficial bladder cancer after i.b. administration and for solid tumors after injection, and the mechanism(s) of action remain undefined.

Other promising second generation photosensitizers are phthalocyanines, hypocrellins, and benzoporphyrin derivatives. These sensitizers have simple molecular characteristics, strong absorption bands of light greater than 650 nm, are cleared from normal tissues within a few hours to days, and have high yields of singlet oxygen.[8,38,41,48] Therefore, they might be applied in treatment of solid tumors, and prolonged skin photosensitivity should not be a problem. However, none of these newer photosensitizers have shown a propensity for selective retention in tumor over

5

normal tissue after injection. More pre-clinical studies are needed for these sensitizers to be applied clinically.

To increase the selectivity of photosensitizer accumulation in tumor, the use of photosensitizers associated with different types of delivery vehicles has received strong interest within the field of PDT.[53,54] Most potent photosensitizers are highly lipophilic. Lipid-based delivery vehicles, such as liposomes and oil emulsions, allow the administration of these water-insoluble photosensitizers, increasing the choice of photosensitizers potentially useful for treating tumors. In some cases, these delivery vehicles increase the selectivity of tumor targeting by favoring photosensitizer uptake in tumor tissue. However, a higher selectivity of tumor targeting could be obtained through the association of photosensitizers with monoclonal antibodies, which can interact specifically with tumor cells. Monoclonal antibody-coupled photosensitizers have been tested mainly *in vitro*, and have shown a high selectivity towards cells expressing specific antigens.[54,55] Only a limited number of reports are available on the biodistribution of immunoconjugated photosensitizers and on their selectivity *in vivo*,[56,57] so that their importance for the selectivity of tumor targeting, especially for solid tumors, has not yet been defined. More systematic pharmacokinetic studies are required in order to assess the precise role of delivery vehicles in tumor targeting of photosensitizers, since the latter can be affected by the nature of the photosensitizer (hydrophilicity/ lipophilicity), the characteristic of the tumor (degree of vascularization) and probably many other factors.

Bladder cancer is the fourth most common cancer in men and the eighth most common cancer among women.[58] Transitional cell carcinoma (TCC) comprises approximately 90% of all malignant tumors primary to the urinary bladder. At least 70% of patients with TCC are diagnosed with superficial tumors (*i.e.* Ta, T1, and carcinoma *in situ* [CIS]) at their initial presentation.[59] Up to 80% of superficial tumors cause a management problem with local recurrences. The risk for recurrence or progression is related to multiplicity of tumor, and the best predictors of tumor progression include tumor grade, stage, status of blood group-antigen expression,

6

DNA ploidy, associated mucosal abnormalities and C/S. Carcinoma *in situ* of the bladder is a pathobiological enigma that continues to challenge pathologists and urologists. The clinical course is highly variable and unpredictable, creating a management dilemma for urologists. Formerly, the grave prognosis of C/S led to the recommendation of radical cystectomy as the treatment of choice for all patients with confirmed C/S. Current results with intravesical therapy, particularly Bacillus Calmette-Guérin vaccine (BCG) immunotherapy, as well as whole bladder photodynamic therapy, have improved to the point that it is now inappropriate to recommend cystectomy as the initial treatment of choice for patients with C/S.[60]

The bladder seems ideally suited to PDT as it is readily accessible and the entire bladder mucosa can be treated as a whole. PDT is considered to be able to eradicate most, if not all, superficial bladder cancer lesions extending into the mucosa or submucosal regions (<1 mm). However, C/S remains the best indication for whole bladder PDT. At present, whole bladder PDT is not indicated for patients who have bladder cancer with any stage greater than T1 or size greater than 2 cm in diameter. Ablation of superficial bladder papillary tumors has been attempted using front surface illumination with either a cleaved fiber or a microlens, and has been followed in some cases by whole bladder PDT using a spherical diffuser-tipped fiber optic in order to ablate micropapillary and remaining carcinoma *in situ* or severely dysplastic lesions. Typical Photofrin doses are between 2 – 5 mg/kg body weight.[2,3,6,17,61] Although Photofrin has proved to be an effective photosensitizer, the major reported dose-dependent morbidity in bladder cancer PDT was sterile cystitis characterized by irritative symptoms of urinary frequency, urgency and dysuria which occurred in 100% of patients. This so-called post-PDT syndrome may vary in duration from a few days to several weeks. Bladder contracture is another serious complication following Photofrin-PDT. Nseyo *et al.*[62] reported severe side effects in all of an initial series of 6 patients undergoing whole bladder PDT. Two patients had such a marked reduction in bladder capacity with incontinence, that they required a cystectomy for these PDT-induced symptoms alone, although their bladders were

7

found to be clear of tumor. Jocham *et al.*[63] reported a reduction in bladder capacity in some of their patients in excess of 50% and 3 still had a 70% reduction one-year after PDT. Both ureteric reflux and ureteric obstruction were seen in the initial series of Nseyo *et al.*[62] but in general no problems with the upper tracts have been mentioned by other authors until a report by Harty *et al.*[6] in which they studied the side effects after PDT in a series of 7 patients who were given whole bladder treatment. Five patients had a significant reduction in bladder capacity after PDT, which persisted one year in four of them. Deep bladder biopsies showed marked fibrosis in the muscle layer. These four patients also developed persistent bilateral hydronephrosis and grade 4 vesico-ureteric reflux. As mentioned above, cutaneous photosensitivity is not uncommon if Photofrin is given systemically.

With so many serious problems it is perhaps surprising that anyone is still trying to use PDT in the bladder. Several of the clinical pioneers did decide to stop clinical work and go back to the laboratory to solve the problems. The most likely solution lies in newer photosensitizers. Other ways of administering photosensitizers have been recommended. However, i.b. administration of Photofrin for treatment of bladder cancer has not been systematically studied.

Prostate cancer is the most common malignancy in men.[64] But the management for this slow-growing carcinoma is still controversial. Radical prostatectomy and radiotherapy have been used as potentially curative forms of treatment for localized prostate adenocarcinoma (stages T1–T3). However, since the majority of patients with prostate cancer are diagnosed at 70 years or older, not every patient can tolerate radical prostatectomy, and complications from both surgery and radiotherapy are not uncommon.[65] Interstitial PDT, which may produce selective tumor destruction by inserting the optical fiber(s) into the tumor, should be another option as a treatment modality for localized prostate cancer.[25,66] However, due to the high attenuation of light in tissue, multiple interstitially placed optical fibers are needed to deliver light for treatment of clinically significant volumes of solid tumors.[66,67]

8

Based upon the above background, this thesis project sought to:

1. Investigate *in vitro* phototoxicity of Photofrin and several second generation photosensitizers to bladder cancer cells using clonogenic assays. These studies may provide fundamental data to *in vivo* photodynamic therapy for these malignancies.

2. Establish and characterize a transplantable orthotopic rat bladder TCC tumor model.   a). Many of the previous studies on photosensitizer biodistribution and PDT were done in normal animal bladders (free of tumor) or in heterotopic tumor models (tumor implanted subcutaneously). Although these studies are important, an orthotopic bladder tumor model (tumor growing in the bladder lumen) is more appropriate for studies of phototoxicity and efficacy regarding tumor biology, histology, and surrounding normal bladder muscle.   b). Carcinogen-induced primary rat bladder tumor models require several months to transform and it is also difficult to predict tumor stages (PDT is recommended to treat superficial bladder cancer at present). Therefore a transplantable bladder tumor model may be a more feasible model system for whole bladder PDT. c). Due to the small size of the bladder and urethra, the mouse model is not suitable for studying whole bladder PDT. The rat bladder and urethral caliber however, are large enough to introduce the drug and optical fiber into the bladder *per urethra*. Our work provided the first transplantable orthotopic superficial rat bladder tumor model.

3. Study the biodistribution of Photofrin and ALA-induced PpIX in both orthotopic and heterotopic rat bladder tumor models, as well as in the heterotopic rat prostate cancer model, after i.v. injection or i.b. instillation of Photofrin or ALA. Using confocal laser scanning microscopy (CLSM), the fluorescence of photosensitizers in tumor and different tissue layers of the bladder can be detected and analyzed. These studies provide essential parameters for optimal PDT in different model systems. These parameters

9

include the feasibility of systemic and intravesical routes of administration of sensitizers; the time interval between administration of sensitizer and light application; the optimal doses of sensitizers; and the differential accumulation and distribution of sensitizers in tumor and normal tissues in both orthotopic and heterotopic models.

4. Explore the photoefficiency and phototoxicity of whole bladder PDT for superficial rat bladder cancer after i.v. injection or i.b. instillation of Photofrin or ALA in the orthotopic model. These pre-clinical investigations may shed light to further clinical PDT of the analogous human lesions.

5. Investigate interstitial PDT in the heterotopic bladder tumor and prostate cancer by inserting multiple optical fibers into the tumor after i.v. injection of ALA. Due to high attenuation of light in tissue, PDT is applied largely to the treatment of superficial tumors. Interstitial PDT might overcome this limitation, and make it possible for PDT to treat solid tumors.

6. Finally, evaluate the penetration and intratumor distribution of photosensitizers (Photofrin and several second generation sensitizers) in an *in vitro* tumor model system (multicellular spheroids) using CLSM. These data are useful for selecting the suitable sensitizer(s) and drug delivery strategies for bladder instillation in both PDT and photo-detection of bladder cancer.

0.1 References:

1. Jocham, D., Baumgartner, R., Stepp, H., and Unsold, E. (1990) Clinical experience with the integral photodynamic therapy of bladder carcinoma. *J. Photochem. Photobiol.*, B: Biology, **6:** 183.

2. Nseyo, U.O., Dougtherty, T.J., and Sullivan, L.(1987) Photodynamic therapy in the management of resistant lower urinary tract carcinoma. *Cancer* **60:** 3113.

3. Prout, G.R., Lin, C.W., Benson, R., Nseyo, U.O., Dale, J.J., Griffin, P.P., Kinsey, J., Tian, M.E., Lao, Y.H., Mian, Y.Z., Chen, X., Ren, F.M. and Qiao, S.J. (1987) Photodynamic therapy with hematoporphyrin derivative in the treatment of superficial transitional cell carcinoma of the bladder. *N. Engl. J. Med.*, **317**: 1251.

4. Henderson, B.W. and Dougtherty, T.J. (1992) How does photodynamic therapy work? *Photochem. Photobiol.*, **55**: 145-157.

5. Dougherty, T.J., Cooper, M.T. and Mang, T.S. (1990) Cutaneous phototoxic occurrences in patients receiving Photofrin. *Lasers Surg. Med.*, **10**: 485-488.

6. Harty, J.I., Amin, M., Wieman, T.J., Tseng, M.T., Ackerman, D. and Broghamer, W. (1989) Complications of whole bladder dihematoporphyrin ether photodynamic therapy. *J. Urol.*, **141**: 1341-1346.

7. Roberts, W.G., Smith, K.M., McCullough, J.L. and Berns, M.W. (1989) Skin photosensitivity and photodestruction of several potential photodynamic sensitizers. *Photochem. Photobiol.*, **49**: 431-438.

8. Miller, G.G., Brown, K., Ballangrud, A.M., Barajas, O., Xiao, Z., Tulip, J., Lown, J.W., Leithoff, J. M., Allalunis-Turner, M.J., Mehta, R.D. and Moore, R.B. (1997) Preclinical Assessment of Hypocrellin B and Hypocrellin B Derivatives as Sensitizers for Photodynamic Therapy of Cancer: Progress Update. *Photochem. Photobiol.*, **65(4)**: 714-722.

9. Santoro, O., Bandieramonte, G., Melloni, E., Maechesini, R., Zunino, F., Lepera, P. and DePalo G. (1990) Photodynamic therapy by topical meso-tetraphenylporphyrine-sulfonate tetrasodium salt administration in superficial basal cell carcinoma. *Cancer Res.*, **50**: 4501-4503.

10. Kriegmair, M., Baumgartner, R., Lumper, W., Waidelich, R. and Hofstetter, A. (1996) Early clinical experience with 5-aminolevulinic acid for the photodynamic therapy of superficial bladder cancer. *Br. J. Urol.*, **77**: 667-671.

11. Van Tappeiner, H.V. and Jesionek, A. (1903) Therapeutische Versuche mit fluoreszierenden stoffe. *Muench Med Wochenschr.*, **47**: 2042-2044.

12. Dougherty T.J. (1974) Activated dyes as anti-tumor agents. *J. Natl. Cancer Inst.*, **51**: 1333-1336.

13. Dougherty, T.J., Grindey, G.B., Fiel, R., *et al.* (1975) Photoradiation therapy II: cure of malignant tumors with hematoporphyrin and light. *J. Natl. Cancer Inst.*, **55**: 115-121.

14. Lipson R.L., E.J. Blades, and A.M. Olsen (1961) The use of hematoporphyrin in tumor destruction, *J. Natl. Cancer Inst.*, **26**: 1-11.

15. Dougherty, T.J., Boyle, D.G., Welshaupt, K.R., *et al* (1983) Photoradiation therapy-clinical and drug advances. In: Porphyrin Photosensitization. Eds: D. Kessel and T.J. Dougherty. New York: Plenum Press. PP. 3-15.

16. Kelly, J.F., and Snell, M.E. (1976) Hematoporphyrin derivative: a possible aid in the diagnosis and therapy of carcinoma of the bladder. *J. Urol.*, **115**: 150-151.

17. Nseyo U.O. (1992) Photodynamic therapy. *Urol. Clin. North. Am.*, **19**: 591-599.

18. Jori G. (1989) In vivo transport and pharmacokinetic behavior of tumor photosensitizers. *Ciba Found Symp.*, **146**: 78-94.

19. Korbelik M., & Hung, J. (1991) Cellular delivery and retention of Photofrin II. The effects of interaction with human plasma proteins. *Photochem. Photobiol.*, **53**: 501-510.

20. Jori G. (1987) Photodynamic therapy of solid tumors. *Radiat. Phys. Chem.*, **30**: 375-380.

21. Jori, G., Beltramini, M., Reddi, E., *et al.* (1984) Evidence for a major role of plasma proteins as hematoporphyrin carriers *in vivo*. *Cancer Lett.* **24**: 291-297.

22. Kessel D.(1986) Porphyrin lipoprotein association as a factor in porphyrin localization. *Cancer Lett.*, **33**: 183-188.

23. Gomer, C.J., Doiron, D.R., Rucker, N., *et al.*(1984) Action spectrum (620-640 nm) for hematoporphyrin derivative induced cell killing. *Photochem Photobiol.* **39**: 365-368.

24. Moore R.B. (1991) PDT induced ischemia. Ph.D. thesis. University of Alberta. Edmonton, Canada.

25. Gonzalez, S., Arnfield, M.R., Meeker, B.E., Tulip, J., Lakey, W.H., Chapman, J.D., and McPhee, M.S. (1986) Treatment of Dunning R3327-AT rat prostate tumors with photodynamic therapy in combination with misonidazole. *Cancer Res.* **46**: 2858-2862.

26. Moan, J., Berg, K., Kvan, E., *et al.* (1989) Intracellular localization of photosensitizers. *Ciba Found Symp.* **146**: 95-111.

27. Chapman, J.D., Stobbe, C.C., Arnfield, M.R., *et al.* (1991) Oxygen dependency of tumor cell killing *in vitro* by light-activated Photofin II. *Radiat. Res.* **126**: 73-79.

28. Girotti A.W. (1990) Photodynamic lipid peroxidation in biological systems. *Photochem. Photobiol.* **51**: 499-509.

29. Okunaka T., Eckhauser, M.L., Kato, H., *et al.*(1992) Correlation between photodynamic efficacy of differing porphyrins and membrane partitioning behavior. *Lasers Surg. Med.*, **12**: 98-103.

30. Kessel D. (1986) Sites of photosensitization by derivatives of hematoporphyrin. *Photochem. Photobiol.* **44**: 489-494.

31. Gomer C.J., Ferrario, A., Hauashi, N., *et al.*(1988) Molecular, cellular and tissue responses following photodynamic therapy. *Lasers Surg. Med.*, **8**: 450-463.

32. Salet C., Moreno, G. (1990) Photosensitization of mitochondria: molecular and cellular aspects. *J. Photochem. Photobiol. B.* **5**: 133-150.

33. Jori G., Spikes, J.D. (1984) Photochemistry of porphyrins. In: Smith K.C. editor. *Topics in photomedicine.* New York: Plenum, 183-318.

34. Evensen J.F., Malik, Z., Moan, J. (1988) Ultrastructural changes in the nuclei of human carcinoma cells after photodynamic treatment with hematoporphyrin derivative and with tetrasodium-meso-tetra-(4-sulphonatophenyl) Porphine. *Lasers Med. Sci.*, **3**: 195-206.

35. Gomer, C.J., Rucker, N., Murphee, A.L. (1988) Differential cell photosensitivity following porphyrin photodynamic therapy. *Cancer Res.*, **48**: 4539-4542.

36. Star, W.M., Marijnissen, J.P.A., Van den Berg-Blok, *et al.* (1986) Destruction of rat mammary tumor and normal tissue microcirculation by hematoporphyrin derivative

photoradiation observed in vivo in sandwich observation chambers. *Cancer Res.*, **46**: 2532-2540.

37. Henderson, B.W., Fingar, V.H. (1987) Relationship of tumor hypoxia and response to photodynamic treatment in an experimental mouse tumor. *Cancer Res.* **47**: 3110-3114

38. Ben-Hut, E., Rosenthal, I. (1995) The phthalocyanines: a new class of mammalian cell photosensitizers with a potential for cancer phototherapy. *Int. J. Radiat. Biol.*, **47**: 145-147.

39. Roberts, W.G., Shiau, F.Y., Nelson, J.S. *et al.* (1988) In vivo characterization of monoasparty chlorin e6 and diaspartyl chlorin e6 for photodynamic therapy. *J. Natl. Cancer Inst.*, **80**: 330-336.

40. Beems, E.M., Dubbelman, TMAR., Lugtenburg, J. *et al.* (1987) Photosensitizing properties of bacteriochlorophillin a and bacteriochlorin a, two derivativers of bacteriochlorophyll a. *Photochem. Photobiol.*, **46**: 639-643.

41. Sternberg, E., Dolphin, D. (1993) An overview of second generation drugs for photodynamic therapy including BPD-MA. In Spinelli P, Dal Fante M, Marchesini R, eds. Photodynamic Therapy and Medical Lasers. *Excerpta Medica* 470-474.

42. Kennedy, J.C., Pottier, R.H. and Pross. DC. (1990) Photodynamic therapy with endogenous protoporphyrin IX: basic principles and present clinical experience. *J Photochem. Photobiol. B: biol.*, **6**: 143-148.

43. Kennedy, J.C. and Pottier, R.H. (1992) Endogenous protoporphyrin IX, a clinical useful photosensitizer for photodynamic therapy. *J. Photochem. Photobiol. B: Biol.*, **14**: 275-292

44. Berlin, N.I., Neuberger, A. and Scott, J.J. (1956) The matabolism of δ-aminolevulinic acid, 2. Normal pathways, studied with the aid of ^{14}C. *Biochem. J.*, **64**: 90-100.

45. Bickers, D.R. (1987) The dermatologic manifestations of human porphyria. *Ann. N.Y. Acad. Sci.* **514**: 261-267.

46. Divaris, D.X.C, Kennedy, J.C., Pottier, K.H. (1990) Phototoxic damage to sebaceous glands and hair follicles of mice after systemic administration of 5-aminolevulinic

acid correlates with localized protoporphyrin IX fluorescence. *Am. J. Pathol.* **136**: 891-897.

47. Moore, R.B., Miller, G.G., Brown, K., *et al* (1995) Urothelial conversion of 5-Aminolevulinic acid to protoporphyrin IX following oral or intravesical administration. *SPIE.* 2371: 284-288.

48. Loh, C.S., Bedwell, J., MacRobert, A.J., Krasner, N., Phillips D. and Bown, S.G. (1992) Photodynamic therapy of the normal rat stomach: a comparative study between di-sulphonated aluminum phthalocyanine and 5-aminolevulinic acid. *Br. J. Cancer.* **66**: 453-462.

49. Bedwell, J., Macroert, A.J., Phillips, D. *et al.*(1992) Fluorescence distribution and photodynamic effect of ALA-induced PpIX in the DMH rat colonic tumor model. *Br. J. Cancer*, **65**: 818-824.

50. Chang, S.C., MacRobert, A.J. and Bown, S.G. (1996) Biodistribution of protoporphyrin IX in rat urinary bladder after intravesical instillation of 5-aminolevulinic acid. *J. Urol.*, **155**: 1744-1748.

51. Grant, W.E., Hopper, C., MacRobert, A.J., *et al.* (1993) Photodynamic therapy of oral cancer: photosensitization with systemic aminolevulinic acid. *Lancet.* **342**: 147-148.

52. Hua, Z., Gibson, S.L., Foster, T.H. and Hilf, R. (1995) Effectiveness of δ-aminonevulinic acid-induced protoporphyrin as a photosensitizer for photodynamic therapy *in vivo. Cancer Res.*, **55**: 1723-1731.

53. Reddi E. (1997) Role of delivery vehicle for photosensitizers in the photodynamic therapy of tumors. *J. Photochem. Photobiol. B: Biol.* **37**: 189-195.

54. Miller, G.G. and Lown, J.W. (1997) Immunophotodynamic therapy: current developments and future prospects (review). *Drug Develop. Res.,* **42**: 182-197.

55. Morgan, J., Lottman, H., Abbou, C.C., and Chopin, D.K. (1994) A comparison of direct and liposomal antibody conjugates of sulfonated aluminum phthalocyanines for selective photoimmunotherapy of human bladder carcinoma. *Photochem. Phtobiol.,* **60**: 486-496.

56. Duska, L.R., Hamblin, M.R., Bamberg, M.P. and Hasan, T. (1997) Biodistribution of charged F(ab')2 photoimmunoconjugates in a xenograft model of ovarian cancer. *Br. J. Cancer.* **75**: 837-844.

57. Goff, B.A., Blake, J., Bamberg, M.P. and Hasan, T. (1996) Treatment of ovarian cancer with photodynamic therapy and immunoconjugates in a murine ovarian cancer model. *Br. J. Cancer.* **74**: 1194-1198.

58. Wingo, P.A., Tong. T., Bolden, S. (1995) Cancer statistics. *CA Cancer J Clin.*, 45: 8-30.

59. Bane, B.L., Rao, J.Y. and Hemstreet, G.P. (1996) Pathology and staging of bladder cancer. *Semi. Oncology.* **23**: 546-570.

60. Nseyo, U.O. and Lamm, D.L. (1996) Therapy of superficial bladder cancer. *Semi. Oncology.* **23**: 598-604.

61. Prout, G.R. Jr., Griffin, P., Daly, J.J. (1987) The outcome of conservative treatment of carcinoma in situ of the bladder. *J. Urol.*, **138**: 766-770.

62. Nseyo, U.O, Dougherty, T.J., Boyle, D.G., *et al* (1985) Whole bladder photodynamic therapy for transitional cell carcinoma of the bladder. *Urology.* **26**: 274-280.

63. Jocham, D., Beer, M., Baumgartmer, R., *et al.* (1989) Long-term experience with integral photodynamic therapy of Tis bladder carcinoma. ed. Boek G and Hornett. S. In: Photosensitizing Compounds: their chemistry; biology and clinical use. *Ciba Foundation Symposium* **146**: 190-208. Chicherster: Wiley.

64. Brasher, P.M.A. (1998) *Alberta cancer registry.* 1.

65. Seay, T.M., Blute, M.L. and Zincke, H. (1998) Long-term outcome in patients with pTxN+ adenocarcinoma of prostate treated with radical prostatectomy and early androgen ablation. *J. Urol.*, **159**: 357.

66. Lee, L.K., Whitehurst, C., Pantelides, M.L., Vernon, D.I., and Moore, J.V. (1996) Interstitial photodynamic therapy in the Dunning R3327-AT prostatic carcinoma. *Lasers Med. Sci.*, 11: 155-161.

67. Lowdell, C.P., Ash, D.V., Driver, I., and Brown, S.B. (1993) Interstitial photodynamic therapy. Clinical experience with diffusing fibers in the treatment of cutaneous and subcutaneous tumors. *Br. J. Cancer.* **67**: 1398-1403.

CHAPTER I

CHARACTERIZATION OF A NOVEL TRANSPLANTABLE ORTHOTOPIC RAT BLADDER TRANSITIONAL CELL TUMOR MODEL

1.1 Introduction

Bladder cancer is the second most frequent urologic malignancy in North America,[1] and the most common urologic cancer in Southeast Asia. More than 90 percent of patients diagnosed with bladder cancer have transitional cell carcinoma (TCC).[2] Patients with superficial tumors (Carcinoma *in situ* [C*IS*], Ta, T1) account for 70–85% of all newly diagnosed cases.[3,4] The first choice of treatment for stages Ta and T1 disease is transurethral resection (TUR). A major problem in the treatment of superficial TCC of the bladder is the high incidence of tumor recurrence following TUR. In addition to the multifocal origin of these tumors, a further explanation for this high rate of recurrence might be the implantation of tumor cells at the time of resection. In follow-up, patients need periodic cystoscopic examinations and adjuvant intravesical (i.b.) therapies to prevent or postpone tumor recurrence.[5] Furthermore, the diagnosis and effective treatment of bladder C*IS* remain dilemmas.

A suitable bladder tumor model that resembles human disease both histologically and in behavior is essential for evaluating new therapeutic agents and modalities. The ideal animal bladder tumor model should include the following characteristics:

1. The tumor should grow intravesically (orthotopically), such that the tumor can be directly exposed to i.b. antitumor drugs in its natural environment.

2. The tumor should be of pure TCC origin, with different stages of disease progression (C*IS*, papillary, and invasive diseases), and, as for the human disease, the majority of the tumors should be superficial, but not progressive.

3. The animal host should be immunocompetent and reasonably large, so it can be treated by various antitumor modalities such as immunotherapy with Bacillus Calmette-Guérin (BCG), chemotherapy, and whole bladder photodynamic therapy (PDT).

4. The tumor should be technically easy to develop within a reasonable time period, and highly reproducible with respect to its natural history.

Rodent primary bladder tumors have been induced by N-[4-(5-nitro-2-furyl)-2-thiazolyl]formamide (FANFT) and other carcinogens for 30 years.[6,7,8,9,10,11,12,13] The induction of primary bladder tumors required 8–11 months, with both TCC and squamous carcinoma induced by carcinogen ingestion.[6,7,8,12,14,15,16] A transplantable animal model appears more feasible as an experimental tool for testing new antineoplastic agents. Soloway showed that bladder tumor cells (MBT-2) could be implanted on the murine bladder mucosa by i.b. tumor inoculation, if the bladder mucosa was pre-treated with N-methyl-N-nitrosourea (MNU).[9] Ibrahiem and colleagues[11] injected rat tumor cells into rat bladder muscularis to develop an invasive bladder tumor model, because of tumor cell growth failure when inoculated on the bladder mucosa using Soloway's procedure. Chin et al. established an orthotopic mouse bladder tumor model by implanting MBT-2 tumor cells on bladder mucosa which was altered by mild acid pretreatment.[17] Compared with Soloway's procedure, the one used by Chin et al. was more convenient. Carcinogen could be avoided and higher tumor takes (75–80%) were achieved.[17] The advantages and limitations of previous animal bladder tumor models were elegantly reviewed by Oyasu.[15] In mice, most of the deeply invasive bladder tumors were squamous cell carcinomas, as opposed to TCC. The carcinomas observed in mice tended to invade into the perivesical organs by direct extension, and seldom showed metastasis to regional lymph nodes or lung as observed in humans. The rat models however, were more closely parallel to human bladder carcinomas than mouse models in regards to configuration and progression.[15] Therefore we adapted the procedure described by Chin et al.[17] by instilling AY-27 TCC cells into syngeneic rat bladders, and monitoring for tumor growth with magnetic resonance imaging (MRI) at weekly intervals. This resulted in efficient establishment of various stages of TCC within a relatively short time period. This orthotopic rat bladder TCC model resembles the

20

human situation resulting from "seeding" of viable tumor cells. Its characteristics and application potentials are discussed.

1.2 Materials and methods

1.2.1 Tumor cells and culture conditions

Fischer F344 rats were used to establish the orthotopic bladder tumor model and to propagate the tumor heterotopically (flank or subcutaneous). The rat bladder TCC cell line AY-27 was established as a primary bladder tumor in Fischer F344 rats by feeding FANFT, and was generously provided by Dr. Steve Selman at the Medical College of Ohio, Toledo. The cells were initiated from frozen stock and cultured *in vitro* as monolayers at 37°C in a humidified atmosphere of 5% CO_2 in air. RPMI 1640 medium (Gibco/BRL) supplemented with 10% fetal bovine serum, penicillin-streptomycin, and 2.0 g /L sodium bicarbonate, was used throughout. Cells were passaged when nearly confluent by standard, limited trypsinization procedures.

1.2.2 Preparation of cells

Single tumor cell suspensions were prepared by mincing the subcutaneous tumor under sterile conditions and plating in sterile plastic T-25 flasks (Corning, NY). The medium was decanted from the adherent cells and replaced with fresh medium 4 h later, and at daily intervals for 3–4 days. When the plated cells neared confluence, the growth medium was removed and the cells were incubated for 10 min in Hank's Balanced Salt Solution (HBSS) without Ca^{++} and Mg^{++}, supplemented with EDTA (ethylenediaminetetraacetic acid, 200 mg/L, Sigma Chemicals) and antibiotics as above. HBSS was replaced by 0.01% trypsin-EDTA in HBSS and incubated for 10 min. The resulting cell suspension was then centrifuged at 75 × g for 5 min, the supernatant discarded and the cells resuspended in 10 mL HBSS with Ca^{++} and Mg^{++}. Cell number was determined with a Coulter Counter (Coulter Industries, Model ZBI). To maintain the phenotypic and cytogenetic fidelity, the AY-27 TCC cell line was also passaged periodically as subcutaneous tumors in the flanks of Fischer F344 rats. A tumor cell stock was maintained by cryopreservation.

21

Cell suspension directly from cell culture was used for both bladder instillation and subcutaneous injection. For orthotopic implantation, 1.5 x 10^6 cells in 0.5 mL HBSS were instilled intravesically. For flank implantation, 1.0 x 10^6 cells in 100 μL HBSS were injected subcutaneously.

1.2.3 Animals

Fischer F344 rats were obtained from Charles River, Canada, and subsequently bred locally in our vivarium. Only female rats (160–200 grams) were recipients for the orthotopic bladder inoculation. Male Fischer F344 rats were utilized for the flank implantation. All animal procedures were performed in compliance with the Canadian Council on Animal Care Guidelines. Sterile technique was used for tumor cell implantation.

1.2.4 Tumor Implantation

Intravesical instillation of the TCC cell suspension followed that described by Chin et al.[17] Briefly, the rats were anaesthetized with intraperitoneal (i.p.) injections of ketamine (50 mg/kg body weight, MTC Pharmaceuticals, Cambridge, Ontario) and xylazine (7.5 mg/kg body weight, Miles Canada Inc. Etobicoke, Ontario). Body temperature was maintained with a homeothermic blanket. The rat bladder was catheterized *via* the urethra with an 18-gauge plastic intravenous (i.v.) cannula (Becton Dickinson, Utah). The 18-gauge cannula was optimal for administration of the various agents, providing a snug fit, with no leakage around the catheter. To facilitate tumor seeding, the bladder mucosa was conditioned with an acid rinse. The conditioning consisted of i.b. administration of 0.4 mL of 0.1 N HCl for 15 seconds and neutralization with 0.4 mL of 0.1 N KOH for 15 seconds. The bladder was then drained and flushed with sterile phosphate-buffered saline (PBS). Histologically, HCl/KOH instillation elicited focal urothelial denudation with slight submucosal blood vessel dilatation. Immediately after bladder conditioning, the AY-27 cells were instilled and left indwelling for at least 1 h. The rats were turned 90 degrees along the long axis every 15 min to facilitate whole bladder exposure to the tumor cell suspension. Initially, TCC cell inocula were varied from 1 x 10^6 to 3 x 10^6 cells to

22

examine dose dependency. Unconditioned bladders were examined for tumor takes as well. After 1 h, the catheter was removed and the rats were allowed to void the suspension spontaneously. After recovery from the anesthetic, the rats were placed into standard cages and monitored daily for hematuria and general health status. Rats were assessed for tumor growth by serial MRI at 8 to 14 days post-inoculation, and were sacrificed and necropsied at intervals following MRI detection of tumor growth.

To evaluate the natural course of tumor progression over time, 12 rats inoculated with 1.5×10^6 AY-27 cells were followed until they developed signs of advanced disease. The rats were monitored daily for general health status, and were sacrificed and necropsied when they had any of the following signs: poor grooming; lethargy; hunching; or palpable abdominal mass. All rats were euthanized prior to onset of significant tumor-related morbidity.

1.2.5 MRI protocol

For MRI assessment of the bladder, the rats were anaesthetized with ketamine and xylazine, their bladders were catheterized *per urethra* and moderately distended with 0.5 mL normal saline. Two rats were simultaneously positioned supine in an MRI knee coil. Turbo STIR (Short-T1 Inversion Recovery sequence) images (TR = 2647, TE = 20, TI = 165) were acquired using 205 x 256 matrix, with a field of view of 100 mm, and 0.49 mm x 0.39 mm in-plane resolution. A Philips Gyroscan ACS-II 1.5T clinical magnet was used to generate 1.8 mm slices with a 0.4 mm interval between slices. No external marker was required to interpret bladder location, which was initially determined by serial scanning of the rats in the transverse and sagittal planes. Typically, STIR images were acquired in both planes, resulting in well defined images capable of monitoring tumors nominally 2 mm in diameter. Imaging of the rats was carried out weekly until sacrificed.

1.2.6 Gross and microscopic histology

Necropsy was performed on all rats. The extent of tumor burden at necropsy was evaluated by gross and microscopic examination of the bladder, as well as the organs within the cranial, thoracic and peritoneal cavities. The presence or absence of

23

tumor was noted, along with the number of foci, morphology, size, and degree of tumor invasion. On removal, the bladders were reflected open and examined for tumor distribution and tumor size. Tissue from the bladders and other organs was fixed in 10% phosphate-buffered formalin, embedded in paraffin, serially sectioned at 4 μm, and stained with hematoxylin-eosin (H&E) for histologic examination.

1.2.7 Immunocytochemistry of AY-27 bladder tumor

To confirm that the AY-27 tumor has and retains the TCC phenotype after several *in vitro* and *in vivo* passages, a three-step, indirect immunoperoxidase staining of paraffin-embedded bladder tumor sections with two monoclonal antibodies directed against cytokeratins 7 and 13 was conducted.[18] Cytokeratin 7 has been shown to be expressed in normal human and rat urothelia, as well as in transitional cell carcinomas, but not in squamous cell cancer.[18,19] Cytokeratin 13 is considered to be a reliable "group marker" for squamous epithelium from different organs, whereas it is absent in pure TCC without squamous differentiation.[18] Briefly, the 4 μm-thick tissue sections were deparaffinized and heated (Microwave processor, Model H2500, Energy Beam Sciences, Inc.) to 100°C for 10 min, and then treated with 0.05% trypsin for 15 seconds before adding the antibody. After labeling with the primary antibody ([either anti-cytokeratin 7 or 13, mouse IgG_1], Boehringer Mannheim Biochemica, Germany), biotin-conjugated second antibody (anti-murine IgG, Dako, USA), and avidin-peroxidase conjugate (Biogenix, Canada), the sections were incubated with diaminobenzidine (DAB), and counter-stained with hematoxylin. For comparison, histological sections of human transitional cell carcinoma, squamous cell carcinoma, rat normal skin, and AY-27 cell monolayer cultures, were stained using identical techniques.

Fas and its ligand are cell surface receptors mediating apoptosis.[28] To examine for Fas or Fas-ligand (FasL) expression on AY-27 cells, the cells were grown to approximately 70% confluence in T-75 flasks, washed once in PBS with 0.04% EDTA, and then incubated in PBS with 0.04% EDTA for 30 min at 37°C. The cells then were harvested by gentle pipetting, pelleted by centrifugation, washed once with

24

PBS, and again pelleted. The cells were then resuspended in 600 μL immunofluorescence (IF) buffer (1% fetal bovine serum, 0.02% sodium azide in PBS) and 200 μL aliquots were transferred to 1.5 mL Eppendorf tubes and placed on ice. Each aliquoted sample received 1 μL of either anti-Fas (Pharmigen, USA), anti-FasL (Pharmigen, USA), or isotype-matched control (X931, Dako, USA) antibody and was incubated for 1 h on ice. Subsequently, the cells were pelleted, washed twice in IF buffer, and resuspended in 200 μL IF buffer with 10% normal goat serum (Dako, USA). Samples were incubated at room temperature for 10 min, then returned to ice. Each sample received 1 μL of goat anti-mouse-IgG-FITC (Pharmigen, USA) and was then incubated on ice in the dark for one hour. The cells were pelleted, washed twice in IF buffer, then resuspended in 500 μL of 1% formaldehyde in PBS. Human T lymphocytes were processed as described above and used as positive control. Following the above processing, the samples were analyzed immediately using a Becton-Dickinson flow cytometer and CellQuest software.

1.3 Results

1.3.1 Orthotopic bladder tumor establishment

Single-cell suspensions of 1.5×10^6 AY-27 cells instilled into normal (non-conditioned) bladders did not result in tumor establishment. The establishment of bladder tumors following AY-27 cell instillation into bladders with pre-conditioned mucosa is summarized in Table 1.1. A total of one hundred and six rats were inoculated intravesically with AY-27 cells. Of these rats, 4 died of complications related to the anesthetic or tumor implantation procedure during early experiments. The overall tumor establishment was 95% (97/102). Of the 102 remaining rats, eight were sacrificed 12 to 13 days after tumor cell instillation. Three of the 8 had no detectable tumor. Carcinoma *in situ* and/or T1 bladder tumors were detected in the remaining five, and none had developed invasive tumor. Rats inoculated with 1.0×10^6 AY-27 cells were included in this initial group. Another 82 rats were euthanized on days 16 to 17 post-implantation following MRI detection of tumor. Only two were tumor-free, 80 rats (97%) developed various stages of bladder tumors: 65% (52/80)

25

with superficial tumors (*CIS*, T1); 29% with T2; and 5 out of 80 with T3 bladder tumors. None of these rats developed distant metastases, although 2 had hydroureteronephrosis, with evidence of secondary infection to tumor obstruction of the ureters. Twelve rats were followed until they were overtly symptomatic, prior to being necropsied on days 22 to 50 (average 41 days) to assess the natural history of disease progression. All these rats developed bladder tumors, 66% (9/12) of which were invasive T2 to T4 bladder tumors. Hydroureteronephrosis due to tumor obstruction was found in 4 rats. In 2 of these 4 rats, tumor cell metastasis to the common iliac artery lymph nodes was detected. Tumor seeding of the peritoneum was detected in only one rat.

Table 1.1. Orthotopic bladder tumor incidence and stage of the 102 rats that received AY-27 cells and were sacrificed at different times post-implantation.

Harvest Time (days)	Number of Rats	Histology*						Bladder Stones	No. of Rats with Tumor (%)
		No Tumor	CIS Only	T1/*CIS*‡	T2	T3	T4		
12 – 13	8	3	3	2	0	0	0	0	5/8
16 – 17	82	2	17	35	23	5	0	7	80 (97%)
22 – 50	12	0	0	3	3	4	2	4	12/12
Total	102	5	20	40	26	9	2	11	97 (95%)

CIS: tumor cells confined to bladder mucosa, no papillary tumor.

T1: papillary tumor invading bladder submucosa, but not beyond.

T2: papillary tumor invading one-half of the bladder wall, but not through it.

T3: papillary tumor penetrating through the bladder wall, no apparent metastasis.

T4: papillary tumor invading adjacent organs or metastasizing to distant organs.

‡Papillary tumors were usually accompanied by *CIS*. If a rat had more than two categories (*CIS*, T1, T2, T3, and T4), it was allocated to the highest category.

26

1.3.2 Gross and microscopic characteristics

Microscopic and gross characteristics of the bladder tumor are presented in Figures 1.1A–D. The malignant cellular features of this bladder tumor included high mitotic activity, high nuclear-to-cytoplasmic ratio, and marked nuclear pleomorphism. These cellular characteristics are identical to those observed for the AY-27 cells in monolayer culture. Different *in vitro* passage numbers yielded similar tumor establishment, but with a slight increase in tumor aggressiveness occurring with later passages. The *in vitro* doubling time of exponentially growing AY-27 cells was approximately 24 h.

The microscopic and gross features observed after i.b. AY-27 cell inoculations followed a pattern which may be divided arbitrarily into three stages: 1) early tumor establishment (post-inoculation days 1–13); 2) mid stage of i.b. progression (days 14–21); and 3) advanced i.b. progression and extravesical spread (days 22–50). Soon after instillation into the bladder, tumor cells implanted on the basement membrane where the urothelium was denuded. Tumor cells grew and extended along the basement membrane, and eventually replaced the surrounding normal urothelium (Fig. 1.1A). At this early stage, the lesions appeared flat and intra-epithelial, and were defined as bladder C*IS*.

During the mid stage, these intra-epithelial lesions developed into papillary tumor, or invasive disease, probably depending upon cellular differentiation and host resistance, since in papillary tumor, moderately differentiated cells were predominant (Fig. 1.1B), while in invasive tumor, more poorly differentiated cells were prominent (Fig. 1.1C). In some cases, lymphocytic and mononuclear cell infiltration around tumor could be seen. The papillary tumor configuration appeared similar to that of the human counterpart. The tumor papillae however, were shorter and less branched (Fig. 1.1B), such that the tumor assumed a broad-based cauliflower-like appearance (Fig. 1.1D). In certain cases, diffuse, fine granularity of tumor covering the entire bladder lumen was seen. During this stage, twenty-nine percent of tumors invaded the submucosa connective tissue and/or superficial detrusor muscle. Only in a few cases

Figure 1.1 Microscopic and gross features of AY-27 bladder tumors of different stages. (A) In the early stage, soon after tumor cells establish on basement membrane where normal urothelium is sloughing (arrows), bladder C*IS* replaces normal urothelium and covers partially or entirely bladder lumen surface. There is a moderate increase in the nuclear-to-cytoplasmic (N/C) ratio in cells. Mitotic figures (arrowheads) are common.

28
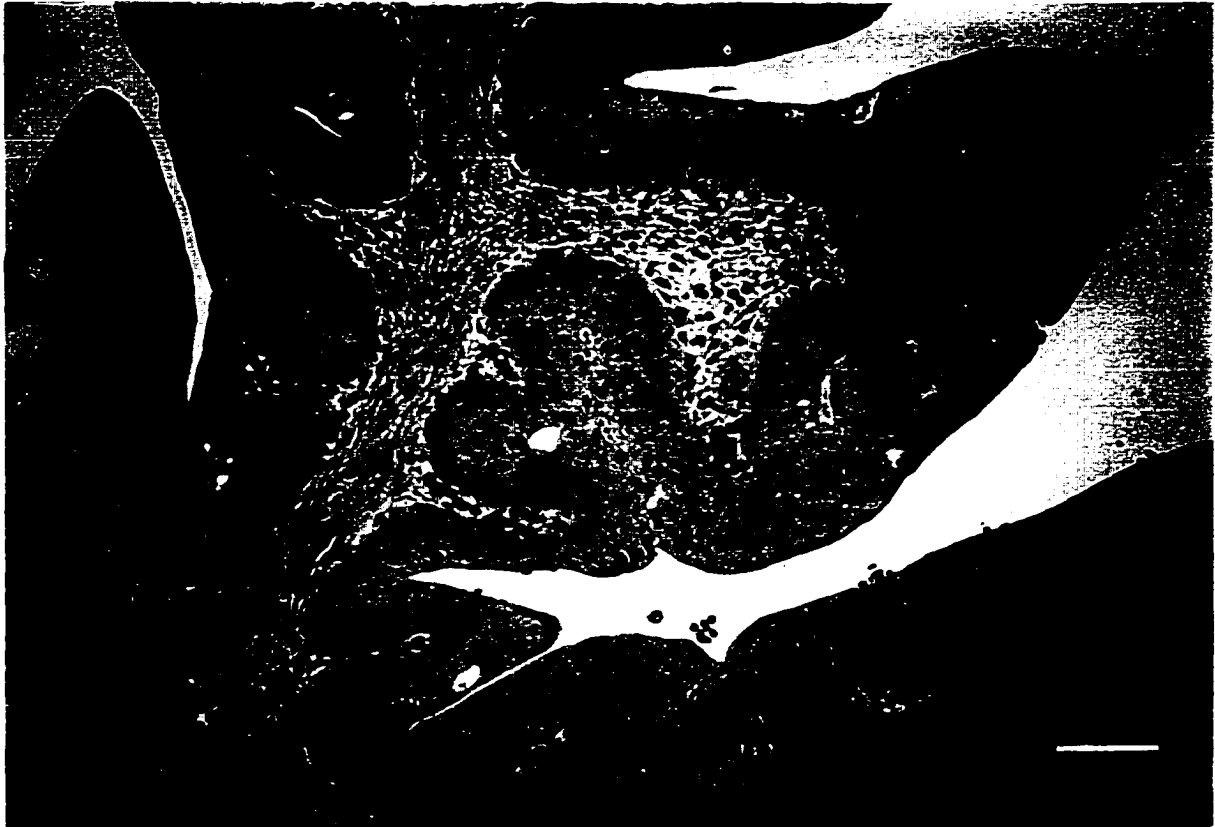
Figure 1.1 (B) Development of papillary tumor is the characteristic of disease progression in the mid stage. The papillae are usually short. The N/C ratio of the cells is moderately increased, the nuclei have slightly irregularly distributed chromatin, and nucleoli are prominent (Grade II).

29
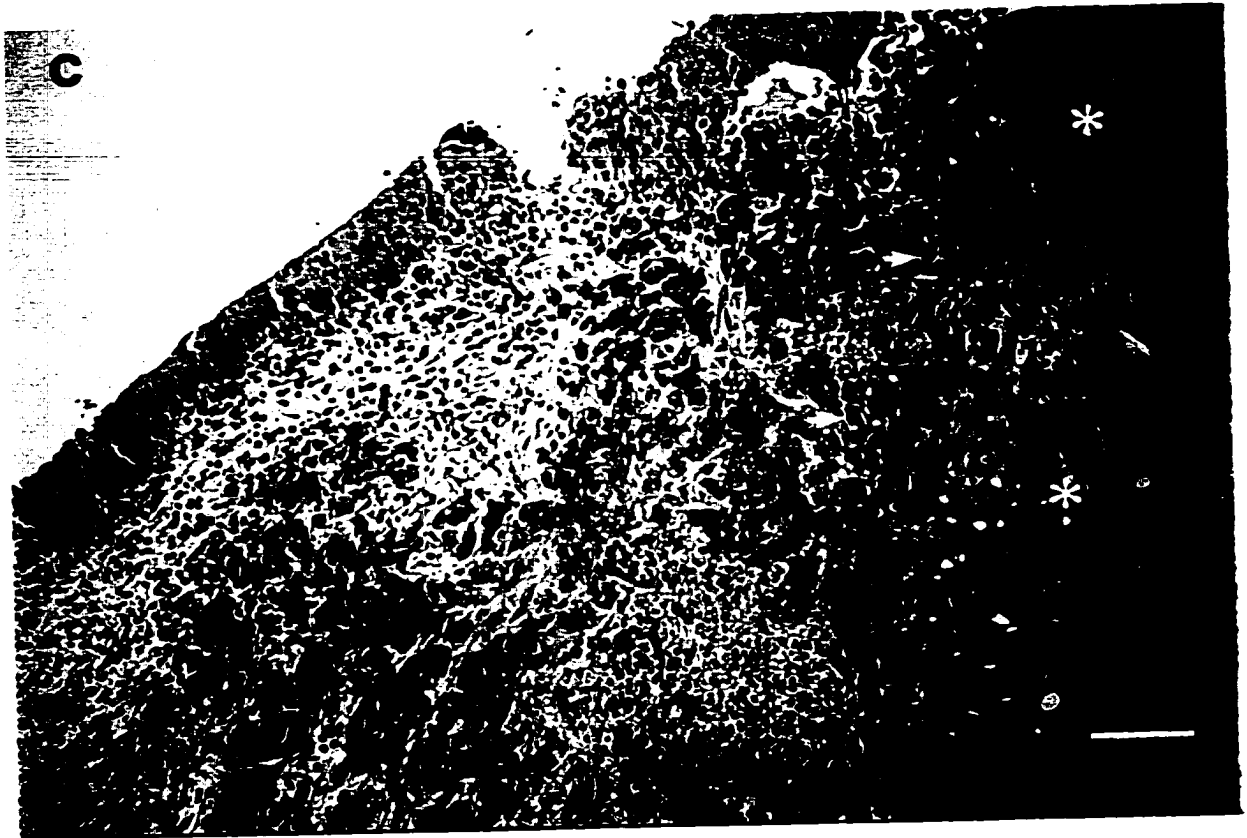
Figure 1.1 (C) In later stages, Grade III tumor cells (*) invade to submucosa and bladder detrusor muscle. There is marked increase in the N/C ratio in cells which form solid sheets. There is markedly increased variation in nuclear size and shape, and mitotic figures (arrows) and nucleoli are frequent and prominent. 'U' denotes normal urothelium. (A–C) H&E stain, Bar = 100 μm.

30
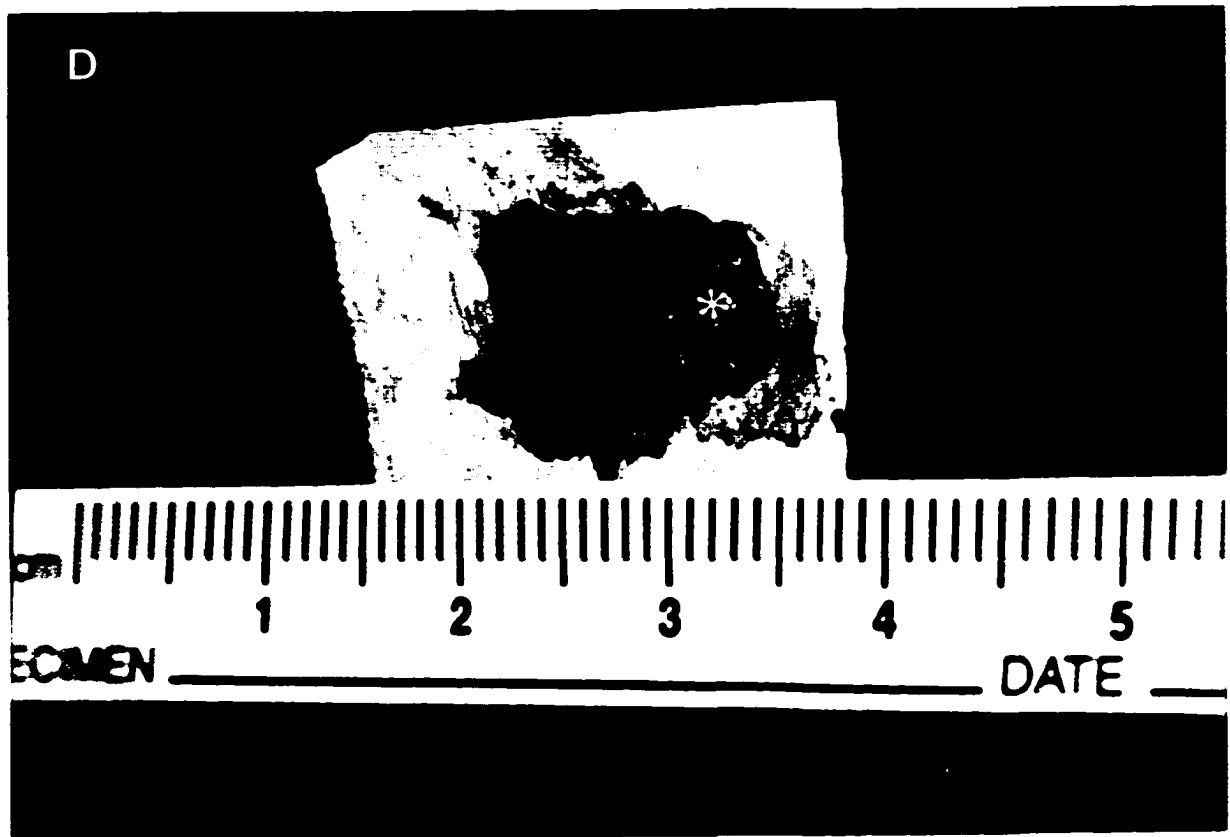
Figure 1.1 (D) Gross view of bladder papillary tumor at mid stage. A solitary tumor (*) locates at bladder posterior-left wall with a cauliflower-like configuration.

31

(5/80) did the tumor invade through the detrusor muscle. Two rats with gross hydroureteronephrosis were found to have evidence of infection secondary to tumor obstruction of the distal ureters.

At the advanced stage, tumor cells penetrated the bladder wall and spread to lymph nodes. The advanced stage was frequently associated with hydroureteronephrosis which also appeared to be caused by direct tumor invasion. Infection following tumor obstruction is the most common life-threatening complication observed in this model. Tumor was detected in the liver in 1 case, with concurrent massive peritoneal seeding and spread of other visceral organs. In all the rats studied, no evidence of tumor spread was found in the lung, brain, heart and pericardial cavity.

1.3.3 MRI

Magnetic resonance imaging demonstrated no evidence of tumor until at least 10 days post-implantation. With further experience, we found it only necessary to begin MRI at post-implant day 13. At this time interval, MRI reliably revealed a thin "filling defect" lesion lining the bladder wall (Fig. 1.2A). By post-implant day 16, part of the bladder lumen was occupied by the "filling defect" lesion (Fig. 1.2B). Necropsy examination revealed a solitary papillary tumor located on the posterior-left bladder wall (Fig. 1.1D). If invasive tumor developed, MRI showed the bladder outline was disrupted and retracted by the invading tumor (Fig. 1.2C). The changes seen on MRI correlated well with the extent of tumor invasion identified histologically.

1.3.4 Immunocytochemistry

Both human and rat urothelia were stained strongly positive with anti-cytokeratin 7, while basal and intermediate cells stained only weakly positive with anti-cytokeratin 13. Human TCC cells were strongly positive with anti-cytokeratin 7 staining, but negative with anti-cytokeratin 13 staining. The AY-27 tumor cells from both *in vivo* bladder tumor and *in vitro* cell cultures were similarly positive with anti-cytokeratin 7 staining, but negative with anti-cytokeratin 13 (Figs 1.1C, 1.3A–B).

32

Figure 1.2 MR images of rat bladders at different post-inoculation days. (A) A thin "filling defect" lesion (open arrow) lining the posterior bladder wall 13 days following tumor cell instillation. 'u' represents the urethra. There is an air bubble (arrow) locating at the bladder dome.

33
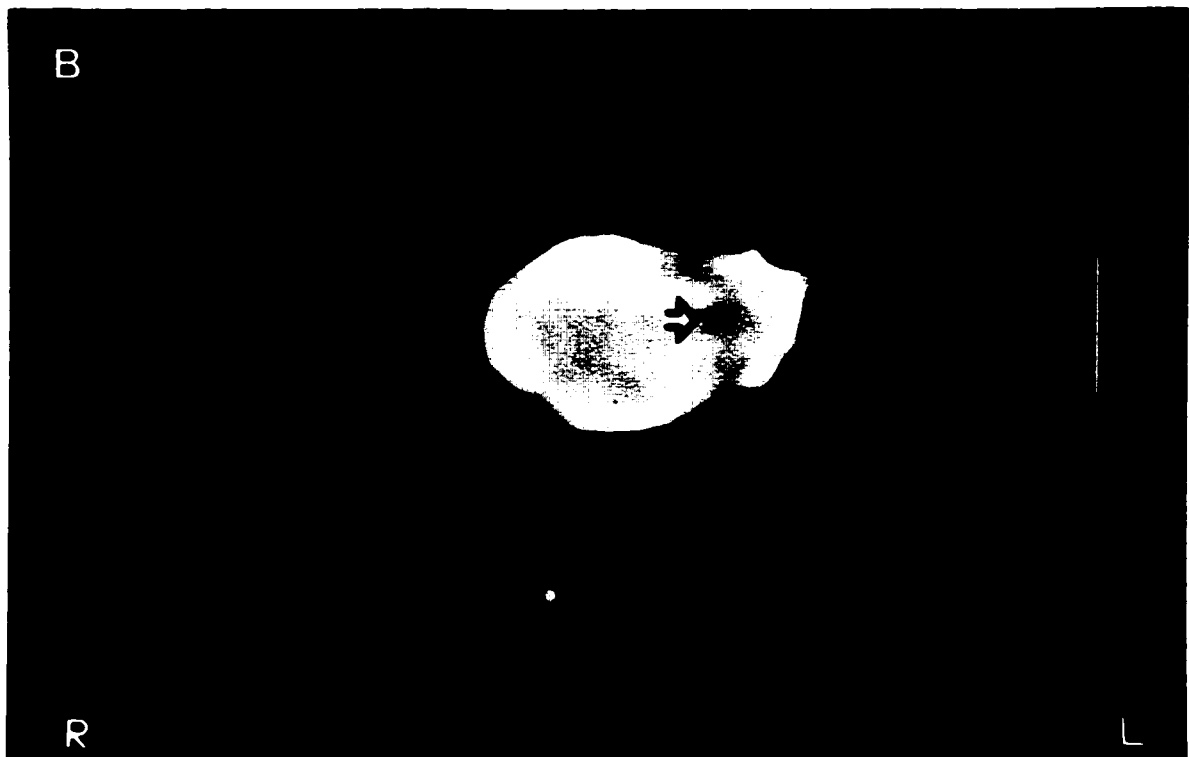
Figure 1.2 (B) A transverse view showing a "filling defect" lesion (arrow) arising from the posterior left bladder wall, protruding into the lumen 16 days post-implantation. The corresponding tumor is shown in Figure 1D.

34

Figure 1.2 (C) A sagittal view showing the bladder is partially filled with tumor (large arrow) that disrupts the bladder outline (small arrow) with retraction due to tumor invasion at 28 days post-implantation. 'S' denotes the stomach. (A–C) Bar = 10 mm.

35
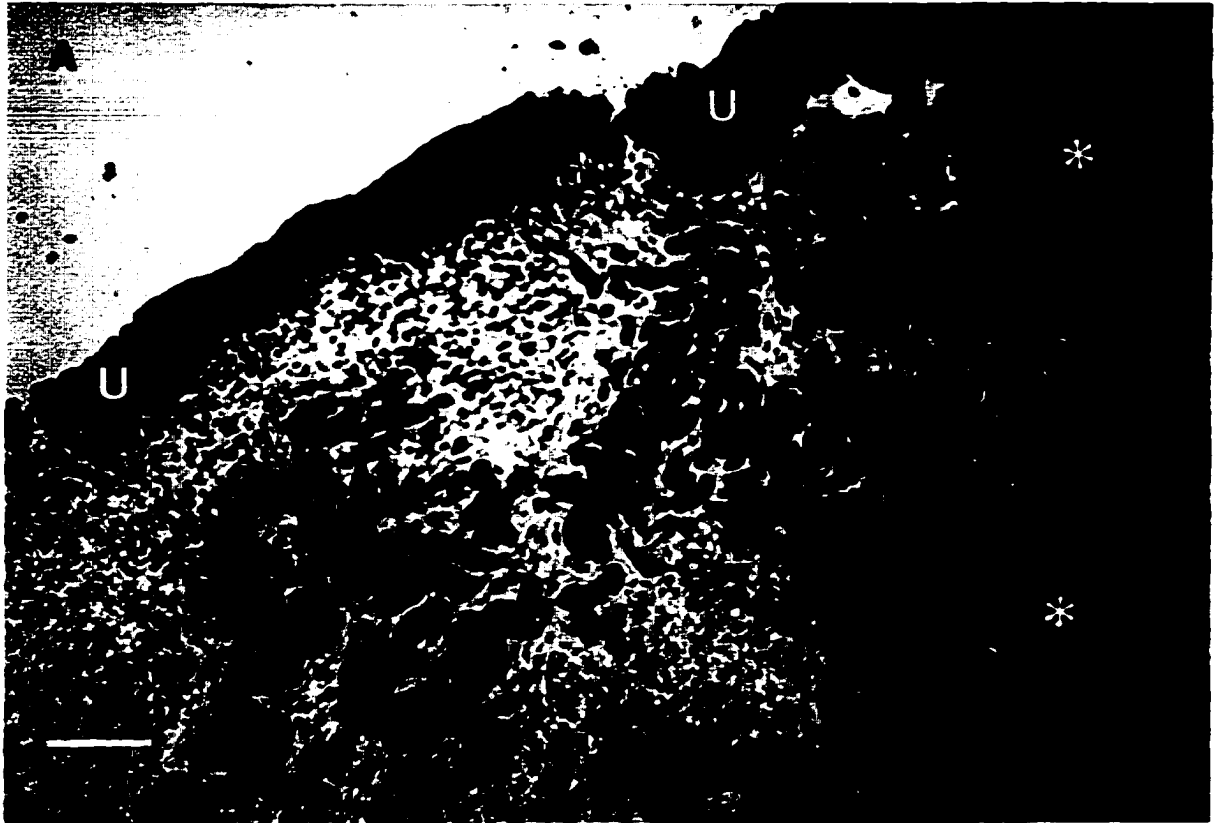
Figure 1.3 Immunoperoxidase staining of formalin-fixed, paraffin-embedded rat bladder sections adjacent to the tissue section shown in Figure 1C. (A) Staining with anti-cytokeratin 7 shows that both normal urothelium (U) and tumor cells (*) are positive (dark brown). Bar = 100 μm.

Figure 1.3 (B) Staining with anti-cytokeratin 13 shows that basal and intermediate cells (arrows) of normal urothelium are only weakly positive (light brown), while tumor cells (*) are negative. Bar = 100 μm.

The AY-27 bladder tumor cells used in this model, therefore maintain urothelial features and demonstrate no evidence of squamous differentiation, both histologically and immunochemically.

Immunofluorescent flow cytometry provides a rapid assay for expression of Fas or FasL. Neither Fas nor FasL is expressed on AY-27 TCC cells, as the fluorescence distribution profiles are not significantly different among control and treated samples (Fig. 1.4).

1.3.5 Other findings

Eleven rats out of 102 developed small bladder stones or calcific encrustation of the tumor surface. Although the reason for calculus formation was not thoroughly investigated, it was evident that stone formation correlated directly with the presence of tumor necrosis, which occurred with heavy tumor burden.

Approximately 2 weeks following tumor implantation, some rats failed to gain body weight. These animals maintained their initial body weight, but did not grow as expected, presumably due to tumor growth. In the few animals with advanced stage T4 disease, the tumor mass could be detected by palpation of the lower abdomen.

1.3.6 Flank Tumor Growth

Tumor establishment following subcutaneous (s.c.) injection of cell suspension (10 rats), or implantation of 3-mm tumor chunks (30 rats) was 100%. Over a period of 4 weeks, the tumors progressively grew to approximately 15 mm in diameter (about 1,700 mm^3). The tumor-volume-doubling time was approximately 4 days. Upon dissection, the tumors demonstrated a smooth thin capsule, with a well-vascularized surface and a zone of central necrosis. The tumor architecture was solid monotonous sheets of TCC cells without papillary growth. No evidence of distant metastasis was found, however there was evidence of local tumor invasion into the underlying striated muscle in 2 rats.

1.4 Discussion

Our primary objective was to develop a bladder tumor model for whole bladder PDT and other i.b. therapies. This requires an orthotopic, superficial, and
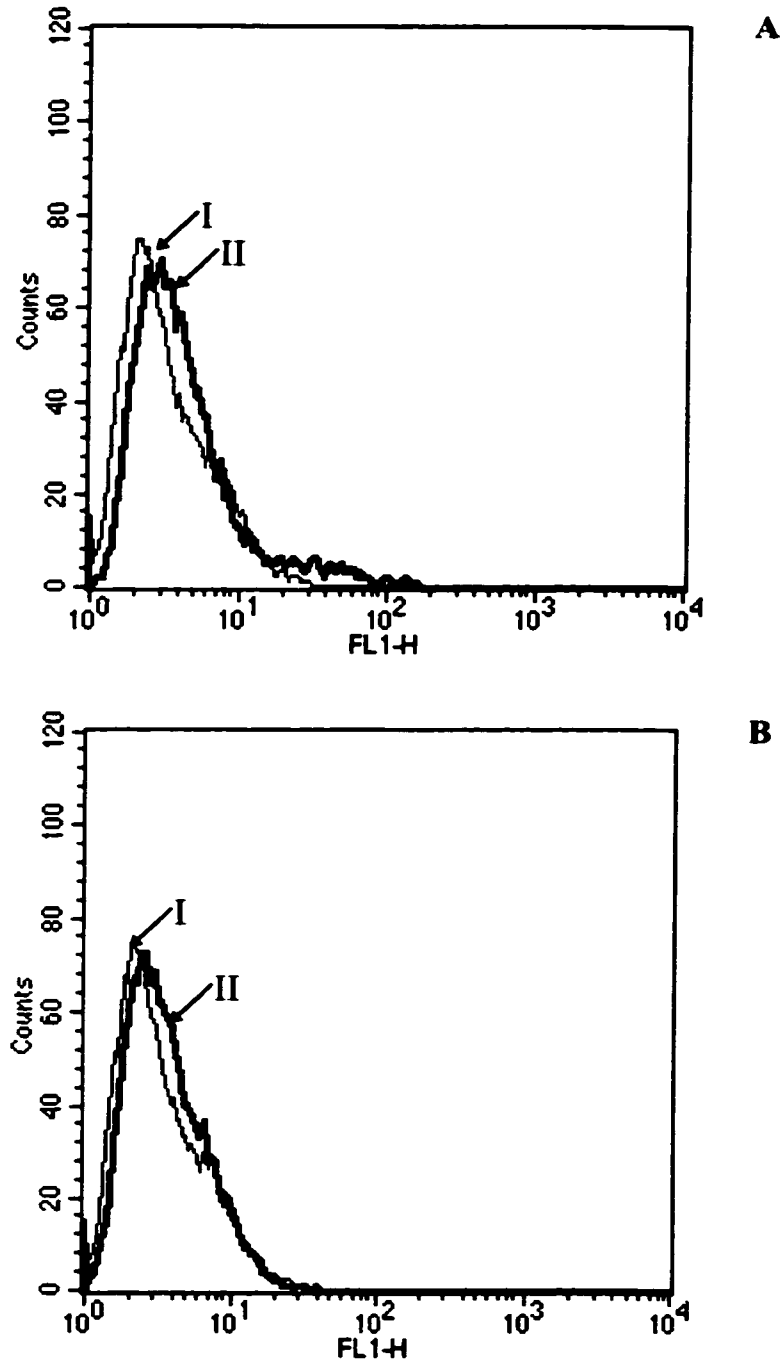
38

Figure 1.4 Fas and FasL expression on AY-27 TCC cells. Cells were incubated first with either anti-Fas (A), anti-FasL (B), or isotype-matched mouse IgG (control), then with goat anti-mouse-Ig-FITC. Samples were read on the FL 1 parameter using a flow cytometer (See *Materials and Methods* for details). The fluorescence distribution profiles are not significantly different among control (I) and treated samples (II).

39

purely TCC model with a reasonable bladder volume and urethral caliber to introduce the laser fiber or other therapeutic agents into the bladder. Spontaneously arising rodent bladder tumors are rare.[20] A suitable rat model may meet these criteria, since carcinogen-induced primary bladder tumors closely parallel the human disease in both morphology and tumor biology.[15] However, several limitations of previously described models exist. For example, induction of primary bladder tumors requires several months, with both TCC and squamous carcinoma being induced, and tissues other than urothelium also being transformed.[6,7,8,14,15,16] The subcutaneous tumor model is unsuited to i.b. antitumor therapies, not only due to its heterotopic growth, but also due to its dissimilarities in biological behavior to the clinical disease, as observed in this study. Therefore, ideally, a transplantable orthotopic rat bladder tumor model appears more relevant as an experimental tool for testing new antineoplastic agents provided it is easy to establish and highly reproducible. Soloway[9] showed that by traumatization of the bladder mucosa by MNU 48 h prior to tumor cell inoculation, the bladder tumor cells (MBT-2) could be implanted intravesically in mouse bladder mucosa. He reported about 60% tumor takes. Ibrahiem and colleagues[11] injected rat bladder tumor cells into the bladder muscle to develop an invasive bladder tumor model after failure to implant the tumor cells on the bladder mucosa using Soloway's technique. Their model did not closely mimic the human counterpart because the tumor was actually invasive and largely covered with normal bladder mucosa.[11,21] Chin and colleagues[17] reported that tumor cells could be efficiently inoculated in mouse bladder mucosa that was pre-treated with mild HCl/KOH. They reported about 80% tumor growth. However, the rat model, because of its size, is easier to work with for i.b. therapies, and furthermore, it may parallel the human disease processes better than a mouse model.[12,15] Detailed characteristics of a transplantable orthotopic rat bladder tumor model, to the best of our knowledge, have not been described.

Using the AY-27 cell line and a modification of the techniques previously described by Chin et al.[17] for the MBT-2 model, we have developed and characterized

40

a highly reproducible, transplantable, purely TCC rat orthotopic bladder tumor model. The procedures are not technically complicated, are well tolerated by the animals, and result in minimal morbidity associated with occasional mild hematuria subsequent to tumor cell instillation. The fact that tumor cells used for i.b. instillation originated from cell cultures rather than directly from solid tumor fragments, might contribute to the high tumor establishment observed. Tumor cells prepared from tumor fragments may also contain stromal cells, lymphocytes, *etc.*, and their viability might be compromised due to mechanical or enzymatic treatment. Initially, tumor cell suspensions prepared directly from tumor fragments were used for both s.c. injection and i.b. instillation. The resulting tumors grew slower with lower tumor establishment (data not shown). Single-cell suspensions of AY-27 cells instilled in normal (unconditioned) bladder did not elicit tumor establishment. Prior to 13 days post-inoculation, all tumors detected are superficial (T1, *CIS*). The relatively lower tumor establishment in this group may be explained either by: 1) small early *CIS*-like lesions escaping detection on histological examination; or 2) this group including three rats inoculated with a lower dose (1.0×10^6) of AY-27 cells. In a group of animals sacrificed on days 16–17 post-inoculation, the tumor establishment is 97% (80/82), with 65% being superficial (T1, *CIS*), 29% superficially invasive (T2), and 6% deeply invasive (T3) disease. Thus 14–16 days post-inoculation seems to be the most suitable time for i.b. therapies such as chemotherapy, immunotherapy, and whole bladder PDT. With time, there is progression of the disease process with invasive tumors detected in 66% of the animals followed 21 – 50 days post tumor inoculation.

Recently, we also have established an orthotopic nude rat model xerografted with human bladder TCC cells (MGH-U3) using similar procedures described in this study (data not shown). While this tumor model may better represent the cellular biology of human disease, greater time, cost, and labor are necessary to maintain the nude rat model than the syngeneic model. As well, the nude model is not

41

reproducible and not appropriate for active immunotherapies like BCG instillation, which currently is the most effective clinical therapy for bladder C*IS*.

In clinical practice, human bladder carcinoma is commonly classified into three types: C*IS*, superficial papillary, and invasive carcinomas. The superficial papillary tumors frequently recur after TUR, but the prognosis is good. The advanced invasive tumors have a very poor prognosis with the median survival being approximately one year despite the use of aggressive regimens.[22] Whether the carcinogenesis of these two entities is different has yet to be determined. Studies on animals using bladder carcinogens suggest that both papillary and invasive tumors may be derived from C*IS* depending on cellular differentiation.[12,15,23] In addition, Orozco *et al.* [24] analyzed 102 patients with primary or secondary bladder C*IS*, and suggested that host resistance to local progression determined the outcome of C*IS*, since bladder C*IS* is cytologically identical to high grade papillary and invasive TCC. Droller *et al.*[25] also found that tumor development was accompanied by decreased lymphocyte cytotoxicity against bladder tumor in rats. Our observations in the transplantable tumor model also support these findings. Bladder C*IS* developed to papillary or invasive tumors depending on both cellular differentiation and possibly host resistance to disease progression. Since the cells are from the same monolayer cultures, the cytology of papillary tumors is similar to that of C*IS*. Clinically however, the latter is usually thought to be the preliminary stage of invasive diseases. These findings may also suggest that the AY-27 cells are heterogeneous. The course of tumor progression observed in our model closely mimics the clinical situation resulting from viable tumor cell implantation at the time of TUR or prior.

In addition to cellular differentiation and host resistance, recent evidence shows that cell-to-cell and cell-to-substrate interactions also play an important role in tumor progression. Inhibiting metastasis by interfering with cancer cell adhesion may be a future therapeutic option, since tumor cells establish bonds with other cells and extracellular matrix by cell adhesion molecules.[26] Cell adhesion molecules consist of multimolecular protein complexes of transmembrane adhesion receptors anchoring

intracellular cytoskeletal structural proteins and signal transdution molecules.[27] Our model could potentially be utilized to conduct studies of using biological agents to prevent tumor cell seeding by interfering with cell adhesion or to induce apoptosis. FasL, a cell surface molecule belonging to the tumor necrosis factor family, binds to its receptor Fas (a type I membrane protein), thus inducing apoptosis of Fas-bearing cells.[28] It has been hypothesized that i.b. administration of FasL could be employed as a treatment option for bladder TCC. In the present study, the expression of Fas and FasL on AY-27 cells has been investigated to explore whether the model would be suitable for studying therapy with Fas or FasL. However, preliminary evidence suggests that neither marker is expressed in the absence of some form of induction.

Cytokeratins are part of the intermediate filament system of the cytoskeleton.[29] The synthesis of cytokeratins is usually maintained during malignant transformation, and this feature serves as one of the hallmarks of epithelium-derived tumors,[30] including tumors of the urinary tract.[18,19,31,32] Cytokeratin 7 has been considered a urothelial marker,[19] while cytokeratin 13 is a squamous cell marker with trace amounts of component 13 expressed in basal and intermediate cells of human urothelium and low-grade TCC.[18] Immunocytochemical studies show that the AY-27 rat bladder tumors retain TCC features, without squamous cell differentiation. The latter, if present, usually associates with high-grade (G2–G3), invasive TCC.[15] Since squamous carcinoma may respond differently to anticancer therapies than TCC carcinoma, this purely TCC tumor model is ideal for preclinical evaluation of antitumor therapies for human bladder TCCs, the most common type of cancers arising from the urothelium.

MRI provides a non-invasive imaging modality that is useful to detect early superficial papillary tumor and monitor tumor growth in rodent models. Previously, confirmation of successful tumor implantation in rodents was based on the detection of a palpable suprapubic mass, gross hematuria, weight loss in the animals, or on a transillumination technique by periodic surgical exposure of the bladder.[11] In the present study, only 2 rats with advanced (stage T4) tumors had a palpable suprapubic

43

mass. The average weight loss was insignificant (0.2%). The changes shown on MRI correlated well with the extent of tumor invasion identified histologically. However, once this tumor model had been characterized for growth kinetics, regular monitoring with MRI added little benefit because of the high reproducibility of this model.

In conclusion, the distinct advantageous features of this model system include: 1) purely TCC carcinomas growing orthotopically in the bladder lumen; 2) highly reproducible tumor growth in a relatively short time; 3) resemblance to high grade human TCC in both morphology and tumor biology; and 4) utility to test varying intravesical therapies such as chemotherapy, active and passive immunotherapies, and whole bladder PDT. This model is currently being used to study PDT,[33] BCG immunotherapy, oncolytic therapy and chemotherapy of bladder cancer in our laboratory.

1.5 References

1. Parker, S.L., Tong, T., Bolden, S. and Wingo, P.A. (1996) Cancer statistics, 1996. *CA. Cancer J. Clin.*, **46**: 1.

2. Lamm, D.L. and Torti, F.M. (1996) Bladder cancer, 1996. *CA. Cancer J. Clin.*, **46**: 93.

3. Lamm, D.L. (1992) Superficial bladder cancer. *Urol. Clin. North Amer.*, **19**: 3.

4. Whitemore, Jr. W.F. (1988) Bladder cancer: an overview. *CA. Cancer J. Clin.*, **38**: 213.

5. Grossman, H.B. (1996) Superficial bladder cancer: decreasing the risk of recurrence. *Oncology* **10**: 1617–1624.

6. Erturk, E., Price, J.M., Morris, J.E., Cohen, S., Letth, R.S., Von Esch, A.M. and Crovetti, A.J. (1967) The production of carcinoma of the urinary bladder in rats by feeding N-[4-(5-Nitro-2-furyl)-2-thiazolyl]formamide. *Cancer Res.*, **27**: 1998–2002.

7. Erturk, E., Cohen, S., Price, J.M. and Bryan, G.T. (1969) Pathogenesis, histology, and transplantability of urinary bladder carcinomas induced in albino rats by oral administration of N-[4-(5-nitro-2-furyl)-2-thiazolyl]formamide. *Cancer Res.*, **29**: 2219–2228.

8. Erturk, E., Cohen, S. and Bryan, G.T. (1970) Urinary bladder carcinogenicity of N-[4-(5-nitro-2-furyl)-2-thiazolyl]formamide in female Swiss mice. *Cancer Res.*, **30**: 1309–1311.

9. Soloway, M.S. (1977) Intravesical and systemic chemotherapy of murine bladder cancer. *Cancer Res.*, **37**: 2918–2929.

10. Arai, M., Cohen, S.M., Jacobs, J.B. and Friedell, G.H. (1979) Effect of dose on urinary bladder carcinogenesis induced in F344 rats by N-[4-(5-nitro-2-furyl)-2-thiazolyl]formamide. *J. Natl. Cancer Inst.*, **62**: 1013–1015.

11. Ibrahiem, E.I., Nigam, V.N., Brailovsky, C.A., Madarnas, P. and Elhilali, M. (1983) Orthotopic implantation of primary N-[4-(5-Nitro-2-furyl)-2-thiazolyl]formamide-induced bladder cancer in bladder submucosa: an animal model for bladder cancer study. *Cancer Res.*, **43**: 617–622.

12. Ohtani, M., Kakizoe, T., Nishio, Y., Sato, S., Sugimura, T., Fukushima, S. and Niuima, T. (1986) Sequential changes of mouse bladder epithelium during induction of invasive carcinomas by *N*-butyl-*N*-(4-hydroxybutyl)nitrosamine. *Cancer Res.*, **46**: 2001–2004.

13. Samma, S., Uchida, K., Seidenfeld, J. and Oyasu, R. (1990) Effect of α-difluoromethylonithine on the development of deeply invasive urinary bladder carcinomas in mice. *Urol. Res.*, **18**: 277–280.

14. Herman, C., Vegt, P.D.J., Debruyne, F.M.J. and Ramaekers, F.C.S. (1985) Squamous and transitional elements in rat bladder carcinomas induced by *N*-butyl-*N*-4-hydroxybutyl-nitrosamine (BBN). A study of cytokeratin expression. *Am. J. Pathol.*, **120**: 419–426.

15. Oyasu, R. (1995) Epithelial tumors of the lower urinary tract in humans and rodents. *Fd. Chem. Toxic.*, **33**: 747–755.

16. Stocker, S., Knuchel, R., Sroka, R., Kriegmair, M., Steinbach, P. and Baumgartner, R. (1997) Wavelength dependent photodynamic effects on chemically induced rat bladder tumors following intravesical instillation of 5-aminolevulinic acid. *J. Urol.*, **157**: 357–361.

17. Chin, J., Kadhim, S., Garcia, B., Kim, Y.S. and Karlik, S. (1991) Magnetic resonance imaging for detecting and treatment monitoring of orthotopic murine bladder tumor implants. *J. Urol.*, **145**: 1297–1301.

18. Moll, R., Achtstatter, T., Becht, E., Balcarova-Stander, J. and Franke, W.W. (1988) Cytokeratins in normal and malignant transitional epithelium: Maintenance of expression of urothelial differentiation features in transitional cell carcinomas and bladder carcinoma cell culture lines. *Am. J. Pathol.*, **132**: 123–144.

19. Cilento, B.G., Freeman, M.R., Schneck, F.X., Retik, A.B. and Atala, A. (1994) Phenotypic and cytogenetic characterization of human bladder urothelia expanded *in vitro*. *J. Urol.*, **152**: 665–670.

20. Van Moorselaar, R.J., Ichikawa, T., Schaafsma, H.E., Jap, P.H., Isaacs, J.T., Van Stratum, P., Ramaekers, F.C., Debruyne, F.M. and Schalken, J.A. (1993) The rat

46

bladder tumor model system RBT resembles phenotypically and cytogenetically human superficial transitional cell carcinoma. *Urol. Res.*, **21**: 413–21.

21. Iinuma, S., Bachor, R., Flotte, T. and Hasan, T. (1995) Biodistribution and phototoxicity of 5-aminolevulinic acid-induced PpIX in an orthotopic rat bladder tumor model. *J. Urol.*, **153**: 802–806.

22. Roth, B.J. (1996) Chemotherapy for advanced bladder cancer. *Sem. Oncol.*, **23**: 633–644.

23. Oyasu, R., Samma, S., Ozono, S., Bauer, K., Wallemark, C.B. and Homma, Y. (1987) Induction of high-grade, high-stage carcinomas in the rat urinary bladder. *Cancer* **59**: 451–458.

24. Orozco, R., Martin, A.A. and Murphy, W.M. (1994) Carcinoma *in situ* of the urinary bladder. Clues to host involvement in human carcinogenesis. *Cancer* **74**: 115–122.

25. Droller, M. and Gomolka, D. (1982) Expression of the cellular immune response during tumor development in an animal model of bladder cancer. *J. Urol.*, **128**: 1385–1389.

26. Ruoslahti, E. (1996) How cancer spreads. *Scientific American* (September): 72–77.

27. Yamada, K.M. and Benjamin, G. (1997) Molecular interactions in cell adhesion complexes. *Cur. Opin. cell biol.*, **9**: 76–85.

28. Nagata, S. and Golstein, P. (1995) The Fas death factor. *Science* **267**: 1449–1456.

29. Steinert, P.M. and Roop, D.R. (1988) Molecular and cellular biology of intermediate filaments. *Annu. Rev. Biochem.*, **57**: 593–625.

30. Tseng, S.C.G., Jarvinen, M.J., Nelson, W.G., Huang, J-W., Woodcock-Mitchell, J. and Sun, T-T. (1982) Correlation of specific keratins with different types of epithelial differentiation: monoclonal antibody studies. *Cell* **30**: 361–372.

31. Moll, R., Franke, W.W., Schiller, D.L., Geiger, B. and Krepler, R. (1982) The catalog of human cytokeratins: patterns of expression in normal epithelia, tumors and cultured cells. *Cell* **31**: 11–24.

47

32. Letocha, H., Nilsson, S., Silen, A., Ekblom, J., Amberg, H., Wiklund, B. and Westlin, J-E. (1993) Immunotargeting with monoclonal cytokeratin 8 antibodies of human urothelial cancer transplanted to nude mice. *Acta oncologia* **32**: 793–800.

33. Xiao, Z., Miller, G.G., McCallum, T.J., Brown, K., Lown, J.W., Tulip, J. and Moore, R.B. (1998) Biodistribution of Photofrin II and 5-aminolevulinic acid-induced protoporphyrin IX in normal rat bladder and bladder tumor models: implications for photodynamic therapy. *Photochem. Photobiol.*, **67**: 573–583.

CHAPTER II

BIODISTRIBUTION OF PHOTOFRIN II® AND 5-AMINOLEVULINIC ACID-INDUCED PROTOPORPHYRIN IX IN NORMAL RAT BLADDER AND BLADDER TUMOR MODELS: IMPLICATIONS FOR PHOTODYNAMIC THERAPY

2.1 Introduction

Photodynamic therapy (PDT) is a promising cancer treatment for small, superficial tumors.[1,2] As such it may be useful to treat dysplastic, premalignant lesions and carcinoma *in situ* (C*IS*) of the bladder that are not amenable to transurethral resection. The basic principle of PDT includes the administration of a photosensitizer which preferentially accumulates to effective therapeutic levels in tumor *vis-à-vis* normal tissues. Following systemic or topical administration of the photosensitizer, light of suitable wavelength (usually laser light) is applied to excite the sensitizer. The resultant photochemical reaction induces the generation of highly reactive species such as singlet oxygen and/or free radicals leading to cell death.[3,4] The bladder is one of the most suitable organs for PDT due to convenient endoscopic access and the multifocal nature of bladder cancer that require the bladder to be treated as a whole. Photofrin II® (Porfimer sodium, or PII), a mixture of porphyrins, is the only photosensitizer approved for clinical use to date. Although PII has proved to be an effective photosensitizer, there are limitations associated with PII-based PDT. These include prolonged cutaneous phototoxicity and lack of tumor selectivity following systemic administration of PII. A major concern in whole bladder PDT with PII has been the development of fibrotic, contracted bladders with upper tract obstruction due to damage of the muscularis.[5,6] As a result of these problems, new photosensitizers are being investigated. One particular agent of interest is 5-aminolevulinic acid (ALA). ALA has been used recently in experimental clinical photodynamic therapy of skin cancers[7,8] and gastrointestinal malignancies.[9] The endogenous intermediate, ALA, is a precursor of heme biosynthesis. Protoporphyrin IX (PpIX), a potent photosensitizer, is, in turn, produced in the penultimate step of heme biosynthesis. There are two rate-limiting steps in this pathway; the first is synthesis of ALA, which

50

is formed by the condensation of glycine and succinyl CoA. This step is feedback-inhibited by heme. The second rate-limiting step is conversion of PpIX to heme by addition of ferrous iron to PpIX. Since the conversion of PpIX to heme is slow, especially in some malignant cells,[10] the presence of excess exogenous ALA can bypass the first rate-limiting step and lead to an accumulation of PpIX.[11,12]

Experimental and preliminary clinical studies suggest several advantages using ALA-based PDT:

1. ALA-induced PpIX is rapidly eliminated from the body if ALA is given systemically, and hence the risk of skin phototoxicity is limited to 24 h.

2. Unlike PII, which accumulates more in the submucosal vascular stroma, ALA-induced PpIX is preferentially accumulated in the mucosa (epithelium) of hollow viscera and consequently, bladder muscle damage may be avoided.

However, no systematic study concerning the uptake of ALA and subsequent conversion to PpIX in bladder tumor has been undertaken. This was probably due to lack of a suitable bladder tumor model that would effectively mimic clinical disease. Additionally, the potential of intravesical administration of both ALA and PII for PDT of bladder cancer has only been cursorily examined and remains to be determined.[13,29,30,31,32]

The objectives of this study are:

1. To characterize the biodistribution of ALA-induced PpIX in bladder tumors and normal bladder, using both heterotopic and orthotopic rat bladder tumor models. Variables include drug dose and biodistribution time, as well as intravenous vs. intravesical administration route of ALA.

2. To explore the suitability of intravesical instillation of ALA for detection and PDT of bladder cancer; and

3. To study the potential of intravesical application of PII for PDT of bladder cancer.

2.2 Materials and methods

2.2.1 *Tumor cells.* AY-27 cells from a FANFT-induced rat bladder TCC cell line were grown as monolayers at 37°C in RPMI-1640 culture medium (Gibco/BRL)

supplemented with L-glutamine and 10% fetal calf serum and penicillin-streptomycin (1%, v/v). The cells' malignant phenotype was maintained by serial implantation in syngeneic Fischer CDF344 rats as a solid subcutaneous tumor.

2.2.2 *Animals and tumor models.* Fischer CDF344 rats were obtained from Charles River, Canada and bred at the Cross Cancer Institute Vivarium. Female CDF344 rats greater than 8 weeks old (160 – 200 g) were used to develop two tumor models: an orthotopic superficial bladder tumor model, and a subcutaneous bladder tumor implant in both flanks (heterotopic or flank model). Male Fischer rats were also utilized in the heterotopic model. All procedures and care of the animals were performed according to the Guidelines of the Canadian Council on Animal Care.[14] To develop the orthotopic model, a tumor transplantation technique previously described by Chin et al.[15] for their murine bladder tumor model was modified for our rat model (see chapter I).[16] Briefly, rats were sedated with Ketamine (MTC Pharmaceuticals, Cambridge, Ontario, 50 mg/kg. body weight) and Xylazine (Miles Canada Inc. Etobicoke, Ontario, 7.5 mg/kg. body weight) by intraperitoneal (i.p.) injection. Access to the bladder was *via* an 18-gauge plastic intravenous cannula. Approximately 2.5 cm of the cannula was inserted into the bladder *per urethra*. For tumor cell grafting the bladder mucosa was mildly disrupted using a 15-second wash with 0.4 mL of 0.1 N HCl, followed by neutralization with 0.4 mL of KOH, and two subsequent phosphate-buffered saline (PBS) washes. A suspension containing 1.5 x 10^6 AY-27 cells was then instilled into the bladder and left for one hour. The rats were maintained under sedation with positional changes at 15-minute intervals prior to the capped cannula being removed. Seven to 14 days later, and at weekly intervals, the animals were imaged with magnetic resonance imaging (MRI) to assess tumor growth. For MRI, rats were sedated with ketamine and xylazine, the bladder was catheterized and distended with 0.5 mL normal saline. The rats were placed in supine position in an MRI knee coil. Turbo STIR (Short-T1 Inversion Recovery) images (TR = 2647, TE = 20, TI = 165) were acquired using a 205 x 256 matrix, and 0.49 mm x 0.39 mm in-plane resolution. A Philips ACS-II Gyroscan 1.5T clinical magnet

52

generated 1.8 mm slices with a 0.4 mm intervening gap. Typically, STIR images were obtained in the transverse and sagittal planes, resulting in well defined images capable of monitoring tumors as small as 2 mm in diameter. The lesion assumed to be tumor appeared as a black intraluminal "filling defect" on the bladder wall against the white background of saline. This technique facilitated non-invasive detection of tumors otherwise undetectable by clinical signs.[15,16] The orthotopic model was used to examine the biodistributions of PII and PpIX following either intravesical (i.b.) or intravenous (i.v.) administration of PII or ALA. To establish the heterotopic model, 3 mm³ chunks of AY-27 tumor tissue from a rat host were implanted subcutaneously into both flanks of Fischer CDF344 rats. The implants grew to approximately 15 mm in diameter, about 4 weeks post-implantation. The heterotopic model was used to characterize the biodistribution of PpIX after i.v. injection of ALA.

2.2.3 *Administration of ALA, PpIX, and PII.* ALA was supplied as a hydrochloride salt (Aldrich Chemical Inc. Milwaukee, WI) with a purity of 98%. ALA powder (molecular weight 167.6) was dissolved in PBS (Sigma Chemicals Inc.) at appropriate concentrations immediately before use (*vide infra*). For the i.v. route, animals bearing heterotopic tumor were anesthetized by Metofane inhalation (Janssen Pharmaceutica, North York, Ontario). ALA in PBS (0.5 to 1 mL) was injected into the tail vein *via* a 27G needle at doses of 100, 250, 500, and 1000 mg/kg body weight. Animals were allowed to recover (in approx. 5 minutes) and were protected from intense light. At intervals of 2, 4, or 6 h after ALA administration, animals were euthanized for study. Groups of 3 to 5 animals were used at each dose and time point. Control animals (3 rats bearing heterotopic tumor) received PBS intravenously and were sacrificed 2 h later. Three further groups (3 rats/group) of animals bearing orthotopic bladder tumor received i.v. injection of ALA (250, 500, and 1000 mg/kg, respectively), and were euthanized 4 h following ALA injection. ALA for i.b. instillation was prepared in concentrations of 5, 10, 25, 50, 100, 200, 400, and 600 m*M* (0.83 – 100 mg/mL) by dissolving in PBS. For concentrations greater than 50 m*M*, ALA solution was adjusted with sodium hydroxide (NaOH) to maintain the pH

53

between 5.5 and 6.5, which is within the physiological pH range of urine. ALA solution with pH less than 7 has been found to be acceptably stable within 6 h at 22°C.[27] Animals bearing orthotopic tumor were anesthetized by i.p. injection of Ketamine and Xylazine. An 18-gauge plastic intravenous cannula was inserted into the bladder *via* the urethra, and 0.5 mL of ALA solution was instilled into the bladder. The cannula remained in the urethra and was capped for 2, 4, or 6 h, during which time the animals were kept anesthetized, placed on a homeothermic blanket at 37°C, and protected from bright light. Groups of 3 to 5 rats were used at each concentration and each biodistribution time point. At the end of the incubation period animals were euthanized for study. Control animals included (a) normal bladder control (2 normal rats) for each ALA concentration and each time point; (b) background fluorescence (no drug) control (3 rats bearing orthotopic tumor and 3 normal rats), which received 0.5 mL of PBS intravesically and were sacrificed 2 h later.

Another group of rats (3 rats bearing orthotopic tumor and 2 normal rats) received 25 mM PpIX (14 mg/mL, 0.5 mL/rat) bladder instillation. PpIX (Sigma Chemical Co., St. Louis, MO. molecular weight 562.7) was solubilized in DMSO (dimethyl sulfoxide, Sigma Chemical Co., St. Louis, MO)/PBS (30%, v/v). The solution was placed in the bladder for 4 h prior to the animals being sacrificed.

PII obtained from QLT PhotoTherapeutics Inc. (Vancouver, BC) was dissolved in 5% dextrose (Abbott Laboratories, Ltd., Montreal, QC). The concentration of PII for i.v. injection was 5 mg/kg body weight, and for i.b. instillation ranged from 0.1 to 2 mg/mL. One group of rats received PII i.v. injection. Another three groups received PII bladder instillations of various concentrations (0.1, 0.5, and 2 mg/mL, 0.5 mL/rat). Each group included 3 rats bearing orthotopic tumors and 2 normal rats. The rats were euthanized at the end of the 4-h incubation. Previous studies suggested that absolute tissue PII levels reach the peak 3 – 4 h after i.v. injection, and that 1 h exposure of PII to the bladder mucosa seemed not long enough for PII uptake.[31,32]

2.2.4 *Fluorescence confocal microscopy.* Imaging and semi-quantification of fluorescence in sections of normal and tumor tissues were achieved using the confocal laser scanning microscope (CLSM). The CLSM system consisted of a Leitz Aristoplan Fluorescence Microscope illuminated by an mercury lamp for direct fluorescence observation and a 15 mW argon-krypton laser with major emissions at 488, 568, and 647 nm for fluorescence excitation scanning. At the end of the incubation period, normal and tumor tissues were harvested and rapidly frozen with dry-ice/methanol in a bed of OCT cryostat embedding compound (Tissue-Tek®, Sakura Finetek USA Inc., Torrance, CA) for tissue sectioning. Five consecutive 8-μm frozen sections were prepared with a cryostat (Miles Scientific Inc. Naperville, IL). Two adjacent sections were stained with hematoxylin and eosin (H&E) for histological analysis (tumor grade and stage) and tissue orientation, and the other three sections were examined by CLSM for PpIX or PII fluorescence analysis several hours after cutting (these sections were kept light-protected at 4°C prior to CLSM). Tissue sections were prepared in subdued light to avoid photobleaching. To further avoid photobleaching, the regions of interest were located using low intensity, bright-field illumination. For each sample parameter, 3 to 5 randomly chosen areas representing heterotopic tumor, orthotopic tumor, normal bladder urothelium, or muscularis in each of three tissue sections were selected, and images were stored on an optical disk for further analysis. Rapid observation and electronic data storage avoided significant photobleaching of the fluorescent porphyrins prior to quantitative analysis. Images were periodically acquired twice to test the effects of laser scanning on photobleaching. No significant diminution of the fluorescence intensity was observed for second scans, indicating that the conditions for image acquisition did not artifactually alter the true fluorescence intensity. Multi-user/multitasking image analysis software developed by *Leica Lasertechnik GmbH* (Heidelberg) was run on a Motorola 68030 CPU workstation, using the OS-9 operating system. For uniformity, all physical parameters pertaining to fluorescence excitation and detection were held constant throughout the study and are listed as follows: 25/0.75 oil-immersion

55

objective lens; KP590 short-pass excitation filter (excitation wavelengths primarily 488 and 568 nm); RSP510 beam-splitter; 590 nm long-pass barrier filter (fluorescence detection); photomultiplier voltage, 790 V; pinhole, 25; offset, -35; pixel size 0.391 x 0.391 μm. Regions of interest were delineated, and the fluorescence intensity was determined from the mean of 30 measurements of the integrated fluorescence intensity within regions of interest. The relative intensity of porphyrin fluorescence, which was used to represent relative tissue concentrations of PpIX or PII, was then corrected by subtraction for autofluorescence level of each respective tissue layer as measured on specimens from control animals to which no photosensitizer had been administered.

To determine factors that might affect tissue fluorescence during storage and processing of specimens, 8-to-10 consecutive sections of each tissue block were cut from several representative groups. These sections were kept protected from light at 22, 4, -20, or -70°C, and viewed with CLSM 3, 7, 14, or 21 days after sectioning. The fluorescence intensities were measured as described above.

2.2.5 *Statistical analysis*. One-way ANOVA test (Pharmacologic calculation system, version 4.2) was used to determine statistically significant differences among mean porphyrin intensities. The semi-quantitative data were analyzed among various sensitizer doses for each different time point. Tumor porphyrin intensities among different time points for each respective dose were also compared. Results were considered statistically significant at $p < 0.05$.

2.3 Results

2.3.1 Characteristics of the animal models.

The orthotopic AY-27 TCC bladder tumor is an excellent model for the human disease and its characteristics were summarized in the previous chapter.[16] In the present study, a total of 86 rats were inoculated with AY-27 cells intravesically. Of these, 4 died (2 due to anesthesia; 2 due to infection). Eighty-two rats remained available for PpIX or PII biodistribution studies. All 82-rat bladders were histologically examined by a series of tissue sections as described in the previous

56

section. The overall tumor establishment was 95% (harvested at 13 – 31 days), while in a group of animals sacrificed at 16 – 17 days, 64/66 animals (97%) developed TCC, the majority of which were superficial. Tumor stage was confirmed by gross pathology and light microscopy. Patchy carcinoma *in situ* could be detected histologically 13 days post-implant. Papillary tumor (papilloma) and invasive diseases developed thereafter. The changes seen on MRI correlated well with the extent of tumor invasion identified histologically.[16]

For the flank tumor model, the tumor growth of 3 mm^3 tumor chunks implanted bilaterally in the flanks was 100%. The tumors progressively grew to approximately 15 mm in diameter 4 weeks post-implant. The tumor-volume-doubling time was approximately 4 days. The tumors showed a smooth, well vascularized surface and thin capsule, with a zone of central necrosis.

2.3.2 Biodistribution of ALA-induced PpIX.

Figures 2.1 to 2.3 represent the relative tissue concentrations, expressed as relative fluorescence intensity of PpIX, at 2, 4, or 6 h following i.v. injection of ALA. When the ALA dose reached 250 mg/kg of body weight or greater, PpIX was selectively accumulated in flank tumor and bladder mucosa, while PpIX concentrations in bladder submucosa, muscularis, and abdominal muscle were just slightly higher than those of the background levels, which ranged from 4 to 8 units on the scale of 256 gray levels (Fig. 2.4a). In the 100 mg/kg dose groups, the tumor PpIX concentration was lower than that of the bladder mucosa, and was barely above the background. The greatest PpIX levels in tumor tissue occurred 4 h following ALA administration, and diminished gradually by 6 h post-injection. The tumor PpIX levels increased with increasing ALA dose. At 4 h, the tumor PpIX level in the 1000 mg/kg group was significantly higher than that in other groups (p < 0.01). Microscopically, the distribution of PpIX fluorescence was more uniform for the higher dose (500 and 1000 mg/kg) groups than for the 250 mg/kg group. In the latter group, the fluorescence was distributed in the tumor surface and scattered in deeper tissue as bright patches surrounded by tissue of lower fluorescence (Fig. 2.5a, b). The

57

Figure 2.1 Mean PpIX fluorescence levels (± SEM) in flank tumor and normal bladder wall 2 h after various doses of ALA i.v. injection. Each value represents the mean of 30 measurements. Single asterisks represent statistically significant (p < 0.01) values when compared with the flank tumor at the 1000 mg/kg dose. Double asterisks represent statistical values of p < 0.05 with respect to the same tumor reference. (a.u. = arbitrary fluorescence units).

58

Figure 2.2 Mean PpIX fluorescence levels (± SEM) in flank tumor and normal bladder wall 4 h after various doses of ALA i.v. injection. Each value represents the mean of 30 measurements. * Significantly different (p < 0.01) from flank tumor PpIX level in the 1000 mg/kg group. (a.u. = arbitrary fluorescence units).

59

Fig. 2.3. Mean PpIX fluorescence levels (± SEM) in flank tumor and normal bladder wall 6 h after various doses of ALA i.v. injection. Each value represents the mean of 30 measurements. (* $p < 0.01$, ** $p < 0.05$, compared with the flank tumor in 1000 mg/kg dose), (a.u. = arbitrary fluorescence units).

Fig. 2.4 Confocal images of, (a) normal bladder wall with background fluorescence (no drug); (b) bladder papilloma sensitized with 25mM (14 mg/mL) PpIX intravesically for 4 h, showing superficial, focal fluorescence distribution.
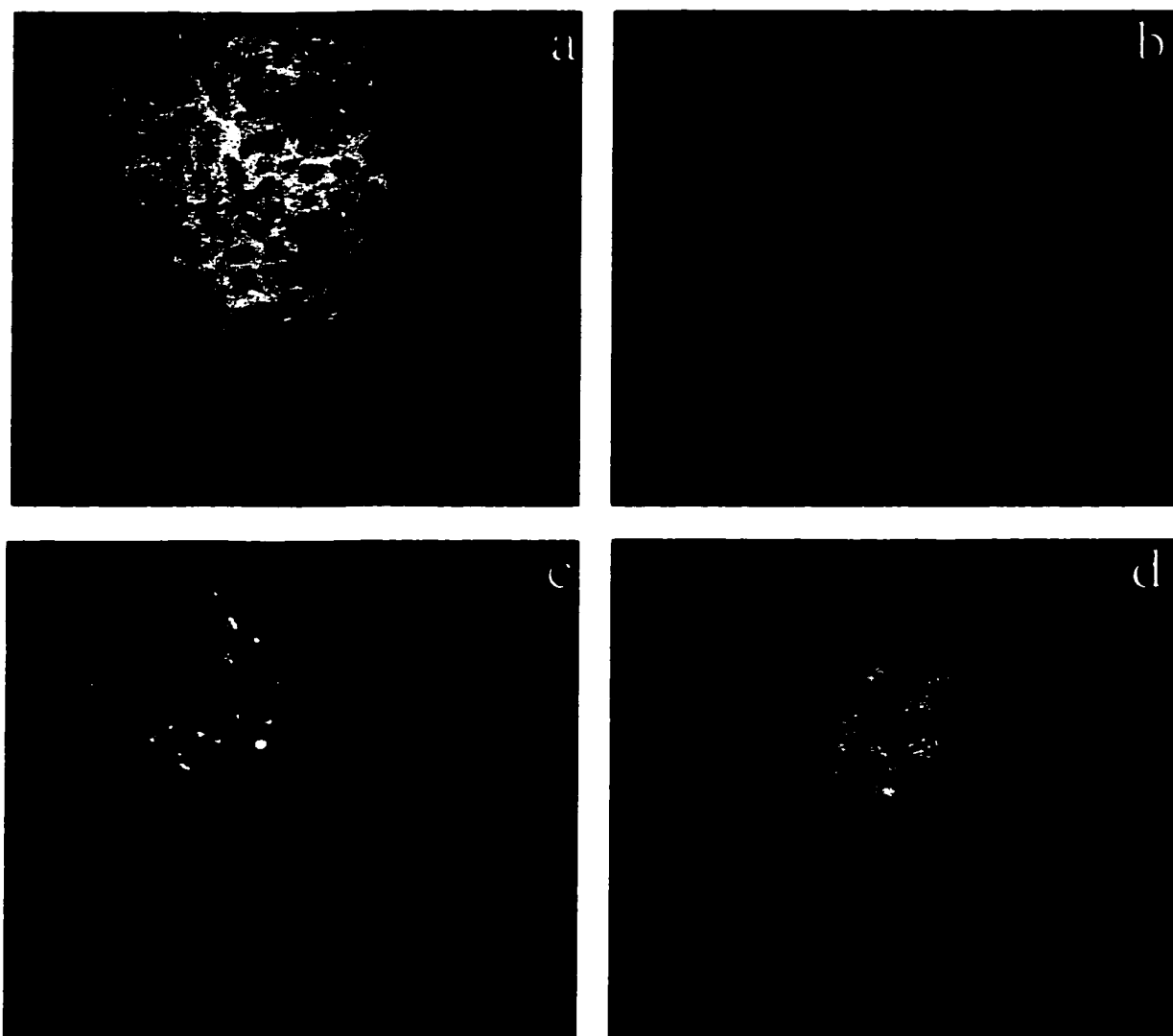
Fig. 2.5 Confocal images of, a) flank tumor sensitized with 1000 mg/kg; b) flank tumor sensitized with 250 mg/kg; c) normal bladder wall sensitized with 250 mg/kg; and d) orthotopic bladder papilloma (stage T2) sensitized with 1000 mg/kg of ALA intravenously for 4 h. (Bar = 25μm).

62

distribution pattern of PpIX in normal bladder mucosa differed from that in tumor. In general, the fluorescence distribution in bladder mucosa was more uniform than that in tumor (Fig. 2.5c). In the 100 mg/kg groups, the peak level of PpIX in normal urothelium occurred at 2 h, whereas in other groups, the peak PpIX levels plateaued between 2 and 4 h, and diminished by 6 h. The PpIX levels in bladder mucosa increased from 100 to 250 mg/kg, but remained relatively constant from 250 to 1000 mg/kg. The PpIX ratios of tumor-to-bladder mucosa increased from 1.2:1 in the 250 mg/kg group to 2.8:1 in the 1000 mg/kg group at 4 h (Table 2.1). The PpIX ratios of tumor-to-bladder muscle layer at 4 h were 3.4:1, 4.9:1, and 8.2:1 in 250, 500, and 1000 mg/kg groups, respectively (Table 2.1). Although the rats could tolerate the high ALA dose of 1000 mg/kg, at this concentration, the ALA solution is highly acidic, and must be infused very slowly.

Table 2.1 PpIX fluorescence intensity ratios of flank tumor to normal bladder tissues 2, 4, or 6 h following i.v. injection of ALA

ALA Dose (mg/kg)	Bladder Mucosa			Bladder Submucosa			Bladder Muscle		
	2 h	4 h	6 h	2 h	4 h	6 h	2 h	4 h	6 h
100	0.57	0.65	0.42	0.91	0.93	0.58	1.53	1.43	0.80
250	0.91	1.21	1.42	1.97	2.51	1.89	2.60	3.37	2.84
500	0.99	1.73	1.65	2.42	3.26	2.13	4.58	4.92	2.69
1000	1.05	2.77	1.52	2.40	4.58	2.74	3.18	8.24	5.04

Figure 2.6 depicts relative PpIX fluorescence intensities of orthotopic bladder tumor and normal bladder wall 4 h after ALA i.v. injection. The PpIX levels in bladder papilloma also showed a dose-dependent increase. The papilloma PpIX level in the 1000 mg/kg group was twice that in the 250 mg/kg group (p < 0.01). In the latter group, the tumor PpIX concentration was even slightly lower than that of normal urothelium. An ALA dose of 500 mg/kg significantly increases the PpIX concentration of the papilloma, with no evidence of augmented uptake and
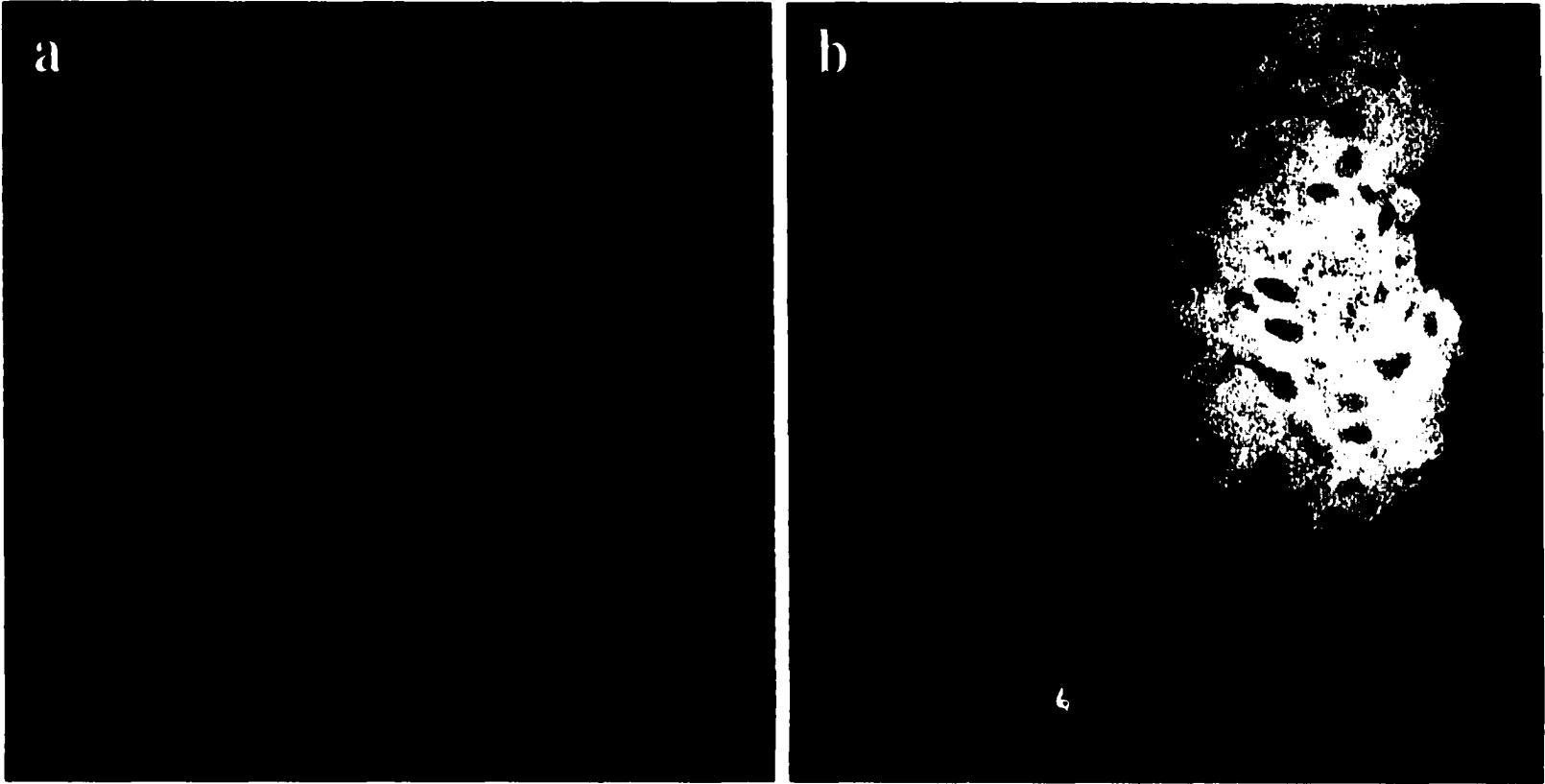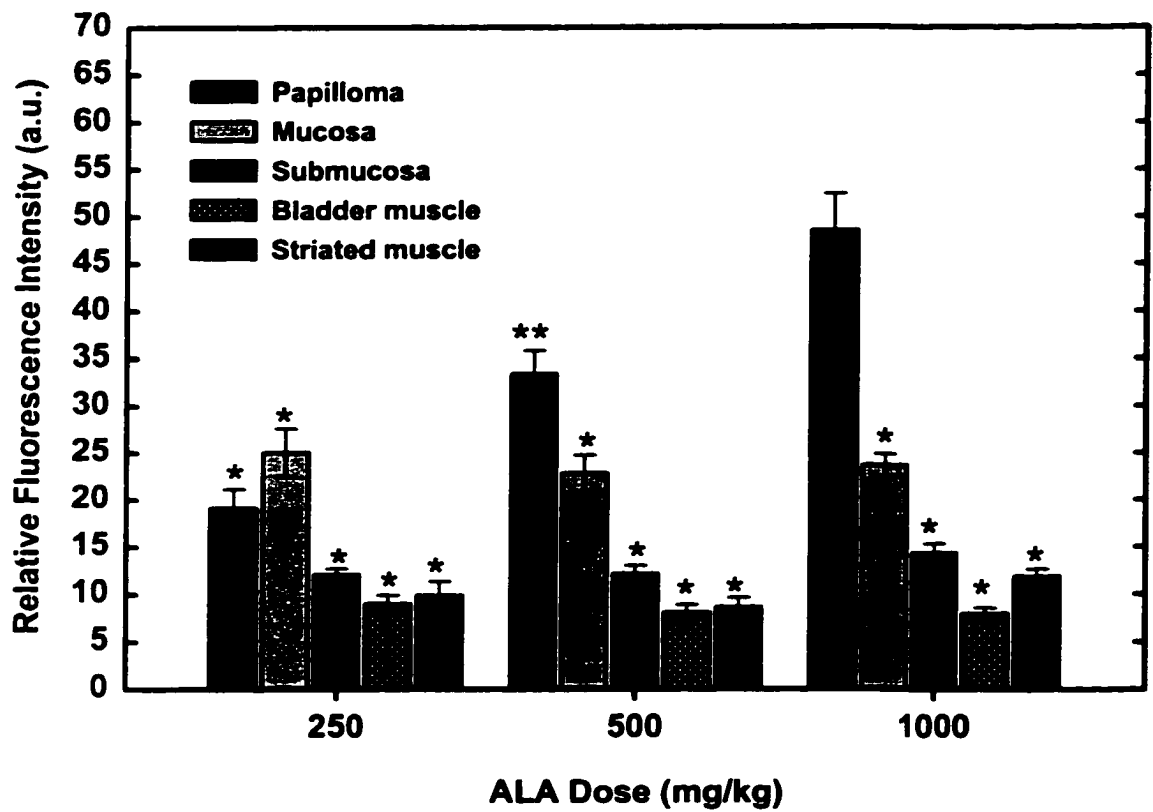
63

Figure 2.6 Mean PpIX fluorescence levels (± SEM) in orthotopic bladder tumors and normal bladder wall 4 h after various doses of ALA i.v. injection. Each value represents the mean of 30 measurements. (* $p < 0.01$, ** $p < 0.05$, compared with the papilloma level in 1000 mg/kg dose), (a.u. = arbitrary fluorescence units).

64

bioconversion in the deeper tissue layers. Microscopically, the PpIX fluorescence in invasive tumor appeared much brighter than in small, superficial tumors, especially in the 1000 mg/kg group. In this group, the PpIX level in superficial tumor was close to that in normal urothelium, while the PpIX intensity in invasive tumor approached that in flank tumor sensitized with the same dose (Fig. 2.5a, d).

Figures 2.7 to 2.9 demonstrate the kinetics of PpIX accumulation in orthotopic bladder tumors and normal bladder tissues 2, 4, and 6 h following i.b. instillation of ALA. It is evident that this administration route provides significant labeling of both tumor and bladder mucosa 4 h post-administration of 400 or 600 mM of ALA. The tumor PpIX level in 600 mM group reached its peak at 4 h, which was significantly higher than that in other groups (p < 0.01). By 6 h, levels of PpIX were diminishing in tumor and bladder tissues. Since PpIX levels were diminished by 6 h in both low and high dose groups, only several representative groups were tested for 6-h timepoint to save animals. There is a dose-dependent increase in PpIX intensity in both tumor and urothelium, without significant ALA conversion in submucosa, bladder muscularis, and abdominal muscle, for doses above 200 mM. At lower ALA concentrations (dose range, 5 – 200 mM), the tumor PpIX levels were just slightly above the background, and lower than those of the normal urothelium. The PpIX intensity in carcinoma *in situ* was usually slightly higher than that of the papilloma. Microscopically, only the tumor surface (approx. 5 – 7 cell layers) was labeled when rats received the lower ALA dose. When sensitized with a higher dose (600 mM), small tumor was evenly labeled from surface to deeper areas (Fig. 2.10a, b, c). Under these conditions however, the high osmolarity (1,100 mOsm) of the ALA solution was somehow toxic, with moderate blood vessel dilation and congestion in bladder submucosa observed in H&E-stained sections. The PpIX intensity ratios of papilloma-to-normal bladder tissues are summarized in Table 2.2. It is readily seen that no selectivity between tumor and urothelium exists, regarding PpIX accumulation. However, the tumor PpIX level was 3 and 5 times that in submucosa and muscularis in the 600 mM group.
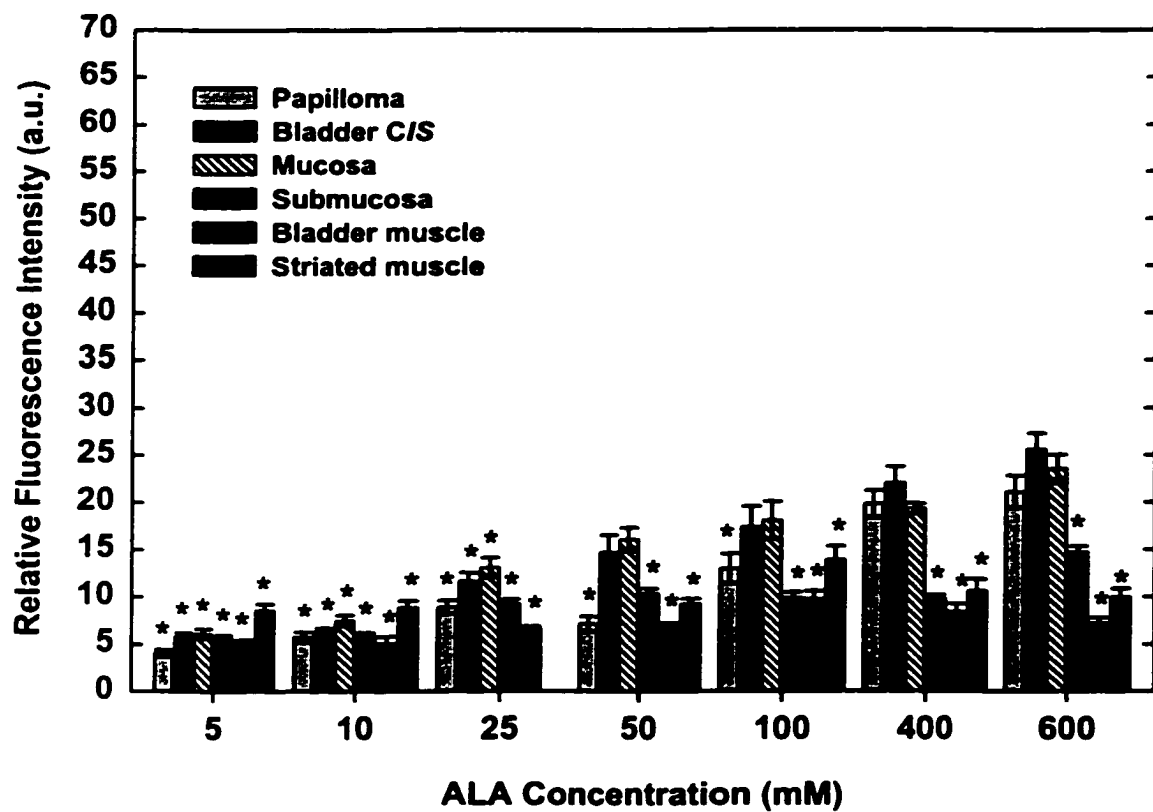
65

Figure 2.7 Mean PpIX fluorescence levels (± SEM) in orthotopic bladder tumors and normal bladder wall 2 h after various doses of ALA i.b. instillation. Each value represents the mean of 30 measurements. (* $p < 0.01$, compared with the papilloma in 600 mM dose), (a.u. = arbitrary fluorescence units).

Figure 2.8 Mean PpIX fluorescence levels (± SEM) in orthotopic bladder tumors and normal bladder wall 4 h after various doses of ALA i.b. instillation. Each value represents the mean of 30 measurements. * Significantly different (p < 0.01) from papilloma PpIX level in 600 mM group. The muscularis and submucosa within the 400 mM ALA dose group also had significantly less PpIX fluorescence than the bladder papilloma (p < 0.01 and 0.05, respectively), (a.u. = arbitrary fluorescence units).

67

Figure 2.9 Mean PpIX fluorescence levels (± SEM) in orthotopic bladder tumors and normal bladder wall 6 h following various doses of ALA i.b. instillation. Each value represents the mean of 30 measurements. * Significantly different (p < 0.01) from papilloma PpIX level in 600 mM group. (a.u. = arbitrary fluorescence units).
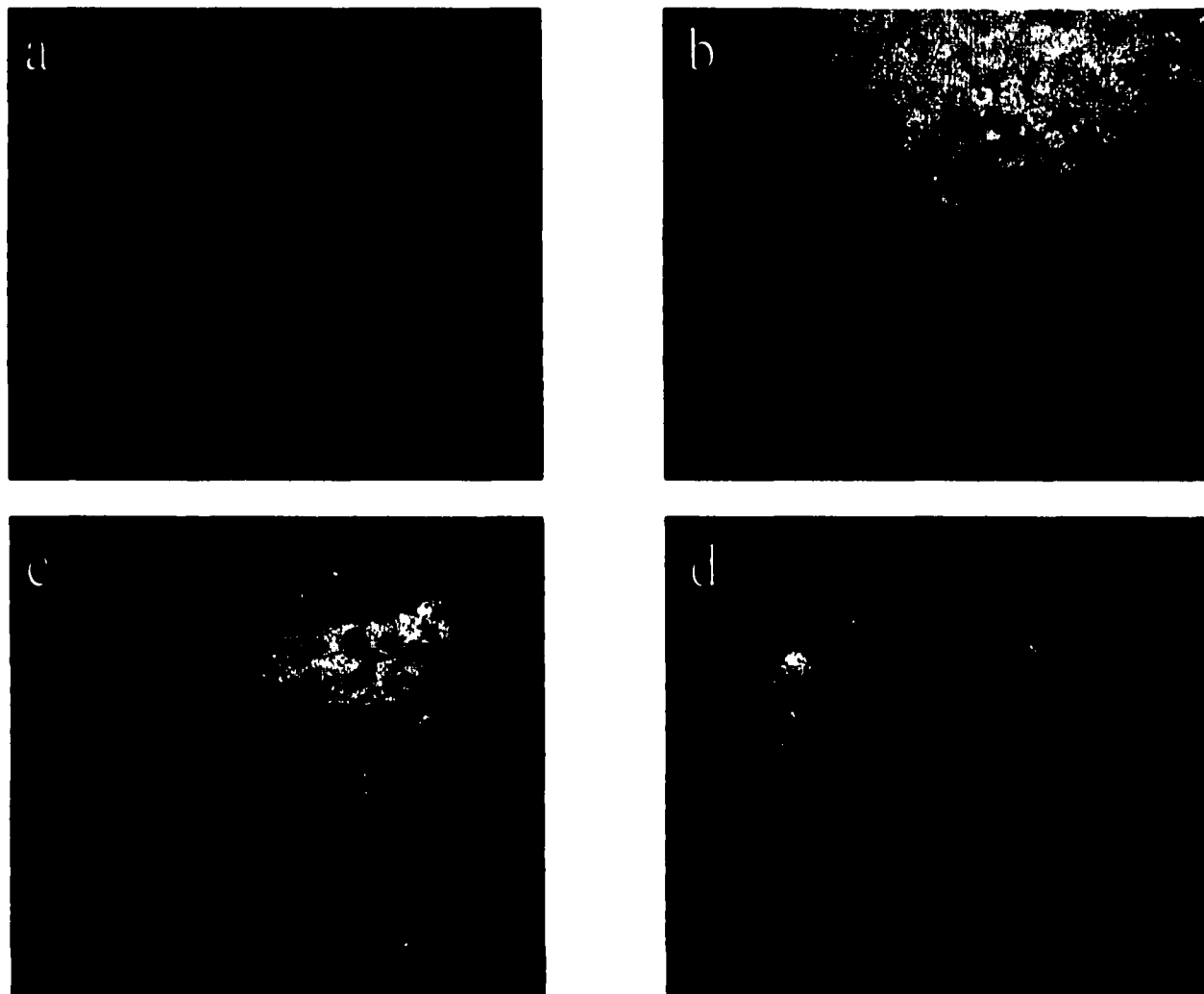
Fig. 2.10 Confocal images of, (a) bladder papilloma sensitized with 100 mM ALA; (b) & (c) bladder papilloma and carcinoma *in situ* sensitized with 600 mM ALA; and (d) bladder papilloma sensitized with 2 mg/mL Photofrin; intravesically for 4 h.

Table 2.2 PpIX fluorescence intensity ratios of bladder papilloma to normal bladder tissues 2, 4, or 6 h following i.b. instillation of ALA

[ALA] (mM)	Bladder Mucosa			Bladder Submucosa			Bladder Muscularis		
	2 h	4 h	6 h	2 h	4 h	6 h	2 h	4 h	6 h
5	0.67	0.60	–	0.71	0.55	–	0.9	0.75	–
10	0.76	0.82	0.78	0.72	1.14	1.23	1.12	1.51	1.04
25	0.68	0.84	–	0.96	1.23	–	1.35	1.38	–
50	0.44	0.75	0.85	0.68	0.96	1.55	1.06	1.33	1.65
100	0.71	1.01	0.94	1.31	1.49	1.50	1.33	1.63	2.20
200	–	1.35	–	–	1.56	–	–	2.07	–
400	1.03	1.01	–	2.04	2.05	–	2.35	4.27	–
600	0.91	1.19	1.23	1.46	3.35	2.39	2.97	4.73	3.20

2.3.3 Biodistribution of PII.

Figure 2.11 shows PII uptake in orthotopic bladder tumors, normal bladder wall, and abdominal muscle 4 h following either i.b. or i.v. administration of PII. After i.v. injection, the highest porphyrin intensity was seen in submucosa, followed by tumor, muscle, and with the lowest in urothelium. After i.b. instillation, there was a dose-dependent increase in porphyrin intensity in both tumor and urothelium, sparing submucosa and muscularis. Tumor porphyrin intensity in the 2 mg/mL group

Table 2.3 Porphyrin fluorescence intensity ratios of bladder papilloma to normal bladder tissues 4 h following Photofrin administration

Photofrin Dose (route) *	Bladder Mucosa	Bladder Submucosa	Bladder Muscularis
0.1 mg/mL (i.b.)	1.07	1.91	1.93
0.5 mg/mL (i.b.)	0.93	1.48	1.89
2.0 mg/mL (i.b.)	1.10	2.31	3.38
5.0 mg/kg (i.v.)	2.32	0.97	1.47

* i.b., intravesical instillation; i.v., intravenous injection.
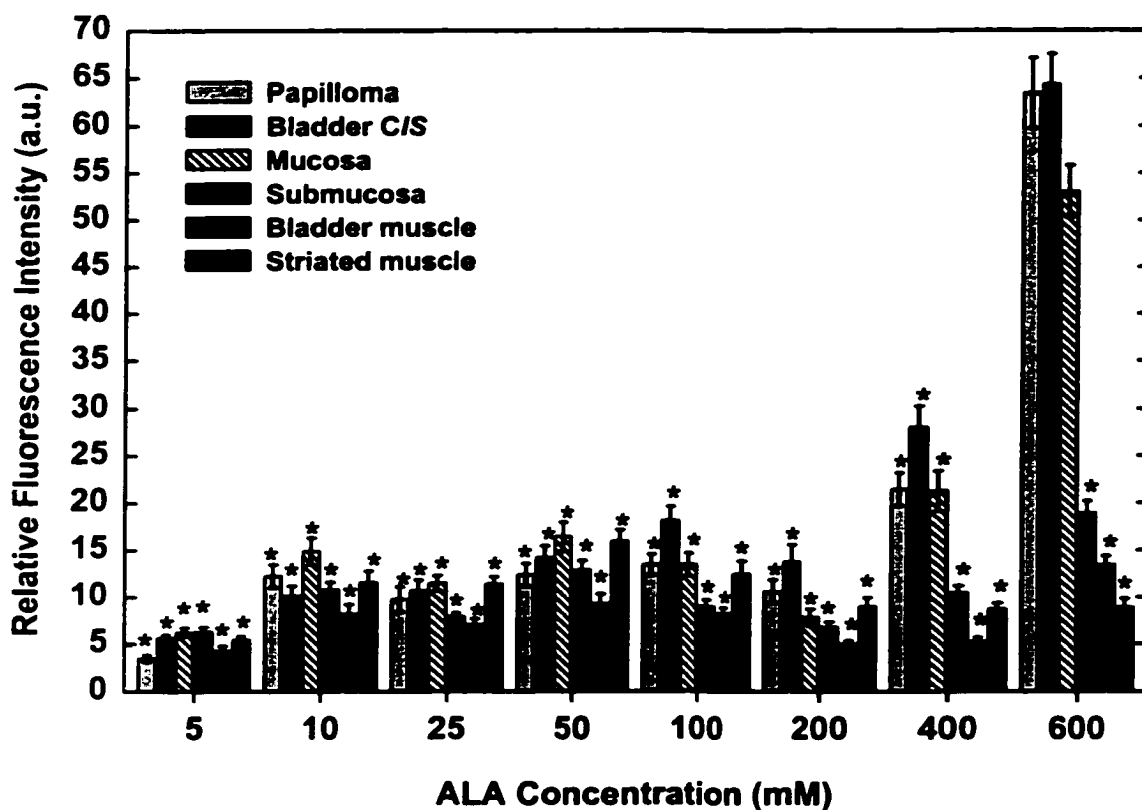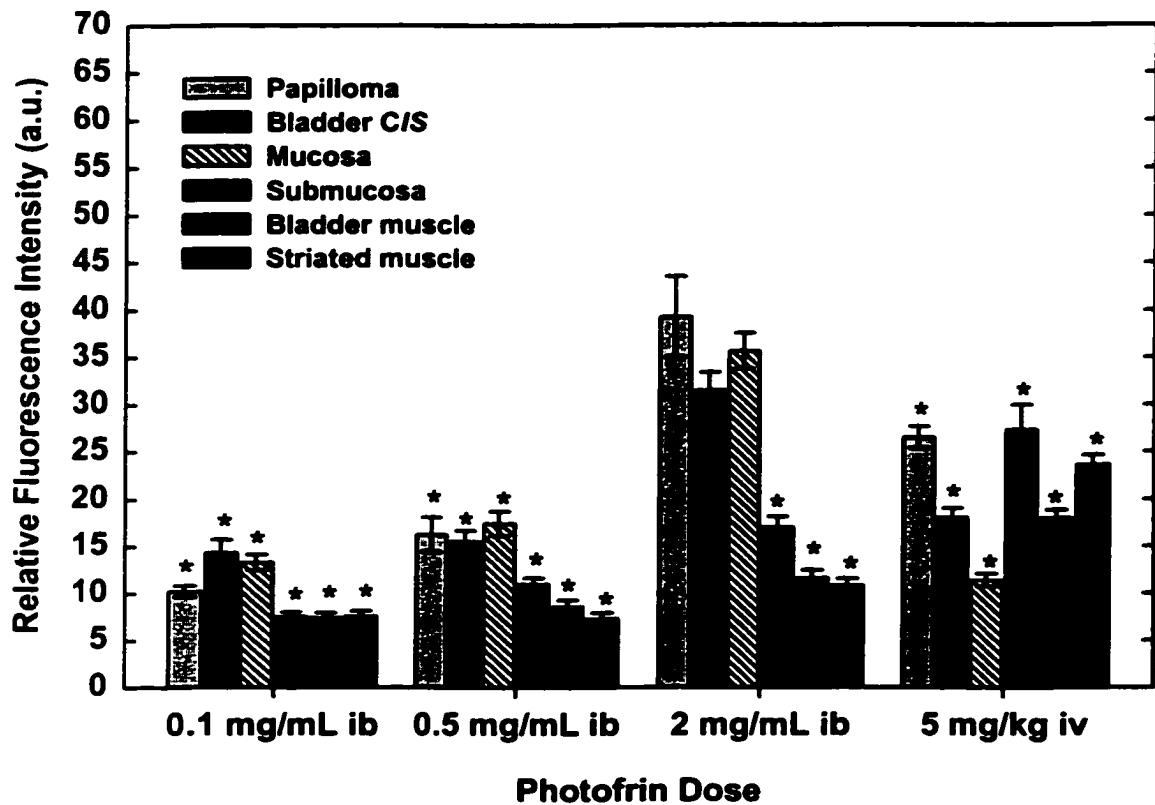
Figure 2.11 Mean porphyrin levels (± SEM) in orthotopic bladder tumors and normal bladder wall 4 h after various doses of PII i.b. instillation or 5 mg/kg of PII i.v. injection. Each value represents the mean of 30 measurements. * Significantly different (p < 0.01) from papilloma porphyrin level in 2 mg/mL i.b. group. (a.u. = arbitrary fluorescence units).

71

was significantly higher than that in other groups (p < 0.01), and was 3 times that of bladder muscularis (Table 2.3). Microscopically, after i.b. instillation the papilloma surface was labeled much brighter than deeper tumor tissue (Fig. 2.10d).

2.3.4 Biodistribution of PpIX.

After i.b. instillation of 25 mM (14 mg/mL) PpIX, the fluorescence distribution in both tumor and normal bladder was highly unpredictable. Some very bright areas were surrounded by totally dark tissue, and only the surface layers of tumor and urothelium were labeled (Fig. 2.4b). Since PpIX is very hydrophobic, 25 mM PpIX saturates, even in 30% DMSO-PBS. This may lead to formation of aggregates which somehow limits penetration.

2.3.4 Tissue handing factors affecting tissue PpIX level.

Table 4 shows tumor PpIX level changes in several selected groups after the sections were stored at different temperatures and time intervals. Both temperature and time had remarkable effect on tissue PpIX intensity. PpIX level increased to 2 and 5 times when sections were kept at 22°C for 3 and 7 days, respectively. PpIX values increased 3-fold when specimens were stored at 4°C from 14 to 21 days. PpIX content was relatively stable during 21 days when sections were kept at –20 or –70°C.

Table 2.4 Effect of temperature and storage time on PpIX fluorescence intensity in tumor tissue

[ALA] and Route	Biocon-version time	Tissue specimen storage time (days) and temperature											
		4°C				22°C		–20°C			–70°C		
		1	7	14	21	3	7	7	14	21	7	14	21
100 mg/kg.iv	4 h	7.8*	—	—	28.7	15.5	37.4	—	—	8.6	—	—	7.5
250 mg/kg.iv	4 h	32.1	—	—	—	—	—	32.6	—	—	29.7	—	—
500 mg/kg.iv	6 h	27.4	—	—	—	—	—	—	—	35.8	—	—	—
200 mM. ib	4 h	10.6	12.1	36.3	—	—	—	8.12	10.3	—	9.0	12.0	—

* Each PpIX value was derived from the mean of 30 measurements. Tissue sections were prepared as described in *Materials and Methods*.

72

2.4 Discussion

A strong correlation has been found previously between sensitive microfluorometric measurements and chemical extraction of tissue PpIX following ALA administration.[17] HPLC analysis of porphyrins extracted from the gastrointestinal tract and tumor has demonstrated that more than 95% of the porphyrin induced by ALA is PpIX in normal colon, stomach and tumor of rats.[17] The fluorescence emission spectra of ALA-sensitized rat stomach, colon, and skin of mice exhibited two emission peaks at 635 and 704 nm, with a maximum at 635 nm.[12,18,19] The advantage of using sensitive fluorescence microscopy over gross tissue extraction measurements has been addressed previously.[12,20] The distribution of photosensitizers in different layers of tissue section, rather than the whole organ, can be analyzed at the microscopic level. In order to destroy superficial bladder tumor while not damaging bladder muscle, thus preserving bladder function, the photosensitizer uptake in tumor and the ratio between tumor and normal bladder muscularis are of crucial importance. Neither gross tissue extraction measurements nor standard fluorescence microscopy can give this information.[20] Furthermore, not only does phototoxicity correlate with localized PpIX fluorescence,[11] but tissue fluorescence of porphyrin photosensitizers (PII) also reflects the photoactive monomers, not the inactive, non-fluorescent aggregates.[32] Thus, data obtained from fluorescence may be more relevant to photodynamic therapy than data obtained with radiolabelled substances.[32] The CLSM system we used is highly sensitive and suitable for detection and semi-quantitative analysis of photosensitizer fluorescence intensities in tissues. Many factors however, can influence the observed tissue fluorescence values. Among these are filter combinations; photomultiplier voltage; objective lens magnification and numerical aperture; offset (background contrast); and pinhole diameter applied. These parameters must be appropriately set and kept unchanged throughout the study, in order to maintain a constant relationship between fluorescence intensity and tissue concentration of the fluorescent compound. Differential quenching of fluorescence among tissues is a possibility, based on tissue-specific differences in interstitial pH

73

and biomolecular constituents.[21] This phenomenon is difficult, if not impossible, to control and must be considered in interpretation of the results.

Aggregation of the photosensitizers either as a result of their differential concentration within various tissues, or of local pH, ionic strength, or hydrophilicity, can influence the fluorescence yield. In addition, we also find both storage time and temperature affect tissue PpIX intensity dramatically (Table 2.4). The reason for this effect remains to be determined. In order to obtain reliable PpIX values, the tissue sections should be viewed as soon as possible, or kept at −70°C in the dark.

Following i.v. administration of ALA, the peak levels of flank tumor PpIX fluorescence are achieved at 4 h except for the lower dose (100 mg/kg) groups, and diminish by 6 h (Figs 1 − 3). Tumor PpIX intensity increases with increasing ALA dose (Fig. 2.2). PpIX levels in normal bladder mucosa peak between 2 and 4 h, and are not dose-dependent when the dose is greater than 250 mg/kg. Our data agree reasonably well with those of others.[18,22] Hua and colleagues reported that PpIX levels in subcutaneous rat mammary tumor were both time- and dose-dependent after i.v. injection of ALA.[22] Loh et al. showed that maximal tissue PpIX fluorescence in stomach, colon, and bladder mucosa was reached between 2 and 4 h after administration (both oral and i.v. injection).[18] The distribution pattern of PpIX in the orthotopic tumor model appears different from that in the heterotopic model. In the latter, smaller tumors are more strongly labeled than larger ones. In the former, however, the PpIX fluorescence in invasive bladder tumor shows much brighter than the superficial papilloma. The PpIX level in invasive bladder papilloma almost approaches that of flank tumor in the 1000 mg/kg groups (Fig. 2.5a, d), while the PpIX intensity in the superficial papilloma is close to that of normal urothelium. A possible explanation for this unanticipated finding is that while the intact basement membrane may limit ALA diffusion to superficial papilloma, invasive bladder tumor breaks down the basement membrane, and thus may be supplied by more aberrant neovasculature. This finding also suggests the orthotopic bladder tumor model may

74

be a more suitable model for PDT of bladder cancer than the heterotopic model, since the latter does not possess anatomic similarity to the clinical disease.

Our earlier studies supported the topical administration of ALA as a means of selective photosensitization of normal bladder epithelium.[23] These data encouraged us to continue examining ALA conversion to PpIX for both diagnostic and therapeutic photosensitization of bladder cancer after i.b. instillation. To our knowledge, this is the first systematic investigation of the biodistribution of ALA induced-PpIX in the orthotopic superficial bladder tumor model. The results of the present study show that i.b. administration of ALA provides comparable tumor labeling with the intravenous route (Figs 2.2, 2.8). ALA diffuses well across the glycosaminoglycan layer due to its cationic nature in urine and its low molecular weight. The mechanism of ALA absorption from the bladder is unknown. Previous studies showed that the bladder wall was at least as permeable as the small intestine and colon to many substances including amino acids.[24,25] ALA is thought to undergo similar absorption processes as amino acids from the alimentary tract.[18] The findings of the present study and those of others[27] suggest that the low molecular weight of ALA, a sufficient concentration gradient across the bladder wall, and the time of drug retention in the bladder, are important factors influencing the PpIX accumulation in both tumor and the bladder wall. For the timepoints tested, the optimal incubation period appears to be 4 h (Figs 2.7 – 2.9). At this time, bladder tumor cells exhibit maximal fluorescence with average levels that are approximately 3 times that of submucosa, and 5 times bladder muscle levels in the high dose group. However, we observed no evident differential between bladder tumor and normal bladder mucosa (Table 2.2). This agrees with the results obtained in the chemically induced rat bladder tumor model,[30] but disagrees with the clinical fluorescence cystoscopic findings by us (unpublished observation) and others.[26] Using violet light-aided cystoscopy, Kriegmair *et al.*[26] found that the tumor showed brighter fluorescence than the surrounding normal mucosa in patients instilled ALA solution before cystoscopic examination. The reason for this disagreement is unclear. There are several possible explanations: 1) Findings from

75

the rat tumor model suggest that PpIX fluorescence level is higher on the tumor surface than in deeper area of the tumor, while the distribution of PpIX fluorescence is more uniform through the depth of normal urothelium. Therefore the average PpIX levels in tumor are not significantly higher than those in urothelium. Clinical observations are viewed from the luminal surface, whereas we observed cross-sections of the bladder wall; 2) PpIX can be quickly bleached by ultraviolet light illumination. The normal urothelium is much thinner (2-3 cell layers when distended) than papillomas that accumulate more PpIX (absolute amount). Thus PpIX in normal urothelium might therefore be more readily bleached than that in tumor; 3) The species difference may also contribute to the discrepancy.

There is a dose-dependent increase above 200 mM, in both tumor and urothelial PpIX concentrations (Fig. 2.8). At lower doses (<200 mM), only the tumor surface is labeled. A high concentration of ALA appears important to drive drug into deeper cell layers of the tumor. However, the high ionic strength of ALA solution (600 mM) seems somewhat toxic to the thin, vulnerable rat bladder wall. Our data are consistent with previous work by Chang et al. who, using normal rats instilled with varying concentrations (0.1 – 10%) of ALA, found that the highest level of PpIX was accumulated in urothelium following 10% (~600 mM) ALA instillation.[27] They also reported some toxicity under this condition (edema of the bladder wall and intraperitoneal exudate).[28] However, compared to rat bladder, human urinary bladder is much thicker and may therefore be more tolerant to the ALA solutions. Patients with superficial bladder tumor treated intravesically with 16% ALA and whole-bladder irradiation at 15 to 60 J/cm^2 complained of occasional dysuria, macro-hemoturia and desquamation of tissue. No other severe complications were reported in this preliminary clinical trial.[29] Since a PpIX ratio of 5:1 between the urothelium and bladder muscle is sufficient to obtain selective destruction of the urothelium and sparing the bladder detrusor muscle,[27,28] a ratio of 5:1 between tumor PpIX level and muscle layer might be sufficient to selectively destroy the tumor without damaging the detrusor muscle layer. However, the tumor is much thicker than the normal

76

urothelium, and the tumor surface usually accumulates more PpIX fluorescence. This may partially explain why ALA-based PDT could previously achieve only incomplete tumor destruction.[30] The risk of incomplete tumor elimination could potentially be reduced by repeated PDT with i.b. administration of ALA. Since the urothelium can regenerate completely shortly after ALA-assisted PDT,[28] the lack of differential between tumor PpIX fluorescence and normal urothelium may not limit phototherapy of bladder cancer, but could limit differential diagnosis of the disease.

Porphyrin photosensitizers (PII) are usually given intravenously.[1] Cutaneous photosensitivity (lasting 6 – 8 weeks) and the risk of development of contracted bladder due to non-selective PII accumulation have been reported.[6] To avoid these undesirable complications, i.b. application of the photosensitizer would be preferable providing there is selective accumulation of the drug in tumor tissue. Previous studies of i.b. administration of PII in normal bladders were not encouraging[31,32] Our findings using the orthotopic rat superficial bladder tumor model strongly support the feasibility of i.b. instillation of PII for PDT of carcinoma *in situ* and small papillary tumors of the bladder. In contrast, after i.v. injection of PII, porphyrin fluorescence is seen mainly in the well-vascularized submucosa, followed by papillary tumor, bladder muscle, and urothelium. Thus direct and indirect cell killing (destruction of tumor vasculature) may be expected after i.v. administration, whereas following i.b. administration, a more direct mechanism of cell killing would be expected. Compared with our study, the previous PII bladder retention time was only 1 h.[31,32] Longer contact with the bladder mucosa and relative higher concentration of PII seem necessary for absorption by tumor. Our data are quite similar to the findings of Bachor *et al.* using Chloroaluminum tetrasulfophthalocyanine bladder instillation.[33]

Following i.b. instillation of PpIX, a patchy, irregular fluorescence distribution pattern is found in urothelium and tumor surface. The bladder mucosa is considered highly permeable to some lipophilic molecules.[25] However, the permeability can be reduced by ~76% in the presence of detergent to dissolve the highly lipophilic molecule.[25] This may be due to the formation of a thin luminal lining of adsorbed

77

detergent or mucopolysaccharide material.[25] This might partially explain why PII can be absorbed more evenly than PpIX by the bladder urothelium and tumor, because PpIX is more lipophilic than PII and requires a high concentration of DMSO solvent. PpIX may contain a larger fraction of aggregates or bigger micelles than PII, and the aggregates may reduce the availability of PpIX to the bladder, as well as penetrate less well than monomers into tissue.

In conclusion, i.b. administration of higher concentrations of ALA provides a feasible route for photosensitization of superficial bladder tumors. Although PpIX is not selectively accumulated in tumor, it is selectively accumulated in epithelial tissues (both tumor and normal urothelium), as opposed to detrusor muscle. Thus detrusor muscle damage and reduction of bladder capacity may be avoided. Our data also show that the biodistribution of ALA-PpIX in the orthotopic model differs from that in the heterotopic model. The former model may be more suitable for experimental treatment of bladder cancer due to its close similarity to the human counterpart.

The distribution patterns of PII within the orthotopic bladder tumors and rat bladder wall after i.b. and i.v. administration are different. Four hours after i.b. instillation of 2 mg/mL PII, porphyrin fluorescence is detected only in tumor and bladder mucosa, and tumor porphyrin intensity is significantly higher than that in 5 mg/kg PII i.v. group. While after i.v. injection, porphyrin fluorescence is detected mainly in the well-vascularized bladder submucosa and tumor stroma, as well as the muscularis. Thus i.b. instillation of PII may be an appropriate and safer route for PDT of superficial bladder cancer.

Further studies are required to evaluate optimal laser light dosimetry for effective PDT using the orthotopic rat bladder tumor model and the optimal photosensitization strategies determined above. Targeted delivery of photosensitizers may be necessary to improve tumor selectivity for both detection and treatment of bladder cancer.

78

2.5 References

1. Dougherty, T.J. and Marcus, S.L. (1992) Photodynamic therapy. *Eur. J. Cancer*. **28A**: 1734-1742.

2. Van Hillegersberg, R., Will, J.K. and Wilson, J.H.P (1994) Current status of photodynamic therapy in oncology. *Drugs*. **48** (4): 510-527.

3. Foote, C.S. (1991) Definition of type I and type II photosensitized oxidation. *Photochem. photobiol.*, **54**: 659.

4. Henderson, B.W. and Dougherty, T.J. (1992) How does photodynamic therapy work? *Photochem. Photobiol.*, **55**: 145-157.

5. Nseyo, U.O., Dougherty, T.J., Boyle, D.G., Potter, W.R., Wolf, R., Huben, R. and Pontes, J.E. (1985) Whole bladder photodynamic therapy for transitional cell carcinoma of the bladder. *Urology*. **26**: 274-80.

6. Harty, J.I., Amin, M., Wieman, T.J., Tseng, M.T., Ackman, D. and Broghamer, W. (1989) Complications of whole bladder dihematoporphyrin ether photodynamic therapy. *J. Urol*. **141**: 1341-1346.

7. Kennedy, J.C., Pottier, R.H. and Pross, D.C (1990) Photodynamic therapy with endogenous protoporphyrin IX: basic principles and present clinical experience. *J. Photochem. Photobiol. B*. **6**: 143-148.

8. Cairnduff, F., Stringer, M.R., Hudson, E.J., Ash, D.V. and Brown, S.B. (1994) Superficial photodynamic therapy with topical 5-aminolevulinic acid for superficial primary and secondary skin cancer. *Br. J. Cancer*. **69**: 605-608.

9. Regula, J., MacRobert, A.J., Gorchein, A., Buonaccorsi, G.A., Thorpe, S.M., Spencer, G.M., Hatfield, A.R. and Bown, S.G. (1995) Photosensitization and photodynamic therapy of esophageal, duodenal, and colorectal tumors using 5-aminolevulinic acid induced protoporphyrin IX - a pilot study. *Gut*. **36**: 67-75.

10. Van Hillegersberg, R., Willen, J., Van den Berg, O., Kort, W.J., Terpstra, O.T., and Wilson, J.H.P. (1992) Selective accumulation of endogenously produced porphyrins in a liver metastasis model in rats. *Gastroenterology*. **103**: 647-651.

79

11. Divaris, D.X.G., Kennedy, J.C. and Pottier, R.H. (1990) Phototoxic damage to sebaceous glands and hair follicles of mice after systemic administration of 5-aminolevulinic acid correlates with localized protoporphyrin IX fluorescence. *Am. J. Pathol.* **136**: 891-897.

12. Bedwell, J., MacRobert, A.J., Philips, D. and Bown, S.G. (1992) Fluorescence distribution and photodynamic effect of ALA-induced PpIX in the DMH rat colonic tumor model. *Br. J. Cancer.* **65**: 818-824.

13. Leveckis, J., Burn, J.L., Brown, N.J. and Reed, M.W.R. (1994) Kinetics of endogenous protoporphyrin IX induction by aminolevulinic acid: preliminary studies in the bladder. *J. Urol.* **152**: 550-553.

14. Olfert, B.M. Cross, and McWilliam, A.A. (1993) *Guide to the Care and Use of Experimental Animals,* Vol. 1, Second Edition and *Canadian Council on Animal Care.* Vol. 2. Bradda Printing Services Inc., Ottawa, Ontario.

15. Chin, J., Kadhim, S., Garcia, B. Kim, Y.S. and Karlik, S. (1991) Magnetic resonance imaging for detecting and treatment monitoring of orthotopic murine bladder tumor implants. *J. Urol.* **145**: 1297-1301.

16. Xiao, Z., McCallum, T.J., Brown, K.M., Miller, G.G., Halls, S.B., Parney, I. and Moore, R.B. (1999) Characterization of a novel transplantable orthotopic rat bladder transitional cell tumor model. *Br. J. Cancer.* (in press)

17. Loh, C.S., Vernon, D., MacRobert, A.J., Bedwell, J., Bown, S.G. and Brown, S.B. (1993) Endogenous porphyrin distribution induced by 5-aminolevulinic acid in the tissue layers of the gastrointestinal tract. *J. Photochem. Photobiol. B.* **20**: 47.

18. Loh, C.S., MacRobert, A.J., Bedwell, J., Regula, J., Krasner, N. and Bown, S.G. (1993) Oral versus intravenous administration of 5-aminolevulinic acid for photodynamic therapy. *Br. J. Cancer.* **68**: 41-51.

19. Pottier, R.H., Chow, Y.F.A., Lapainte, J.P., Truscott, T.G., Kennedy, J.C. and Beiner, L.A. (1986) Non-invasive technique for obtaining fluorescence excitation and emission spectra *in vivo. Photochem. Photobiol.,* **44**: 679-687.

20. Pope, A.J., MacRobert, A.J., Phillips, D. and Bown, S.G. (1991) The detection of phthalocyanine fluorescence in normal rat bladder wall using sensitive digital imaging microscopy. *Br. J. Cancer.* **64:** 875-879.

21. Spikes, J.D. (1992) Quantum yields and kinetics of the photobleaching of hematoporphyrin, Photofrin II, tetra(4-sulfonatophenyl)-porphine and uroporphyrin. *Photochem. Photobiol.,* **55(6):** 797-808.

22. Hua, Z., Gibson, S.L., Foster, T.H. and Hilf, R. (1995) Effectiveness of δ-aminolevulinic acid-induced protoporphyrin as a photosensitizer for photodynamic therapy *in vivo. Cancer Res.,* **55:** 1723-1731.

23. Moore, R.B., Miller, G.G., Brown, K., Bhatnagar, R., Tulip, J. and McPhee, M.S. (1995) Urothelial conversion of 5-aminolevulinic acid to protoporphyrin IX following oral or intravesical administration. *SPIE.* **2371:** 284-286.

24. Morris, C.R. and Bryan, G.T. (1966) Absorption of ^{14}C-labeled tryptophan, its metabolites, glycine and glucose by the urinary bladder of the mouse. *Invest. Urol.,* **3:** 577-585.

25. Bridges, J.W., Sargent, N.S.E. and Upshall, D.G. (1979) Rapid absorption from the urinary bladder of a series of n-alkyl carbamate: a route for the recirculation of drug. *Br. J. Pharmacol.* **66:** 283-289.

26. Kriegmair, M., Baumgartner, R., Knuchel, R., Stepp, H., Hofstadter, F. and Hofstetter, A. (1996) Detection of early bladder cancer by 5-aminolevulinic acid induced porphyrin fluorescence. *J. Urol.,* **155:** 105-110.

27. Chang, S.C., MacRobert, A.J. and Bown, S.G. (1996) Biodistribution of protoporphyrin IX in rat urinary bladder after intravesical instillation of 5-aminolevulinic acid. *J. Urol.,* **155:** 1744-1748.

28. Chang, S.C., MacRobert, A.J. and Bown, S.G. (1996) Photodynamic therapy on rat urinary bladder with intravesical instillation of 5-aminolevulinic acid: light diffusion and histological changes. *J. Urol.,* **155:** 1749-1753.

29. Kriegmair, M., Baumgartner, R., Lumper, W., Waidelich, R. and Hofstetter, A. (1996) Early clinical experience with 5-aminolevulinic acid for the photodynamic therapy of superficial bladder cancer. *Br. J. Urol.*, **77**: 667-671.

30. Stocker, S., Knuchel, R., Sroka, R. Kriegmair, M., Steinbach, P. and Baumgartner, R. (1997) Wavelength dependent photodynamic effects on chemically induced rat bladder tumors following intravesical instillation of 5-aminolevulinic acid. *J. Urol.*, **157**: 357-361.

31. Taari, K., Talja, M., Riihela, M., Rannikko, S. and Mokka, R. (1992) Morphological effects of photodynamic therapy on rabbit bladder using Photofrin II and Photosan intravesically and intravenously. *Br. J. Urol.*, **70**: 616-621.

32. Windahl, T., Peng, Q., Moan, J., Hellsten, S., Axelsson, B. and Lofgren, L. (1993) Uptake and distribution of intravenously or intravesically administered photosensitizers in the rat. *Cancer lett.*, **75**: 65-70.

33. Bachor, R., Hautmann, R., and Hasan, T. (1994) Comparison of two routes of photosensitizer administration for photodynamic therapy of bladder cancer. *Urol. Res.*, **22**: 21-23.

CHAPTER III

WHOLE BLADDER PHOTODYNAMIC THERAPY OF ORTHOTOPIC SUPERFICIAL RAT BLADDER CANCER: A COMPARATIVE STUDY BETWEEN INTRAVENOUS AND INTRAVESICAL ADMINISTRATION OF PHOTOSENSITIZERS

3.1 Introduction

Transitional cell carcinoma (TCC) comprises approx. 90% of all malignant tumors primary to the urinary bladder. The remaining 10% consist of other less common bladder cancers including squamous, adenocarcinoma, undifferentiated, and mixed carcinomas.[1] At least 70% of patients with TCC are diagnosed as superficial tumors (Ta, carcinoma *in situ*, T1) at their initial diagnosis.[1] The treatment of choice for superficial bladder cancer is transurethral resection of bladder tumor (TURBT). Up to 80% of these tumors cause a management problem with local recurrences. The risk for both recurrence and progression is related to tumor grade, depth of invasion, DNA ploidy, associated C/S and mucosal abnormalities. Intravesical chemotherapy and immunotherapy have been advocated for patients at high risk of tumor recurrence or progression. Intravesical chemotherapy has shown a decrease in short-term tumor recurrence rates, and can be beneficial in the treatment of C/S with reported complete response rates ranging from 34% to 42%. Bacillus Calmette-Guérin vaccine (BCG) is currently the most effective intravesical agent for the therapy and prophylaxis of superficial bladder cancer. Long-term follow-up studies have consistently shown prolonged protection from tumor recurrence.[2] Although BCG appears to have its highest efficacy rates in patients with C/S, a number of patients will fail or will relapse after an initial response. Furthermore, unlike chemotherapy, BCG is a living organism, which can produce local, regional, or systemic infection. In addition, like intravesical chemotherapy, BCG therapy requires a prolonged, repeated treatment protocol.[3]

Photodynamic therapy (PDT) was first introduced for the therapy of superficial bladder cancer by Kelly and Snell in 1976.[4] PDT was approved by Health Canada in 1993 for the prophylaxis and treatment of bladder cancer. Photofrin® is so

far the only photosensitizer approved for clinical use, and is administered by intravenous (i.v.) injection. A randomized study that addressed prophylaxis of superficial disease with PDT *versus* observation alone had recurrences of 39% and 81% in PDT and observation groups respectively. The median time to recurrence was 13 and 3 months respectively.[5] Patients with C*IS* who failed BCG therapy could respond well to PDT.[6] However, prolonged skin photosensitivity and end-stage bladder contracture are two major complications associated with whole bladder PDT.[7,8,9,10] These problems are possibly due to the poor tumor selectivity of Photofrin after systemic administration. The reduction of bladder capacity may be the result of bladder muscle damage with fibrous healing.[8] Previous biodistribution studies in animal models from our laboratory and others demonstrated that intravesical (i.b.) instillation of Photofrin might avoid or reduce these complications.[11,12,13] Another possible resolution for these side effects obviously lies on the discovery of improved photosensitizers. Ideally, these second generation photosensitizers should have simple molecular characteristics, and be cleared from normal tissues within a few hours to days. Endogenous protoporphyrin IX (PpIX), derived from 5-aminolevulinic acid (ALA), is such a photosensitizer. This novel approach, which combines short sensitizer half-life and topical applicability, was first introduced by Kennedy *et al*[14] for the treatment of skin cancers by using ALA. ALA is the first intermediate of the heme synthesis pathway,[15] the second last step of which is the production of PpIX. Under normal conditions the synthesis of heme is controlled by a feedback mechanism in which the presence of free heme inhibits the synthesis of ALA from glycine and succinyl CoA in mitochondria. However, an excess of exogenous ALA overcomes this negative feedback control mechanism and results in the transient intracellular accumulation of PpIX. Certain malignant cells may produce more porphyrins than their slower growing normal counterparts, leading to an increased accumulation of PpIX in tumor cells (see Figure 3.1).

Studies in rodents showed that after systemic ALA administration, selective accumulation of porphyrins (predominantly PpIX, with small amounts of

85

coproporphyrin) was found in surface-lining tissues such as epidermis, mucosae of bladder and gastrointestinal tract, endometrium *etc.*, but not in underlying muscle layers.[16,17,18] Relatively selective porphyrin accumulation in tumor has also been reported.[19] ALA-induced PpIX is rapidly eliminated from the body when ALA is given systemically, therefore, the risk of skin photosensitivity is limited to 24 hours.[20,21]
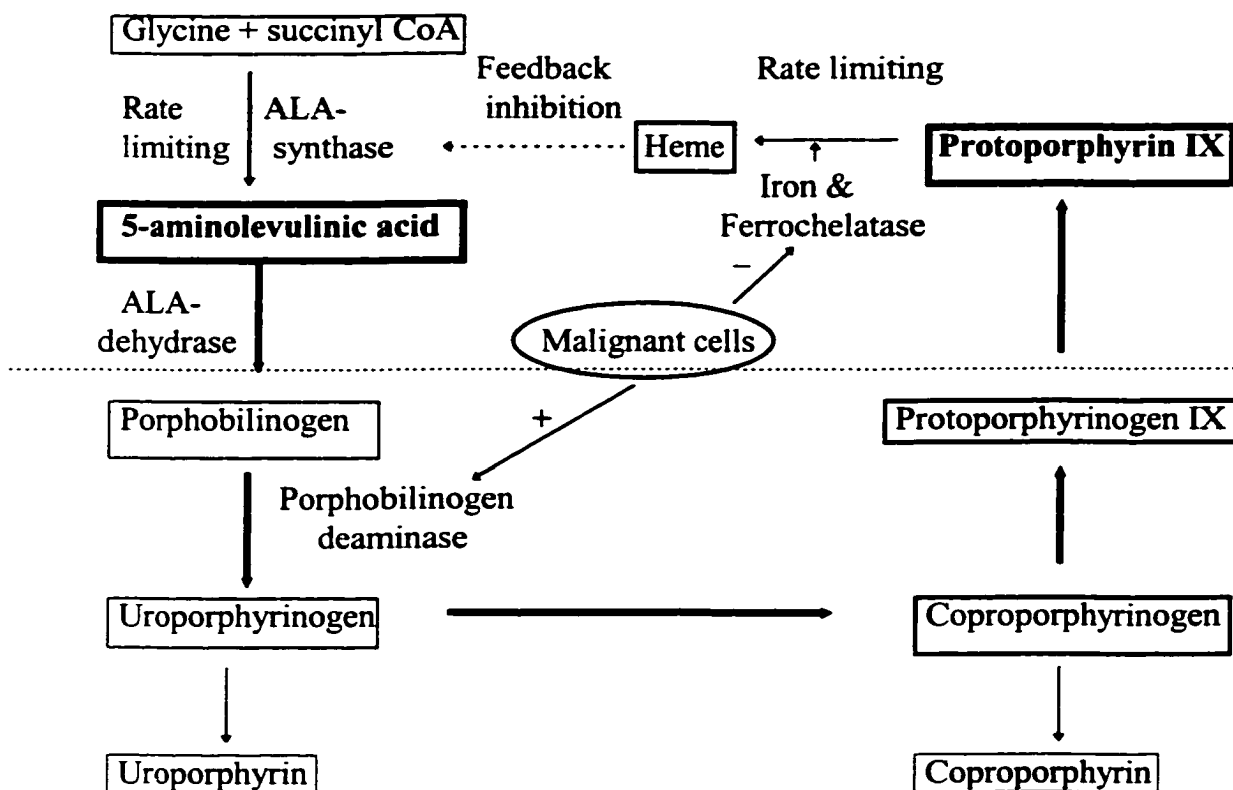
Figure 3.1 Schematic biosynthetic pathway of heme. The first intermediate is 5-aminolevulinic acid (ALA), which is formed by the condensation of glycine and succinyl CoA. This rate-limiting step can be bypassed by administration of exogenous ALA at high concentrations. Therefore, protoporphyrin IX (PpIX), which is the potential photosensitizer, is synthesized and accumulated in cells. Reactions above the dotted line take place in the mitochondria. Others take place in the cytosol.

Preliminary clinical results of whole bladder PDT after intravesical ALA instillation did not show any sign of bladder contracture.[22] According to our biodistribution studies in the orthotopic model, tumor PpIX levels are comparable between i.v. injection and i.b. instillation of ALA (see chapter II).[11] In this study, the

86

photoefficiency and phototoxicity of intravesical Photofrin or ALA-induced PpIX in the orthotopic superficial bladder tumor model were investigated, and compared with that of intravenous Photofrin. The feasibility of i.b. administration of sensitizers for PDT of bladder cancer has been discussed.

3.2 Materials and methods

3.2.1 Tumor cells. AY-27 cells from a rat bladder TCC cell line were grown in RPMI-1640 culture medium (Gibco/BRL) supplemented with L-glutamine and 10% fetal calf serum and antibiotics (1%, v/v). Cells were incubated at 37°C in a 5% CO_2 humidified atmosphere. In order to maintain the phenotypic characteristics, the cells were periodically transplanted in syngeneic Fischer CDF344 rats as a solid subcutaneous tumor.

3.2.2 Animal model. All animal procedures were performed in compliance with Canadian Council on Animal Care Guidelines and approved by the local Animal Care Committee of the Cross Cancer Institute. Female Fischer CDF344 rats (150-180 grams) were obtained from Charles River, Canada, and subsequently bred in the Cross Cancer Institute Vivarium. They were utilized as recipients for the orthotopic bladder tumor implantation. The procedures to establish the orthotopic bladder cancer model have been described in detail in the previous chapters. Briefly, the rats were anaesthetized with a combination of ketamine (50 mg/kg body weight, MTC Pharmaceuticals, Cambridge, ON) and xylazine (7.5 mg/kg body weight, Miles Canada Inc. Etobicoke, ON) given by intraperitoneal (i.p.) injection. When the rat reached anaesthetic surgical plane, the bladder was accessed *via* the urethra with an 18-gauge plastic intravenous cannula (Becton Dickinson Inc., Sandy, Utah). And the bladder mucosa was pre-conditioned with 0.4 mL of 0.1 N HCl for 15 seconds and neutralized with 0.4 mL of 0.1 N KOH for 15 seconds, then bladder was immediately flushed with sterile phosphate-buffered saline (PBS). After the bladder mucosal conditioning, a 0.5 mL of cell suspension containing 1.5 x 10^6 AY-27 cells was instilled into the bladder and left indwelling for one hour. After one hour the catheter was removed and the rat was allowed to void the cell suspension. The rats were

87

housed in standard cages and monitored daily for overall health status. With this tumor implantation procedure, more than 95% of the rats developed tumor, and the majority of these tumors were stage T1 or C*IS* approximately two weeks post-implantation (see previous chapters). Thirteen days post-implantation the rats were randomized into different treatment groups: a) true control (no sensitizer, no light); b) light only control (100 J/cm^2, no sensitizer); c) drug only control (0.5 mL of 300 m*M* ALA instillation, no light); d) Photofrin-i.v.-50 J/cm^2; e) Photofrin-i.v.-100 J/cm^2; f) Photofrin-i.b.-50 J/cm^2; g) Photofrin-i.b.-100 J/cm^2; and h) ALA-i.b.-75 J/cm^2.

3.2.3 Administration of Photofrin and ALA. Photofrin was supplied from QLT PhotoTherapeutics Inc. (Vancouver, BC) as a lyophilized powder. The same batch (Lot # DP-73) of the drug was used throughout the study. The Photofrin powder was dissolved in 5% dextrose (Abbott Laboratoties, Ltd., Montreal, QC) and filtered by a 0.20 µm sterile filter (Corning, NY) immediately before use. The concentration of Photofrin for i.v. injection was 5 mg/kg body weight, and for intravesical instillation was 2 mg/mL. For i.v. injection, animals were sedated by Metofane inhalation (Janssen Pharmaceutica, North York, ON), and the Photofrin solution (approx. 0.5 mL) was injected into the tail vein. Animals were allowed to recover (in approx. 5 minutes) and were protected from bright light in the following 3 days. For bladder instillation, the rats were anesthetized by i.p. injection of Ketamine and Xylazine, 0.5 mL of Photofrin solution was instilled *per urethra via* an 18-gauge plastic cannula, and 2 hours later, the bladder was emptied, another 0.5 mL of Photofrin was refilled to avoid dilution of the drug and over-distention of the bladder. Four hours after administration of Photofrin, the bladder was gently washed with PBS, and irradiated with 630 nm light.

ALA was supplied as a hydrochloride salt (Sigma Chemicals Co., St. Louis, MO). ALA powder (molecular weight 167.6) was dissolved in PBS (Sigma Chemicals Co.) and filtered by a 0.20 µm sterile filter (Corning, NY). The pH of the ALA solution was adjusted between 6.0 and 7.0 with 5 *N* NaOH immediately before use. The ALA concentration was 300 m*M* (approx. 50 mg/mL) except as stated

88

otherwise. With the rats anesthetized by i.p. injection of Ketamine and Xylazine, 0.5 mL of ALA solution was instilled into the bladder. Approx. 2 hours later, the bladder was emptied and another 0.5 mL of ALA solution was re-instilled to avoid dilution of the drug. Four hours after initial ALA instillation, the bladder was irradiated with 630 nm laser light.

3.2.4 In vitro light distribution. The entire bladder mucosa needed to be irradiated with uniform illumination to treat the multifocal bladder tumors (whole bladder PDT). Whole bladder PDT may be achieved by using a special optical fiber with a spherical diffusing tip,[9] or by instilling a light scattering medium into the bladder when an optical fiber with a flat-cleaved tip is used.[23] In this study the flat-cleaved tip fiber was used because of the relatively small urethral caliber of the rats and less cost than the fiber with spherical diffusing tip. To understand light distribution in the rat bladders, a locally constructed glass bulb (Technical Services, University of Alberta, Edmonton) was used as a model of the rat bladder. The bulb's volume was approx. 0.5 mL with a diameter of 1.1 cm. Therefore both the shape and the volume of the glass bulb approximated the rat bladder filled with 0.5 mL of light scattering medium (in this case, intralipid). The bulb was filled with graded concentrations (0 – 1%) of intralipid/saline (v/v) and fixed on the optical bench with a transition stand. A silicon coated 400-μm quartz laser fiber with flat-cleaved tip, which basically delivered light in a forward direction only, was fixed by the same stand as the glass bulb, so that the quartz fiber could be inserted into the glass bulb along its axis. This delivery (source) fiber was coupled to the argon-pumped dye laser which was tuned to 630 nm with power output of 100 mW at the fiber tip (Coherent, Inc., Palo Alto, CA). A detector fiber was fixed perpendicularly to the source fiber and connected with an integrating sphere-61 optometer (Model 2500, United Detector Technology, Hawthorne, CA). The light intensity on the glass bulb surface at different directions was measured when the source fiber was inserted into the glass bulb at 1, 3, 5, or 7 mm, respectively (Figure 3.2). These studies showed

Source fiber
(coupled to 630 nm →
laser light)

1

Glass bulb
(filled with →
0–1% intralipid)

.... **2**

Detector fiber
(positioned at →
1, 2, 3, or 4)

3

4
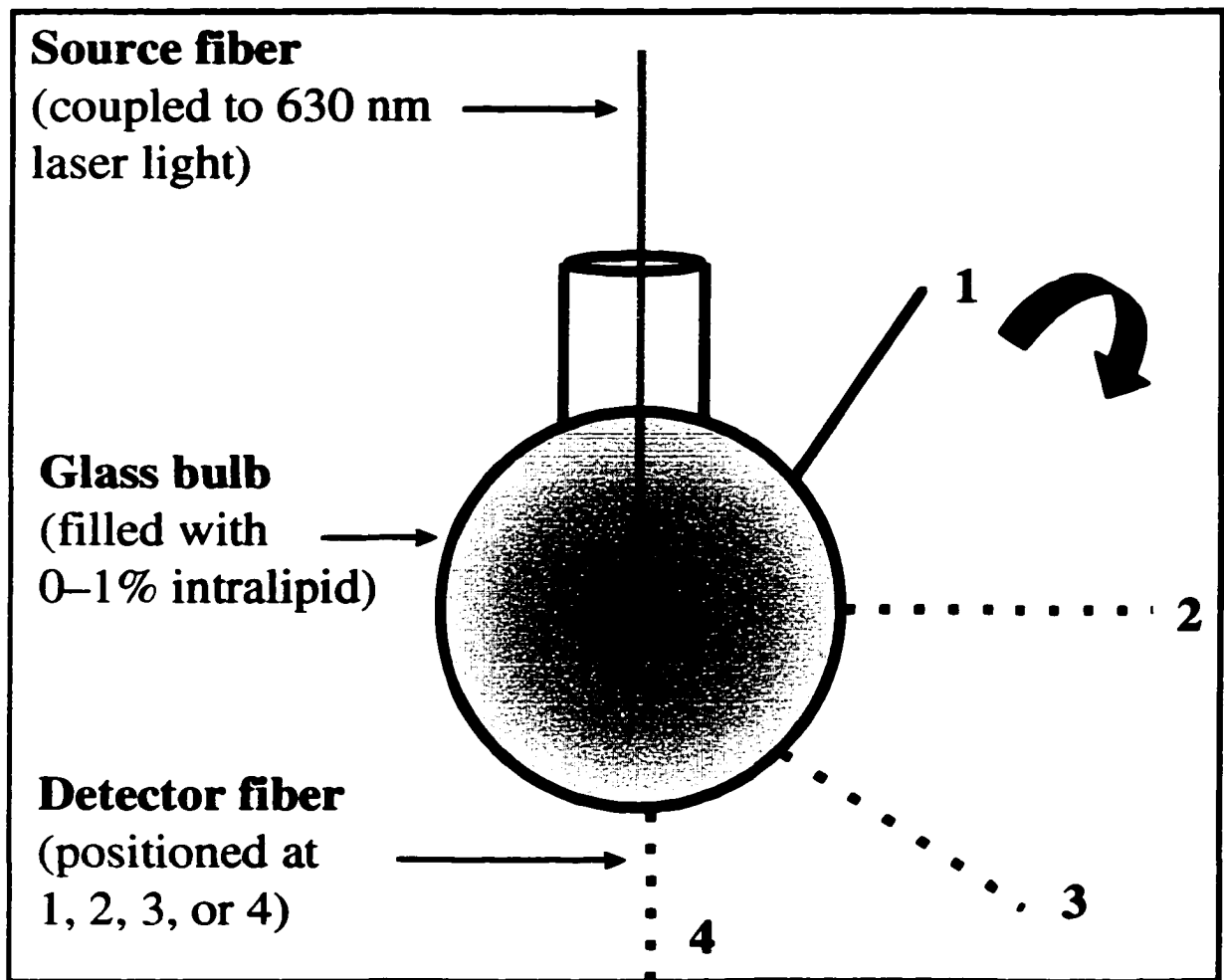
Figure 3.2 The schematic of *in vitro* measurement of light distribution.

that when the source fiber tip was located at the mid-point of the glass bulb filled with 1% intralipid, the light distribution in all directions was almost homogeneous.

3.2.5 Setup of whole bladder PDT. Figure 3.3 depicts the setup of whole bladder PDT. Four hours after administration of drugs, the rats were anaesthetized with Ketamine and Xylazine and catheterized with a 16G plastic i.v. cannula. This cannula fit perfectly to allow snug passage of the silicon coated 400-μm quartz fiber into the bladder, with sufficient distention of the urethra, so that no leakage occurred during laser therapy. After flushing with PBS, the bladder was filled with 0.5 mL of 1% intralipid *via* a urethral cannula. The cannula was lightly clamped by a small hemostat and the optical fiber with a flat-cleaved tip was then inserted into the bladder with the tip positioned at the mid-point of the long axis of the bladder. This was done by measuring the length between the bladder dome and the end of the cannula (A), and the length between the suprapubic rim (corresponding to the bladder neck) and the end of the cannula (B). The difference between (A) and (B) was the length of the bladder (long axis) (C). The length of (C) was approximately 1.5 cm when the bladder was filled with 0.5 mL of intralipid. Therefore, the measured length of B + ½C was assumed the mid-point of the bladder. However, it was very difficult to position the fiber tip in the true anatomic center of the bladder, especially in the anterior-posterior direction. The optical fiber was coupled to the argon-pumped Kiton red dye laser which was tuned to 630 nm with power output of 90 mW at the fiber tip. This was verified each time before and after PDT by a power meter (LaserTherapeutics, Inc., Buellton, CA). Hyperthermic effects on tissue induced by PDT using 90 mW/fiber are negligible.[24,25] The light doses for rats receiving Photofrin were 50 or 100 J/cm^2, and for rats receiving ALA was 75 J/cm^2. The latter was based on a pilot study of light-dose escalation, in which animals receiving 300 mM or 600 mM ALA instillations were irradiated with graded light doses from 15 to 100 J/cm^2. Animals (n = 6) treated with 300 mM ALA and 15 to 25 J/cm^2 died of tumor progression 44 days post-implantation (31 days post-PDT). Animals (n = 6) survived 65 days (52 days post-PDT) when irradiated with 50 to 75 J/cm^2, and no rat
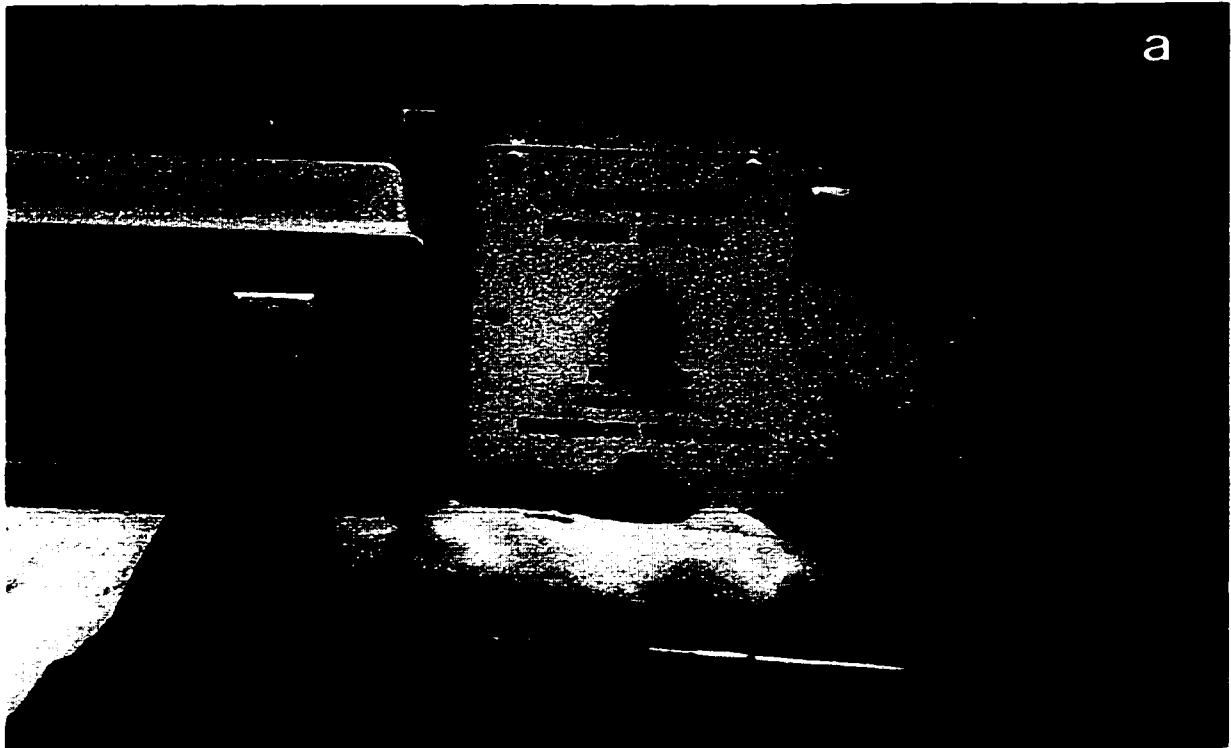
91

Figure 3.3 Setup of whole bladder PDT of rats bearing orthotopic bladder tumors. (A) The bladder was catheterized and filled with 0.5 mL of 1% intralipid, and the laser output at the fiber tip was checked before and after each session. (B) The fiber was inserted into the bladder *per urethra* and positioned in the center of the bladder.

92

died of PDT complications. Rats treated with 300 mM ALA and 100 J/cm^2 irradiation had similar survival time to those irradiated with 75 J/cm^2. One-third (3 out of 9) of the animals treated with 600 mM ALA and 100 J/cm^2 irradiation died of PDT complications (*i.e.* bladder wall damage).

Since the bladder shape is not exactly spherical, the bladder surface area, the treatment time, and the light dose were calculated according to a standard formula with the following parameters:[6]

Intended Dose = D_i [J/cm^2]

Laser Power at Fiber Tip = P_{tip} [watts]

Bladder Treatment Volume = BV [mL]

Surface area (SA) = 4.83 (BV)$^{2/3}$ [cm^2]

Power Density (P_{dns}) = P_{tip}/SA [W/cm^2]

Treatment Time = D_i/P_{dns} [seconds]

The calculated surface area of the rat bladder filled with 0.5 mL of 1% intralipid solution was 3.043 cm^2 (*i.e.* 4.83 × (0.5)$^{2/3}$). This area was used to calculate the power density (*i.e.* 0.090/3.043). Treatment times ranged from 28.1 min to 56.2 min, to yield incidental light doses of 50 J/cm^2 to 100 J/cm^2. If irradiated for longer than 30 min, the bladder was emptied of intralipid 28 min after initial illumination, and refilled with 0.5 mL of fresh 1% intralipid to keep the bladder volume relatively constant. To prevent systemic infection from the urinary tract resulting from the procedures of PDT, the rats were injected (i.p.) with Ampicillin (50 mg/kg) 4 hours prior to and post PDT, and once a day for 4 days thereafter.

3.2.6 Urodynamic assessment of bladder compliance. In order to examine whether rat bladder compliance changed after whole bladder PDT, a filling cystometrogram was performed using a modified Vitatek® electrocardiogram/blood pressure monitoring apparatus (Hillsboro, Oregon). This pressure monitoring system comprised a 10-cc syringe mounted on a syringe pump (Sage pumps, Orion Research Inc., Boston, MA), which can be set up for different filling speeds; a pressure transducer; and a display monitor which displays both digital and linear recordings of

93

pressure. A 'Y'-tubing arrangement enabled the syringe to continually fill the bladder, while the bladder pressure was simultaneously measured with a transducer which was connected to the display monitor. Immediately prior to and 14 days post tumor cell implantation, and every 30-days post PDT, the rats were catheterized with an 18G catheter (under anesthesia), placed supine on the low energy general-purpose collimator of a General Electric 400 AC gamma camera head. The bladder was emptied of urine and the catheter was connected to the 'Y'-tube to allow the syringe to constantly fill the bladder (0.1 mL/min) with ^{99m}Technetium (^{99m}Tc) diluted with saline (10 MBq/mL) up to one mL or until the bladder pressure reached 30 mm Hg. The ^{99m}Tc was used to monitor vesicoureteric reflux. At 30-second intervals, the average values of the bladder pressure of each treatment group were taken to create a compliance curve (pressure *vs.* filled bladder volume). Statistical differences among these curves were analyzed by non-linear regression (exponential growth) test (GraphPad Prism™, version 2.0, San Diego, CA). At the same time as bladder pressure measurement, the dynamic change of the bladder volume and any vesico-ureteric reflux were imaged by the gamma camera. The data were stored and analyzed by a Picker Odyssey computer.

3.2.7 Histopathology. After phototherapy, all rats were monitored carefully for any signs of distress, hematuria, urine retention, abdominal mass, and body weight changes. Animals surviving 80 days after tumor implantation (67 days post PDT) were defined as long-term survivors (LTS). Previous experiments in this laboratory showed that without treatment, rats could only survive from 22 to 56 days (average 41 days) post implantation.[26] The rats were sacrificed 67 days post PDT except those that had to be terminated earlier due to PDT complications or tumor progression. Necropsy was performed on all rats. The bladders were excised immediately after sacrifice. The extent of tumor burden within the bladder was evaluated by gross and microscopic examination. The bladders were opened longitudinally, fixed in 10% buffered formalin, embedded in paraffin, and cut at 4-μm from the central part of the bladder. Sections were stained with hematoxylin and eosin (H&E) for histology, and

94

with Masson Trichrome[27] (M.T.) to assess collagen deposition during healing. The kidneys and ureters were also routinely sent for histologic examination. In the presence of bladder tumor(s), organs within the cranial, thoracic and peritoneal cavities were carefully examined. Lymph nodes in the pelvis and tissues with suspected tumor metastasis were taken for histologic examination.

3.2.8 Statistical analysis. Plots of survival distributions for the different treated groups as well as controls were generated according to the Kaplan-Meier method. The log-rank test (SAS® Proprietary Software, 1996, SAS Institute Inc., NC, USA) was used to compare the survival curves between each treated group and the control.

3.3 Results

3.3.1 Hematuria and weight loss

Hematuria was seen in almost all the animals treated with i.v. injection of Photofrin and irradiation, while only in a few animals treated with bladder instillation of either Photofrin or ALA and irradiation. Hematuria ceased 3 to 5 days after PDT if there was no tumor progression. Light or drug alone did not result in hematuria. All animals treated with i.v. injection of Photofrin and phototherapy became clinically ill and lost weight in the first week post PDT. These rats regained their body weight to pre-treatment level in more than two weeks. Animals treated with i.b. instillation of either Photofrin or ALA and phototherapy remained healthy and regained their body weight to pre-treatment levels by 7 to 10 days.

3.3.2 Histopathology

The submucosal and muscular layers of rat bladders, which were treated with light illumination only (n = 9) or ALA instillation only (n = 5), were histologically identical to those of untreated control rat bladders (n = 5) (Figure 3.4). There was neither abnormal fibrin collagen deposition in the thin submucosa, nor evidence of inflammatory cells in muscular layers (Figure 3.5). The extent of damage to the rat bladders and other organs resulting from PDT depended on the treatment protocols, *i.e.* the routes of drug administration and light doses applied. Photofrin administered

95

Figure 3.4 (A) Histology of untreated rat bladder wall showing mucosa, submucosa, and muscularis. There are some mononuclear cells scattering in the well-vascularized thin submucosal layer. (B) 14 days after bladder tumor was treated with 100 J/cm^2 light only, no evident histologic change in tumor and submucosa ($\times$ 125, H&E stain).
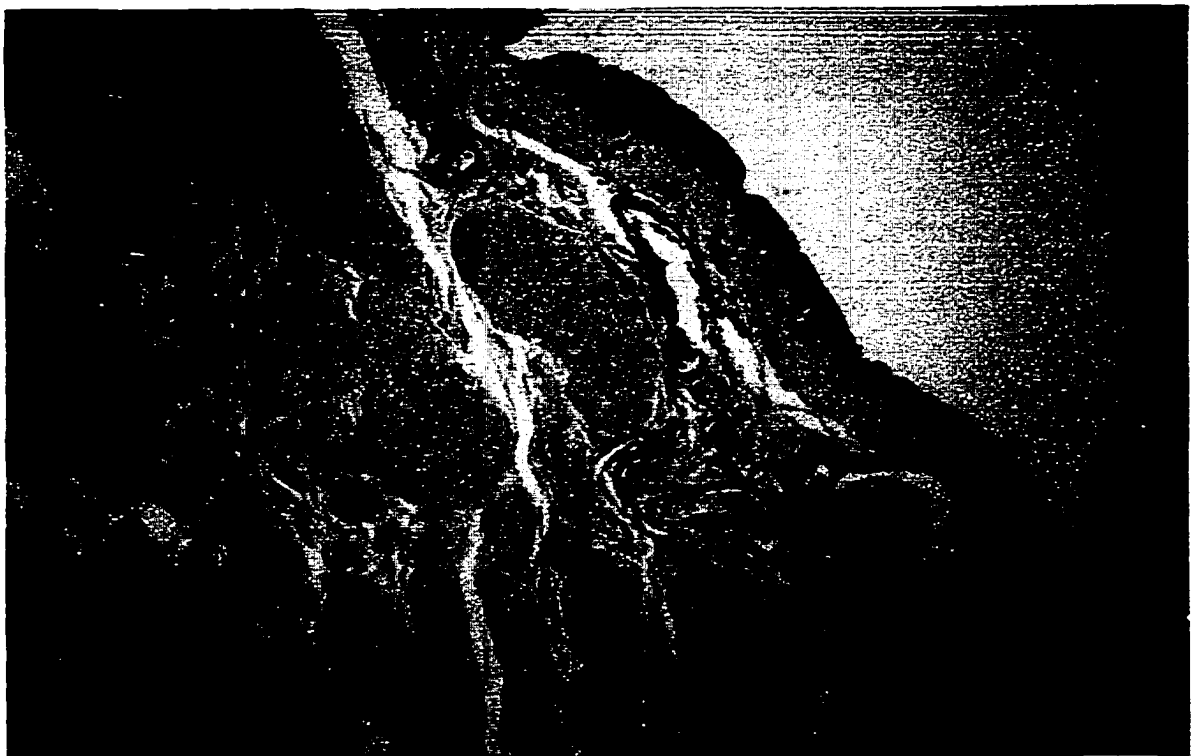
96

Figure 3.5 Untreated bladder wall showing scanty collagen fibrils (blue) in submucosa and serosa, especially surrounding small blood vessels. (× 125, Masson Trichrome stain).
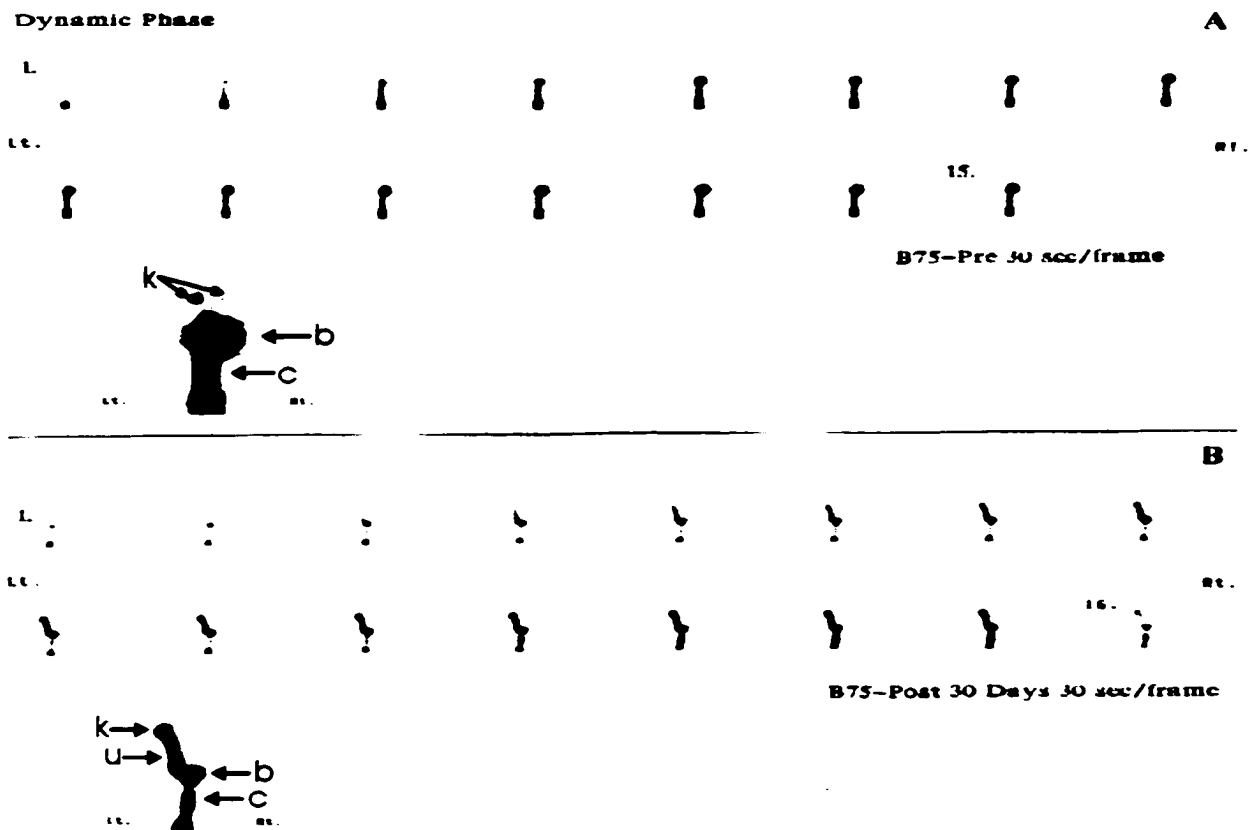
by i.v. injection together with 50 or 100 J/cm^2 of irradiation resulted in the most severe damage to the urinary bladders and other organs (*i.e.* rectum, vagina, and other perivesical tissues). Among the rats irradiated with 100 J/cm^2, 6 of 10 died or had to be euthanized at 3 to 10 days post-PDT. Postmortem examination revealed that the bladders became grossly pale with areas of hemorrhage, and highly distended cysts. Intrathoracic and intraperitoneal exudate was found in 2 of them, suggesting renal failure or sepsis. Dark red discharge in rectum was seen in 3 of them, indicating damage to the rectum. Hemorrhage in perivesical ligments was common. On microscopic examination, the most prominent findings in these bladders were extensive coagulative necrosis of the urothelium, tumor, and submucosa. In some cases, the entire bladder epithelium was denuded; with full thickness damage extending from the urothelium through the muscle to the serosa was seen (Figure 3.6). Hemorrhage, and sometimes acute inflammatory cell infiltration, mostly polymorphonuclear and plasma cells, were seen in the edematous submucosal and muscular layers. When the light dose was reduced to 50 J/cm^2 (n = 10), 2 of 10 rats had to be sacrificed (due to PDT damage to bladders) at 5 and 7 days post-PDT. The microscopic findings of the bladders were similar to that treated with 100 J/cm^2 described above, but with less severity (Figure 3.7). Another 2 rats had to be sacrificed at 15 and 45 days post-PDT. Microscopic examination showed that there was only focal C*IS* in one bladder, and the other rat was tumor free. However, focal full thickness damage (resulting from PDT) of the bladder wall with evident mononucleated cell infiltration was seen in both rats, as well there was evidence of a perivesical abscess and upper urinary tract infection in one of these rats. Among the rats surviving more than 8 weeks after PDT, only one rat developed a contracted bladder with hydroureteronephrosis and infection due to calcification of the bladder lumen surface (Figure 3.8), all other bladders regained their normal architecture except for mild to moderate collagen deposition in the submucosa, and sometimes in the superficial muscular layer (Figures 3.9 & 3.10).

Figure 3.6 Bladder section showing total denudation of the urothelium (arrows), extensive intramural hemorrhage and tissue necrosis except the serosa of the bladder, 3 days after PDT with Photofrin 5 mg/kg, i.v. and light dose of 100 J/cm² (× 125, H&E stain).
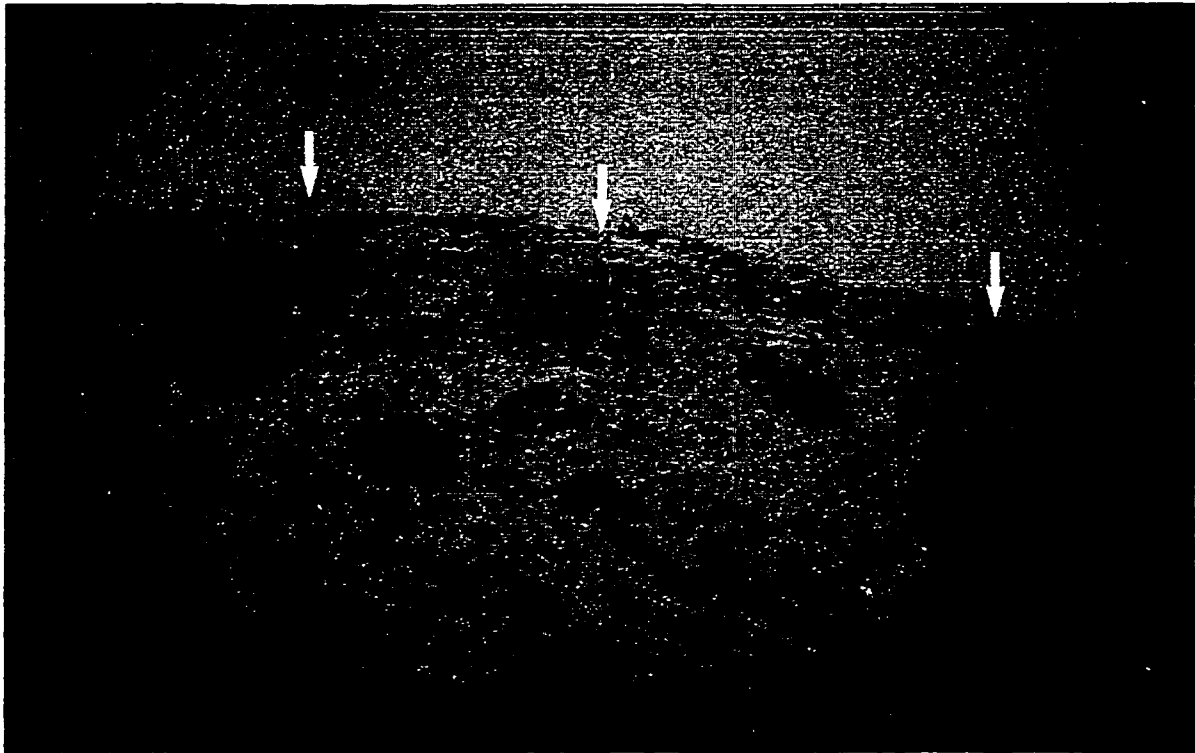
Figure 3.7 Bladder section showing total denudation of the urothelium (arrows), blood vessel dilatation with congestion in the edematous submucosa and muscular layers, which were also infiltrated with inflammatory cells, 5 days after PDT with Photofrin 5 mg/kg, i.v. and light dose of 50 J/cm² (× 125, H&E stain).

Dynamic Phase

A

L.

Lt.

15.

B75-Pre 30 sec/frame

k←
b←
c←

Lt.

B

L.

Lt.

16.

B75-Post 30 Days 30 sec/frame

k→
u→
b←
c←

Lt.

Figure 3.8 Dynamic scintigrams (30 seconds/frame) of a rat imaged with filling cystometrography show the bladder (b) and kidneys (k) after 0.8 mL of ^{99m}Tc-saline is infused into the bladder pre-implantation of tumor cells (A); and (B) a shrunken bladder (b) with left side vesico-ureteric reflux and hydroureteronephrosis in the same rat 30 days after whole bladder PDT with Photofrin injection and 50 J/cm^2 irradiation. Insets are magnifications of images A-15 and B-15. 'c' denotes the canula in the urethra;'u'denotes the ureter.

101

Figure 3.9 Bladder section showing slight increase in collagen fibrils in the bladder wall with small blood vessel proliferation in the submucosa 67 days after PDT with Photofrin 5 mg/kg, i.v. and light dose of 50 J/cm² (× 125, Masson Trichrome stain).
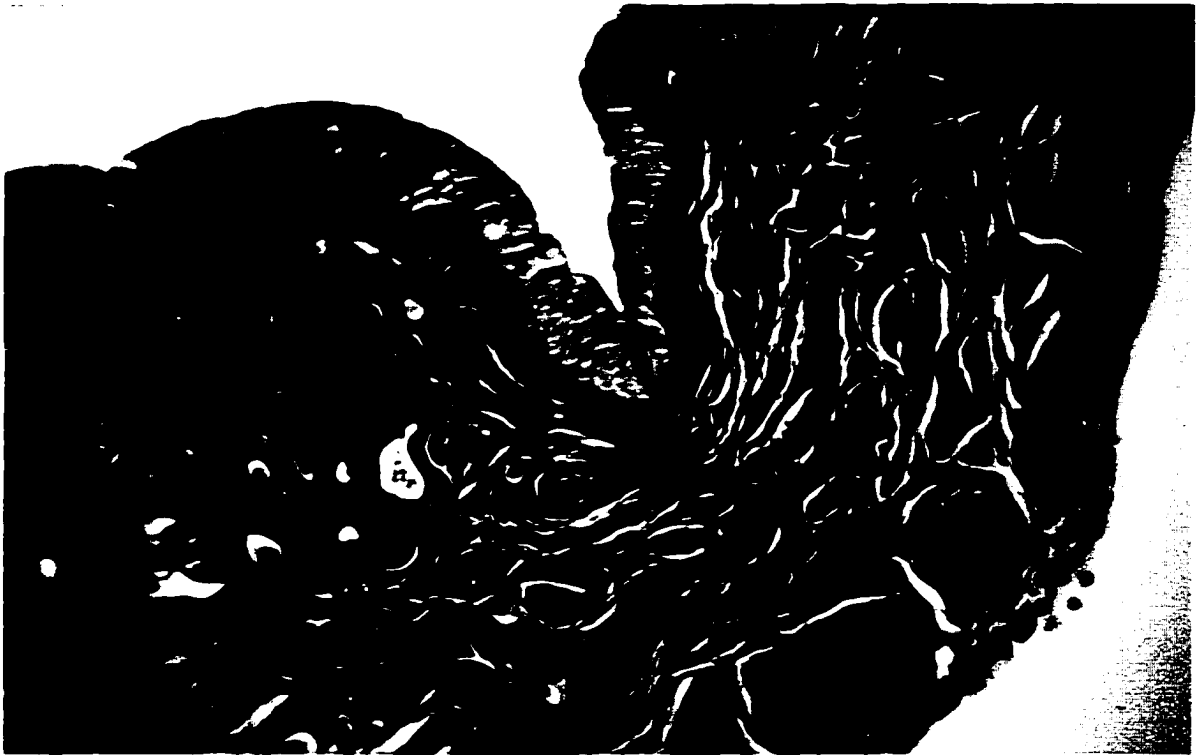
Figure 3.10 Bladder section showing moderate increase in collagen fibrils in the bladder wall with small blood vessel proliferation in the submucosa 67 days after PDT with Photofrin 5 mg/kg, i.v. and light dose of 100 J/cm^2 ($\times$ 125, Masson Trichrome stain).

103

There were no PDT-related deaths in the other groups. Animals were sacrificed at 67 days after PDT except those needing to be sacrificed earlier with signs of tumor progression, *i.e.* rapid loss of body weight, abdominal mass, and poor grooming. Overall the rats were sacrificed at various times post PDT as determined by their health status. Although focal damage of the superficial bladder muscle was also seen in some of the rats treated with intravesical instillation of Photofrin and 50 J/cm^2 (n = 10) or 100 J/cm^2 (n = 10) irradiation, the extent of tissue damage among these rats was largely confined to the bladder urothelium and submucosa (Figure 3.11). After instillation of ALA and 75 J/cm^2 of illumination (n = 10), only 2 rats needed to be sacrificed earlier than 80 days post-implantation due to tumor obstruction and/or progression. No obvious histopathologic changes were seen in the bladder muscular layer two months after PDT with i.b. instillation of ALA or Photofrin (Figure 3.12).

3.3.3 PDT effect on survival for rats implanted with AY-27 TCC cells

The Kaplan-Meier probability of survival for animals implanted with 1.5×10^6 AY-27 TCC cells and treated with whole bladder PDT 14 days post-implantation are displayed graphically in Figure 3.13. Other details are also tabulated as mean survival time (MST), increased life span compared with control (ILS), long-term survivor (LTS), and long-term tumor-free survivor (TFS) after different treatments (Table 3.1). Half of the rats receiving Photofrin injection and irradiated with 100 J/cm^2 died of PDT damage to multiple organs. There were 4 long-term survivors in this group, 3 of them were tumor-free. Two of 10 rats receiving Photofrin injection and 50 J/cm^2 irradiation were terminated at 5 and 7 days after PDT, while 5 of the 6 long-term survivors were tumor-free. None of the rats treated with bladder instillation of either Photofrin or ALA, and 50 to 100 J/cm^2 irradiation died of PDT complications. For the 10 rats treated with ALA instillation and 75 J/cm^2 irradiation, there were 8 long-term survivors, 6 of them were tumor-free. Likewise, half of the rats receiving Photofrin instillation and laser therapy were tumor-free long-survivors (Table 3.1). Analysis by the log-rank test, which accounts for proportional survivals over time
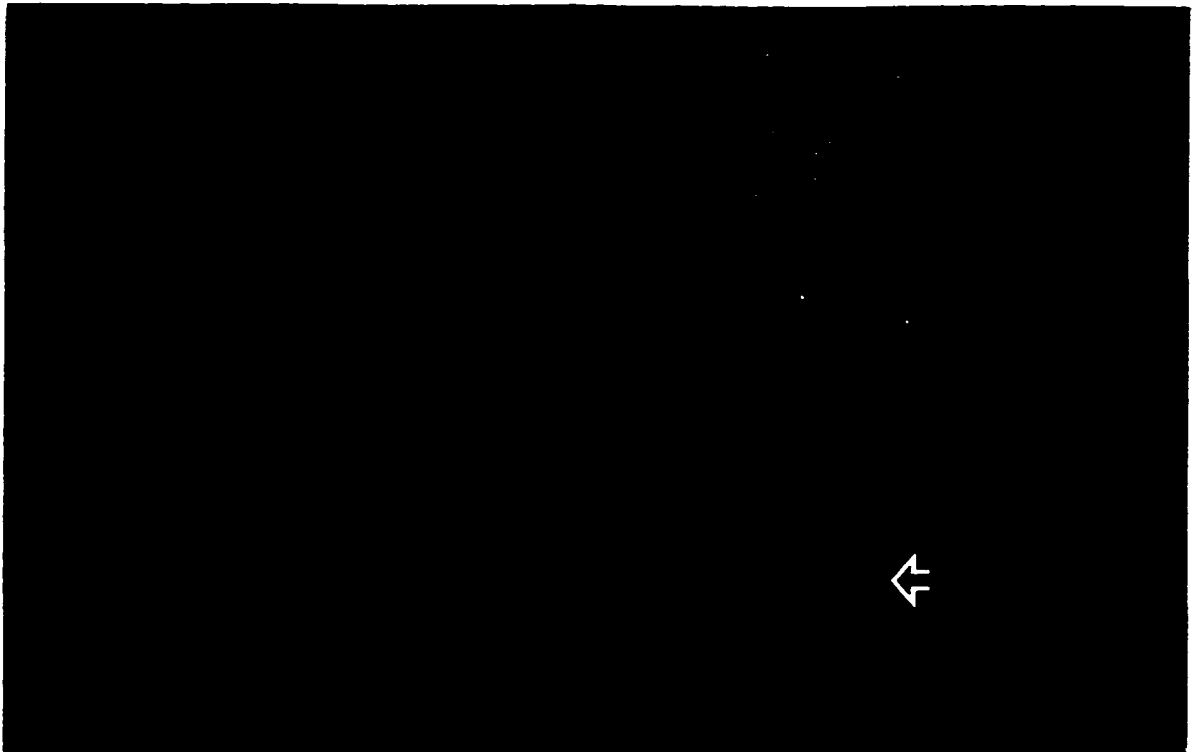
104

Figure 3.11 Histology of bladder wall showing patchy urothelium sloughing (right upper corner) with areas of undamaged C*IS* (right lower corner), 12 days after PDT with Photofrin 2 mg/mL, i.b. and light dose of 50 J/cm^2. There are many mononuclear cells infiltrating the bladder wall ($\times$ 125, H&E stain).
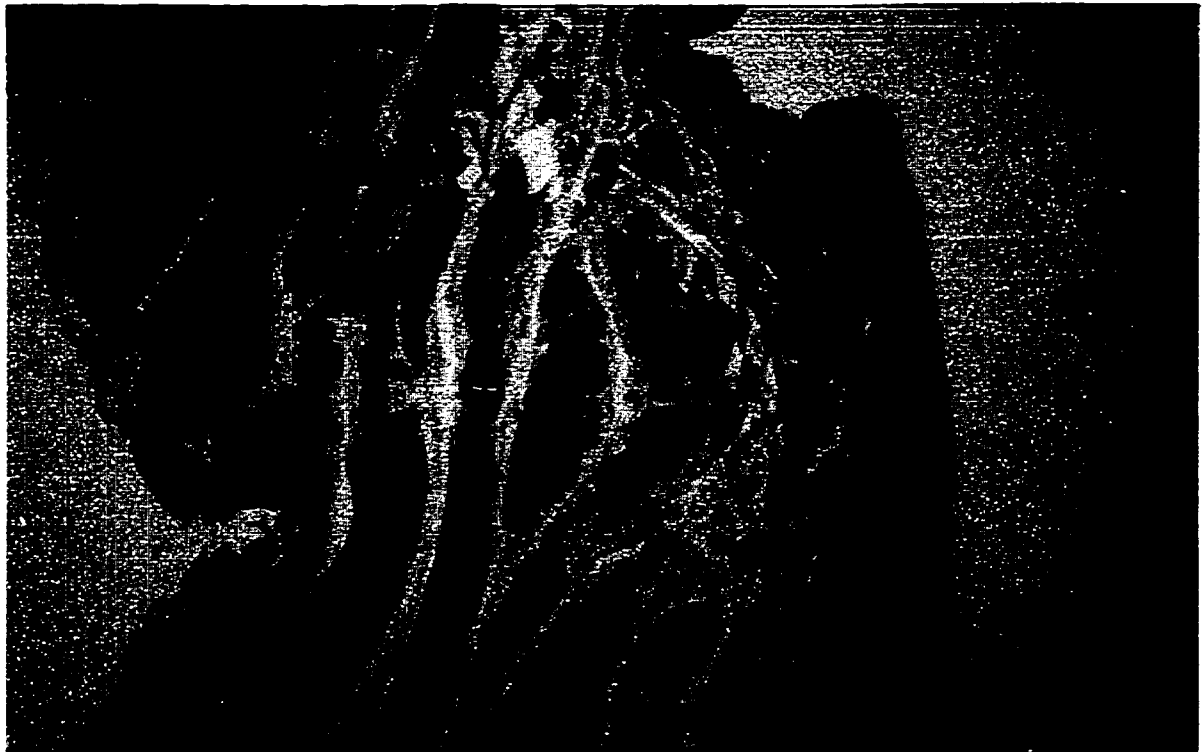
Figure 3.12 Histology of bladder wall 67 days after PDT with ALA 300 m*M*, i.b. and a light dose of 75 J/cm² showing apparently normal bladder architecture without abnormal collagen fibril deposition (× 125, Masson Trichrome stain).
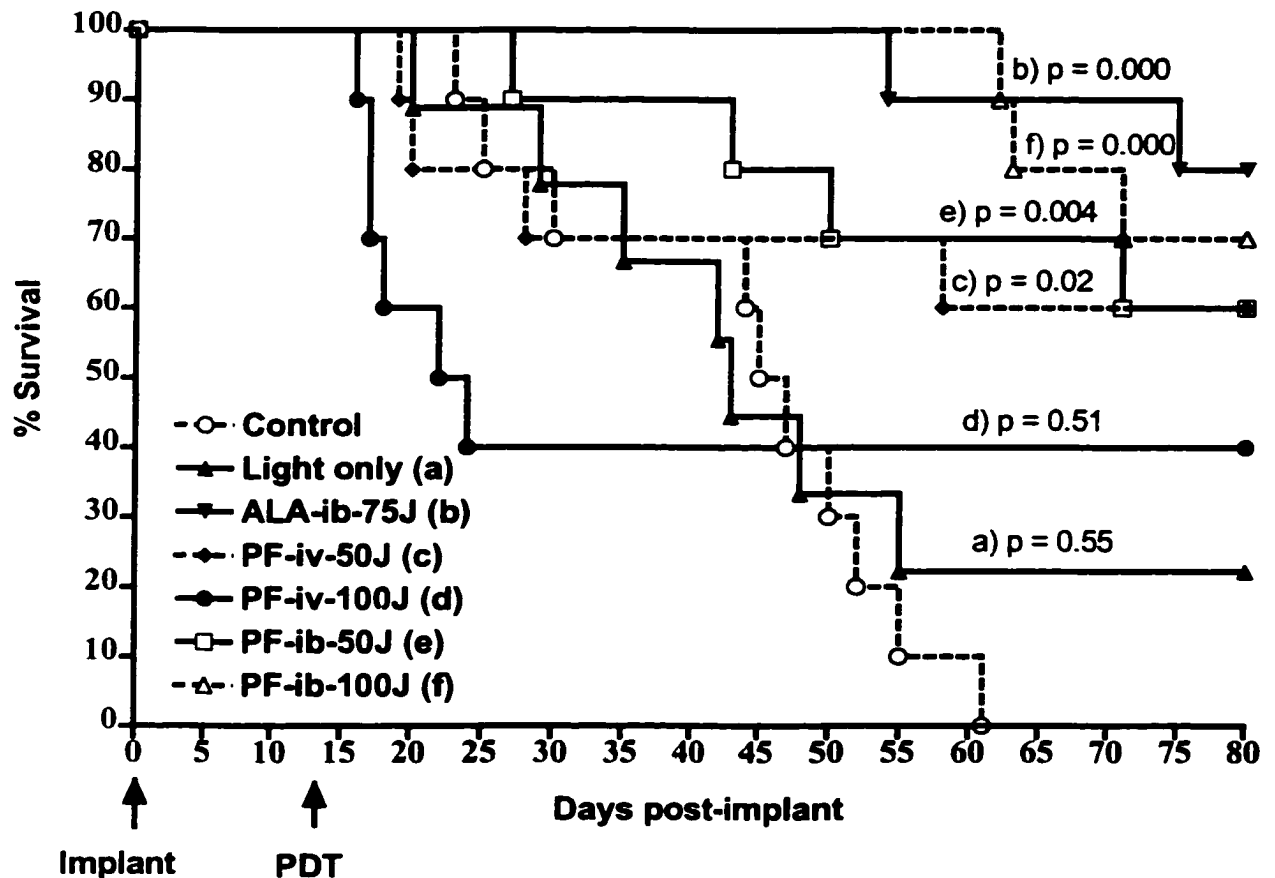
Figure 3.13 Kaplan-Meier probability of survival for Fischer rats implanted with AY-27 TCC cells and treated with whole bladder PDT at 14 days post-implantation. Treated groups are: a) 100 J/cm^2 light only (n=9); b) ALA, 300 mM, i.b. with 75 J/cm^2 (n=10); c) PF*, 5 mg/kg, i.v. with 50 J/cm^2 (n=10); d) PF, 5 mg/kg, i.v. with 100 J/cm^2 (n=10); e) PF, 2 mg/mL, i.b. with 50 J/cm^2 (n=10); and f) PF, 2 mg/mL, i.b. with 100 J/cm^2 (n=10). Control rats were treated with ALA, 300 mM, i.b. (n=5), or no drug no light (n=5). * Photofrin.

(days), revealed no significant differences between the groups of light only vs. control (p = 0.55), Photofrin i.v. with 100 J/cm^2 vs. control (p = 0.51). However, the groups receiving ALA i.b. with 75 J/cm^2, Photofrin i.v. with 50 J/cm^2, and Photofrin i.b. with 50 and 100 J/cm^2 groups had significant differences vs. the control group (p = 0.0001, 0.02, 0.004, and 0.0001, respectively).

Table 3.1 Summary of survival for rats implanted with 1.5 x 10^6 AY-27 TCC tumor cells in the bladders and treated with whole bladder PDT at 14 days post-implantation.

Group	No. of rats	Drug dose	Light dose (J/cm^2)	No. of rats died of PDT	MST[a] Mean ± SD (days)	ILS[b] (%)	LTS[c] (≥80 days)	TFS[d] (≥80 days)
Control 1	5	none	none	N/A	44 ± 12.3	–	0/5	0/5
Control 2	5	300 mM ALA, i.b.	none	N/A	42.4 ± 14.9	0	0/5	0/5
Light only	9	none	100	0/9	48 ± 20.8	9	1/9	0/9
ALA-i.b.[e]	10	300 mM	75	0/10	76.9 ± 8.2	74.8	8/10	6/10
PF[f]-i.v. (a)	10	5 mg/kg	50	2/10	60.5 ± 27.29	37.5	6/10	5/10
PF-i.v. (b)	10	5 mg/kg	100	6/10	43.4 ± 31.6	0	4/10	3/10
PF-i.b. (c)	10	2 mg/mL	50	0/10	67.1 ± 19.7	52.5	6/10	5/10
PF-i.b. (d)	10	2 mg/mL	100	0/10	75.6 ± 7.45	71.8	7/10	6/10

[a], mean survival time; [b], % increased life span compared with that of control; [c], long-term survival; [d], long-term tumor-free survival; [e], intravesical; [f], Photofrin.

3.3.4 Bladder compliance

The changes in bladder compliance prior to and after different treatments are displayed in Figure 3.14. Basically, the bladder pressure profiles were increasing exponential curves, with the pressure less than 5 mm Hg when the bladder was filled to less than 0.5 mL of saline, and a marked pressure increase thereafter. However, one pressure curve did not follow this trend, the pressure exceeded 5 mm Hg when the bladder was filled only with 0.2 mL of saline in the group treated with Photofrin injection and 50 J/cm^2 irradiation 60 days after PDT. Compared to compliance ascertained prior to tumor implantation, there was no significant change in bladder compliance after different treatment regimens. However, these data should be interpreted with caution, because there were many factors which could affect the
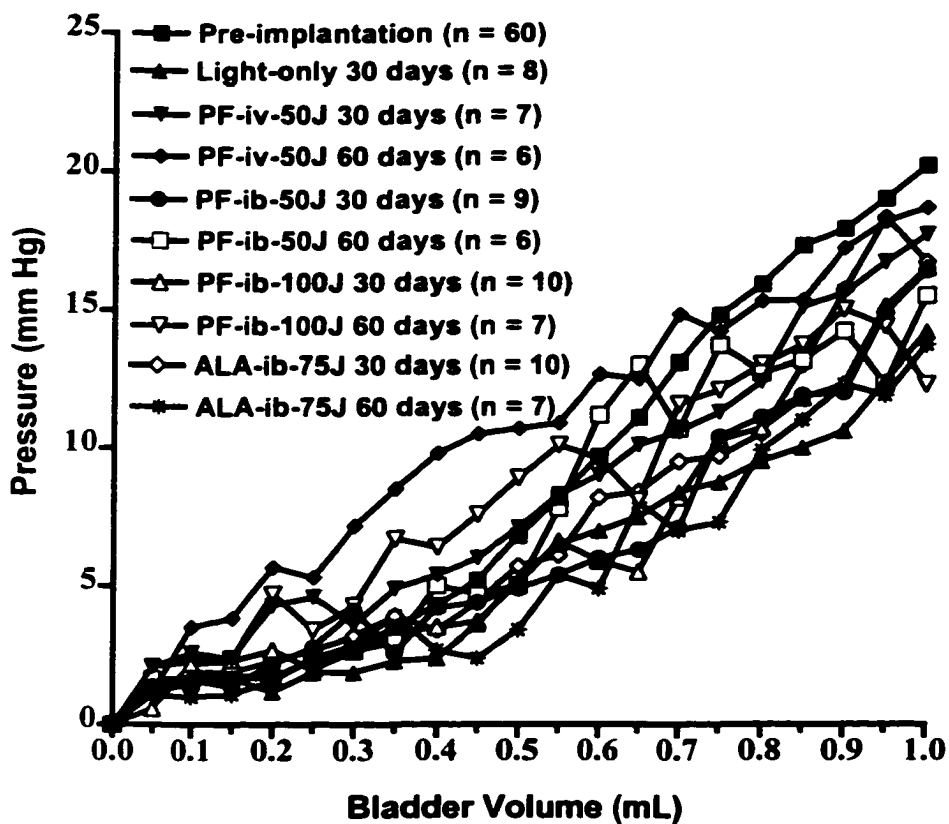
108

Figure 3.14 Bladder pressure as a function of filled bladder volume in rats
prior to, 30 days and 60 days after whole bladder PDT. The bladders
were constantly filled with ^{99m}Tc-saline at infusion rate of 0.1 mL/min.
The bladder pressure was measured simultaneously. Points: mean
value from each group at every 30-seconds.

bladder pressure. These factors will be discussed below. Vesico-ureteric reflux was commonly seen in rats prior to tumor implantation (Figure 3.8). Scintigraphic evidence of ureterorenal reflux was seen in images in 34 out of 82 rats pre-implantation, and in 19 out of 54 and 13 out of 37 rats 30-day and 60-day post-PDT respectively. Interestingly, some of the vesico-ureteric reflux observed prior to PDT disappeared and new reflux showed up after PDT. Only one bladder contracture with hydroureteronephrosis developed in the Photofrin injection group (Figure 3.8).

3.4 Discussion

The efficacy of PDT using systemically administered Photofrin has been demonstrated in both animal tumor models[28] and clinical trials.[6] However, in addition to a prolonged skin phototoxicity,[7] another severe complication following whole bladder PDT is reduction of bladder capacity secondary to fibrotic healing of muscle injury.[8,10] Intravesical administration of Photofrin could potentially avoid these problems, with limited uptake of the drug by tissues deeper than the bladder mucosa and submucosa. Previous studies in our laboratory showed different distribution patterns of porphyrin fluorescence in the orthotopic bladder tumor model after i.v. or i.b. administration of Photofrin (see chapter II).[11] After i.v. injection, the highest porphyrin level was observed in the submucosa and papillary tumor, followed by bladder muscle and urothelium. While after i.b. instillation, the highest porphyrin level was detected in the bladder tumor and urothelium, sparing the bladder muscular layer. The results from whole bladder PDT in this study further demonstrate the differential phototoxicity following i.v. or i.b. administration of Photofrin. It is obvious that animals receiving Photofrin injection can tolerate much less light dose than animals receiving Photofrin instillation, while the tumor responses to both routes of therapy are comparable (Table 3.1, Figure 3.13). Incomplete tumor destruction has been observed in groups receiving either i.v. or i.b. administration of Photofrin (Figure 3.11). Based on the data collected in these experiments, the maximal tolerable light dose for rats receiving 5 mg/kg of Photofrin injection appears less than (but close to) 50 J/cm^2. However, care must be taken when comparing light doses

reported from different authors. Some authors described light dose as J/rat bladder.[29] When the rat bladder is filled with 0.3 mL of light scattering medium as described by Chang *et al.*, the surface area of the bladder should be 2.16 cm^2 according to the formulas used in this study. Thus 100 J/rat bladder as they reported equates no more than 50 J/cm^2. Others have assumed the rat bladder surface area to be 0.5 cm^2 when the bladder was filled with 0.3 mL of saline.[30] Therefore, 100 J/cm^2 reported by them means 50 J/rat bladder, or approximately 25 J/cm^2 according to our calculations. Furthermore, the concentration of light scattering medium can influence the light intensity. Generally speaking, the higher the concentration of the intralipid, the more absorption of the light by the medium, the lesser the light intensity. If the bladder was filled with saline (and illuminated with a spherical diffuser fiber), the measured light dose on bladder mucosa reached more than 3 times the intended light dose, because the bladder lumen surface could scatter and reflect light.[31]

The therapeutic efficacy following topical 5-ALA application has been documented in treatment of patients with skin malignancies.[14] Selective accumulation of ALA-induced PpIX in bladder tumor and urothelium *vs.* bladder muscle in our biodistribution studies suggests that i.b. instillation of ALA may be an attractive strategy of photosensitization for whole bladder PDT.[11] In this study, the tumor destruction/growth delay in orthotopic superficial bladder tumors following i.b. instillation of ALA has been confirmed. None of the rats died of PDT complications. And there was no morphological evidence of bladder damage or functional detriment observed among the long-term survivors. However, the reason for the inconsistent tumor destruction following whole bladder PDT remains to be determined. Various stages of tumor burden or aggressiveness in different animals; inhomogenous distribution of PpIX in tumors; and potentially inhomogenous light distribution in the bladder; may contribute to incomplete tumor destruction. Interestingly, residual tumors observed in these rats were largely located near the bladder neck. It is not clear whether this is due to tumor extension from neighboring locations or due to inadequate light distribution to the bladder neck. It seems that further increase in

111

ALA concentration or light dose from our preliminary experiments is unlikely improve the antitumor effectiveness, because one third of the rats died of PDT complications. Previous results from this laboratory and others suggest that ALA concentration higher than 600 mM (approx. 10%) can cause rat bladder damage due to chemical effects.[11,32] Since PpIX fluorescence level was higher on the tumor surface, multiple sessions of PDT may improve the antitumor efficacy for those rats with papillary tumors.

Compared with pre-implantation (normal bladder) compliance, the changes after PDT with different treatment parameters is not significantly different. It appears that the rat bladder compliance is not an ideal criterion for bladder damage after whole bladder PDT, because there are many other factors which may also affect the bladder compliance. These factors include: 1) bladder volume change (which may increase as the rats mature); 2) tumor invasion to the bladder muscular layers which could either increase or reduce bladder pressure due to compromised bladder muscle contraction; 3) full thickness damage of the bladder wall due to PDT which impairs bladder contraction; 4) vesico-ureteric reflux; and 5) fibrosis in bladder submucosa or superficial muscularis. The vesico-ureteric reflux in this model is not a complication of whole bladder PDT, since it is commonly seen in normal rats when the bladder pressure reaches to 15 mm Hg or greater. Although damage of the bladder wall and loss of function are common shortly after PDT with Photofrin injection and bladder shrinkage developed in one rat, no evidence of muscular fibrosis was observed in other long-term surviving animals. The reason for this remains undefined. Because porphyrin fluorescence intensity was much higher in the submucosa than in other tissue layers after i.v. injection of Photofrin,[11] PDT damage to the bladder submucosa (with some degree of muscle damage) may be sufficient to result in the loss of bladder tone and contractility in the very thin muscular layer. Therefore, fibrosis in the thin rat bladder muscularis may be much less than in the much thicker human bladder detrusor muscle. Our data agreed reasonably well with others, that although bladder

112

damage was commonly seen, no long-term bladder muscular fibrosis was observed after whole bladder PDT in rodents.[29,33,34]

3.5 Conclusions

Intravesical instillation of Photofrin and ALA can achieve the same photoefficiency as i.v. injection of Photofrin in orthotopic rat bladder tumor model, with less phototoxicity to normal tissues. The incident light dose applied for whole bladder PDT with Photofrin injection should be less than (but close to) 50 J/cm^2 if other parameters are kept the same as those in this study. Bladder compliance is not an ideal indication of bladder damage from PDT in this model, because many other factors can affect the bladder contraction and pressure. Bladder muscular fibrosis appears not to be a consequence of whole bladder PDT in this rat model system. Clinical trials are needed to verify these findings.

3.6 References

1. Bane, B.L., Rao, J.Y. and Hemstreet, G.P. (1996) Pathology and staging of bladder cancer. *Semi. Oncology*. **23**: 546-570.

2. Nseyo, U.O. and Lamm, D.L. (1996) Therapy of superficial bladder cancer. *Semi. Oncology*. **23**: 598-604.

3. Lamm, D.L., Steg, A., Gibod, L., Morales, A., Hanna Jr, M., Pagano, F., Alfthan, O., Brosman, S., Fisher, H.A.F., Jakse, G., Chisholm, G.D., van der Meijden, A.P.M. and Debruyne, F.M.J. (1989) Complications of Bacillus Calmette-Guérin immunotherapy: review of 2602 patients and comparison of chemotherapy complications. *EORTC Genitourinary Group Monograph*, **6**: 335-355.

4. Kelly J.F. and M.E. Snell (1976) Hematoporphyrin derivative: a possible aid in the diagnosis and therapy of carcinoma of the bladder. *J. Urol.*, **115**: 150-151.

5. Dugan, M., Crawford, E., Nseyo, U., *et al.* (1991) A randomized trial of observation (OBS) vs phototodynamic therapy (PDT) after transurethral resection (TUR) for superficial papillary bladder carcinoma (SPBC). *Pro. Amer. Soc. Clin. Oncol.* **10**: 554 (abstract)

6. Nseyo, U.O. (1992) Photodynamic therapy. *Urol. Clin. North Am.*, **19**: 591-599.

7. Dougherty, T.J., Cooper, M.T. and Mang, T.S. (1990) Cutaneous phototoxic occurrences in patients receiving Photofrin. *Lasers Surg. Med.*, **10**: 485-488.

8. Harty, J.I., Amin, M., Wieman, T.J., Tseng, M.T., Ackerman, D. and Broghamer, W. (1989) Complications of whole bladder dihematoporphyrin ether photodynamic therapy. *J. Urol.*, **141**: 1341.

9. Nseyo, U.O, Dougherty, T.J., Boyle, D.G., *et al* (1985) Whole bladder photodynamic therapy for transitional cell carcinoma of the bladder. *Urology* **26**: 274-280.

10. Jocham, D., Beer, M., Baumgartmer, R., *et al.* (1989) Long-term experience with integral photodynamic therapy of Tis bladder carcinoma. ed. Boek G and Hornett. S. In: Photosensitizing Compounds: their chemistry; biology and clinical use. *Ciba Foundation Symposium* **146**: 190-208. Chicherster: Wiley.

11. Xiao, Z., Miller, G.G., McCallum, T.J., Brown, K.M., Lown, J.W., Tulip, J. and Moore, R.B. (1998) Biodistribution of Photofrin II and 5-aminolevulinic acid - induced protoporphyrin IX in normal rat bladder and bladder tumor models. *Photochem. Photobiol.*, **67** (5): 513-518.

12. Taari, K., Talja, M., Riihela, M., Rannikko, S. and Mokka, R. (1992) Morphological effects of photodynamic therapy on rabbit bladder using Photofrin II and Photosan intravesically and intravenously. *Br. J. Urol.*, **70**: 616-621.

13. Windahl, T., Peng, Q., Moan, J., Hellsten, S., Axelsson, B. and Lofgren, L. (1993) Uptake and distribution of intravenously or intravesically administered photosensitizers in the rat. *Cancer lett.*, **75**: 65-70.

14. Kennedy, J.C., Pottier, R.H. and Pross. DC. (1990) Photodynamic therapy with endogenous protoporphyrin IX: basic principles and present clinical experience. *J Photochem. Photobiol., B: biol.* **6**: 143-148.

15. Berlin, N.I., Neuberger, A. and Scott, J.J. (1956) The matabolism of δ-aminolevulinic acid, 2. Normal pathways, studied with the aid of 14C. *Biochem. J.*, **64**: 90-100.

16. Divaris, D.X.C, Kennedy, J.C., Pottier, K.H. (1990) Phototoxic damage to sebaceous glands and hair follicles of mice after systemic administration of 5-aminolevulinic acid correlates with localized protoporphyrin IX fluorescence. *Am. J. Pathol.*, **136**: 891-897.

17. Moore, R.B., Miller, G.G., Brown, K., *et al* (1995) Urothelial conversion of 5-Aminolevulinic acid to protoporphyrin IX following oral or intravesical administration. *SPIE.* 2371: 284-288.

18. Loh, C.S., Bedwell, J., MacRobert, A.J., Krasner, N., Phillips D. and Bown, S.G. (1992) Photodynamic therapy of the normal rat stomach: a comparative study between di-sulphonated aluminum phthalocyanine and 5-aminolevulinic acid. *Br. J. Cancer.* **66**: 453-462.

19. Bedwell, J., Macroert, A.J., Phillips, D. *et al.*(1992) Fluorescence distribution and photodynamic effect of ALA-induced PpIX in the DMH rat colonic tumor model. *Br. J. Cancer.* **65**: 818-824.

20. Kennedy, J.C. and Pottier, R.H. (1992) Endogenous protoporphyrin IX, a clinical useful photosensitizer for photodynamic therapy. *J. Photochem. Photobiol. B: Biol.*, **14**: 275-292.

21. Grant, W.E., Hopper, C., MacRobert, A.J., *et al.* (1993) Photodynamic therapy of oral cancer: photosensitization with systemic aminolevulinic acid. *Lancet.* **342**: 147-148.

22. Kriegmair, M., Baumgartner, R., Lumper, W., Waidelich, R. and Hofstetter, A. (1996) Early clinical experience with 5-aminolevulinic acid for the photodynamic therapy of superficial bladder cancer. *Br. J. Urol.*, **77**: 667-671.

23. Jocham, D. (1987) Photodynamic technique in the treatment of bladder cancer. In *Advances in urologic oncology. General perspectives.* (ed.) Williams, R.D. MacMillan Pub. Co: New York.

24. Moore, R.B., Chapman, J.D., Mokrzanowski, A.D., Arnfield, M.R., McPhee, M.S. and McEwan, A.J. (1992) Non-invasive monitoring of photodynamic therapy with 99Technetium HMPAO scintigraphy. *Br. J. Cancer.* **65**: 491-497.

25. Lee, L.K., Whitehurst, C., Pantelides, M.L., Vernon, D.I. and Moore, J.V. (1996) Interstitial Photodynamic therapy in the Dunning R3327-AT6 Prostatic Carcinoma. *Lasers Med. Sci.*, **11**: 155-161.

26. Xiao, Z., McCallum, T.J., Brown, K.M., Miller, G.G., Halls, S.B., Parney, I. and Moore, R.B. (1999) Characterization of a novel orthotopic transplantable rat bladder transitional cell carcinoma model. *Br. J. Cancer.* (in press).

27. Raphael, S.S. (1976) Lynch's Medical Laboratory Technology. Volume II. 3rd Edition. Philadelphia, W.B. Saunders, Co.,

28. Henderson, B.W. and Dougherty, T.J. (1992) How does photodynamic therapy work? *Photochem. Photobiol.*, **55**: 145-157.

29. Chang, S.C., MacRobert, A.J. and Bown, S.G. (1996) Photodynamic therapy on rat urinary bladder with intravesical instillation of 5-aminolevulinic acid: light diffusion and histological changes. *J. Urol.*, **155**: 1749-1753.

30. Stocker, S., Knuchel, R., Sroka, R., Kriegmair, M., Steinbach, P. and Baumgartner, R. (1997) Wavelength dependent photodynamic effects on dhemically induced rat

baldder tumors following intravesical instillation of 5-aminolevulinic acid. *J. Urol.*, 157: 357-361.

31. Star, W.M. (1997) Light dosimetry in vivo. *Phys. Med. Biol.*, **42**: 763-787.

32. Chang, S.C., MacRobert, A.J. and Bown, S.G. (1996) Biodistribution of protoporphyrin IX in rat urinary bladder after intravesical instillation of 5-aminolevulinic acid. *J. Urol.*, **155**: 1744-1748.

33. Stewart, F.A., Oussoren, Y., te Poele, J.A.M., Horenblas, S. & Mooi, W.J. (1992) Functional and histological damage in the mouse bladder after photodynamic therapy. *Br. J. Cancer.* **65**: 884-890.

34. Pope, A.J. & Bown, S.G. (1991) The morphological and functional changes in rat bladder following photodynamic therapy with phthalocyanine photosensitization. *J. Urol.*, **145**: 1064-1070.

CHAPTER IV

INTERSTITIAL PHOTODYNAMIC THERAPY IN SUBCUTANEOUS RAT BLADDER AND PROSTATE TUMORS AFTER INTRAVENOUS ADMINISTRATION OF 5-AMINOLEVULINIC ACID

4.1 Introduction

Photodynamic therapy (PDT) of solid malignancies is still an experimental cancer treatment modality. Interstitial PDT utilizes multiple optical fibers to deliver activating light to deeply seated tumors and produces selective tumor destruction.[1,2] PDT efficacy is dependent upon the concentration of photosensitizer in the tumor and the light energy available to activate the sensitizer. The resultant photochemical reactions generate cytotoxic species such as singlet oxygen ($^1O_2$) which cause damage to biomembranes by lipid peroxidation.[3,4] Hematoporphyrin derivative (HpD) and the active fraction of HpD (Photofrin®), have been the most frequently used photosensitizers in both animal models and in clinical PDT. However, Photofrin is not selectively accumulated in malignant tissue to any therapeutic advantage. As well, prolonged generalized skin photosensitivity that can last for 6–8 weeks is a major drawback of this agent after injection.[5] An alternative and interesting approach to PDT is the administration of a heme precursor, 5-aminolevulinic acid (ALA), that is transformed to a photosensitizer *in situ*.[6,7,8] ALA is synthesized from condensation of glycine and succinyl CoA at the first committed step in heme biosynthesis.[6,9] The penultimate step of the heme synthesis pathway is the production of protoporphyrin IX (PpIX), an effective photosensitizer. Since the conversion of PpIX to heme is slow, an excess of exogenous ALA bypasses the normal negative feedback control mechanism by heme and leads to an accumulation of PpIX. Photosensitization of tumors by PpIX induced from ALA has been demonstrated *in vitro* and *in vivo*,[6-8,10,11] and has been used in clinical investigations with reasonable success for the treatment of superficial cutaneous lesions[6] and gastrointestinal malignancies.[12,13] In this study, we investigated the therapeutic efficacy of ALA-induced PpIX for interstitial PDT of solid genitourinary malignancies including the slow-growing R3327-H rat prostate tumor and the rapidly-growing AY-27 rat bladder tumor.

119

4.2 Materials and methods

4.2.1 Tumor cells. AY-27 cells from a rat bladder TCC cell line were provided by Dr. S. Selman at the Ohio University Medical School, and grown in RPMI-1640 culture medium (Gibco/BRL) supplemented with L-glutamine and 10% fetal calf serum and antibiotics (1%, v/v). Cells were incubated at 37°C in a 5% CO_2 humidified atmosphere and periodically propagated *in vivo* as subcutaneous tumors in syngeneic Fischer CDF 344 rats. The Dunning R3327 rat prostate adenocarcinoma arose spontaneously in a male Copenhagen rat in 1960. Since initial isolation, several sublines have been developed and are well characterized.[14] The R3327-H subline obtained from the Papanicolaou Institute (Miami, FL) is well differentiated, hormonally sensitive, diploid and slow-growing. The R3327-H tumor shows histological and therapeutic similarities to human prostate adenocarcinoma. The R3327-H cells were grown in basal Eagle's medium (Gibco/BRL) supplemented with 12.5% fetal calf serum, and has been passaged in Fischer × Copenhagen rats at the Cross Cancer Institute for over 15 years.

4.2.2 Animal tumor models. All procedures done on the animals were performed according to the Guidelines of the Canadian Council on Animal Care and approved by the Cross Cancer Institute Animal Welfare Committee. Fischer CDF344 male rats (Charles River Canada, QC) were utilized as recipients of AY-27 tumor implants. Tumors which were to serve as donor material for transplantation were selected at volumes not exceeding 5,000 mm^3. Selected tumors were cut into approx. 2.5 mm cubes in sterile Hank's balanced salts solution (HBSS), and implanted into flanks of Fischer rats. After 10 to 14 days of growth latency, the AY-27 tumors became palpable and had a doubling time of 3 to 5 days. First generation (F_1) males from the mating of Fischer (female) and Copenhagen (male) rats served as host for the R3327-H tumor. Donor R3327-H tumors were cut into cubes of approx. 3 mm on the side, and implanted s.c. into flanks of Fischer × Copenhagen rats. A latency period of 16 to 20 weeks was typically observed with the R3327-H tumors before they became

120

palpable. These tumors displayed a doubling time of 15 days or greater. Animal-to-animal tumor transplantation was limited to three passages. Histological examination of the experimental tumor material was made at least twice a year and compared with the archived histology of the original tumor material. Tumors in either group which demonstrated tumor cell drift by either histological or growth kinetic criteria were not used as donor material.

When the tumor nodules became palpable they were measured twice a week with calipers in 3 mutually orthogonal directions. Tumor volumes (V) were then calculated using the formula $V = \frac{\pi}{6} \times D_1 \times D_2 \times D_3$. We have found that this ellipsoidal computation of tumor volume gives a reasonable approximation of actual tumor volume.[15] Animals bearing either AY-27 TCC or R3327-H prostate tumors were randomized to specific treatment protocols when their tumors had reached a volume of approx. 1000 mm^3. Experiments were designed with at least 3 rats randomized to each treatment group. In these studies, the day of treatment was designated as day 0. Tumor volume response to various therapies are shown graphically with percentage of average pre-treatment tumor volume plotted versus time after treatment, or tabulated as time in days after treatment for tumors to grow to an average volume of 4000 mm^3 (approx. 4× treatment vol.). When tabulating these results, statistical analysis given by mean ± SD of time to regrow to 4× treatment volume was used. Dunnett multiple comparing test (ANOVA, GraphPad Prism™, San Diego, CA) was used to determine significant differences between each group and the controls. Tumors that became impalpable more than 100 days following treatment were classified as long-term tumor-free response.

4.2.3 Administration of ALA. ALA was supplied as a hydrochloride salt (Sigma Chemicals Co., St. Louis, MO). ALA powder (molecular weight 167.6) was dissolved in PBS (Sigma Chemicals Co.) and filtered by a 0.20 μm sterile filter (Corning, NY) immediately before use. The ALA dose was 500 mg/kg body weight for animals bearing either AY-27 bladder tumors or R3327-H prostate tumors. With the animals anesthetized by Metofane inhalation (Janssen Pharmaceutica, North York,

ON), the ALA solution (approx. 0.5 mL) was injected into the tail vein 4 hours prior to laser therapy. Animals were allowed to recover (in approx. 5 minutes) and were protected from bright light.

4.2.4 Biodistribution of ALA-induced PpIX. Fluorescence analysis of ALA-induced PpIX in sections of normal and tumor tissues from animals bearing AY-27 tumors has been described in detail in previous chapters. Biodistribution of ALA-induced PpIX in animals bearing R3327-H tumors was similarly examined. Briefly, animals bearing R3327-H tumors were injected with graded doses of ALA, and euthanized at intervals of 2, 4, or 6 hours after ALA injection. Control animals were given PBS, and were sacrificed 2 hours later. Groups of 3 rats were used at each concentration and time-point. Tumor tissues were harvested and rapidly frozen with dry-ice/methanol in a bed of OCT cryostat embedding compound (Tissue-Tek®, Sakura Finetek USA Inc., Torrance, CA) for tissue sectioning. Tissue sections (8-μm thickness) were prepared with a cryostat (Miles Scientific Inc. Naperville, IL), and were examined by confocal laser scanning microscope (CLSM) for PpIX fluorescence analysis. The physical parameters pertaining to fluorescence excitation and detection by CLSM have been reported in previous chapter (see chapter II). Regions of interest (ROI) were delineated, and the fluorescence intensity was determined from the mean of 30 measurements. The relative intensity of PpIX fluorescence from a ROI was then corrected for the background level measured on specimens from control animals to which no ALA had been administered. This relative fluorescence intensity was used as a representative of the tissue concentration of PpIX.

4.2.5 Interstitial phototherapy. Figure 4.1 shows the experimental setup used to irradiate both the subcutaneous AY-27 TCC and the R3327-H prostate tumors. A Coherent CR-599 argon-pumped dye laser (Coherent Inc., Palo Alto, CA) was tuned to emit at a wavelength of 630 nm at variable power intensities to a maximum of 4 watts. The laser light beam was split by a series of beam splitters into eight beams of equal intensity and directed down quartz fibers with 1-cm long cylindrical diffusing tips.[16] Interstitial phototherapy was carried out with seven of these fibers inserted into
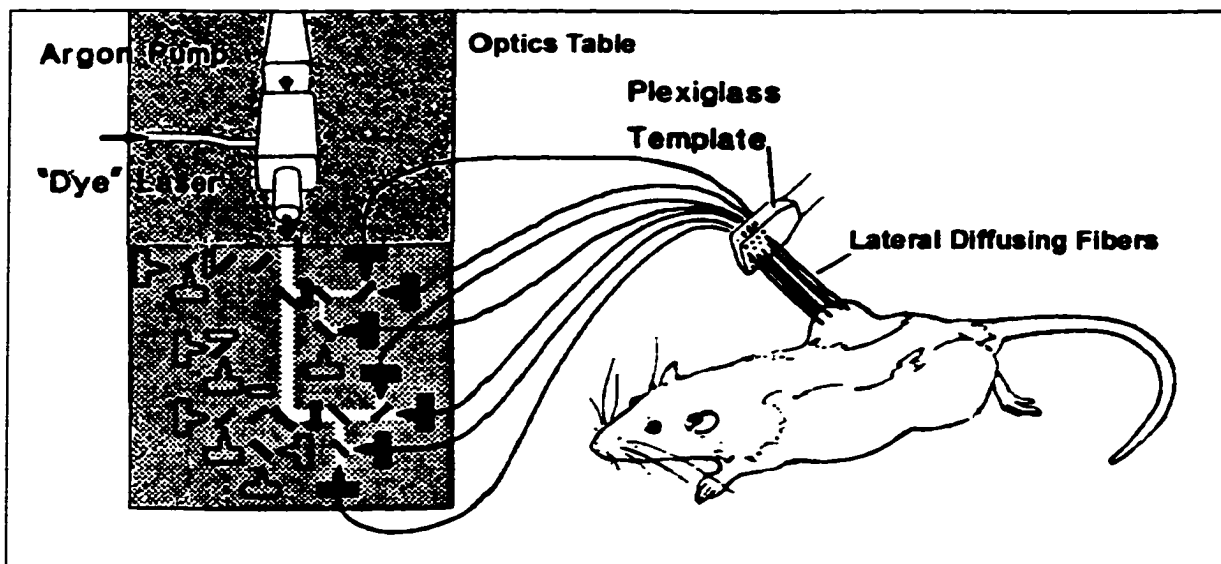
Figure 4.1. Experimental setup of interstitial laser therapy of subcutaneous rat AY-27 and R3327-H frank tumors. The argon-pumped dye laser (λ = 630 nm) was split and coupled to optic fibers which were inserted into the tumor through a template.

acetal plastic needles which were implanted into the tumor through a template, in a hexagonal pattern of equilateral triangles, 7 mm apart. A power meter (LaserTherapeutics, Inc., Buellton, CA) was used to check the power output (dose rate) of each fiber and to confirm the wavelength. The 8th fiber was placed in the power meter to continuously monitor the power output. The power output was kept constant at approx. 80 mW/fiber and the time of exposure was varied from 30 to 90 min to yield light-doses of 1000 J to 3000 J. The rat body was protected from light leaving only the tumor site exposed during PDT. Previous experiments in our laboratory showed that intratumor temperature did not exceed 40°C at a light dose rate of 90 mW/fiber for 60-min irradiation.[1] Therefore, monitoring for hyperthermic effects on tumor during phototherapy was not performed in this study.

4.2.6 Scintigraphy. In an attempt to explore if there were any relationship between vascular injury and tumor response in ALA-based interstitial PDT, the radiopharmaceutical ^{99m}Technetium hexamethylpropyleneamine oxime (^{99m}Tc-HMPAO) was used to study PDT-induced vascular shut-down in the well perfused Dunning R3327-H tumors. ^{99m}Tc-HMPAO has been shown to be a good marker of

123

tumor perfusion in both experimental animal tumors [1,17] and human lung tumors.[18] ^{99m}Tc-HMPAO was prepared by adding 5 mL of second elution ^{99m}Tc sodium pertechnetate to a lyophilized preparation of HMPAO in stannous chloride. Animals bearing R3327-H tumors were imaged with ^{99m}Tc-HMPAO scintigraphy 24 hours prior to and 48 hours post PDT. One mL (100 MBq) of ^{99m}Tc-HMPAO was injected *via* a tail vein. After allowing a minimum of 5 min for distribution, static images were obtained by placing the animals both supine and prone on the low-energy general purpose collimator of a Siemens ZLC gamma camera. With a 129-151 KeV window, 2-min images were acquired on a Picker PCS 512 computer using a 128 by 128 matrix. Quantitative data on regional activity were obtained from the digitized image using the region of interest (ROI) program.

4.3 Results

### 4.3.1 Biodistribution of ALA-induced PpIX.

The R3327-H tumor is a slow-growing, well-differentiated, well-perfused tumor. Little necrosis was found in the tumor center at volumes up to 3000 mm^3.[1,15] The AY-27 tumor however, had much shorter doubling time (3 to 5 days), grew to approx. 1000 mm^3 at about 28 days post tumor implantation. The periphery of the AY-27 tumor appeared well vascularized, but the tumor center became necrotic at volumes of about 1000 mm^3.[19] Despite the striking difference in histology and biology, the average PpIX levels in both AY-27 and R3327-H tumors were close, except the fluorescence distribution was more uniform in the R3327-H. Figure 4.2 shows the ALA-induced PpIX levels in the Dunning R3327-H tumors. The tumor PpIX level showed a dose-dependent increase at 4 hours after ALA administration. The PpIX level decreased at 6 hours. The biodistribution of ALA-induced PpIX in animals bearing AY-27 tumors has been discussed previously (also see chapter II).[19]

4.3.2 Interstitial PDT effects on the AY-27 and the R3327-H tumors.

Animals with tumors of volume approx. 1000 mm^3 were administered ALA (500 mg/kg) i.v. 4 hours prior to exposure to laser light. Figure 4.3 shows the AY-27 tumor volume as percentage of treatment volume after administration of ALA and
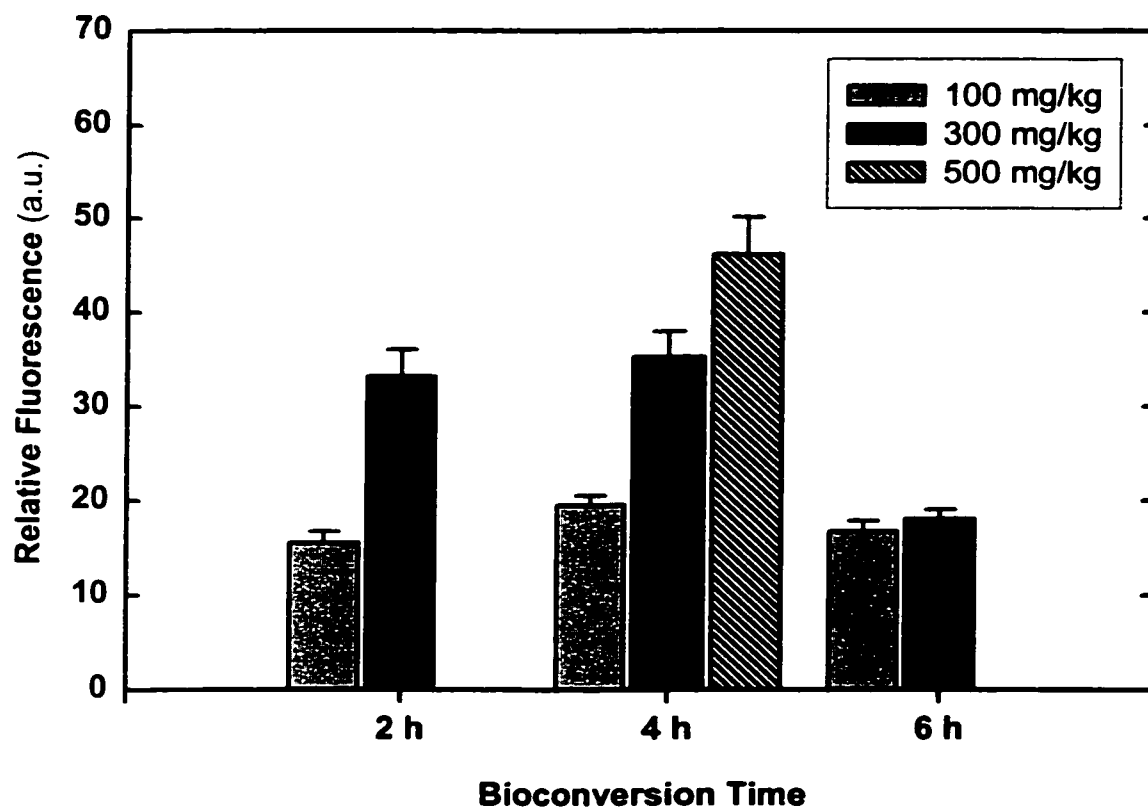
124

Figure 4.2 Relative mean PpIX fluorescence intensity in s.c. rat R3327-H prostate tumor after i.v. injection of ALA. Each value represents the mean of 30 measurements. (Error bar = SEM, a.u. = arbitrary fluorescence units).

125
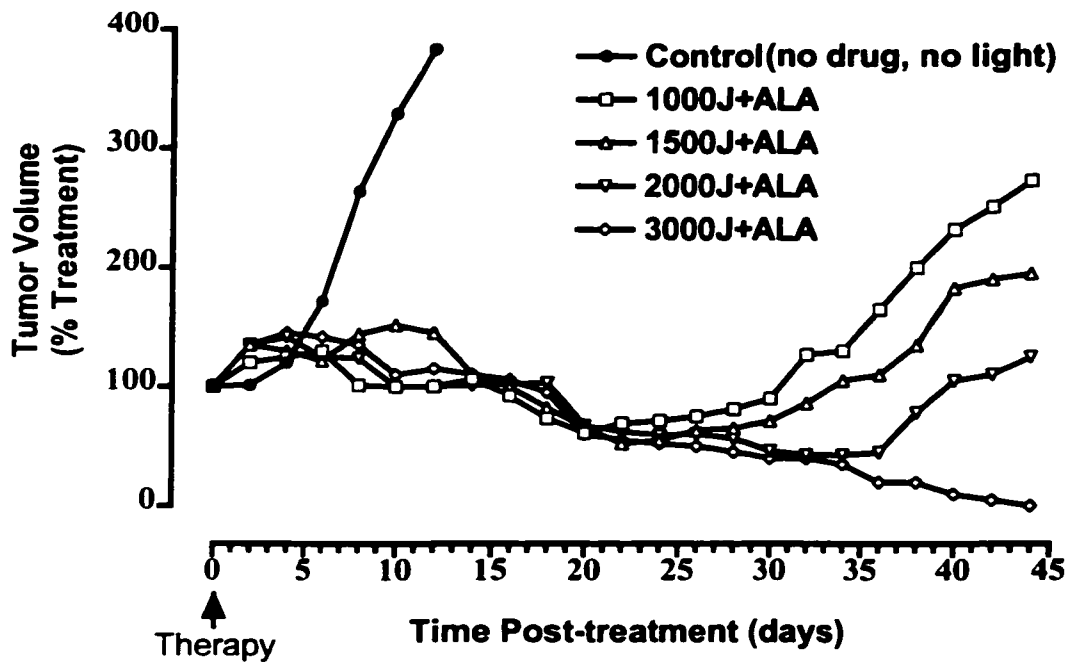
Fig. 4.3 Effect of total light dose in PDT of the AY-27 tumors growing s.c. in flanks of Fischer rats. Points, % pre-treatment tumor volume from 3 rats in each group.

126

irradiation with total light doses of 1000, 1500, 2000, and 3000 J. Tumor growth delays were measured for the respective light treatments (Table 4.1). The differences

Table 4.1 Growth delays of AY-27 and R3327-H tumors affected by PDT with various total light doses 4 h after i.v. injection of ALA

Treatment group	No. of rats	ALA dose (mg/kg)	Light dose (J)	Days to regrow to 4x treatment vol.	P value	No. of TFS* (>100 days)
A. AY-27	15					
Control	3	0	0	13.7 ± 3.1^a	−	0/3
Light dose 1	3	500	1000	179.3 ± 90.4	<0.05	2/3
Light dose 2	3	500	1500	183.3 ± 65.7	<0.05	2/3
Light dose 3	3	500	2000	185.7 ± 60.3	<0.05	2/3
Light dose 4	3	500	3000	250 ± 0^b	<0.01	3/3
B. R3327-H	12					
Control	3	0	2000	79.7 ± 27.3	−	0/3
Light dose 1	3	500	1000	159 ± 29.5	<0.05	0/3
Light dose 2	3	500	2000	169.3 ± 41.2	<0.05	1/3
Light dose 3	3	500	3000	250 ± 0^b	<0.01	3/3

^{a} Mean ± SD.

^{b} Estimated growth delay. If tumor was cured, 250 days was assumed for tumor regrow to 4x treatment volume. Overall, only one tumor recurred.

* Long-term tumor-free survivor.

between each treatment group (from 1000 to 3000 J) and control (no ALA, no light) were statistically significant (Table 4.1). Figure 4.4 shows the effect of ALA and total light doses of 1000, 2000, and 3000 J on R3327-H tumor volume. Likewise, tumor growth delays were measured for the respective light treatments (Table 4.1). Again, the differences between each group and control (light only) were also statistically significant (Table 4.1). These data showed a light dose-dependent tumor response to PDT in both tumor models, with more long-term tumor-free survival in the 3000 J groups. The immediate response to PDT was rapidly developing edema in the treatment field, progressing to scar formation overlying the tumor. The scar was usually detached from the tumor within two weeks. This was sometimes followed by the development of an open wound with necrotic tumor tissue exposed. The wound usually healed without evidence of tumor. However, tumors treated by light only

127
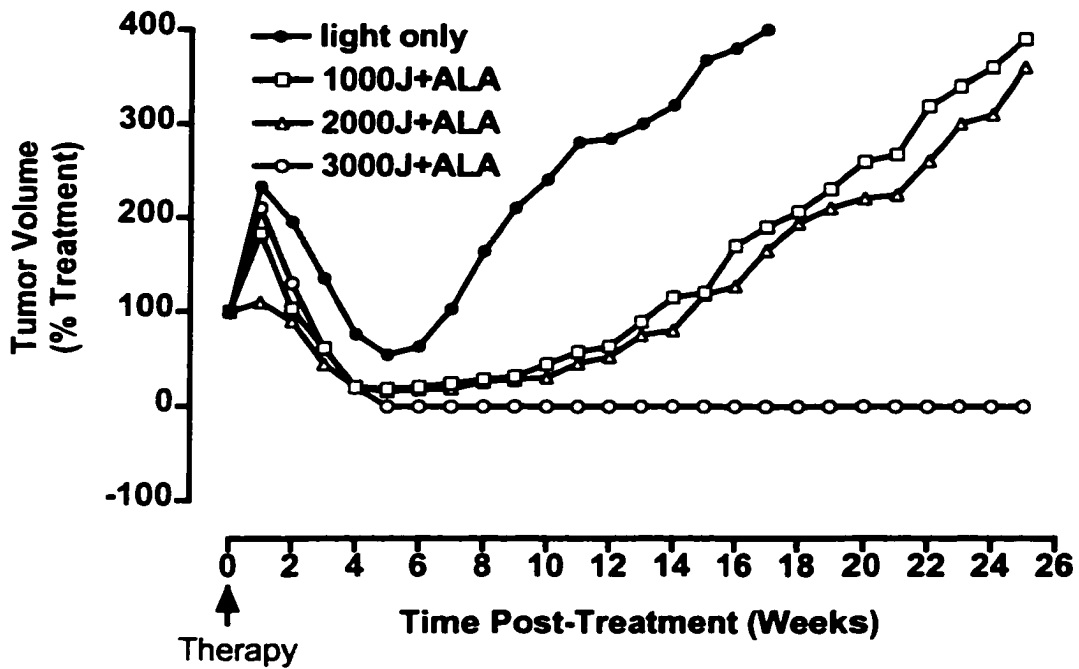
Fig. 4.4 Effect of total light dose in PDT on R3327-H tumors growing in flanks of Fischer x Copenhagen rats. Points, % pre-treatment tumor volume from 3 rats in each group.

128

(2000 J) also became edematous a few days after PDT probably due to insertion (trauma) of the fibers to tissues.
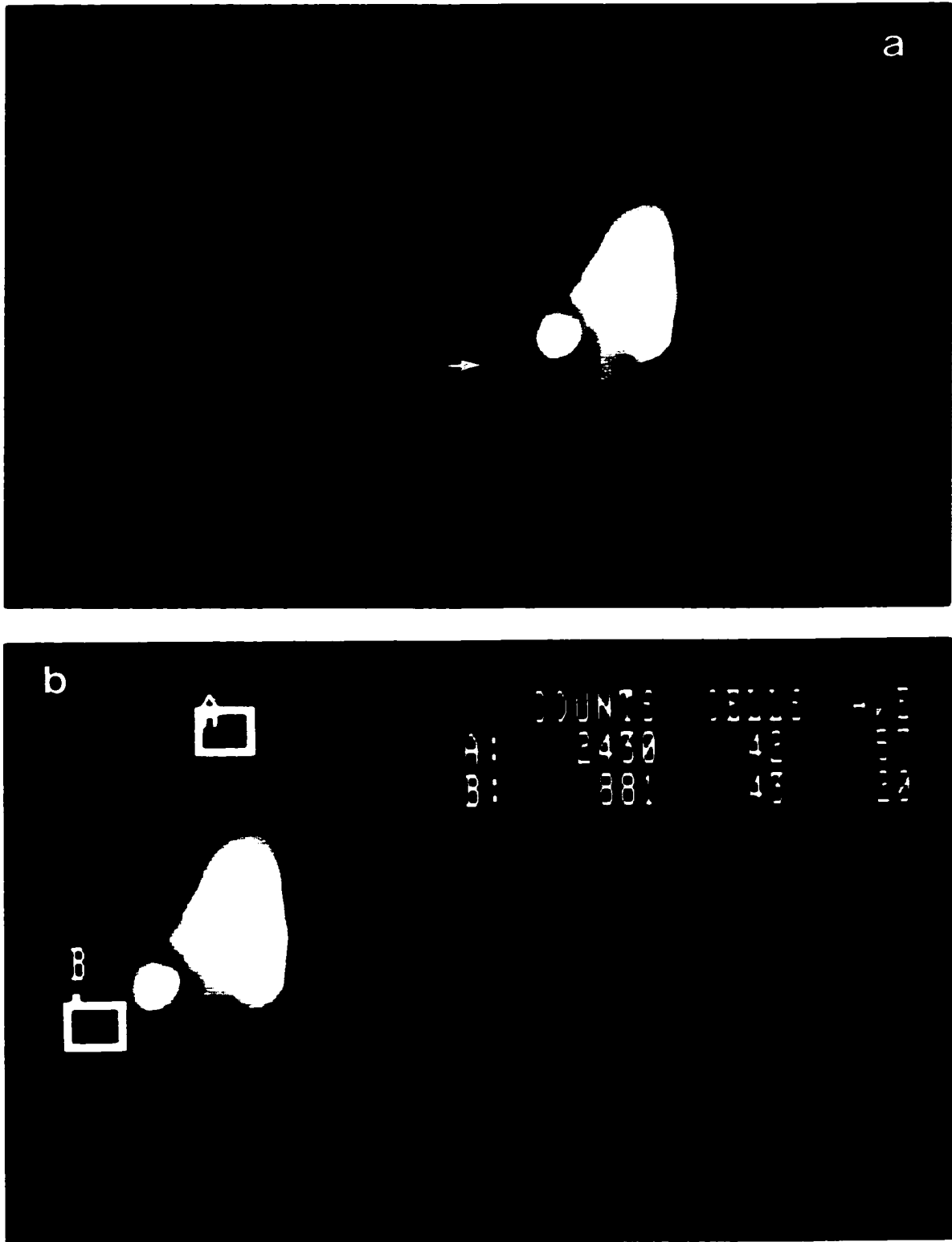
4.3.3 ^{99m}Tc-HMPAO Scintigraphy.

Figure 4.5a shows a pre-PDT scintigram of a rat bearing the well differentiated R3327-H tumor in its right flank. This tumor is reasonably well perfused when compared to the essential organs, with a tumor/brain ratio of ^{99m}Tc-HMPAO activity about 0.5 (Figure 4.5b). Using the ROI program, quantitative analysis of pre- and post-PDT scintigrams demonstrated a slight perfusion shutdown following PDT with 1000 to 3000 J total light dose. This change in perfusion however did not reach statistical significance (p = 0.35) (Table 4.2). As well, this study could not demonstrate a difference among the different light dose groups due to the small sample size.

Table 4.2 Tumor to brain ratios of ^{99m}Tc-HMPAO as a measure of
R3327-H tumor perfusion prior to and post PDT

Prior to PDT	Post PDT
0.375	0.243
0.549	0.356
0.445	0.514
0.449	0.185
0.260	0.447
0.329	0.401
0.367	0.234
0.350	0.080
Mean ± SD 0.390 ± 0.09	$0.307 \pm 0.20; p = 0.35$

4.4 Discussion

In this study, the AY-27 TCC and R3327-H prostate tumors that have remarkably different growth kinetics and vascularization have been chosen to investigate the antitumor efficacy and tumor perfusion changes after interstitial PDT with ALA. ALA-PDT appears clinically effective on a variety of superficial cancers,[7,12,13] but its effectiveness for solid tumors is still undefined. We have previously demonstrated an excellent response of the AY-27 tumors to ALA-mediated

129

Figure 4.5 Digitized ^{99m}Tc-HMPAO scintigrams of a rat bearing the R3327-H tumor (arrow) in his right flank pre-PDT (a), and (b) showing the ROIs within tumor and brain used to measure tumor/brain ratios.

PDT in the orthotopic bladder tumor model. This cell line therefore provided a known starting point for comparative response. Since the 630 nm light is attenuated in tissue rapidly,[1,16] illumination from the tumor surface resulted in only incomplete tumor destruction with a viable tumor base.[20] Previous studies from our laboratory demonstrated that the penetration of 'effective' light after a total dose of 2400 J was limited to tumor zones within 3 mm from each diffusing fiber when the tumor was sensitized with Photofrin.[1] Therefore, tumor volumes of 1700 to 2000 mm^3 should be effectively treated using seven fibers placed interstitially in an icosahedral array 8 mm apart. Using similar light delivery strategies in the present study, tumor growth delays and the possible underlying mechanism(s) of tumor response to ALA-based PDT have been investigated. Data from this study indicate that selective, complete tumor destruction is possible with interstitial PDT in small solid tumors. The higher proportion of long-term tumor-free response in the high light dose groups suggests that a sufficient total PDT dose (drug concentration × light dose) is needed for complete tumor destruction. One of the advantages of ALA-based PDT over Photofrin-based PDT is that PpIX derived from ALA is cleared from the body within 24 hours, thus prolonged skin phototoxicity encountered in Photofrin-PDT may be avoided.[5,7,8,20] The reason for tumor volumes increasing within a few days after PDT and returning to pretreatment volume in about 7 days may be due to edema of the skin and tumor induced by insertion of the fibers, since tumors treated with light only also have similar changes (Figure 4.4).

Although there is a striking difference in tumor doubling time and vascularization between the AY-27 and R3327-H tumors,[15,19] the tumor PpIX levels are unexpectedly close. It suggests that ALA could be diffused from the well-perfused periphery of the AY-27 tumor to the deeper cell layers and converted to PpIX. The locally converted PpIX may be accumulated *in situ* for a longer time due to the compromised lymphatic and vascular drainage in AY-27 tumor than in the well-vascularized R3327-H tumor. The similar PpIX levels in the two tumor models may also account for the similar tumor response to PDT. It appears that a major

131

component of this tumor response is the result of the direct cytotoxic effects of ALA-based PDT, which are dependent upon the total PDT dose.

However, whether tumor perfusion shutdown, a prominent mechanism of tissue destruction with Photofrin-PDT,[1,4] also plays a role in ALA-based photodamage of tumor is still to be determined. The initially reported absence of fluorescence from vascular structures has led to the speculation that ALA-based PDT is specific for tumor cells.[7,8] On the other hand, damage to the endothelium and the basal lamina of vascular walls has been observed following ALA-based PDT and in murine protoporphyria models.[21,22] Furthermore, vascular damage is an important hallmark of human porphyrias.[23] The data of this study show that the ratios of tumor/ brain perfusion remain almost the same prior to and 48 hours after PDT. Although we did not monitor the tumor blood flow during and immediately after PDT, tumor vascular shutdown appears to play a minimal role, if any, in ALA-mediated photodamage of tumor. Previous studies demonstrated that Photofrin-based PDT-induced vascular shutdown reached a maximum shortly after PDT and progressed thereafter.[1,24] Our results of perfusion changes after ALA-based PDT coincide well with others. Henderson *et al.* examined the vascular shutdown after ALA-PDT (surface illumination) in murine Colo26 tumors using fluorescein exclusion tests.[20] They reported only transient, incomplete perfusion shutdown after high ALA-PDT dose. The authors concluded that the transient shutdown might be due to a vasoconstrictive/ vasospastic effect. Roberts *et al.* also obtained an 80% reduction in vascular perfusion after ALA-PDT, with perfusion recovering with time.[25]

4.5 Conclusions

Interstitial PDT by inserting multiple optical fibers into the tumor appears an effective treatment modality for deeply seated tumors. The mechanism of ALA-based PDT may rely on direct cellular damage, rather than tumor perfusion shutdown. Further studies with larger sample size are needed to determine the light dose effect on both vascular shutdown and tumor response. These findings in the animal model support further exploration of ALA for interstitial PDT of human prostate cancer.

132

4.6 References:

1. Moore, R.B., Chapman, J.D., Mokrzanowski, A.D., Arnfield, M.R., McPhee, M.S. and McEwan, A.J. (1992) Non-invasive monitoring of photodynamic therapy with 99Technetium HMPAO scintigraphy. *Br. J. Cancer.* **65**: 491-497.

2. Lee, L.K., Whitehurst, C., Pantelides, M.L., Vernon, D.I. and Moore, J.V. (1996) Interstitial Photodynamic therapy in the Dunning R3327-AT6 Prostatic Carcinoma. Lasers Med. Sci., 11: 155-161.

3. Gomer C.J., Ferrario, A., Hauashi, N., *et al.* (1988) Molecular, cellular and tissue responses following photodynamic therapy. *Lasers Surg. Med.*, **8**: 450-463.

4. Henderson, B.W. and Dougtherty, T.J. (1992) How does photodynamic therapy work? *Photochem. Photobiol.*, **55**: 145.

5. Dougherty, T.J., Cooper, M.T. and Mang, T.S. (1990) Cutaneous phototoxic occurrences in patients receiving Photofrin. *Lasers Surg. Med.*, **10**: 485-488.

6. Kennedy, J.C., Pottier, R.H. and Pross. DC. (1990) Photodynamic therapy with endogenous protoporphyrin IX: basic principles and present clinical experience. *J Photochem. Photobiol. B: biol.* **6**: 143-148.

7. Kennedy, J.C. and Pottier, R.H. (1992) Endogenous protoporphyrin IX, a clinical useful photosensitizer for photodynamic therapy. *J. Photochem. Photobiol. B: Biol.*, **14**: 275-292.

8. Bedwell, J., Macroert, A.J., Phillips, D. *et al.*(1992) Fluorescence distribution and photodynamic effect of ALA-induced PpIX in the DMH rat colonic tumor model. *Br. J. Cancer.* **65**: 818-824.

9. Berlin, N.I., Neuberger, A. and Scott, J.J. (1956) The matabolism of δ-aminolevulinic acid, 2. Normal pathways, studied with the aid of 14C. *Biochem. J.*, **64**: 90-100.

10. Iinuma, S., Farshi, S.S., Ortel, B. and Hasan, T. (1994) A mechanistic study of cellular photodestruction with 5-aminoevulinic acid-induced porphyrin. *Br. J. Cancer.* **70**: 21.

133

11. Hua, Z., Gibson, S.L., Foster, T.H. and Hilf, R. (1995) Effectiveness of δ-aminonevulinic acid-induced protoporphyrin as a photosensitizer for photodynamic therapy *in vivo*. *Cancer Res.*, **55**: 1723-1731.

12. Grant, W.E., Hopper, C., MacRobert, A.J., *et al.* (1993) Photodynamic therapy of oral cancer: photosensitization with systemic aminolevulinic acid. *Lancet*. **342**: 147-148.

13. Regula, J., MacRobert, A.J., Gorchein, A., Buonaccorsi, G.A., Thorpe, S.M., Spencer, G.M., Hatfield, A.R. and Bown, S.G. (1995) Photosensitization and photodynamic therapy of esophageal, duodenal, and colorectal tumors using 5-aminolevulinic acid induced protoporphyrin IX - a pilot study. *Gut*. **36**: 67-75.

14. Isaacs, J.T. (1987) Development and characteristics of the available animal model systems for the study of prostate cancer. In Coffey, D.S., Bruchovsky, N., Gardener, W.A., Resnick, M.I. & Cur, J.P. (eds), *Current concepts and approaches to the study of prostate cancer*. Pp. 513-576. New York: Alan R. Liss.

15. Thorndyke, C., Meeker, B.E., Thomas, G., Lakey, W.H., McPhee, M.S. and Chapman, J.D. (1985) The radiation sensitivities of R3327-H and R3327-AT rat prostate adenocarcinomas. *J. Urol.*, **134**: 191-198.

16. Arnfield, M.R., Gonzalez, S., Lee, P., Tulip, J. & McPhee, M.S. (1986) Cylindrical irradiator fiber tip for photodynamic therapy. *Lasers Surg. Med.*, **6**: 150.

17. Hammersley, P.A.G., McCready, V.R., Babich, J.W. and Coghlan, G. (1987) 99mTc-HMPAO as a tumor blood flow agent. *Eur. J. Nuc. Med.*, **13**: 90.

18. Rowell, N.P., McReady, V.R., Tait, D. et al. (1989) Technetium-99m HMPAO and SPECT in the assessment of blood flow in human lung tumors. *Br. J. Cancer*. **59**: 135.

19. Xiao, Z., Miller, G.G., McCallum, T.J., Brown, K.M., Lown, J.W., Tulip, J. and Moore, R.B. (1998) Biodistribution of Photofrin II and 5-aminolevulinic acid - induced protoporphyrin IX in normal rat bladder and bladder tumor models. *Photochem. Photobiol.* **67** (5): 513-518.

134

20. Henderson, B.W., Vaughan, L., Bellnier, D.A., van Leengoed, H., Johnson, P.G. and Oseroff, A.R. (1995) Photosensitization of murine tumor, vasculature and skin by 5-aminolevulinic acid-induced porphryrin. *Photochem. Photobiol.*, **62**: 780-789.

21. Konrad, K., Hönigsmann, H., Gaschnatt, F. and Wolff, K. (1975) Mouse model for protoporphyria II. Cellular and subcullular events in the photosensitivity flare of the skin. *J. Invest. Dermatol.*, **65**: 300-310.

22. Peng, Q., Moan, J., Warloe, T., Nesland, J.M. and Rimington, C. (1992) Distribution and photosensitizing efficiency of porphyrins induced by application of exogenous 5-aminolevulinic acid in mice bearing mammary carcinoma. *Int. J. Cancer.* **52**: 433-443.

23. Brickers, D.R. (1987) The dermotologic manifestations of human porphyria. *Ann. N.Y. Acad. Sci.*, **514**: 261-267.

24. Star, W.M., Marijnissen, H.P.A., van den Bergblock, A.E., Versteg, J.A.C., Franken, K.A.P., and Reinhold, H.S. (1986) Destruction of rat mammary tumor and normal tissue microcirculation by hematoporphyrin deriveritive photoirradiation observed in vivo in sandwich observation chambers. *Cancer Res.*, **46**: 2532.

25. Roberts, D.J.H., Cairnduff, F., Driver, I., Dixon, B. and Brown, S.B. (1994) Tumor vascular shutdown following photodynamic therapy based on polyhaematoporphyrin or 5-aminolevulinic acid. *Int. J. Oncol.*, **5**: 763-768.

135

CHAPTER V

USING MULTICELL SPHEROIDS FOR STUDYING INTRATUMOR DISTRIBUTION OF PHOTOSENSITIZERS: A CONFOCAL MICROSCOPY STUDY

5.1 Introduction

In photodynamic therapy (PDT), a photosensitizer, light, and oxygen are used to cause photochemically induced cell death.[1] Several mechanisms of cytotoxicity have been proposed to be responsible for tumor destruction, including direct and indirect cell killing.[2,3] Direct cell killing depends on selective accumulation of appropriate amounts (>threshold level) of a photosensitizer in tumors.[3] The physicochemical properties of a sensitizer can influence the distribution and accumulation in target tissue. For instance, lipophilic photosensitizers need to be incorporated into lipid-based delivery vehicles for administration and associate predominantly with cellular membranes. *In situ* photoactivation is therefore likely to result in direct cell killing.[4,5] The selectivity of tumor targeting may be facilitated and enhanced when the sensitizer is incorporated into liposomes and conjugated with monoclonal antibodies specific for tumor antigens.[5,6,7,8,9] In contrast, hydrophilic sensitizers, such as tri- and tetrasulfonated porphyrins and phthalocyanines, tend to bind in a noncovalent fashion to plasma proteins (albumin and globulins) after systemic administration and subsequently localize in the vascular stroma.[10,11] Photoactivation causes damage to the tumor microvasculature, leading to vascular stasis, infarction, and tumor necrosis (indirect cell killing).[12] Targeting of the microvasculature seems also a prominent feature of *in vivo* tumor response with Photofrin (porfimer sodium),[1,3] the only approved sensitizer for clinical use. Patients treated with Photofrin-PDT however, exhibit prolonged skin phototoxicity.[13] This side effect is caused by the accumulation and prolonged retention of the photosensitizer in the skin. As well, the treatment depths of 630 nm light which is required to activate Photofrin are less than 0.5 cm^3. These disadvantages of Photofrin-PDT have prompted the search for better photosensitizers. Newer sensitizers, such as phthalocyanines. benzoporphyrin derivatives, and hypocrellins,

137

offer greater light absorption in the red spectrum with the potential for deeper tissue damage. As well, monomeric molecules of these second-generation sensitizers offer more rapid clearance from normal tissues.[14,15,21]

Superficial bladder cancer represents a favorable target for PDT[16] and other novel intravesical therapies. To avoid systemic side effects such as prolonged skin phototoxicity, topical administration of photosensitizers seems more suitable for PDT of superficial bladder carcinomas, if tumor tissue can take up an appropriate amount of photosensitizer. On the other hand, intravesical administration of drugs, especially liposomal formulations, might facilitate photosensitizer uptake in tumor tissue, due to direct contact of the drug with tumors, thereby avoiding uptake by the macrophages of the reticuloendothelial system. Intratumoral distribution and accumulation of photosensitizers are critical in whole bladder PDT in which preservation of normal bladder function is equally important to tumor destruction. Multicell spheroids have been suggested as reasonable *in vitro* tumor models for studying distribution and efficacy of chemo- and radio-therapeutic agents.[17,18,19] In this study, the penetration and distribution of several second-generation photosensitizers in MGH-U3 spheroids were investigated by laser scanning microscopy, compared with that of Photofrin and liposomal formulations of hypocrellins, to explore the potential of these photosensitizers for PDT of bladder cancers after intravesical administration. These studies aimed to provide important information for selecting photosensitizers and optimal drug delivery strategies for PDT and photo-detection of bladder cancer.

5.2 Materials and methods

5.2.1 Tumor cell and spheroid growth kinetics. The spheroids were generated from a well-to-moderately differentiated human transitional cell carcinoma cell line (MGH-U3), which was generously provided by Dr. Y. Fradet at the University of Laval, Quebec. MGH-U3 cells express a M_r 54,000 surface glycoprotein (gp54) antigen, which reacts specifically with a monoclonal antibody, 48-127 mAb.[20] Spheroids were generated by adding 2×10^6 cells to 60 mL of Dulbecco's modified Eagle's medium [D-MEM (Gibco/BRL, Burlingon, ON)] supplemented with 10%

fetal calf serum and antibiotics. The spheroids grew in a 200 mL spinner flask on a stir-plate at standard cell culture conditions (37°C, 5% CO_2). Half of the medium was replaced with fresh medium 4 days later and every other day thereafter. To establish the growth kinetics of the spheroids, samples were taken every two days. The spheroids' size was measured by microscopy. Spheroids reaching 300 μm in diameter (at 8 – 10 days) were processed for histology to determine if there were necrotic cells in the center, or for scanning electron microscopy (SEM) to look at cell-cell attachment on the spheroid surface and in cross section.

5.2.2 Photosensitizers. 1) Photofrin was provided by QLT PhotoTheraputics Inc., Vancouver. It was first dissolved in 5% dextrose (Abott Laboratories, Montreal, QC), then diluted with serum-free medium immediately before incubation with spheroids. 2) Hypocrellin B (HBs) included HBEA-R1/R2 (ethanolaminated HB, M_r 614), HBBA-R2 (n-butylaminated HB, M_r 636), liposomal HBEA-R1/R2, liposomal HBBA-R2, and immunoliposomal HBBA-R2 (with 48-127 mAb or non-specific, isotype matched mouse anti-OVCAR3 mAb). The physical and chemical properties of hypocrellins have previously been reported in detail by this laboratory.[21] The chemical structures of HBEA-R1 and HBBA-R2 are illustrated in Figure 5.1. The hypocrellins used in this study were provided by Altarex Corp. (Edmonton, AB). The free hypocrellins were first dissolved in chloroform/ethanol, and then diluted with serum-free medium. The (immuno)liposomal preparations will be discussed below. 3) Aluminum phthalocyanine chloride (AlPC) was provided by Acros Organics (M_r 575). 4) Protoporphyrin IX (PpIX, M_r 562.7) was purchased from Sigma Chemical Co. (St. Louis, MO). Both AlPC and PpIX were first dissolved in dimethyl sulfoxide (DMSO), and then diluted with serum-free medium. And, 5) 5-aminolevulinic acid (ALA) was supplied as a hydrochloride salt with a purity of 98% (Sigma Chemical Co.). The ALA powder (M_r 167.6) was dissolved in serum-free medium and the pH was adjusted to ~7 with 5 N NaOH immediately before use.

5.2.3 Liposomal and immunoliposomal photosensitizer formulations. The procedures of liposome preparation were described elsewhere.[22,23,24] 2-iminothiolane,

139
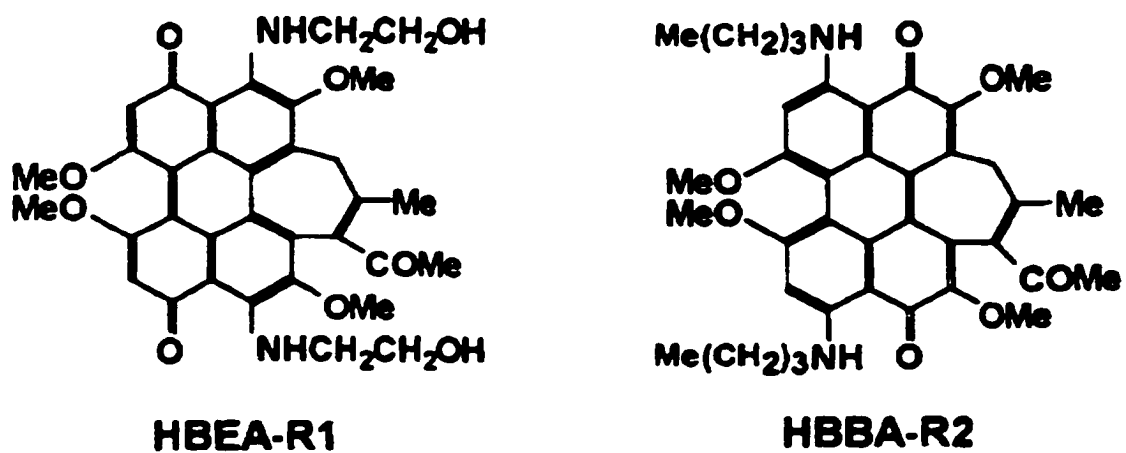
Figure 5.1 Chemical structures of ethanolaminated HB
(HBEA-R1) and butylaminated HB (HBBA-R2).

140

dipalmitoyphosphatidylcholine (DPPC), distearolphosphatidylethanolamine (DSPE), distearolphosphatidylcholine (DSPC), dipalmitoyphosphatidylglycerol (DPPG), polyethylene glycol (PEG, M_r 2000), and maleimide-PEG2000-DSPE were obtained from Sigma (St. Louis. MO). The 48-127 mAb is directed against the MGH-U3 cell surface antigen (gp54).[20] The anti-OVCAR3 mAb specifically recognizes the OVCAR3 antigen presented on human ovarian carcinomas.[25] The long circulating, sterically stabilized (Stealth) HBBA-R2 and HBEA-R1/R2 liposome (SL) and immunoliposome (SIL) formulations were composed of DPPC/maleimide-PEG2000-DSPE (94:6 molar ratio) and DSPC/cholesterol/maleimide-PEG2000-DSPE (64:30:6 molar ratio) respectively. The maleimide-PEG2000-DSPE was incorporated into the liposomal bilayer to couple the antibody covalently to the PEG terminus. Classic HBBA-R2 liposomes (CL) were formulated with DPPC/DPPG at a 9:1 molar ratio.

Two methods were used to load hypocrellins into liposomes. HBBA-R2 was loaded into pre-formed SL and SIL by a solvent injection method at a 15:1 lipid to drug molar ratio. HBBA-R2 was loaded into CL (15:1, lipid:drug) and HBEA-R1/R2 was loaded into SL (2:1, lipid:drug) by a solvent dilution method. For the solvent injection method, liposomes were first prepared by hydrating a dried thin film, of various lipids, to a final concentration of 10 mM with either 20 mM HEPES, 140 mM NaCl, pH 7.4 for SL preparations or 20 mM MOPSO, 140 mM NaCl, pH 6.7 for SIL preparations. The drug, dissolved in solvent (approx. 10 – 20 mM in methanol or approximately 5 – 10 mM in PEG300), was heated to 65°C and injected, dropwise, into a 65°C solution of liposomes. For the solvent dilution method, the lipids and drug were first mixed together from stock solutions in organic solvent then dried. Either methanol or PEG300 was then added to give a final lipid concentration of 200 mM or 50 mM respectively. Liposomes were formed when the lipid and drug solution was slowly diluted to 10 mM lipid at 65°C with the addition of small aliquots of heated buffer (20 mM HEPES, 140 mM NaCl, pH 7.4).

The resulting hypocrellin-liposomes were extruded through 80 nm polycarbonate membranes using a Lipex® Biomembranes extrusion device to give an

141

average vesicle size of 100 nm. The liposomes were then purified by gel filtration and assayed for lipid and drug concentrations. The final lipid to drug molar ratio of 20:1 was usually obtained for all formulations.

The preparation of immunoliposomes was described recently.[24] The antibodies (anti-OVCAR3 and 48-127 mAb) were first dissolved in 20 mM pyrophosphate buffer (pH 8.0), then incubated with 15 molar excess of 2-iminothiolane for 1 hour at 22°C. The thiolated antibody was purified and the pH lowered by gel chromatography using 20 mM MOPSO 140 mM NaCl, pH 6.7 buffer. The thiolated antibody was then incubated at a concentration of 50-μg mAb/μM lipid overnight at 22°C with maleimide-liposomes. Unbound antibody was removed by gel filtration, eluting with 20 mM HEPES, 140 mM NaCl, pH 7.4 buffer. Lipid phosphate was determined by the colorimetric method, and the amount of protein coupled to the liposomes was determined by the amino acid analysis (Beckman System 6300 Amino Acid Analyzer, Alberta Peptide Institute). The final mAb/lipid ratios in SIL were 25 μg/μM for anti-OVCAR3 mAb and 7 μg/μM for 48-127 mAb.

5.2.4 Photosensitizer distribution in spheroids. Spheroids 200- to 400-μm in diameter were incubated with graded doses (0 – 20 μM) of the above photosensitizers (HBEA-R1/R2, HBBA-R2, liposomal HBEA-R1/R2, liposomal HBBA-R2, immunoliposomal HBBA-R2, AlPC, PpIX), except Photofrin (0 – 15 μg/mL) and ALA (0 – 100 mM), for different timepoints (1 – 4 h). The concentrations of lipids in these tests ranged from 0 to 300 μM. Plain liposomes (300 μM lipids) were also incubated with spheroids for lipids only control. More than 5 spheroids were incubated in a 35-mm suspension culture dish (Corning, NY) in 2-mL of solution containing various drugs at 37°C. At the end of the incubation, the spheroids were gently washed with phosphate-buffered saline (PBS) three times, and optically scanned using a confocal laser scanning microscope (CLSM). The CLSM system (Molecular Dynamics, CA) consisted of an argon-krypton laser for excitation scanning, a Nikon inverted microscope to focus on the spheroids by using transmitted light or epifluorescent illumination, and ImageSpace® software (version 3.2,

142

Molecular Dynamics, CA) to explore the images (analyzing intensity profile, 3–D rendering). For consistency, all physical parameters pertaining to fluorescence excitation and detection were kept constant throughout the study, and are listed as follows: 20×/0.55 objective lens; 488/568 nm exciting wavelengths (for AlPC, 647 nm was applied); 488/568 nm beam-splitter (for AlPC, 647 nm beam-splitter was used); 590 nm long-pass (LP590) barrier filter for fluorescence detection (for AlPC, a LP660 filter was used); photomultiplier voltage 600 V; laser power 40 mW; pinhole 50; image size 512×512 (μm); pixel size 1.0×1.0 (μm); step size (interval between optical slices) $2 - 3$ μm. Three to five typical spheroids from each group were scanned from the surface to the center, and images were stored in the computer for further analysis.

The fluorescence intensity, which represents the photosensitizer concentration, in the central section of each spheroid was measured using the ImageSpace® software. The area under the intensity vs. spheroid diameter curve was calculated with the trapezoid area formula, and normalized by each spheroid's diameter.

5.3 Results

5.3.1 Growth characteristics of MGH-U3 spheroids

The spheroids' growth kinetics is shown in Figure 5.2. At $8 - 10$ days, the average diameter of the spheroids was around 300 μm. The spheroids continued to grow to $600 - 700$ μm at $4 - 5$ weeks, and then attached to each other and disintegrated thereafter due to shearforce of stirring. Histological examination showed all the cells from the periphery to the center were healthy in spheroids less than 400 μm in diameter. In those spheroids greater than 500 μm, a central zone of degenerative changes was observed (Figure 5.3). Scanning electron microscopy showed tight cell-cell interdigitations of microvilli at both spheroid surface and cross section (Figs 5.4, 5.5). The cells in the center were also as healthy as in the periphery when the spheroid was less than 400 μm (Figure 5.5).

143
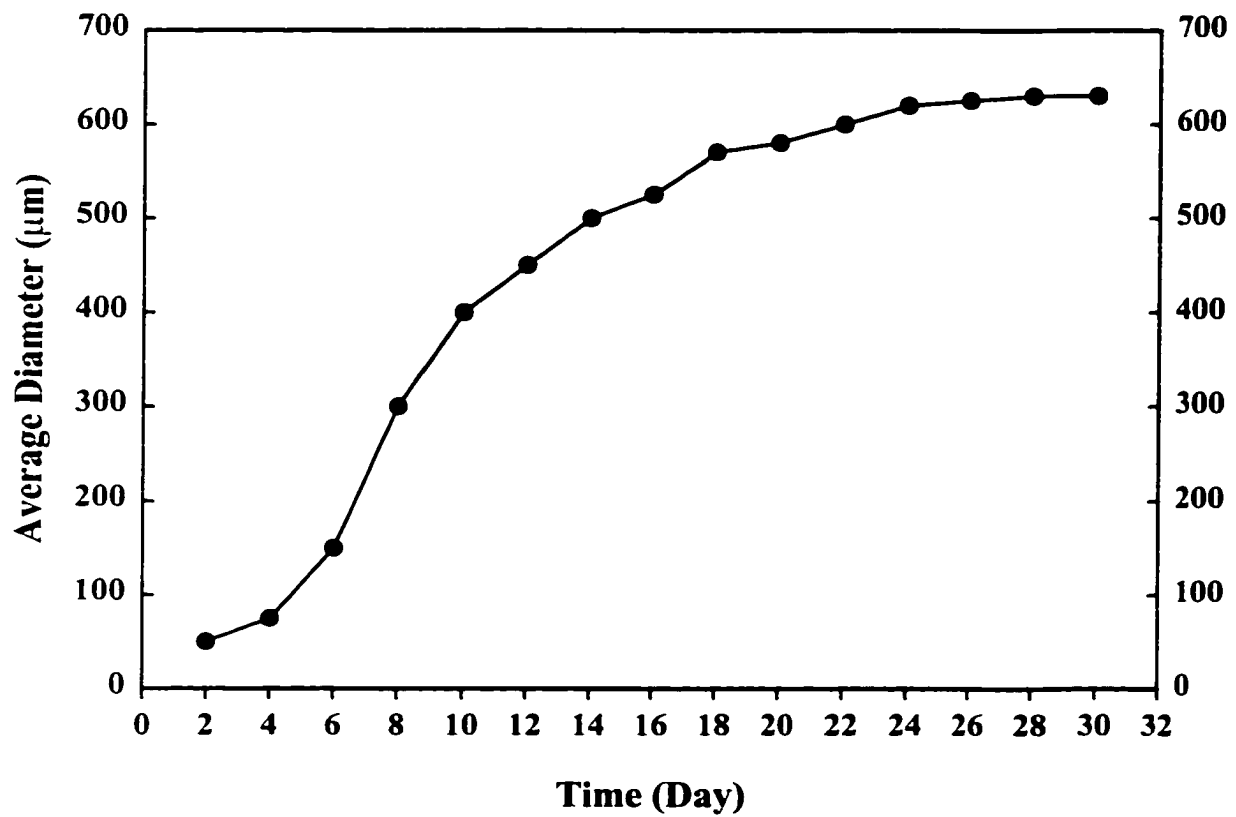
Figure 5.2 Growth kinetics of MGH-U3 spheroids cultured in spinner flask

144
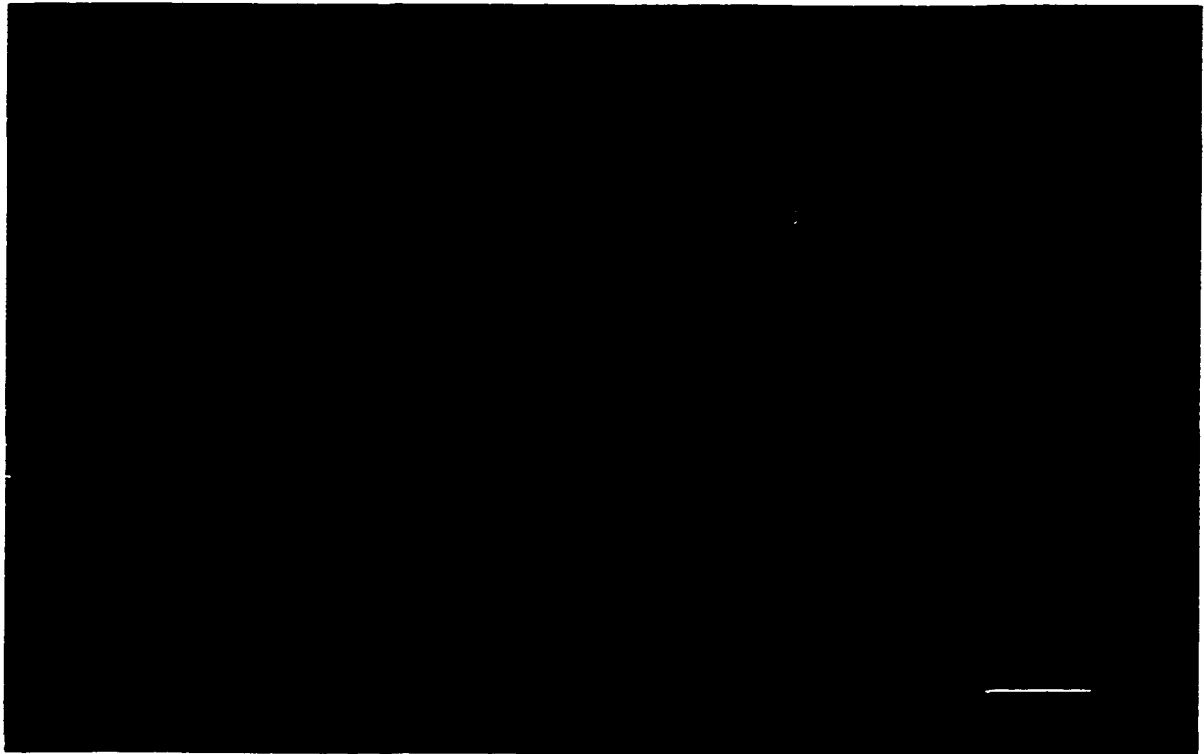
Figure 5.3 Histologic section of a large MGH-U3 spheroid showing healthy cells on the periphery, while the cells in the center show early degenerative changes. The clefts between cells are artifacts due to processing (H&E stain). Bar = 100 μm.

145

881435 2.0 kV   X200   i50µm
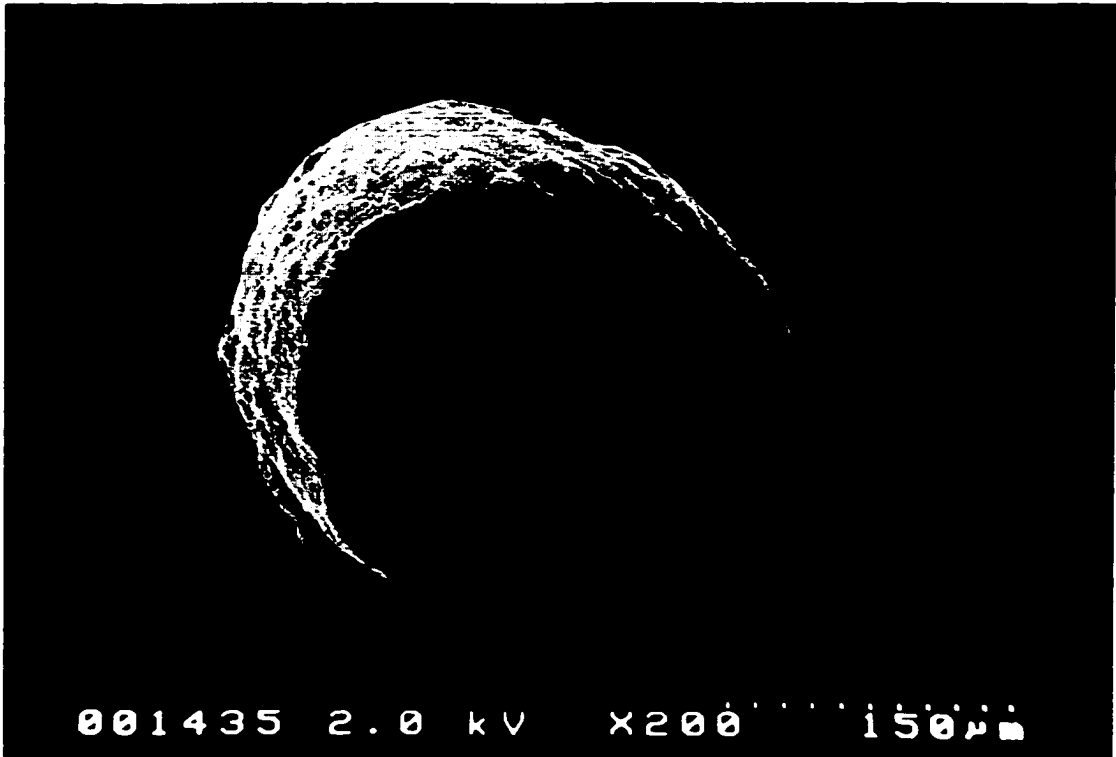
Figure 5.4 SEM microphotograph of a MGHU3 spheroid (~300 nm in diameter) which models a small tumor aggregate comprised of tightly adhesive epithelial cells .

146
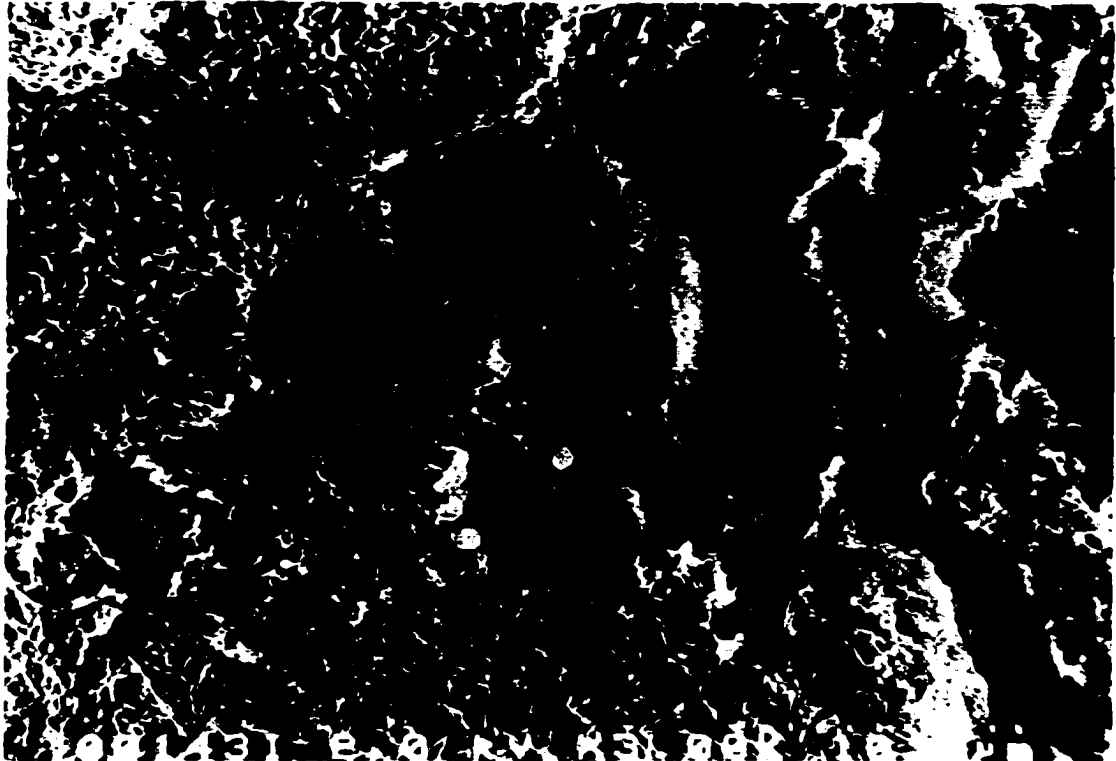
Figure 5.5 SEM microphotograph of a cross section of a spheroid displaying cohesive cells with peripheral microvillous projections.

147
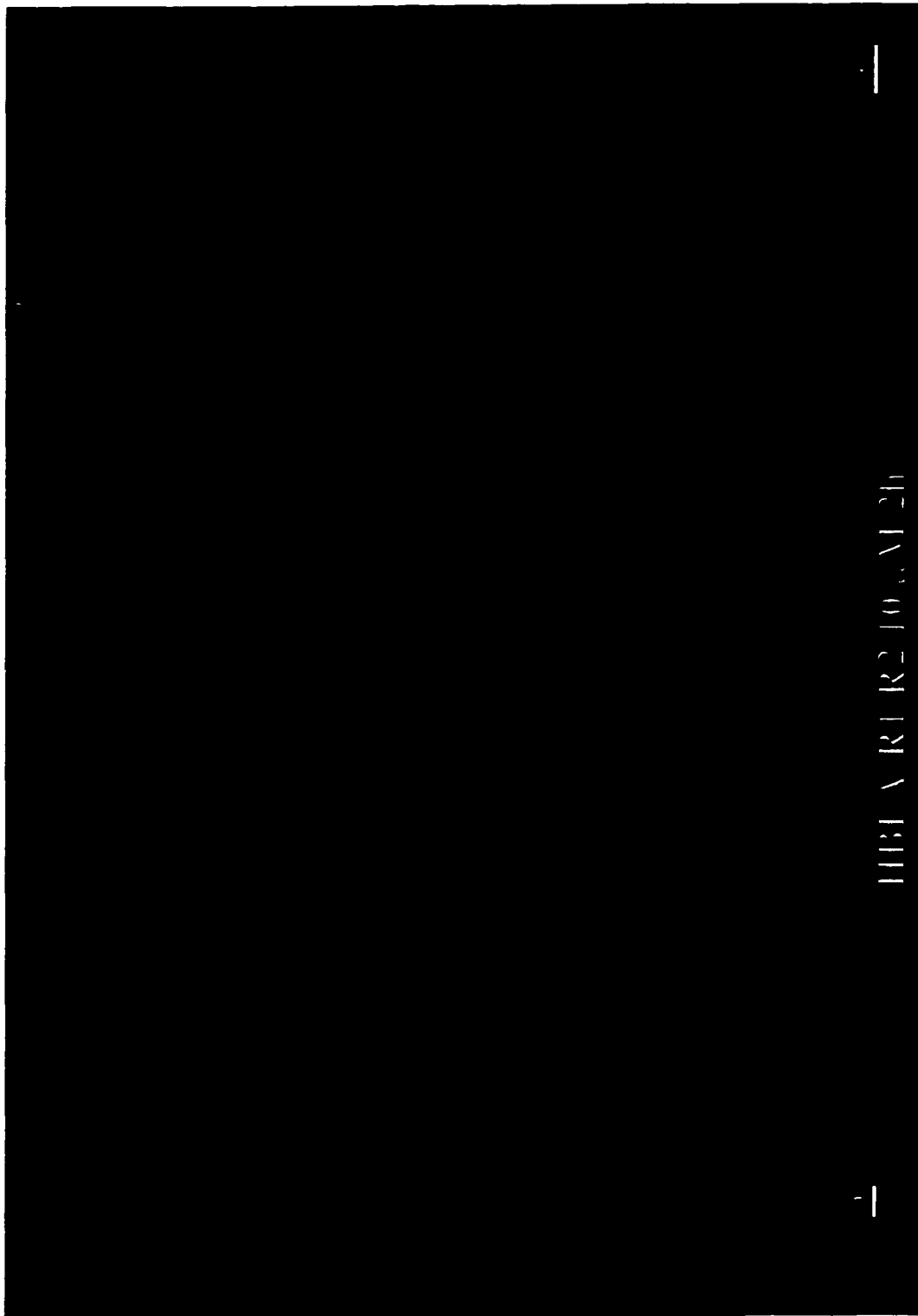
Fig. 5.6 Confocal sections of a MGH-U3 spheroid incubated with HBEA-R1/R2 for 2 h. Inset, 3-D projection of the spheroid. Bars denote μm.

148

5.3.2 Intraspheroid distribution of photosensitizers

Figure 5.6 shows a series of confocal sections scanned from the surface to the center of a spheroid incubated with HBEA-R1/R2, the 3-D projection of this spheroid is also shown. The penetration depths of various agents and the fluorescence intensity profiles in the central cross sections of spheroids are displayed in Figures 5.7 – 5.20, and the average normalized areas under the intensity *vs.* spheroid diameter curve are summarized in Table 5.1. In terms of penetration of free drugs, hypocrellins, especially HBEA-R1/R2, were distributed much more uniformly than AlPC, Photofrin, and PpIX (Figs 5.7, 5.9 – 5.12). HBEA-R1/R2 could penetrate well into the spheroid center (Figs 5.6, 5.7). The penetration of HBBA-R2 however, was not as good as HBEA-R1/R2, leading to higher fluorescence in the spheroid surface (Figure 5.8). The normalized fluorescence intensities of hypocrellins were also much higher than that of other agents in the spheroids based on a molar basis (Table 5.1). Compared with the free hypocrellins, the liposomal formulations of HBEA-R1/R2 and HBBA-R2 delivered the photosensitizers more efficiently into the spheroids leading to much higher fluorescence intensity (Figs 5.7, 5.8, 5.13, 5.16, & Table 5.1).

The intraspheroid distribution pattern of liposomal formulations depended on the lipophilicity of the sensitizer loaded. The more lipophilic the drug, the less the penetration depth, and the higher fluorescence intensity in the spheroid periphery relative to the center (Figs 5.13, 5.14). The liposomal HBEA-R1/R2 delivered the drug into spheroids more uniformly (from the periphery to the center) than the liposomal HBBA-R2 (Figs 5.13, 5.14, 5.16), probably because HBEA-R1/R2 is less lipophilic than HBBA-R2 (Figure 5.1), and part of the amphiphilic HBEA-R1/R2 leaked from liposomes. Therefore the intraspheroid distribution patterns of the liposomal formulations were similar to that of the corresponding free drugs (Figs 5.7, 5.8, 5.13, 5.14). These results suggested that the immunoliposomal HBEA-R1 might be not suitable for photo-detection of bladder cancer. Different liposomal (classical, Stealth®, and immunoliposomal) preparations of HBBA-R2 showed quite similar intraspheroid distribution patterns (Figs 5.15 – 5.18), whereas the fluorescence

149
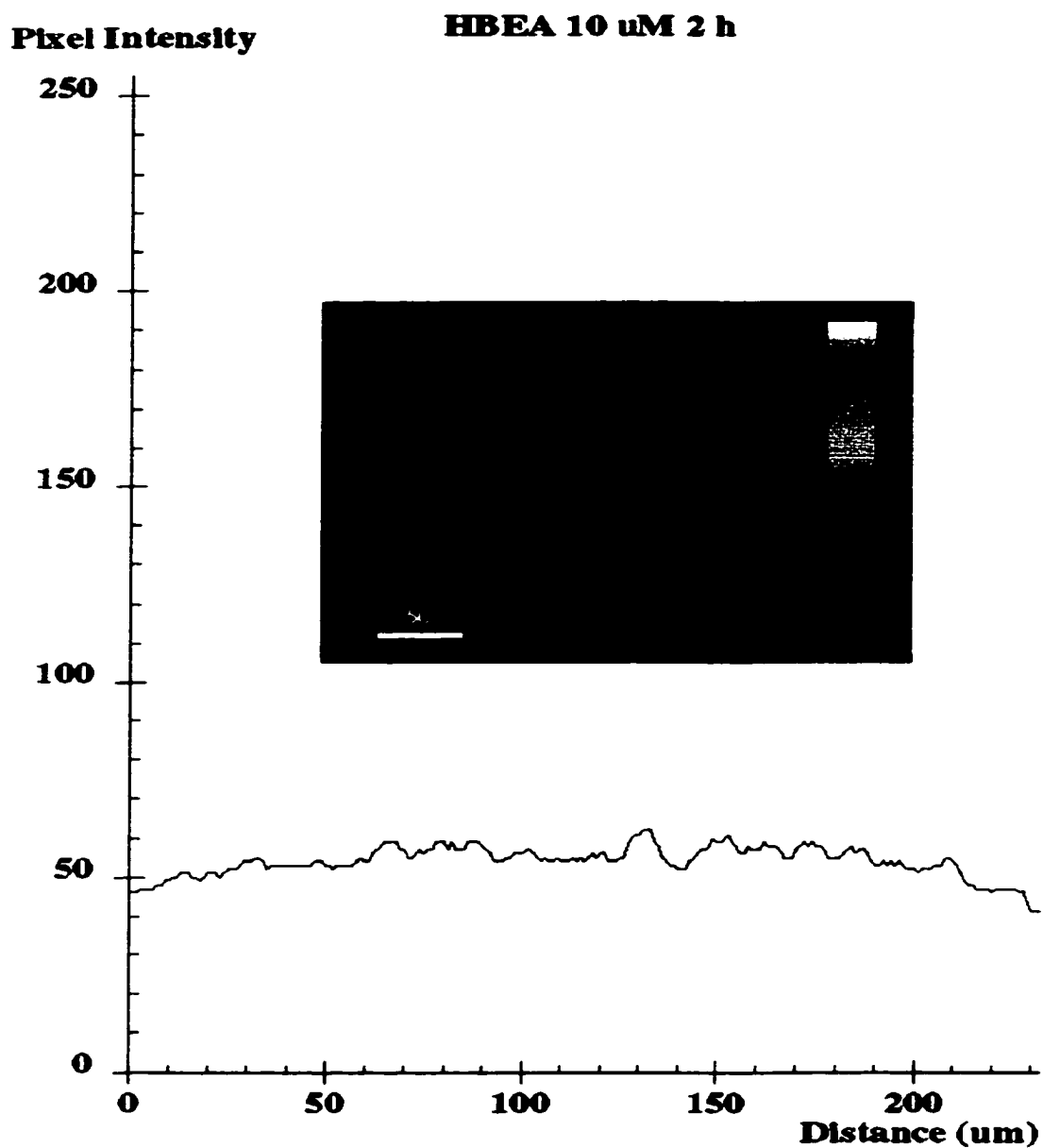
Fig. 5.7 Intraspheroid drug distribution and intensity profile
in the central section of a spheroid incubated with HBEA-R1/R2
10 μM for 2 h. Bar = 50 μm.

150
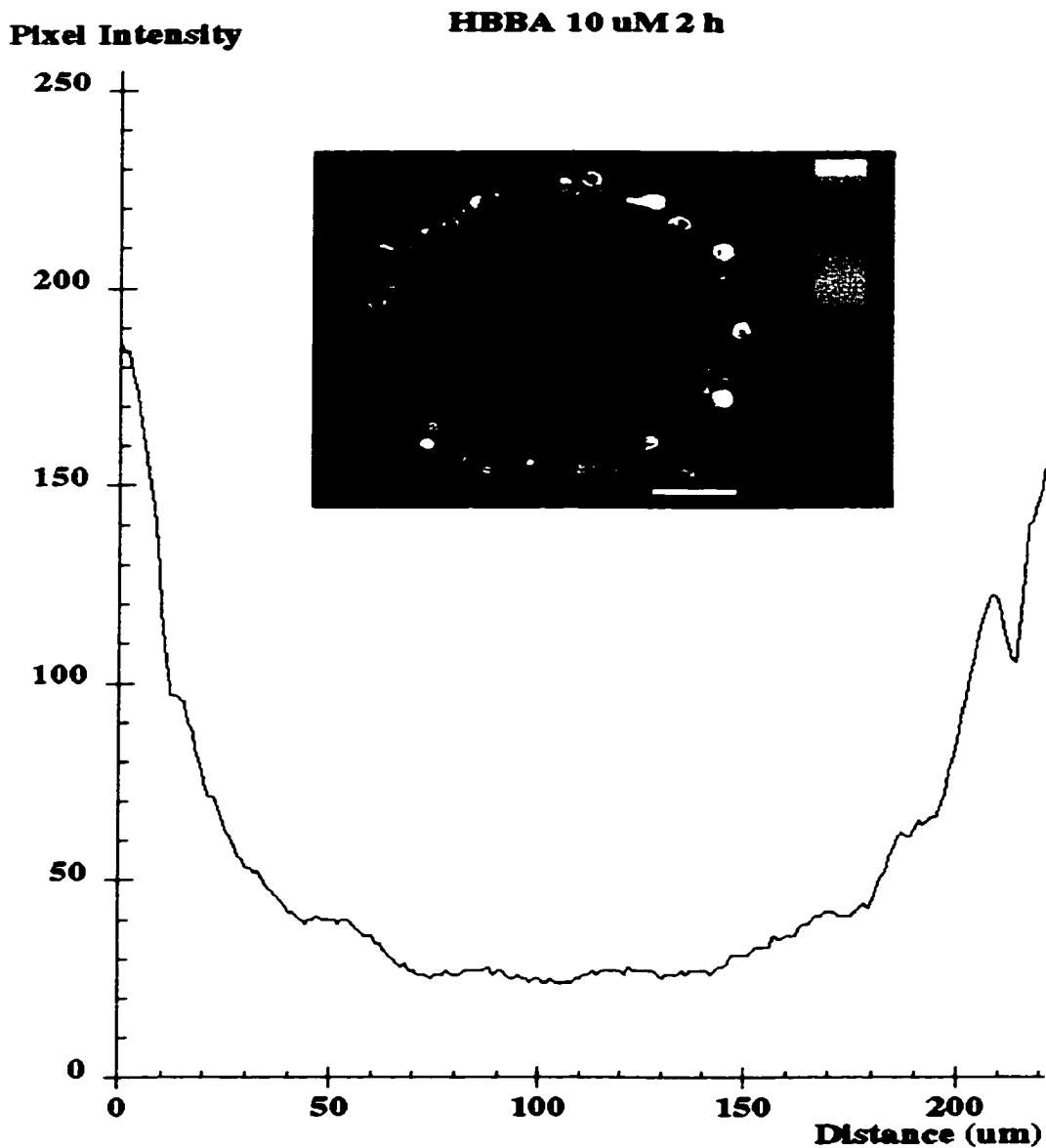
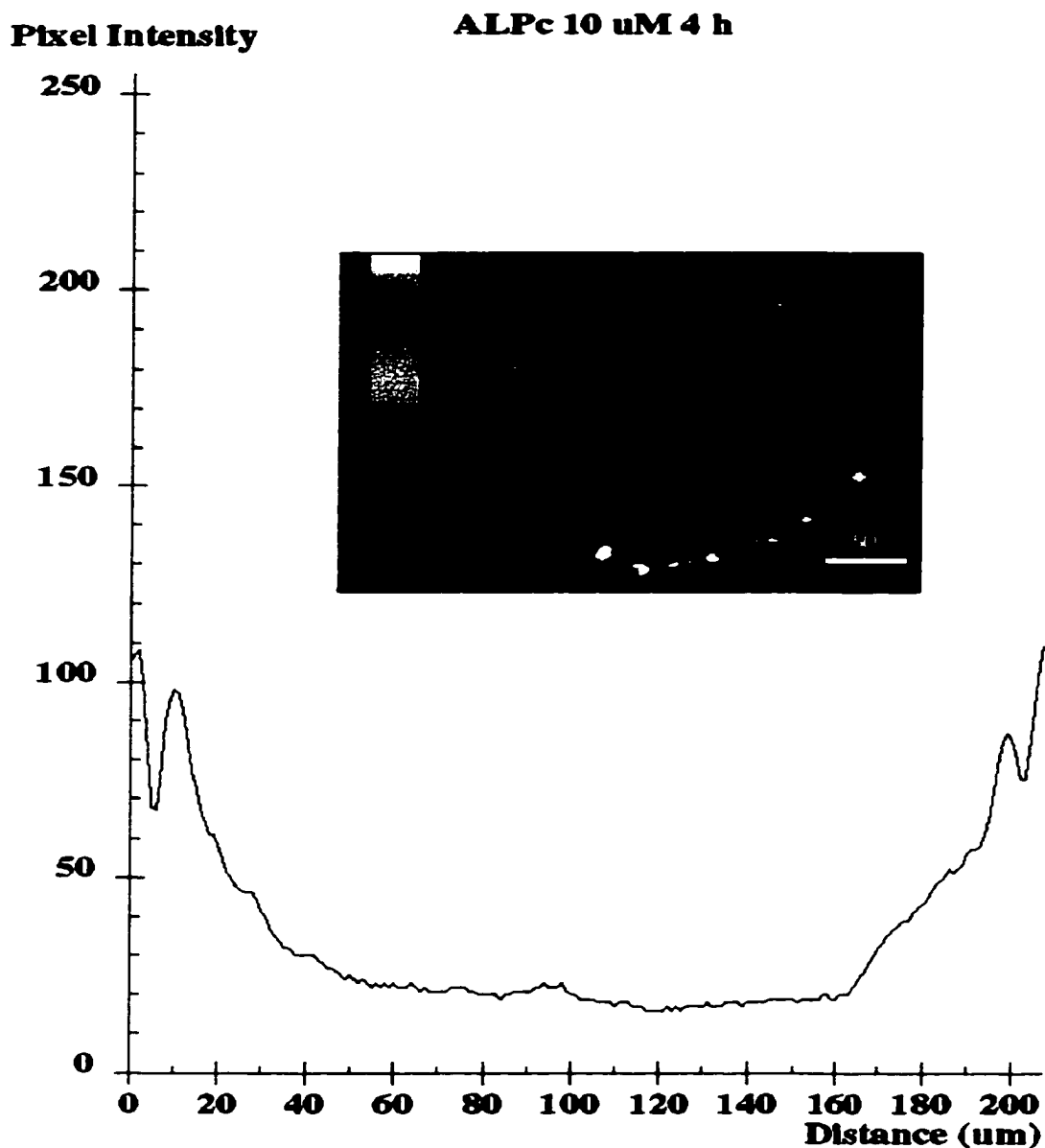**Fig. 5.8** Intraspheroid drug distribution and intensity profile in the central section of a spheroid incubated with HBBA-R2 10 μM for 2 h. Bar = 50 μm.

151
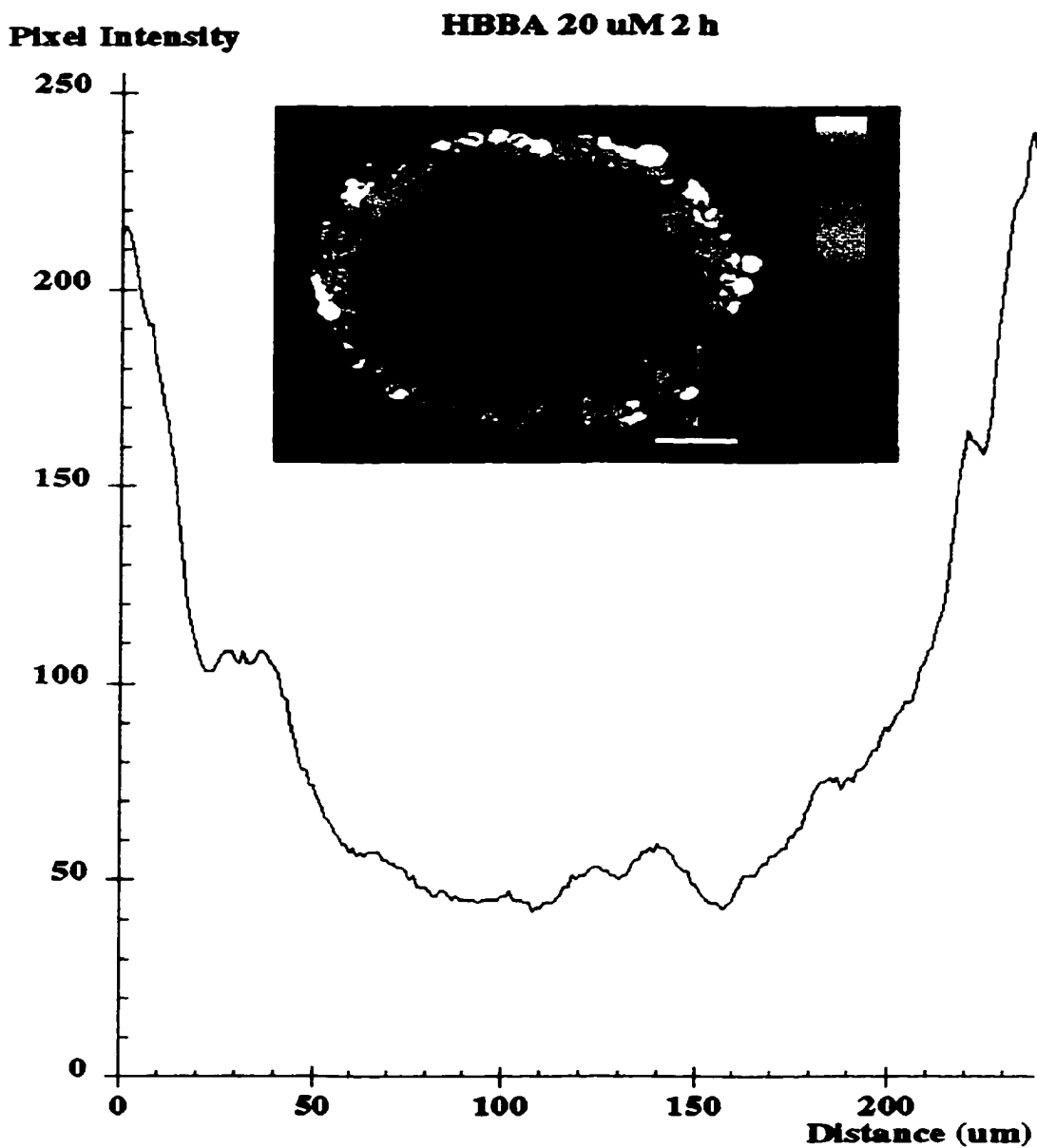
Fig. 5.9 Intraspheroid drug distribution and intensity profile in the central section of a spheroid incubated with HBBA-R2 20 μM for 2 h. Bar = 50 μm.

152

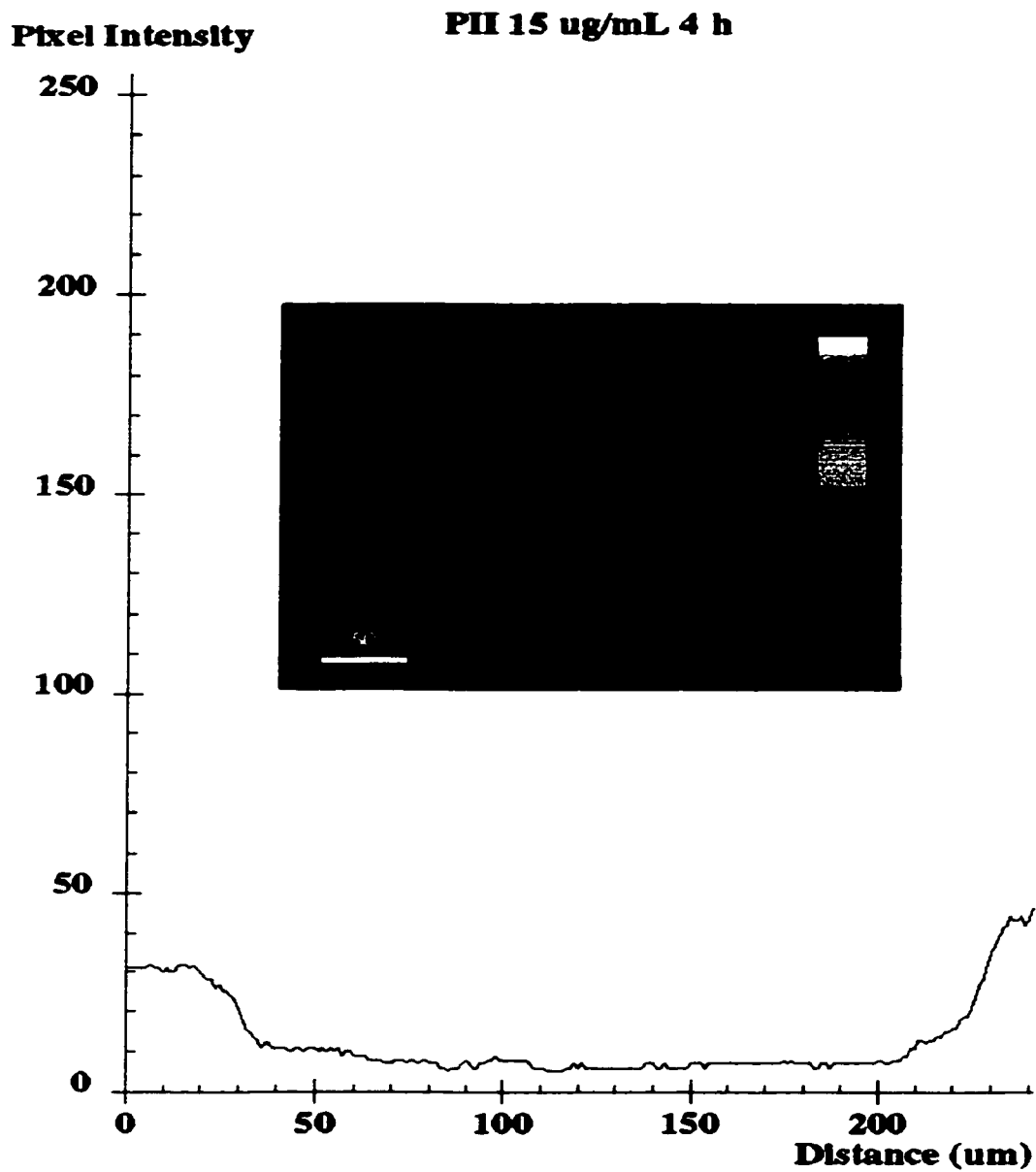Fig. 5.10 Intraspheroid drug distribution and intensity profile
in the central section of a spheroid incubated with Aluminum
Phthalocyanine Chloride 10 μM for 4 h. Bar = 50 μm. The
bright spot in the center is an artifact of the microscope.

PII 15 ug/mL 4 h

Fig. 5.11 Intraspheroid drug distribution and intensity profile in the central section of a spheroid incubated with Photofrin 15 μg/mL for 4 h. Bar = 50 μm.
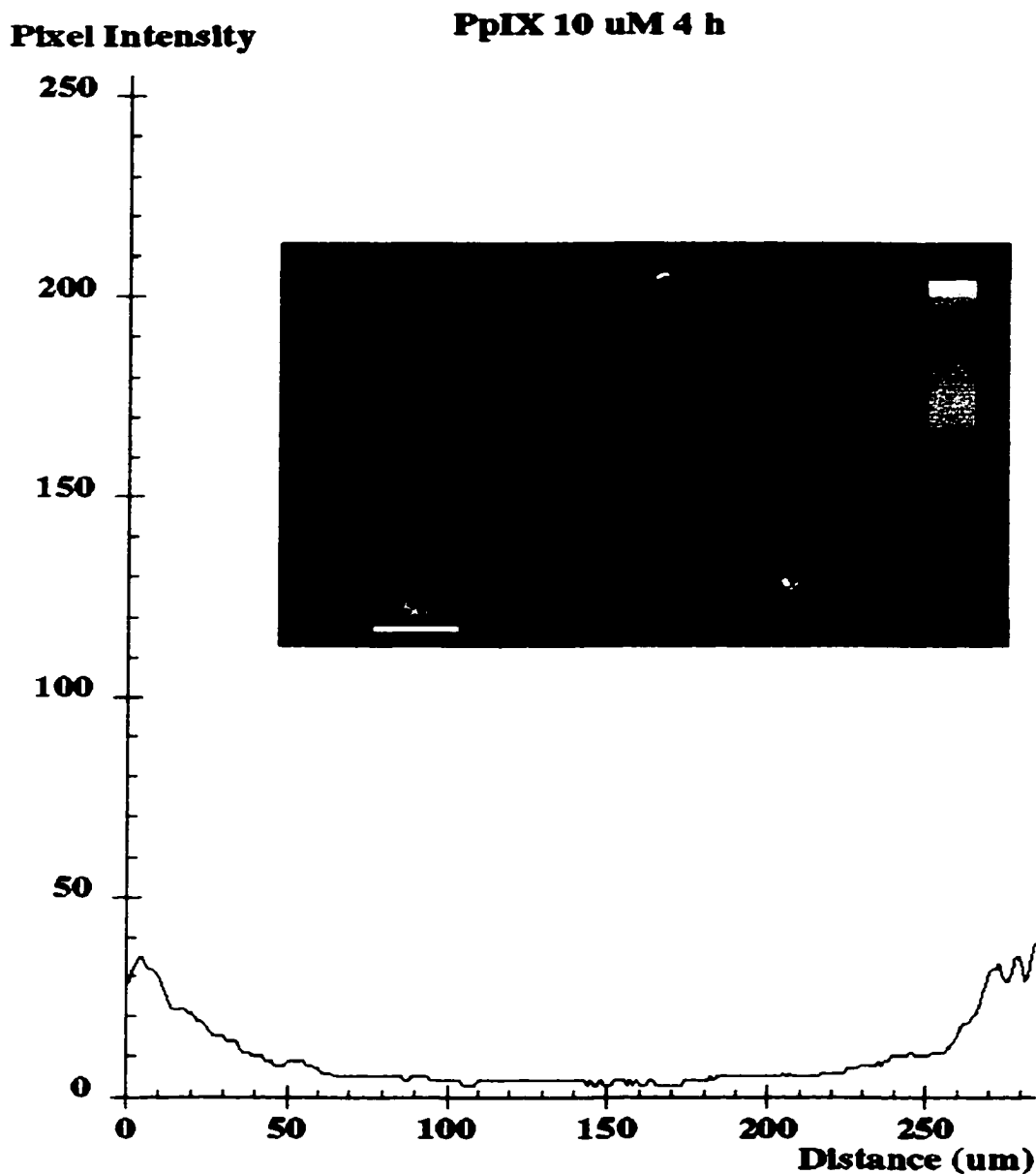
154

Fig. 5.12 Intraspheroid drug distribution and intensity profile in the central section of a spheroid incubated with PpIX 10 μ*M* for 4 h. Bar = 50 μm.

Fig. 5.13 Intraspheroid drug distribution and intensity profile in the central section of a spheroid incubated with Stealth liposomal HBEA-R1/R2 10 μ*M* for 2 h. Bar = 50 μm.

Fig. 5.14 Intraspheroid drug distribution and intensity profile in the central section of a spheroid incubated with Stealth liposomal HBBA-R2 10 μM for 2 h. Bar = 50 μm.

Fig. 5.15 Intraspheroid drug distribution and intensity profile in the central section of a spheroid incubated with classic liposomal HBBA-R2 10 μM for 4 h. Bar = 50 μm.
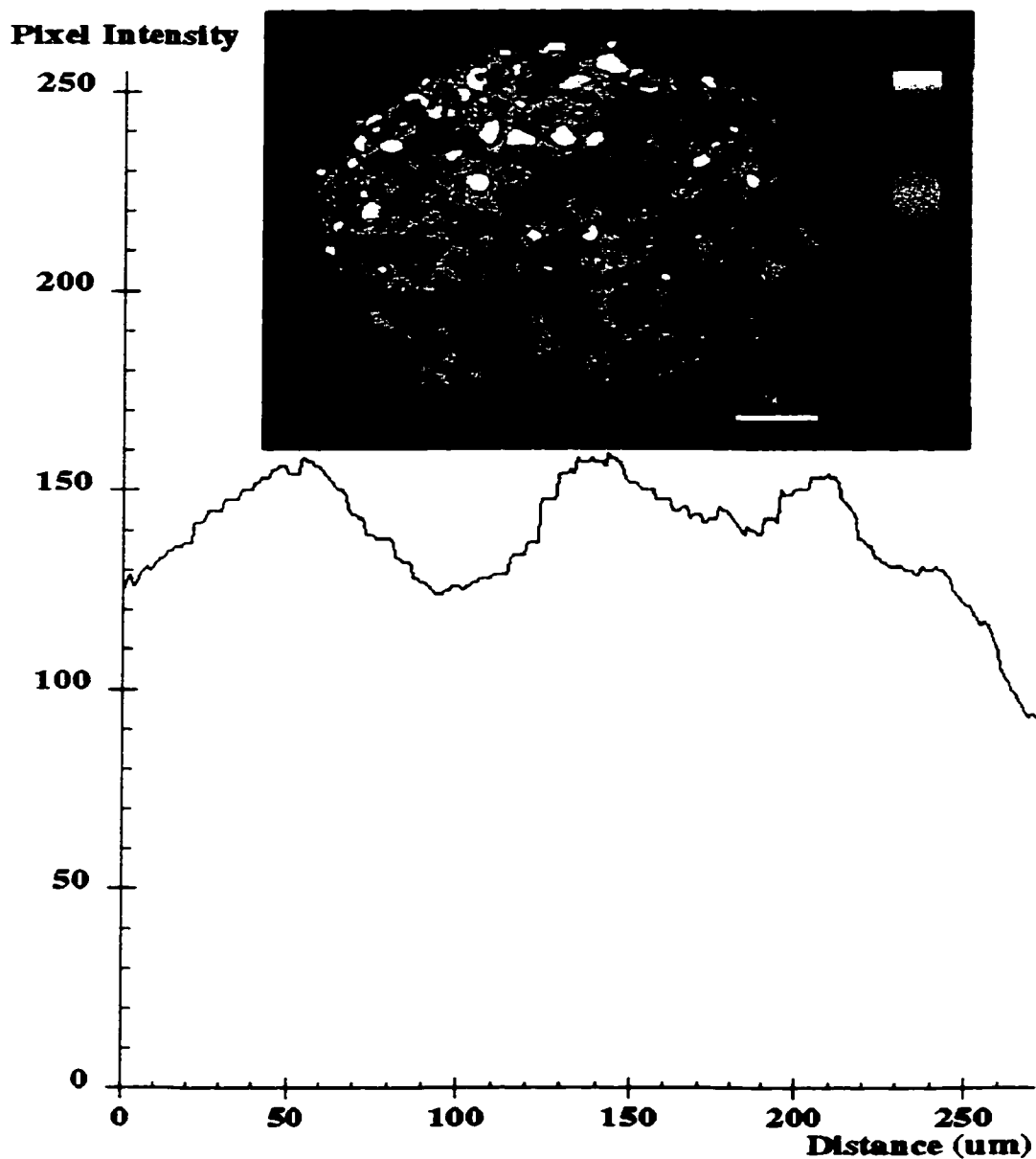
Fig. 5.16 Intraspheroid drug distribution and intensity profile in the central section of a spheroid incubated with Stealth liposomal HBBA-R2 10 μM for 4 h. Bar = 50 μm.

Fig. 5.17 Intraspheroid drug distribution and intensity profile in the central section of a spheroid incubated with specific SIL-HBBA-R2 10 μM for 2 h. Bar = 50 μm.
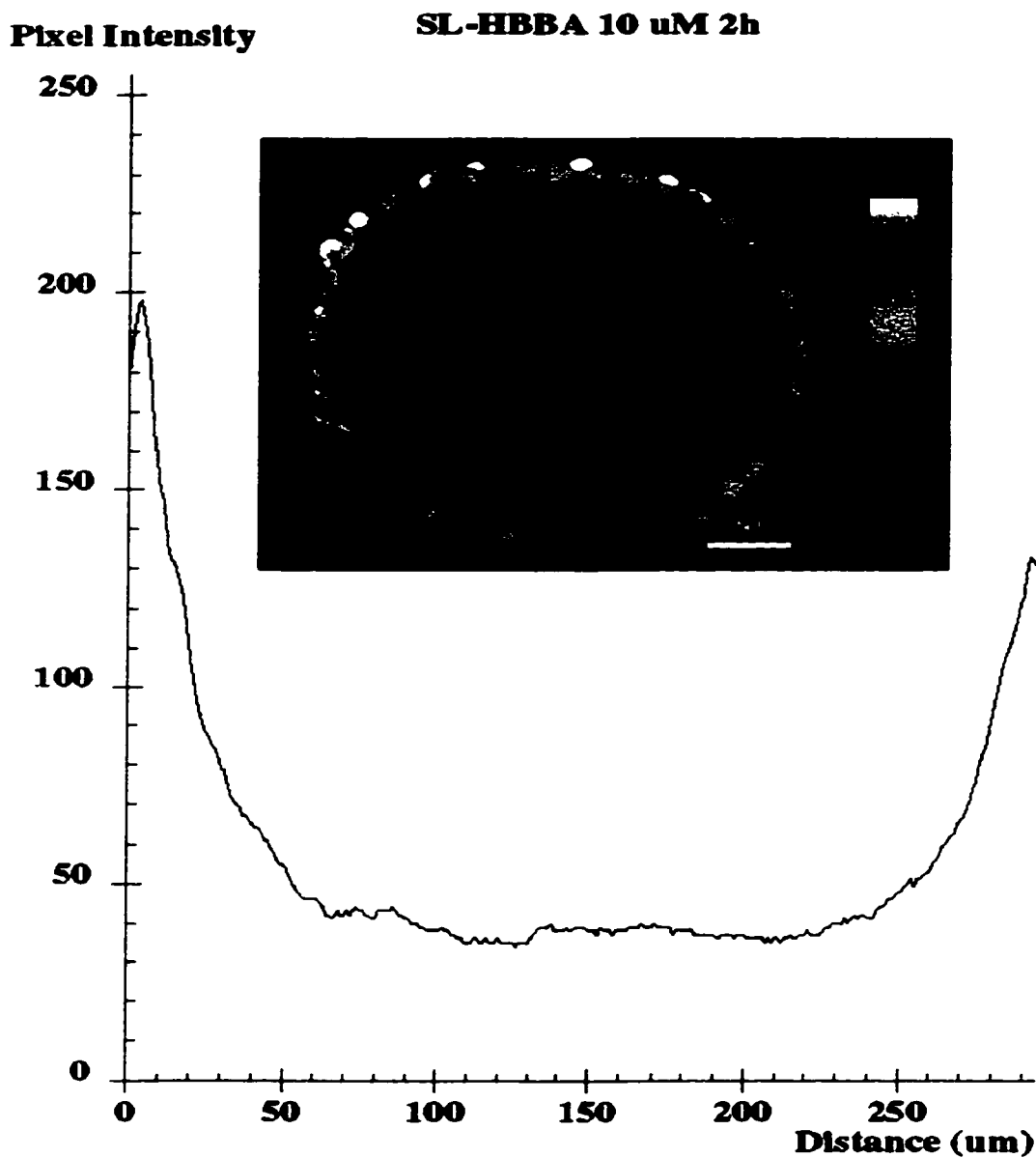
160

Fig. 5.18 Intraspheroid drug distribution and intensity profile in the central section of a spheroid incubated with non-specific SIL-HBBA-R2 10 μ*M* for 2 h. Bar = 50 μm.
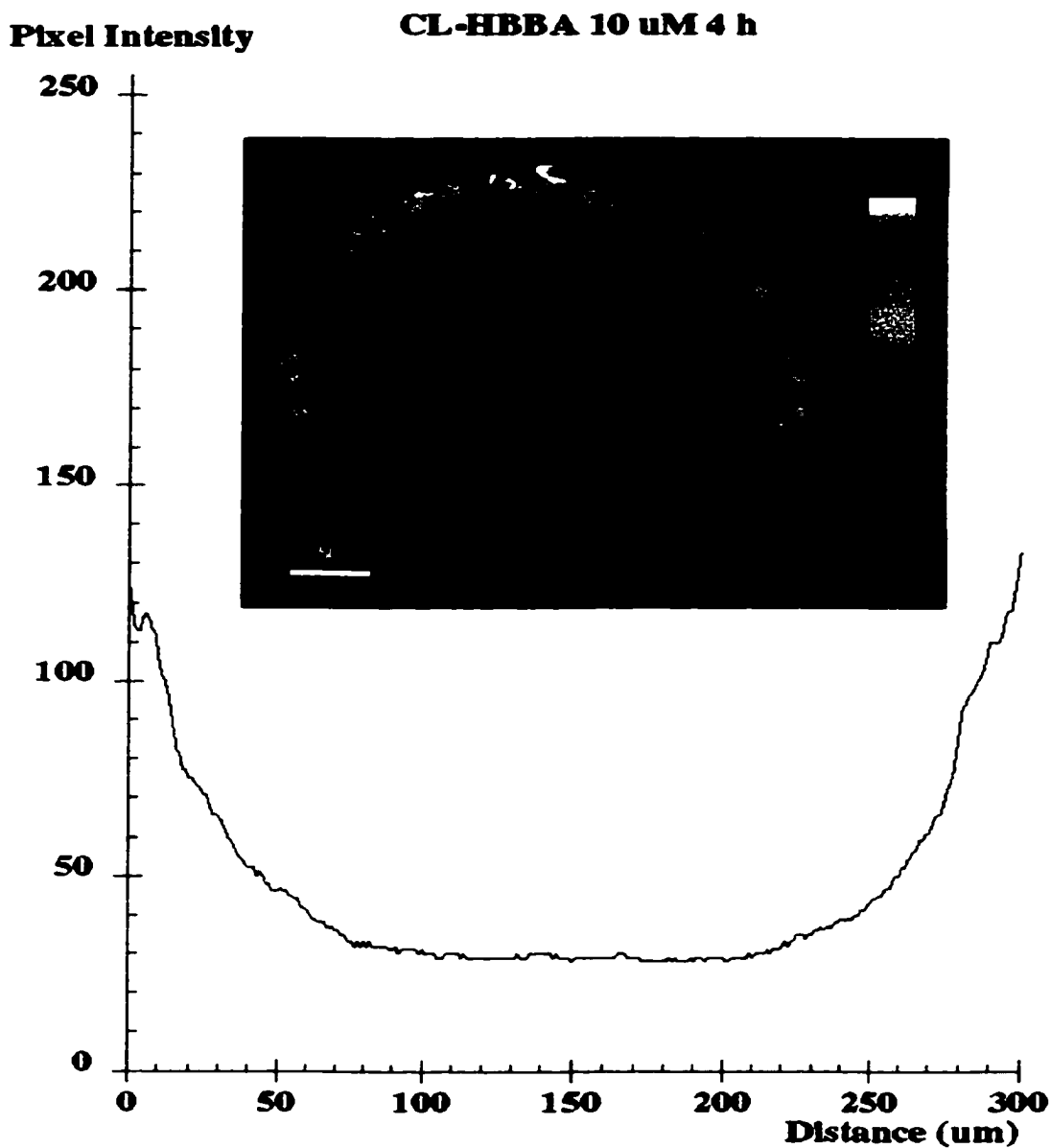
Fig. 5.19 Intraspheroid PpIX distribution and intensity profile in the central section of a spheroid incubated with ALA 1 m*M* for 4 h. Bar = 50 μm.

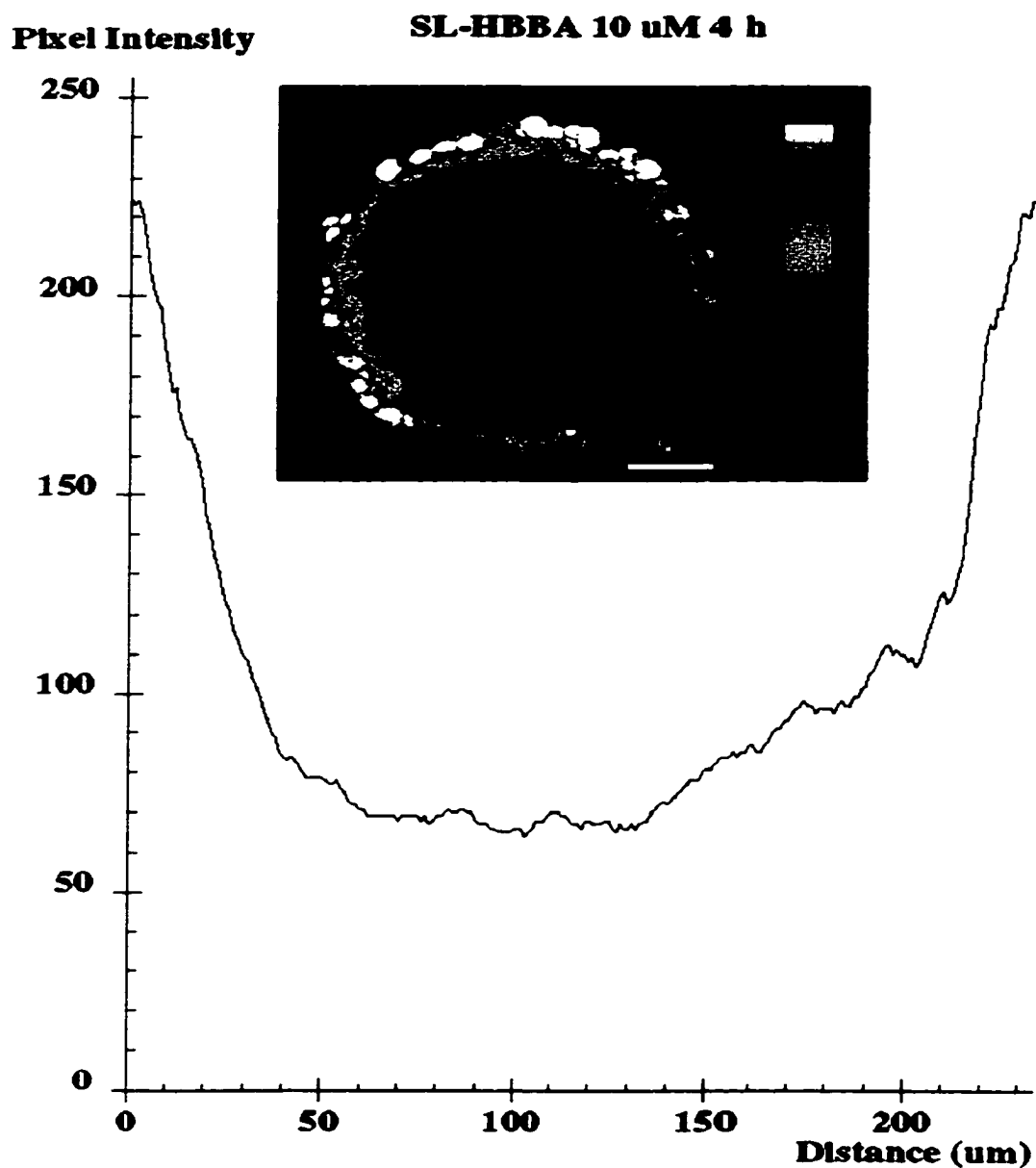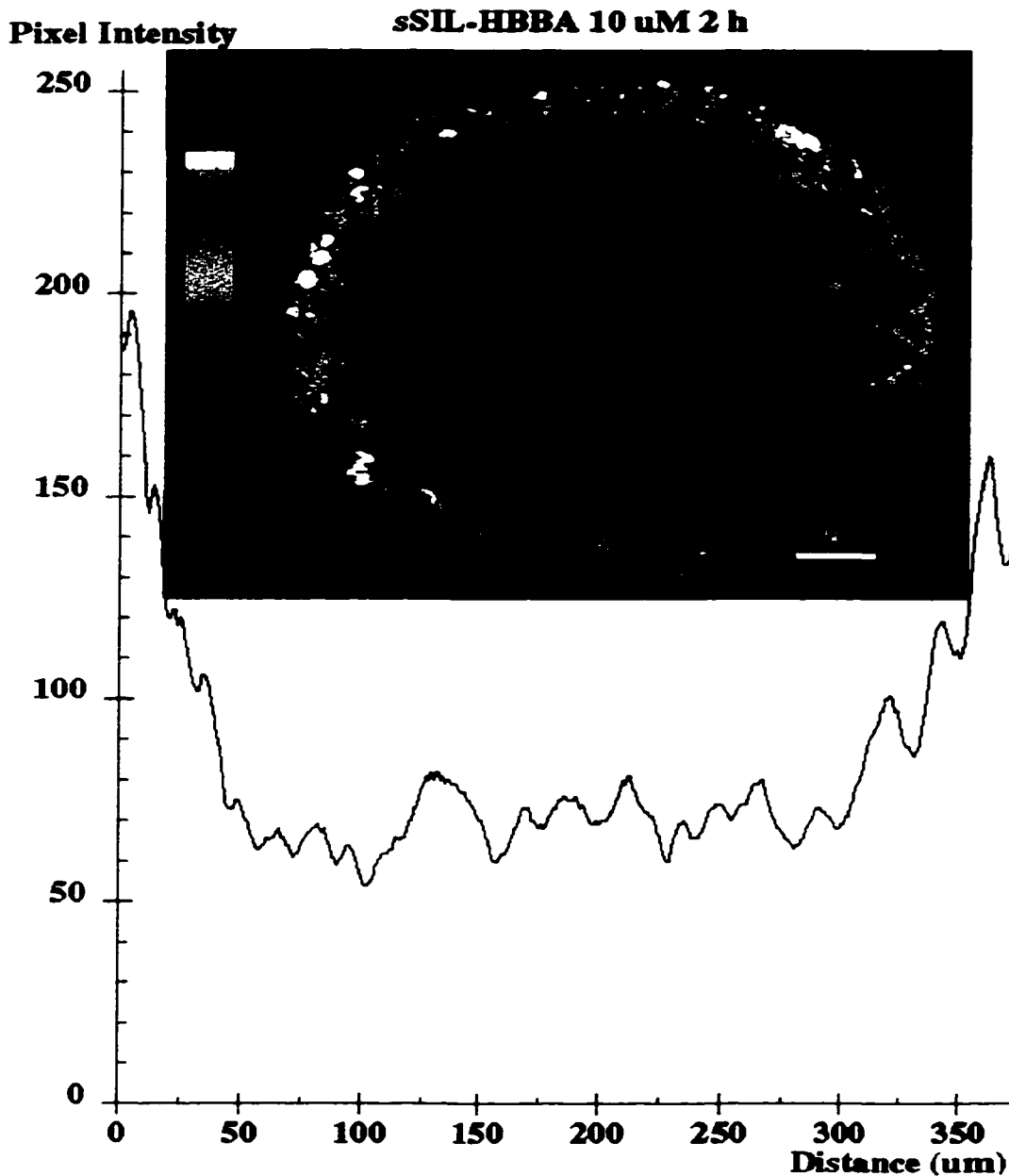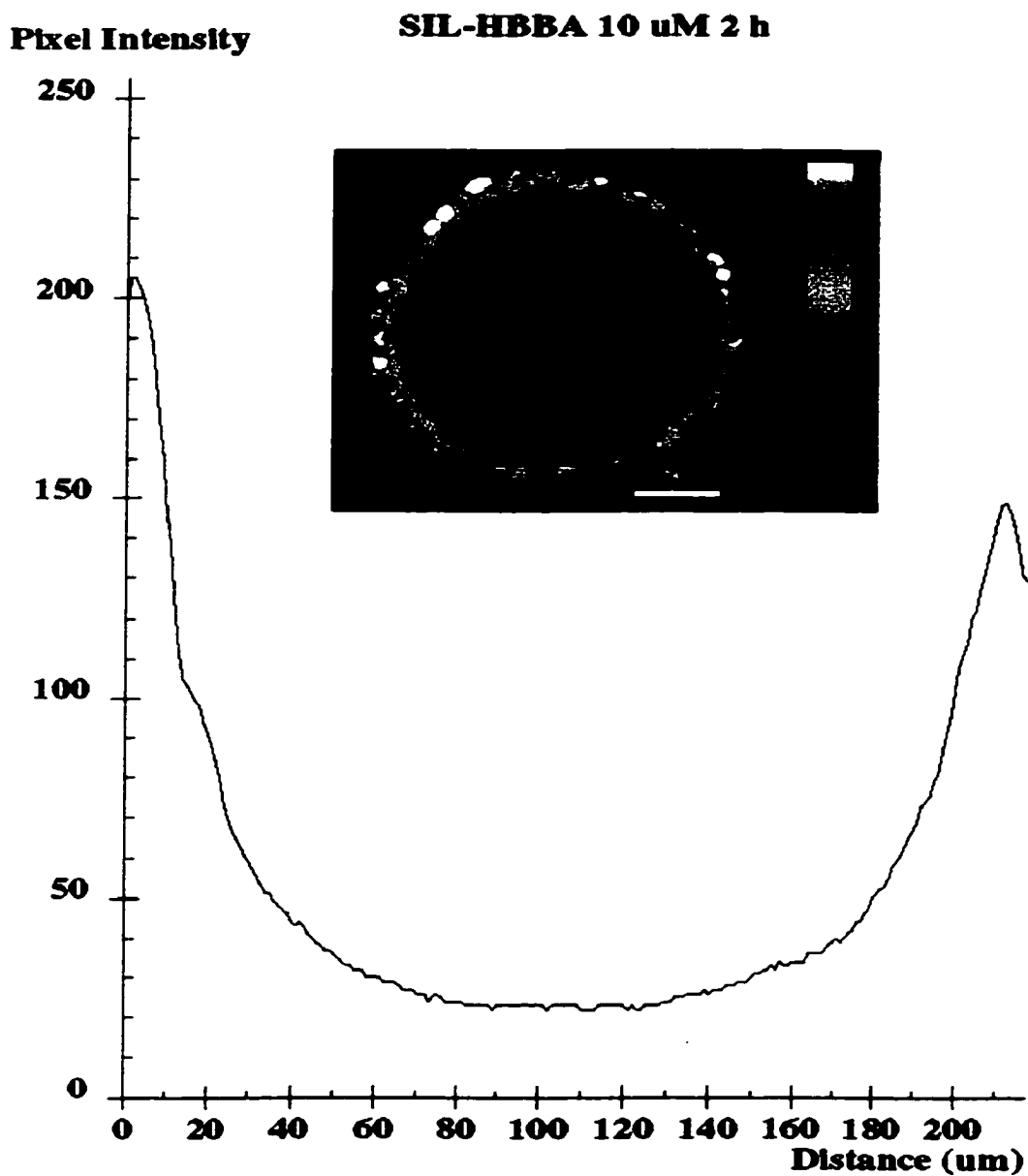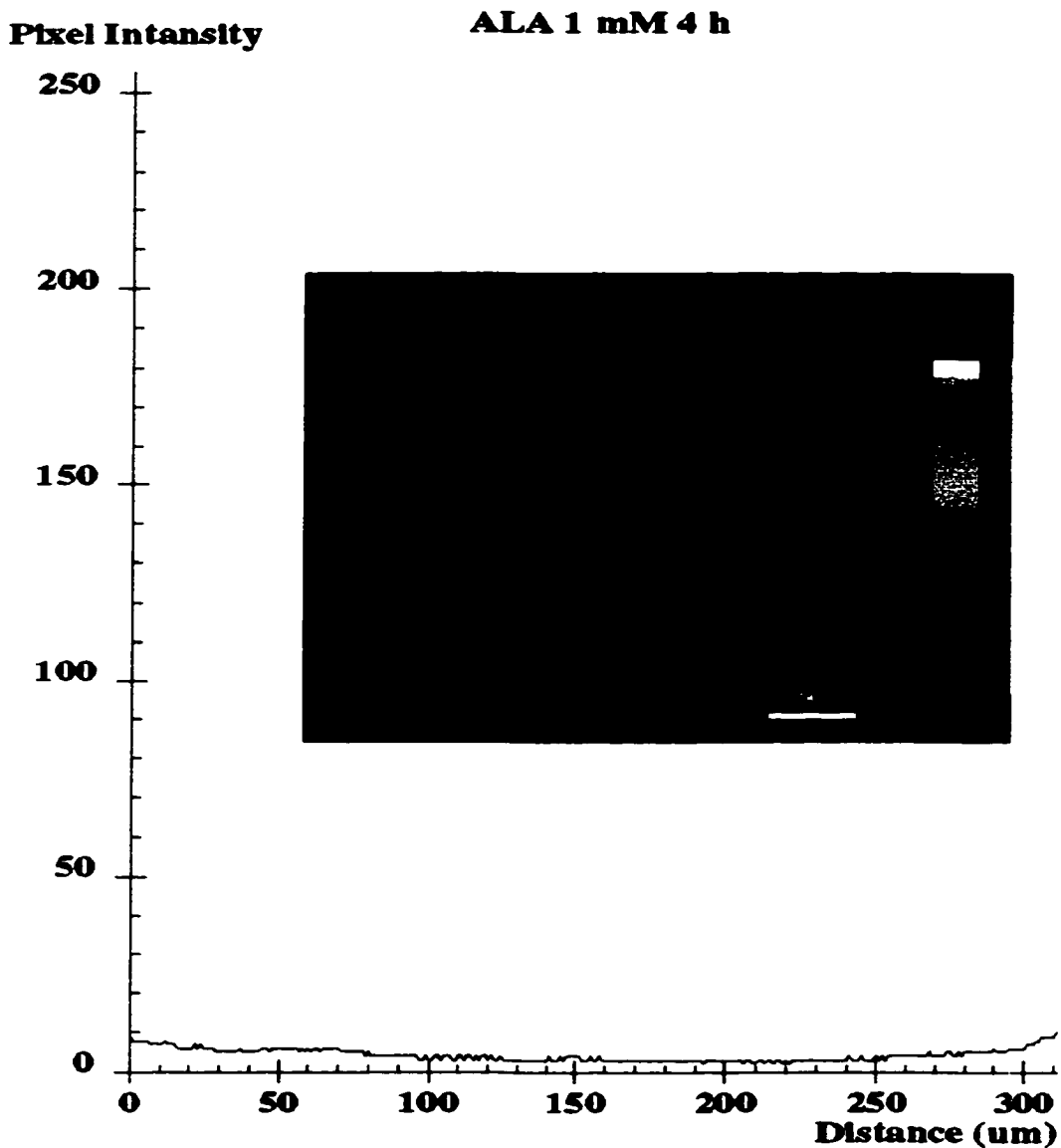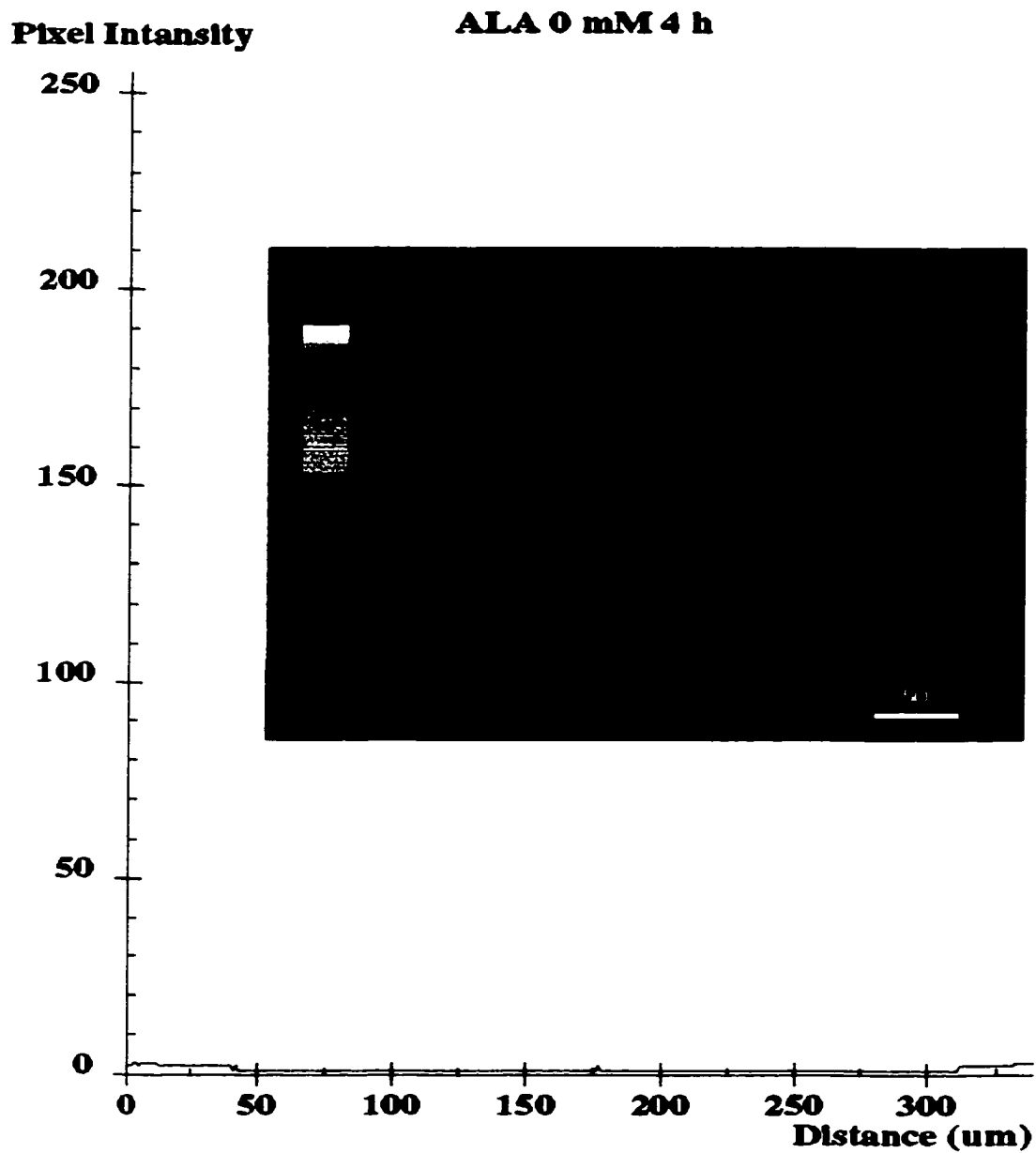**Fig. 5.20** Intensity profile in the central section of a spheroid incubated only with serum-free medium for 4 h. Bar = 50 μm.

163

intensity was slightly higher in spheroids incubated with specific SIL preparation (with 48-127 mAb) than other (*i.e.* plain SL and non-specific SIL) preparations (Table 5.1). The rank order of intraspheroid penetration depth of the tested compounds was: HBEA-R1/R2 $\cong$ liposomal HBEA-R1/R2 > HBBA-R2 $\cong$ liposomal HBBA-R2 > Photofrin $\cong$ AlPC > PpIX. The fluorescence intensity of graded doses of ALA-induced PpIX in the spheroids was only 5 − 8 units above the background level (Figs 5.19, 5.20, & Table 5.1).

Table 5.1 Summary of normalized areas under intensity *vs.* spheroid diameter curve (unit ·µm/pixel). Spheroids were incubated with graded doses of various tested drugs for different intervals and scanned by confocal laser scanning microscopy. The intensity profiles in the central sections of spheroids were taken to calculate the areas under the intensity *vs.* spheroid curve. Each group included 3 to 5 spheroids.

Time (h)	PF* (5 µg)	PF (10 µg)	PF (15 µg)	PpIX (10 µM)	PpIX (20 µM)	AlPC (0 µM)	AlPC (5 µM)	AlPC (10 µM)	AlPC (20 µM)
1	–	–	–	–	–	–	–	10.74	11.84
2	1.84	6.92	7.73	4.75	3.38	–	21.76	25.84	43.38
4	8.21	8.75	14.42	7.71	11.19	2.01	23.76	34.55	35.76

Time (h)	HBEA (5 µM)	HBEA (10 µM)	HBEA (20 µM)	HBBA (5 µM)	HBBA (10 µM)	HBBA (20 µM)	CLHBA (1 µM)	CLHBA (5 µM)	CLHBA (10 µM)
1	6.44	12.48	15.70	–	–	–	–	12.76	–
2	22.24	41.16	54.23	20.31	50.94	76.27	10.17	–	27.40
4	12.71	29.65	42.82	–	46.17	101.8	25.97	38.22	45.07

Time (h)	SLHBEA (5 µM)	SLHBEA (10 µM)	SLHBBA (5 µM)	SLHBBA (10 µM)
2	122.7	163.1	41.45	60.69
4	127.7	178.4	66.98	77.24

Time (h)	sSILHBBA (5 µM)	nSILHBBA (5 µM)	nSILHBBA (10 µM)	Liposome only (300 µM lipids)
2	85.22	50.66	52.38	0.53
4	68.40	–	–	–

Time (h)	ALA (0 mM)	ALA (1 mM)	ALA (8 mM)	ALA (15 mM)	ALA (30 mM)	ALA (60 mM)	ALA (100 mM)
4	1.44	4.32	5.68	4.04	3.21	1.81	1.23

* For abbreviations in this table, see the "abbreviations" list.

164

5.4 Discussion

Both histological and electron microscopic data show that the MGH-U3 spheroids share similarity in morphology and cell-to-cell connection to small tumor aggregates. These characteristics render the spheroids as reasonable *in vitro* tumor models to study intratumor distribution of new drugs. The disadvantage of the spheroids as tumor models is the deficiency of vasculature and lymphatic drainage system. However, this disadvantage may be also an advantage for studying drug penetration and distribution, because variability of vascular and lymphatic drainage in different tumor stages can be ignored. Furthermore, the requirement of animals can be avoided by using the spheroids. The objectives of intravesical instillation of photosensitizers are to increase the local tissue (*i.e.* tumor) concentration and decrease systemic distribution of the drug, and thus to reduce the undesired side effects. In whole bladder PDT, a differential accumulation of the photosensitizer in tumor *vs.* bladder muscle is very important, not only for ablating the tumor, but also for maintaining normal bladder function. *In vitro* studies of intraspheroid distribution of photosensitizers may provide essential information for guiding intravesical instillation of photosensitizers, because the drug is directly in contact with the tumor in both situations.

Hypocrellins (HBEA-R1, HBBA-R2) have been documented as potent photosensitizers *in vitro*[21] and *in vivo*.[26,27] They are available in pure monomeric form with high singlet oxygen yield. However, the lipophilic HBBA-R2 is not suitable for systemic administration without being incorporated into liposomes or other drug carriers. Aluminum phthalocyanine can be sulfonated to different levels.[28] It was found that the lipophilic lower sulfonates of phthalocyanine (AlPC and AlPCS$_1$) exhibited more potent photoefficiency to tumor cells, less subcellular redistribution and therefore less fluctuation of fluorescence intensity by light activation.[14,28,29] Photofrin is a mixture of porphyrins which belong to amphiphilic sensitizers.[30] Data from this study demonstrate that among the photosensitizers tested, hypocrellins (especially HBEA-R1/R2) distribute more uniformly (penetrate deeper) into the

spheroids than other compounds. The fluorescence intensities of spheroids incubated with hypocrellins also show much higher levels than those incubated with other compounds (Table 5.1). Previous sensitive fluorescence microscopic studies suggest that the fluorescence intensity correlates well with the tissue photosensitizer concentration.[31,32,33] Assuming that this correlation holds in the present study, the MGH-U3 spheroids appear to take up more hypocrellins than other photosensitizers. However, different photosensitizer may have quite varying fluorescent yields and quenching in cells and liposomes, especially when different wavelengths of light have been used to excite them. Therefore, care must be taken when analyzing intensity levels quantitatively among different kinds of compounds. Other assays like chemical extraction of sensitizers from spheroids may be more appropriate for quantitatively comparing different drugs in spheroids. However, the spatial distribution (the distribution pattern) of these photosensitizers in spheroids can not be demonstrated by chemical extraction assay.

In terms of the intensity levels of each photosensitizer, a dose-dependent relationship exists from 1 to 20 μM (or 5 – 15 μg/mL for PF), as well as a time-dependent increase from 1 to 2 hours. Most intensity levels remain relatively constant from 2 to 4 hours, except for that of liposomal HBBA-R2 which still increases from 2 to 4 hours (Figs 5.14, 5.16, Table 5.1). These data imply that the contact time between the free photosensitizer and tumor needs to be about 2 hours. As well more than 2 hours are needed for liposomal drugs if administrated topically, and an appropriate concentration gradient is also critical for a tumor to take up sufficient amounts of drug. The lipophilicity of the photosensitizer appears to be a key determinant of its penetration into spheroids. The amphiphilic HBEA-R1/R2 penetrates better than the lipophilic HBBA-R2 and other photosensitizers tested. We still do not know the exact reason contributing to this phenomenon. One possibility may be that the lipophilic HBBA-R2 tends to aggregate in the culture medium.[21,26] The larger the aggregated molecule, the less the penetration depth, the less availability of the drug for uptake by tumor cells. The observation that the liposomal

166

formulations of the hypocrellins can more efficiently deliver the drugs into the spheroids than the free drugs suggests that the liposomes may serve as solvents for the lipophilic drugs to reduce aggregation.[34] However, other factors like endocytosis/pinocytosis of the liposome-drug package by the cells may also play a role. In addition, it was found that the subcellular distribution of HBEA-R1 was different from that of HBBA-R2.[35] The distribution of HBEA-R1 was primarily in the Golgi apparatus and lysosomes. For HBBA-R2, it was prominently distributed in cell membrane, lysosomes and endoplasmic reticulum.[35] However, how this discrepancy of subcellular distribution influences the intratumor distribution of the HBEA-R1 and HBBA-R2 remains to be determined. Apart from the physicochemical properties, the purity and molecular size of the drug seem also playing a role in intratumor distribution, because the amphiphilic HBEA-R1/R2 penetrates much better than the amphiphilic Photofrin (Figs 5.7, 5.11), probably because the latter is a mixture of porphyrins which form di-, tri, and tetra-porphyrin ether/esters.

The liposomal hypocrellins show a similar distribution pattern as the corresponding free drug. The liposomal HBEA-R1/R2, like HBEA-R1/R2, can penetrate well to the spheroid center, while the liposomal HBBA-R2, like HBBA-R2, shows much higher fluorescence intensity in the spheroid periphery. An interesting finding is that the liposomal HBEA-R1/R2 shows 3 – 4 times higher fluorescence intensity than the free HBEA-R1/R2 regarding the same drug concentration (Figs 5.7, 5.13 & Table 5.1). We speculate that some of the HBEA-R1/R2 may leak out of the liposomes due to its amphiphilicity. Therefore, free HBEA-R1/R2 can penetrate well to the spheroid center, and liposomal HBEA-R1/R2 may be taken up by cells more efficiently as liposome-drug package than the free HBEA-R1/R2. On the other hand, this leaking out is a limitation in formulating liposomal HBEA-R1. Since HBBA-R2 can be steadily incorporated in liposomes, liposomal HBBA-R2 seems more appropriate as an immunoliposomal preparation for diagnosis of bladder C*IS* than liposomal HBEA-R1/R2. Liposomal HBEA-R1/R2 however, as well as its free drug, may be more appropriate for treatment of multifocal tumors in the bladder, the high

167

selectivity between tumor and normal urothelium has less importance than in diagnosis, but the penetration depth is a priority. Compared with the non-specific formulation, the specific immunoliposomal HBBA-R2 shows slightly higher fluorescence intensity in the spheroid periphery after 2-hour incubation. However, we do not have enough data to conclude that this is due to the specific binding of the immunoliposome with the spheroid, because the antibody density on the liposome is quite low in studies we have performed to date. The optimal antibody density on liposome should be from 25 to 40 $\mu g/\mu M$ (protein/total lipid) in terms of antigen-recognition and cost.[24] Theoretically, immunoliposomes should be the most cost efficient strategy to deliver photosensitizers compared with antibody-photosensitizer conjugates. However, it is not easy to produce immunoliposomes with the above optimal antibody density, because the antibody is too fragile to the steps of formulation procedures.

The ALA-induced PpIX intensity levels in spheroids are very low. When the ALA concentration was greater than 60 mM, the spheroids started to disintegrate. This result agrees with our previous data from monolayer cells cultured with graded doses of ALA, where only low intensity levels could be detected by confocal microscopy (data not shown). However, in animal model systems, the ALA-induced PpIX levels in both tumor and urothelium are quite high and dose-dependent.[36] The low PpIX level in the spheroids may be due to rapid leakage of PpIX into the culture medium due to the concentration gradient.[37] This however, needs to be further determined by sequentially studying the PpIX levels in the medium..

5.5 Conclusions

The multicell MGH-U3 spheroids model small tumor aggregates in many aspects. Of the photosensitizers tested, HBEA-R1/R2 and its liposomal formulation seem to be the best candidates for intravesical administration for PDT of bladder cancer. The liposomal HBBA-R2 may be utilized in both diagnosis and treatment of bladder CIS if tagged with specific antibody. These data need to be verified in animal model systems.

168

5.6 References

1. Henderson, B.W. and Dougtherty, T.J. (1992) How does photodynamic therapy work? *Photochem. Photobiol.*, **55**: 145-157.

2. Dougherty, T.J., Grindey, G.B., Fiel, R., *et al.* (1975) Photoradiation therapy II: cure of malignant tumors with hematoporphyrin and light. *J. Natl. Cancer Inst.*, **55**: 115-121.

3. Van Hillegersberg, R., Will, J.K. and Wilson, J.H.P (1994) Current status of photodynamic therapy in oncology. *Drugs.* **48** (4): 510-527.

4. Peng, Q., Moan, J., Farrants, G., Danielsen, H.E. and Rimington, C. (1990) Localization of potent photosensitizers in human tumor LOX by means of laser scanning microscopy. *Cancer Lett.*, **53**: 129-139.

5. Cuomo, V., Jori, G., Rihter, B., Kenney, M.E. and Rodgers, M.A.J. (1990) Liposome-delivered Si(IV)-naphthalocyanine as a photodynamic sensitizer for experimental tumors: pharmacokinetic and physiotherapeutic studies. *Br. J. Cancer.* **62**: 966-970.

6. Reddi E. (1997) Role of delivery vehicle for photosensitizers in the photodynamic therapy of tumors. *J. Photochem. Photobiol. B: Biol.* **37**: 189-195.

7. Miller, G.G. and Lown, J.W. (1997) Immunophotodynamic therapy: current developments and future prospects (review). *Drug Develop. Res.,* **42**: 182-197.

8. Morgan, J., Lottman, H., Abbou, C.C., and Chopin, D.K. (1994) A comparison of direct and liposomal antibody conjugates of sulfonated aluminum phthalocyanines for selective photoimmunotherapy of human bladder carcinoma. *Photochem. Phtobiol.,* **60**: 486-496.

9. Love, W.G., Duk, S., Biolo, R., Jori, G. and Taylor, P.W. (1996) Liposome-mediated delivery of photosensitizers: localization of Zinc (II)-Phthalocyanine within implanted tumors after intravenous administration. *Photochem. Photobiol.,* **63**: 656-661.

10. Kessel, D., Thompson, P., Saatio, K. and Nantwi, K.D. (1987) Tumor localization and photosensitization by sulfonated derivatives of tetraphenyporphine. *Photochem. Photobiol.,* **45**: 787-790.

11. Jori, G. and Reddi, E. (1990) Strategies for tumor targeting by photodynamic sensitizers. In *Photodynamic Therapy of Neoplastic Disease* (Edited by D. Kessel), pp. 117-130. CRC Press, Boca Raton, FL.

12. Henderson, B.W., Waldow, S.M., Mang, T.S., Potter, W.R., Malone, P.B. and Dougherty, T.J. (1985) Tumor destruction and kinetics of tumor cell death in two experimental mouse tumors following photodynamic therapy. *Cancer Res.*, **45**: 572-576.

13. Dougherty, T.J., Cooper, M.T. and Mang, T.S. (1990) Cutaneous phototoxic occurrences in patients receiving Photofrin. *Lasers Surg. Med.*, **10**: 485-488.

14. Ben-Hut, E., Rosenthal, I. (1995) The phthalocyanines: a new class of mammalian cell photosensitizers with a potential for cancer phototherapy. *Int. J. Radiat. Biol.*, **47**: 145-147.

15. Sternberg, E., Dolphin, D. (1993) An overview of second generation drugs for photodynamic therapy including BPD-MA. In Spinelli P, Dal Fante M, Marchesini R, eds. Photodynamic Therapy and Medical Lasers. *Excerpta Medica* 470-474.

16. Nseyo U.O. (1992) Photodynamic therapy. *Urol. Clin. North. Am.*, **19**: 591-599.

17. Knuchel, R., Hofstadter, F., Jenkins, W.E.A, and Masters, J.R.W. (1989) Sensitivities of monolayers and spheroids of the human bladder cancer cell line MGH-U1 to the drugs used for intravesical chemotherapy. *Cancer Res.*, **49**: 1397-1401.

18. Erlichman, C. and Vidgen, D. (1984) Cytotoxicity of adriamycin in MGH-U1 cells grown as monolayer cultures, spheroids, and xenografts in immune-deprived mice. *Cancer Res.*, **44**: 5369-5375.

19. Sasaki, T., Yamamoto, M., Yamaguchi, T. and Sugiyama, S. (1984) Development of multicellular spheroids of Hela cells cocultured with fibroblasts and their response to X-irradiation. *Cancer Res.*, **44**: 345.

20. de Harven, E., Fradet, Y., Connolly, J.G., Hanna, W., He, S., Wang, Y., Choi, B.C.K., McGroarty, R., Bootsma, G., Tilups, A. and Christensen, H. (1992) Antibody drug carrier for immunotherapy of superficial bladder cancer: Ultrastructural studies. *Cancer Res.*, **52**: 3131-3137.

21. Estey, E.P., Brown, K., Diwu, Z., Liu, J., Lown, J.W., Miller, G.G, Moore, R.B., Tulip, J. and McPhee, M.S. (1996) Hypocrellins as photosensitizers for photodynamic therapy: a screening evaluation and pharmacokinetic study. *Cancer Chemother. Pharmacol.*, **37**: 343-350.

22. Allen, T.M. and Hansen, C.B. (1991) Pharmacokinetics of stealth versus conventional liposomes: effect of dose. *Biochim. Biophys. Acta.*, **1068**: 133-141.

23. Allen, T.M., Hansen, C.B. and Guo, L.S.S. (1993) Subcutaneous administration of liposomes: a comparison with the intravenous and intraperitoneal routes of injection. *Biochim. Biophys. Acta.*, **1150**: 9-16.

24. Hansen, C.B., Kao, G.Y., Moase, E.H., Zalipsky, S. And Allen, T.M. (1995) Attachment of antibodies to sterically stablilized liposomes: evaluation, comparison and optimization of coupling procedures. *Biochim. Biophys. Acta.*, **1239**: 133-144.

25. Hamilton, T.C., Young, R.C., McKoy, W.M., Grotzinger, K.R., Green, J.A., Chu, E.W., Whang-Penn, J., Rogan A.M., Green, W.R. and Ozols, R.F. (1983) Characterization of a human ovarian carcinoma cell line (NIH:OVCAR-3) with androgen and estrogen receptors. *Cancer Res.*, 43: 5379-5389.

26. Diwu, Z. (1995) Novel therapeutic and diagnostic applications of hypocrelins and hypericins. *Photochem. Photobiol.*, **61**:529-539.

27. Miller, G.G., Brown, K., Ballangrud, A.M., Barajas, O., Xiao, Z., Tulip, J., Lown, J.W., Leithoff, J. M., Allalunis-Turner, M.J., Mehta, R.D. and Moore, R.B. (1997) Preclinical Assessment of Hypocrellin B and Hypocrellin B Derivatives as Sensitizers for Photodynamic Therapy of Cancer: Progress Update. *Photochem. Photobiol.*, **65(4)**: 714-722.

28. Peng, Q., Farrants, G.W., Madslien, K., Bommer, J.C., Moan, J., Danielsen, H.E. and Nesland, J.M. (1991) Subcellular localization, redistribution and photobleaching of sulfonated aluminum phthalocyanines in a human melanoma cell line. *Int. J. Cancer.* **49**: 290-295.

29. Ruck, A., Beck, G., Bachor, R., Akgun, N., Gschwend, M.H. and Steiner, R. (1996) Dynamic fluorescence changes during photodynamic therapy in vivo and in vitro of

hydrophilic Al (II) phthalocyanine tetrasulfonate and lipophilic Zn(II) phthalocyanine administered in liposomes. *J. Photochem. Photobiol.*, **36**: 127-133.

30. Boyle, R. and Dolphin, D. (1996) Structure and biodistribution relationships of photodynamic sensitizers (review). *Photochem. Photobiol.*, **64**: 469-485.

31. Bedwell, J., MacRobert, A.J., Philips, D. and Bown, S.G. (1992) Fluorescence distribution and photodynamic effect of ALA-induced PpIX in the DMH rat colonic tumor model. *Br. J. Cancer.* **65**: 818-824.

32. Loh, C.S., Vernon, D., MacRobert, A.J., Bedwell, J., Bown, S.G. and Brown, S.B. (1993) Endogenous porphyrin distribution induced by 5-aminolevulinic acid in the tissue layers of the gastrointestinal tract. *J. Photochem. Photobiol. B.* **20: 47**.

33. Pope, A.J., MacRobert, A.J., Phillips, D. and Bown, S.G. (1991) The detection of phthalocyanine fluorescence in normal rat bladder wall using sensitive digital imaging microscopy. *Br. J. Cancer.* **64: 875-879**.

34. Reddi E. (1997) Role of delivery vehicle for photosensitizers in the photodynamic therapy of tumors. *J. Photochem. Photobiol. B: Biol.* **37**: 189-195.

35. Miller, G.G., Brown, K., Moore, R.B., Diwu, Z.J., Liu, J., Huang, L., Lown, J.W., Begg, D.A., Chlumecky, V., Tulip, J. and McPhee, M.S. (1995) Uptake kinetics and intracellular localization of hypocrellin photosensitizers for photodynamic therapy: a confocal microscopy study. *Photochem. Photobiol.*, **61**: 632-638.

36. Xiao, Z., Miller, G.G., McCallum, T.J., Brown, K.M., Lown, J.W., Tulip, J. and Moore, R.B. (1998) Biodistribution of Photofrin II and 5-aminolevulinic acid - induced protoporphyrin IX in normal rat bladder and bladder tumor models. *Photochem. Photobiol.*, **67** (5): 513-518.

37. Iinuma, S., Farshi, S.S., Ortel, B. and Hasan, T. (1994) A mechanistic study of cellular photodestruction with 5-aminolevulinic acid-induced porphyrin. *Br. J. Cancer.* 70: 21.

CHAPTER VI

GENERAL DISCUSSION

So far, neither surgery, nor radiotherapy, nor chemotherapy can eradicate cancer without damaging normal tissues. Photodynamic therapy (PDT) is a novel cancer treatment modality, which offers the potential for selectively destroying malignant tumors, especially small multifocal lesions. Such lesions include carcinoma *in situ* (C/S) and small transitional cell carcinoma (TCC) of the bladder;[1] malignant mesothelioma of the pleura;[2] superficial carcinoma of the oral cavity and gastrointestinal tract;[3,4] and superficial basal and squamous cell carcinomas of the skin.[5] Many of these malignancies are refractory to management with conventional cancer treatment modalities. However, with the current lack of, or minimal selectivity of photosensitizer for tumors, it remains a major challenge for both research scientists and clinicians to avoid the undesired side effects while maintaining or improving the antitumor efficacy of PDT. In an attempt to improve on the current limitations, the commonly used photosensitizer, Photofrin® (porfimer sodium), and several second-generation sensitizers have been administrated intravenously (the most common route of administration) and intravesically, to compare the pharmacokinetics, photoefficiency, and phototoxicity in both heterotopic and orthotopic rat bladder tumor models.

The data obtained through out this study are encouraging. First, the orthotopic rat bladder TCC tumor model established in our laboratory not only mimics the human disease, but can be reproduced with a very high tumor engraftment rate (> 97%). Furthermore, by understanding the growth kinetics of the tumor, different stages of tumor can be predicted and selected for different research purposes. Secondly, intravesical administration of appropriate doses of Photofrin or 5-aminolevunilic acid (ALA) can achieve comparable tumor photosensitization to i.v. injection, while sparing the underlying normal bladder muscle, which provides a rationale for the intravesical administration of these drugs for whole bladder PDT. On the other hand, the different biodistribution patterns of ALA-induced PpIX in heterotopic and orthotopic bladder tumor models suggest a relevant tumor model is

174

very important for preclinical studies. Thirdly, whole bladder PDT of orthotopic rat superficial bladder tumors further demonstrates that intravesical administration of photosensitizers may prove an effective, safer, and more acceptable avenue of fighting superficial bladder cancer. Furthermore, deeply seated solid tumors may be eradicated by interstitial PDT.

Photosensitizers can be arbitrarily classified into lipophilic, hydrophilic and amphiphilic categories.[6] Lipophilic photosensitizers are administered in liposomes or other lipid-based drug carriers. After i.v. administration, these sensitizers are, in general, bound to lipoproteins, transported to the malignant tissue. Following receptor-mediated endocytosis, the sensitizers preferentially accumulate in the biomembranes of tumor cells.[7] *In situ* photo-activation of the sensitizers can directly destroy these biomembranes and associated enzymes, leading to leakage of intracellular components, release of biochemically active ions and activation of the complement system.[8] After i.v. administration of hydrophilic photosensitizers, the drugs are largely carried by albumin and other serum proteins, and distributed in the interstitial space and the vascular stroma of the tumor tissue.[6,8] In general, photo-activation of these sensitizers kill neoplastic cells indirectly by damaging blood vessels and interrupting the supply of oxygen and other essential nutrients. This indirect cell killing is not selective *per se*. However, both *in vitro* and *in vivo* studies also show direct cell killing of hydrophilic sensitizers if the target tissue can contact with drugs and in the present of oxygen.

Intravesical administration of photosensitizers may facilitate drug delivery to tumor tissue by direct contact of the tumor with the drug. Direct cell killing may be the dominant mechanism of action in this case. Therefore the intratumor drug concentration may be directly related with the antitumor efficacy. Photosensitizer delivered in liposomes, especially in immunoliposomes, may further enhance tumor selectivity.[9] The distribution and the site of localization of the sensitizer still depend on the lipophilic or hydrophilic character of the drug. The results of drug penetration into MGH-U3 spheroids suggest that HBBA-R2 can be readily incorporated into

175

liposomes and effectively delivered into small tumor cell aggregates. Therefore, immunoliposomal HBBA-R2 may be an attractive formulation for intravesical administration.

There are several limitations of PDT at present, which deter its widespread application in the clinic. The first limitation is the currently available clinical photosensitizer, Photofrin, which is a mixture of monomers and oligomers of porphyrins.[10] Even with the standardized commercial production of lyophilized Photofrin, the biological potency is variable between different lots.[11] The multiple active chemical components in this mixture make it very difficult to define both photosensitizer concentration and light dose to predict tumor response, due to complicated pharmacokinetics after systemic administration.[12] These characteristics have been blamed for the poor tumor selectivity and unwanted side effects after Photofrin-mediated PDT. Second generation photosensitizers, like hypocrellins, phthalocyanines, benzoporphyrin derivatives, and ALA-induced protoporphyrin IX (PpIX), can partly overcome the above limitation, since all of these drugs have a single chemical structure and predictable pharmacokinetics.

Our group has investigated hypocrellins, a group of perylenequinonoid pigment photosensitizers, for several years.[13,14] The photosensitizing properties of hypocrellins in biological systems have been recognized for the past two decades.[15,16] Features of hypocrellins include efficient red light absorption by the parent hypocrellins A and B (658 nm),[16] and high singlet oxygen yield.[13] Hypocrellins are available in pure monomeric forms such as HBEA-R1 (ethanolaminated HB) and HBBA-R2 (n-butylaminated HB), it has been shown that these photosensitizers have improved pharmacokinetics.[16] However, like other potent photosensitizers the lipophilic nature of HBBA-R2 proved troublesome for administration. To improve on the delivery of these compounds they may be administered in liposomes. When the liposomal formulations are tagged with monoclonal antibody against bladder tumor, specific photodetection and destruction of bladder C*IS* may be possible.[17,18] The PDT-induced cytotoxity and tumoricidal effects of hypocrellins have been

176

demonstrated in EMT6/Ed monolayer culture *via* clonogenic assay and in mice bearing the EMT6/Ed tumor.[14] The phototoxicities of hypocrellins and the liposomal formulation to the monolayer AY-27 TCC cells were assessed by clonogenic assay and were compared with that of Photofrin, PpIX and aluminum phthalocyanine chloride (AlPC). Exponentially growing AY-27 TCC cells were seeded in 3-cm tissue culture Petri plates 1 day prior to each experiment. Graded doses of various sensitizers dissolved in dimethyl sulfoxide (DMSO) were mixed into serum-free medium (RPMI-1640) overlaying 5.0×10^4 monolayer cells. Following a 2 h incubation, drug was removed, the cells were washed with Hank's balanced salts solution (HBSS) and illuminated with graded doses of 630-nm light (690-nm light for AlPC) in room air. The cells were trypsinized, counted, and plated at a known density in RPMI-1640 medium containing 10% fetal calf serum for 6 days. Survival fraction for each drug concentration was corrected for plating efficiency of cells treated with light only (no sensitizer). The survival fractions are shown in Figure 6.1. These preliminary data suggest that the photoefficiency of HBEA-R1/R2 is slightly better than that of HBBA-R2, the latter has similar phototoxicity as its liposomal formulation to the AY-27 cells. The phototoxicity of the hypocrellins is superior to that of Photofrin, PpIX and AlPC on a molar basis. These data agree well with a previous study examining phototoxicity with EMT6/Ed cells.[14] The results from clonogenic assay and confocal microscopy, as well as previous preclinical studies, indicate hypocrellins are promising photosensitizers for whole bladder PDT of bladder cancer. Immunoliposomal HBBA-R2 is currently being tested for tumor selectivity in animal models.

Compared with Photofrin, ALA-induced PpIX is preferentially accumulated in epithelial layers, sparing the underlying connective tissue and muscular layers. Thus multifocal urothelial dysplasia and bladder C*IS* can be eliminated at the expense of normal urothelium injury. The latter can regenerate very rapidly.[19] However, studies in animal tumor models, and in the clinic demonstrated that ALA-based PDT could only destroy the surface of solid tumors, with a fairly high recurrence.[5,12] One of the
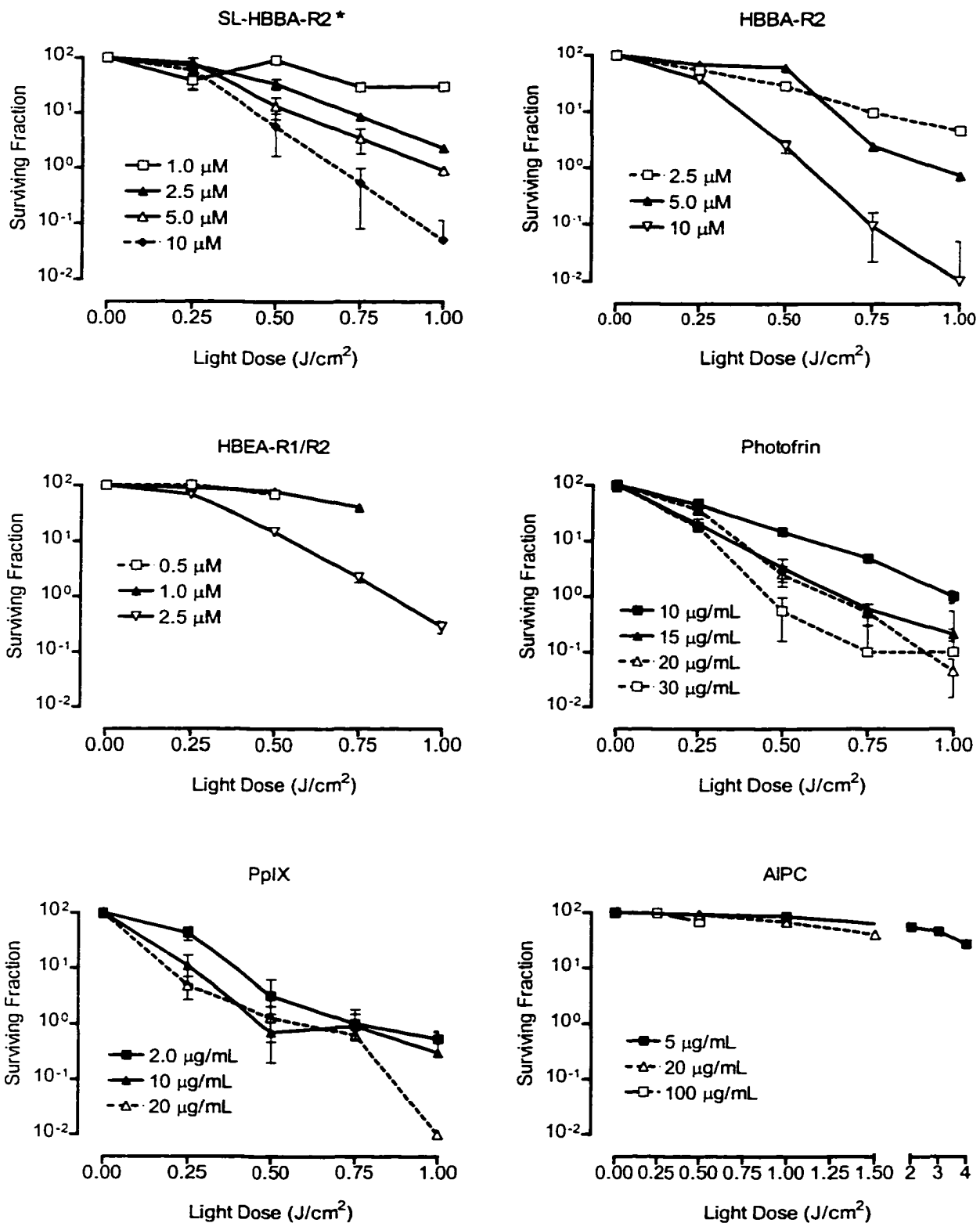
177

Figure 6.1 Phototoxicity of different drugs to AY-27 monolayer cells by clonogenic assay. The argon-pumped dye laser was tuned to 630 nm and 150 mW of output power except for illumination of AlPC (690 nm and 150-200 mW). The surviving fraction is the % control. 1 μM HBEA-R1 = 0.6 μg/ml, 1 μM HBBA-R2 = 0.63 μg/ml. * Stealth liposomal HBBA-R2.

178

factors responsible for the observed incomplete tumor destruction after ALA-based PDT may be the rapid photobleaching of PpIX.[12] This is exemplified by the data in Figure 6.2 which show that PpIX dissolved in DMSO is photobleached rapidly when irradiated with 422 to 630 nm light. The shorter the wavelength, the quicker the photobleaching. And there is no active photo-product from this process.

The second limitation of current PDT is the limited penetration of 630 nm light in tissue. The "effective" penetration depth of 3 mm greatly limits the interstitial application of PDT for deeply seated tumors.[20] Hemoglobin and melanin pigments are primarily responsible for attenuation of 630 nm light. By using light with wavelengths greater than 630 nm there is less absorption by hemoglobin and therefore greater tissue penetration.[21] The remedy for this limitation lies in the development of new photosensitizers and light sources. Photosensitizers, like hypocrellins, phthalocyanines, benzoporphyrin derivatives, all have efficient red light absorption close to 700 nm.[14,22,23] The commonly used dye lasers have the advantage of being tunable over the projected absorption spectrum for the second generation photosensitizers. However, their high costs, complexity and poor reliability make them less than desirable for clinical application. The more compact, reliable, and easy to use diode lasers emitting from 630 to 730 nm light are currently available. The only limitation is their power, which is rapidly being overcome with superconductor technology. With the development of new photosensitizers, tumor-specific drug delivery strategies, light sources, and light delivery instruments, the application of PDT will become more widespread than it is currently.

The diagnosis of carcinoma *in situ* of the bladder remains a dilemma for clinicians. On the other hand, early cancer detection may well enable a more effective treatment and improve survival for patients with bladder cancer. Preliminary studies with ALA instilled into bladders of patients with bladder cancer suggested that ALA-induced PpIX might be useful for detection of bladder C*IS* and small papillary tumors, which can otherwise be easily overlooked by white light cystoscopy.[24] However, both selectivity and specificity of this fluorescence-aided photodetection of early bladder

179
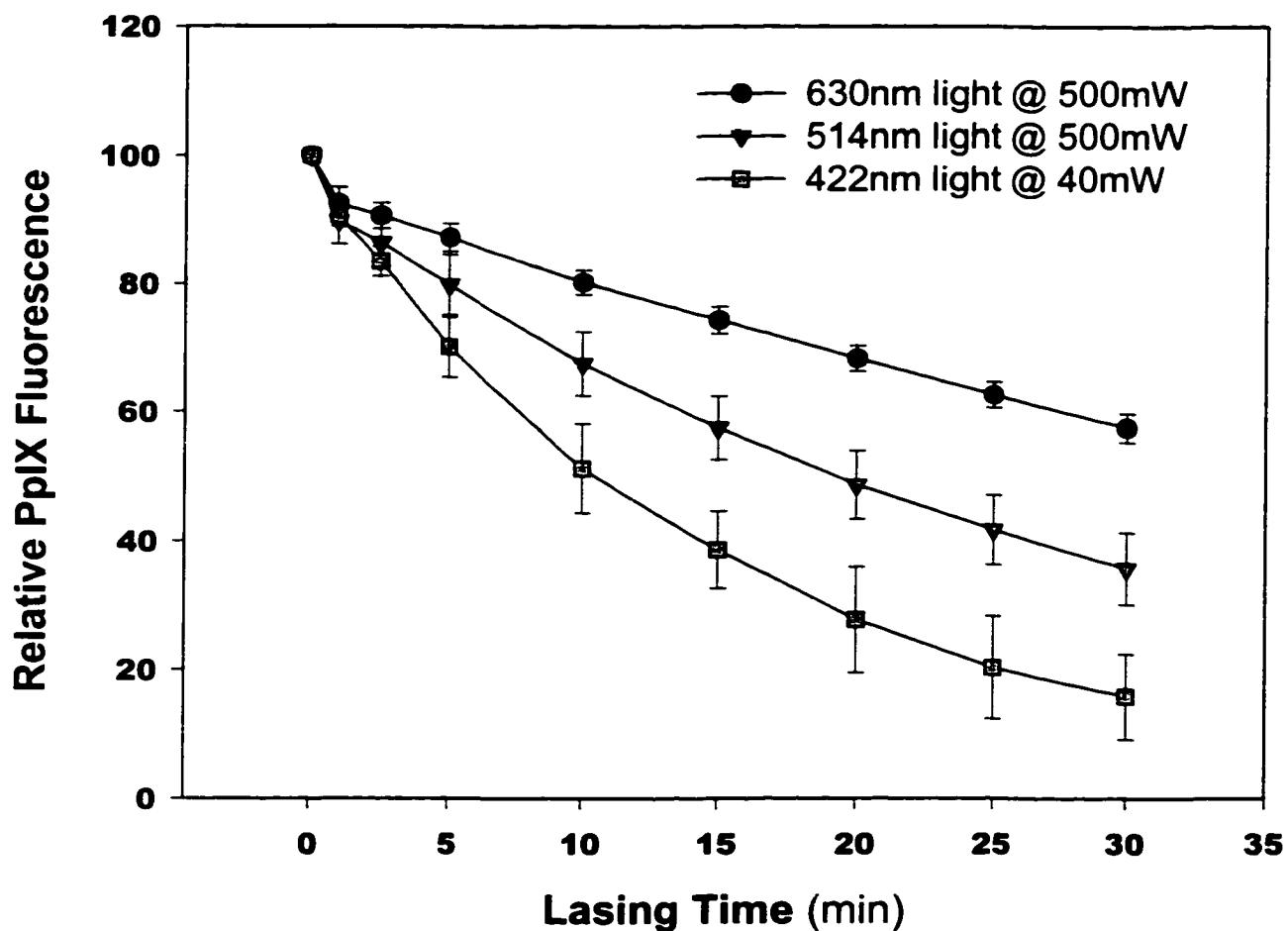
Fig. 6.2 Effect of wavelength on PpIX photobleaching. PpIX was first dissolved in DMSO, then diluted with PBS to a final concentration of 100 ng/mL, and illuminated with light of different wavelength.

tumor need to be improved. Furthermore, data from systematic studies in animal models demonstrated that there was no significant difference of ALA-induced PpIX fluorescence intensity between bladder tumor and normal urothelium.[25,26] Improvement in detection sensitivity and specificity has recently been reported.[27] After esterification of ALA to obtain an amphiphilic derivative, the ALA-hexylester enables a gain in the clinical 'drug dose – photodetection efficiency' of nearly two orders of magnitude.[27] Another reliable and specific way for improving detection of early bladder tumor may be the utilization of immunoliposomal photosensitizers.

With the development of second-generation photosensitizers, which can be activated by 700 nm or greater light, interstitial PDT of localized prostate cancer appears to be a selective, minimally invasive treatment modality. This will broaden the application of PDT from treatment of superficial cancers to deeply seated tumors.

6.1 References

1. Nseyo U.O. (1992) Photodynamic therapy. *Urol. Clin. North. Am.*, **19**: 591-599.

2. Dougherty, T.J. and Marcus, S.L. (1992) Photodynamic therapy. *Eur. J. Cancer.* **28A**: 1734-1742.

3. Grant, W.E., Hopper, C., MacRobert, A.J., *et al.* (1993) Photodynamic therapy of oral cancer: photosensitization with systemic aminolevulinic acid. *Lancet.* **342**: 147-148.

4. Regula, J., MacRobert, A.J., Gorchein, A., Buonaccorsi, G.A., Thorpe, S.M., Spencer, G.M., Hatfield, A.R. and Bown, S.G. (1995) Photosensitization and photodynamic therapy of esophageal, duodenal, and colorectal tumors using 5-aminolevulinic acid induced protoporphyrin IX - a pilot study. *Gut.* **36**: 67-75.

5. Kennedy, J.C. and Pottier, R.H. (1992) Endogenous protoporphyrin IX, a clinical useful photosensitizer for photodynamic therapy. *J. Photochem. Photobiol. B: Biol.*, **14**: 275-292.

6. Boyle, R. and Dolphin, D. (1996) Structure and biodistribution relationships of photodynamic sensitizers (review). *Photochem. Photobiol.*, **36**: 127-133.

7. Jori, G., Beltramini, M., Reddi, E., Salvato, B., Pagnan, A., Ziron, L., Tomio. L. And Tsanov, T. (1984)   Evidence for a major role of plasma lipoproteins as hematoporphyrin carriers in vivo. *Cancer Lett.*, **24**: 291-297.

8.   Ochsner, M. (1997)   Photophysical and photobiological processes in the photodynamic therapy of tumors (review). *J. Photochem. Photobiol. B: biol.*, **39**: 1-18.

9. Reddi, E. (1997)   Role of delivery vehicle for photosensitizers in the photodynamic therapy of tumors. *J. Photochem. Photobiol. B: Biol.*, **37**: 189-195.

10. Byrne, C.J., Marshallsay, L.V. and Ward, A.D. (1990)   The composition of Photofrin II. *J. Photochem. Photobiol. B: Biol.*, **6**: 13-27.

11. Chapman, J.D., Stobbe, C.C., Arnfield, M.R., Santus, R. and McPhee, M.S. (1991) The effectiveness of short-term versus long-term exposure to Photofrin II in killing light activated tumor cells. *Radiat. Res.*, **128**: 82-89.

12. Van Hillegerberg, R., Will, J.K. and Wilson J.H.P. (1994)   Current status of photodynamic therapy in oncology. *Drugs.* **48**: 510-527.

13. Diwu, Z. and Lown, J.W. (1992)   Photosensitization by anti-cancer agents 12. Perylene quinonoid pigmments, a novel type of singlet oxygen sensitizer. *J. Photochem. Photobiol. A Chem.*, **64**: 273-287.

14. Miller, G.G., Brown, K., Ballangrud, A.M., Barajas, O., Xiao, Z., Tulip, J., Lown, J.W., Leithoff, J. M., Allalunis-Turner, M.J., Mehta, R.D. and Moore, R.B. (1997) Preclinical Assessment of Hypocrellin B and Hypocrellin B Derivatives as Sensitizers for Photodynamic Therapy of Cancer: Progress Update. *Photochem. Photobiol.*, **65(4)**: 714-722.

15.   Wan, X.Y. and Chen, Y.T. (1981)   Hypocrellin A, a new drug for photochemotherapy. *Kexue Tongbao* (English version). **26**: 1040-1042.

16. Estey, E.P., Brown, K., Diwu, Z., Liu, J., Lown, J.W., Miller, G.G, Moore, R.B., Tulip, J. and McPhee, M.S. (1996)   Hypocrellins as photosensitizers for photodynamic therapy: a screening evaluation and pharmacokinetic study. *Cancer Chemother. Pharmacol.*, **37**: 343-350.

17. Miller, G.G. and Lown, J.W. (1997) Immunophotodynamic therapy: current developments and future prospects (review). *Drug Develop. Res.*, **42**: 182-197.

18. Morgan, J., Lottman, H., Abbou, C.C., and Chopin, D.K. (1994) A comparison of direct and liposomal antibody conjugates of sulfonated aluminum phthalocyanines for selective photoimmunotherapy of human bladder carcinoma. *Photochem. Phtobiol.*, **60**: 486-496.

19. Chang, S.C., MacRobert, A.J. and Bown, S.G. (1996) Photodynamic therapy on rat urinary bladder with intravesical instillation of 5-aminolevulinic acid: light diffusion and histological changes. *J. Urol.*, **155**: 1749-1753.

20. Moore, R.B., Chapman, J.D., Mokrzanowski, A.D., Arnfield, M.R., McPhee, M.S. and McEwan, A.J. (1992) Non-invasive monitoring of photodynamic therapy with ^{99m}Technetium HMPAO scintigraphy. *Br. J. Cancer.* **65**: 491-497.

21. Moore R.B. (1991) PDT induced ischemia. Ph.D. thesis. University of Alberta, Edmonton, Canada.

22. Ben-Hut, E., Rosenthal, I. (1995) The phthalocyanines: a new class of mammalian cell photosensitizers with a potential for cancer phototherapy. *Int. J. Radiat. Biol.*, **47**: 145-147.

23. Sternberg, E., Dolphin, D. (1993) An overview of second generation drugs for photodynamic therapy including BPD-MA. In Spinelli P, Dal Fante M, Marchesini R, eds. Photodynamic Therapy and Medical Lasers. *Excerpta Medica* 470-474.

24. Kriegmair, M., Baumgartner, R., Knuchel, R., Stepp, H., Hofstadter, F. and Hofstetter, A. (1996) Detection of early bladder cancer by 5-aminolevulinic acid induced porphyrin fluorescence. *J. Urol.*, **155**: 105-110.

25. Stocker, S., Knuchel, R., Sroka, R. Kriegmair, M., Steinbach, P. and Baumgartner, R. (1997) Wavelength dependent photodynamic effects on chemically induced rat bladder tumors following intravesical instillation of 5-aminolevulinic acid. *J. Urol.*, **157**: 357-361.

26. Xiao, Z., Miller, G.G., McCallum, T.J., Brown, K.M., Lown, J.W., Tulip, J. and Moore, R.B. (1998) Biodistribution of Photofrin II and 5-aminolevulinic acid -

induced protoporphyrin IX in normal rat bladder and bladder tumor models.

Photochem. Photobiol. **67** (5): 513-518.

27. Van den Bergh, H., Lange, N. and Jichlinski, P. (1999) ALA hexylester: a second-generation precursor for protoporphyrin IX in photodynamic therapy and photodetection of early bladder cancer. *Photodynamics News.* **2** (1): 4-8.